MULTIFUNCTIONAL NANOPARTICLE-BASED APPROACHES TO ENHANCE THE TREATMENT OF CANCER

By

PERRY TO-TIEN YIN

A dissertation submitted to the

Graduate School-New Brunswick

Rutgers, The State University of New Jersey

and

The Graduate School of Biomedical Sciences

in partial fulfillment of the requirements

for the degree of

Doctor of Philosophy

Graduate Program in Biomedical Engineering

Written under the direction of

Professor Ki-Bum Lee

and approved by

_____

_____

_____

_____

New Brunswick, New Jersey

January, 2016

ABSTRACT OF THE DISSERTATION

MULTIFUNCTIONAL NANOPARTICLE-BASED APPROACHES TO ENHANCE THE TREATMENT OF CANCER

By

PERRY TO-TIEN YIN

Dissertation Director:

Professor Ki-Bum Lee

Magnetic nanoparticles (MNPs) hold tremendous potential for various biomedical applications, including cancer diagnosis and treatment, owing to their unique ability to be manipulated by magnetic fields. In particular, cancer applications of MNPs have primarily utilized MNPs as MRI contrast agents, drug delivery vehicles, and as agents for magnetic hyperthermia. Significant progress has already been made in the advancement of MNP-based therapies to the clinic; however, tumor targeting and chemoresistance remain significant challenges. Addressing these challenges, this thesis focuses on the development of novel multifunctional MNP-based combination therapies.

In the first half of this thesis, novel MNP and magnetic core-shell nanoparticle (MCNP)-based combination therapies are developed to enhance the treatment of cancer by sensitizing cancer cells to subsequent therapies. To this end, MNPs are first developed for the dual purpose of delivering microRNA and inducing magnetic hyperthermia for the treatment of brain cancer. We demonstrate that the combination of lethal-7a microRNA (let-7a), which targets a number of survival pathways, can sensitize cancer cells to

subsequent magnetic hyperthermia. Moreover, we demonstrate the use of MCNPs that are composed of a magnetic core and a mesoporous silica shell for the simultaneous delivery of let-7a and doxorubicin, wherein let-7a was found to sensitize breast cancer cells to subsequent doxorubicin chemotherapy.

In the second half of this thesis, to overcome poor tumor targeting, a stem cell-based gene therapy is developed. Specifically, MCNPs are reported for the dual purpose of delivering and activating a heat-inducible gene vector that encodes TNF-related apoptosis-inducing ligand (TRAIL) in adipose-derived mesenchymal stem cells (AD-MSCs) for the treatment of ovarian cancer. These engineered AD-MSCs retained their innate ability to home to tumors, making them ideal cellular carriers for cancer therapy. Moreover, mild magnetic hyperthermia resulted in the selective expression of TRAIL in the engineered AD-MSCs thereby inducing significant cancer cell death.

Overall, this thesis has demonstrated two multifunctional MNP-based approaches for cancer therapy: 1) combined MNP-based delivery of microRNA and magnetic hyperthermia to sensitize cancers to subsequent chemotherapy and 2) MCNP-based activation of heat-inducible genes in stem cells for targeted cancer treatment.

Acknowledgements

After reflecting on the past five and a half years that I have spent at Rutgers University, there are a number of people that have had a significant impact on my graduate career and whom I would like to acknowledge. First and foremost, I would like to thank my advisor, Dr. Ki-Bum Lee. It was Dr. Lee who first attracted me to Rutgers University and, more importantly, without his support and guidance, none of my graduate work would have been possible. As such, it has truly been a pleasure working with Dr. Lee. In particular, working in his lab has provided me with the unique opportunity to not only explore and develop my own research projects, but also take on considerable responsibility through my participation in grant proposal and review paper writing. As a result, my horizons and knowledge base have been greatly expanded. Moreover, outside of research, Dr. Lee has always whole-heartedly supported me in my career goals. To this point, I would like to give a special thanks to him for allowing me to gain industrial experience through internships at Merck & Co. and Microlin Bio, Inc. as well as allowing me to participate in the NSF I-Corps, which was a very enlightening experience. I would also like to take a moment to thank my committee members, Drs. Li Cai, Charles Roth, and Nanjoo Suh. They have always made themselves available to me and provided me with great advice, which has greatly facilitated and accelerated my research progress.

I am also honored to have formed an excellent network of friends and colleagues during my time at Rutgers University, which I believe will last long after I graduate and throughout my career. Specifically, I would like to acknowledge all of my lab mates in the KBLEE group, especially Shreyas Shah, Tae-hyung Kim, Sahishnu Patel, Nicholas

Pasquale, Aniruddh Solanki, and Birju Shah with whom I most closely collaborated. In particular, I would like to give a special thanks to Shreyas Shah for always being open to discussing science, specific projects, proposals, careers, and any other miscellaneous topics that have come up over the years. I am sure that we will both succeed in our respective fields and I hope we continue to collaborate in the future. I would also like to thank Tae-hyung Kim, who has been a great friend both inside and outside of lab. Though, I'm sorry that you were never able to convince me to become a professor. Finally, I would also like to thank all of my friends and colleagues in the Department of Biomedical Engineering and the NIH Biotechnology Training Program.

Outside of Rutgers, I would like to thank my girlfriend, Xi Chen, for taking the time to visit me almost every weekend for the last year. You have definitely always challenged me and kept me grounded. I also really appreciate your honesty and the fact that you have put up with me being a student and always changing my career plans. I would also like to give a special shout out to my best friends Jean-Paul Leva and Sarah Choi for taking the time and effort to come visit me at Rutgers as often as they could and always getting me to go out and have fun. Finally, I would like to thank my close friends Daniel Cabrera and Teresa Lii for always keeping in contact and welcoming me with open arms every time I see them in New York City.

Finally, but also most importantly, I would like to thank my parents as well as my extended family. They have always been very supportive of me in all my endeavors, especially during my graduate career. More specifically, I would like to give a special thanks to my mother, Tai-yun Yang. She has always known me the best and always knows exactly what to say when I become unsure of myself or the path that I am taking.

Table of Contents

List of Tables

List of Figures

Chapter 1 :

Introduction

The text and images used in this chapter have been previously published, at least in part, in Advanced Healthcare Materials as an original manuscript (Yin PT, Han E, Lee KB. Adv Healthc Mater, 2015 [Epub ahead of print]) and Perry Yin was the first author.

1.1. Nanoparticles for Cancer Therapy

Nanoparticles are generally defined as particles that are between 1 and 100 nanometers in diameter.[1] Due to their nanometer size, nanoparticles can act as a bridge between bulk materials and atoms. For instance, while bulk materials generally have physical properties that remain constant regardless of their size, nanoparticles exhibit size-dependent properties (e.g. unique optical, catalytic, magnetic, and electrical properties) owing to their high surface-to-volume ratio, which dominates over the small bulk of the material that exists at the nanoscale.[2] As such, several nanoparticle-based approaches have been developed, including lipid-based nanoparticles (e.g. liposomes and micelles),[3] polymeric nanoparticles (e.g. dendrimers, hydrogels, and nanofibers),[4] metallic nanoparticles (e.g. quantum dots, magnetic, gold, silver, and titanium),[5] carbon nanostructures (e.g. carbon nanotubes, graphene),[6] and inorganic nanoparticles (e.g. silica),[7] for various biomedical applications such as cancer therapy.

Cancer is currently a leading cause of death worldwide and is the second leading cause of death in the United States with the World Health Organization (WHO) estimating that, in 2012 alone, there were approximately 14 million new cases and 8.2

million cancer-related deaths. In the case of solid tumors, the current gold standard for treatment typically consists of aggressive surgical resection to remove as much of the tumor mass as possible followed by adjuvant chemotherapy and radiotherapy to exterminate the tumor cells that remain. However, despite recent advances in cancer therapy such as immunotherapy and other targeted therapies, the front line nonsurgical methods that are used to treat solid tumors (e.g. radiation therapy and chemotherapy) still rely heavily on agents that aim to just generally kill cells and, as such, do not have good specificity for cancer cells. For example, anticancer drugs, such as doxorubicin and paclitaxel, typically target cells that are rapidly proliferating by intercalating with the DNA and disrupting microtubules, respectively.[8] Moreover, despite these aggressive therapies, cancers often gain chemoresistance, either through adaptive or acquired mechanisms, thereby resulting in recurrence. As such, to improve our ability to treat cancers, there are two general issues that must be addressed. First, there is a pressing need to improve our understanding of cancer physiopathology in order to discover new, potentially more targeted, cancer therapies. Second, there is a desperate need for novel treatments to overcome chemoresistance. As such, novel technologies, in the form of novel drug delivery platforms and/or novel targeted treatment strategies (e.g. stem cell-based therapies, hyperthermia), must be developed.[9]

Owing to their size and unique properties, nanoparticles are emerging as a highly promising class of therapeutics for cancer.[1] In fact, several nanoparticle-based drug therapies have already moved into the clinic and some are now FDA approved.[10] Two of the most well-known nanoparticle-based cancer therapies are Doxil (Janssen), which is a liposomal nanoparticle that contains doxorubicin, and Abraxane (Celgene), which is a

protein nanoparticle composed of albumin-bound paclitaxel. These nanoparticles are both FDA approved and the use of these nanotherapeutics has been shown to not only improve the solubility of their chemotherapeutic cargos but also allows them to remain in circulation longer while ameliorating some of the adverse side-effects that are seen when using free doxorubicin or paclitaxel for the treatment of cancer.

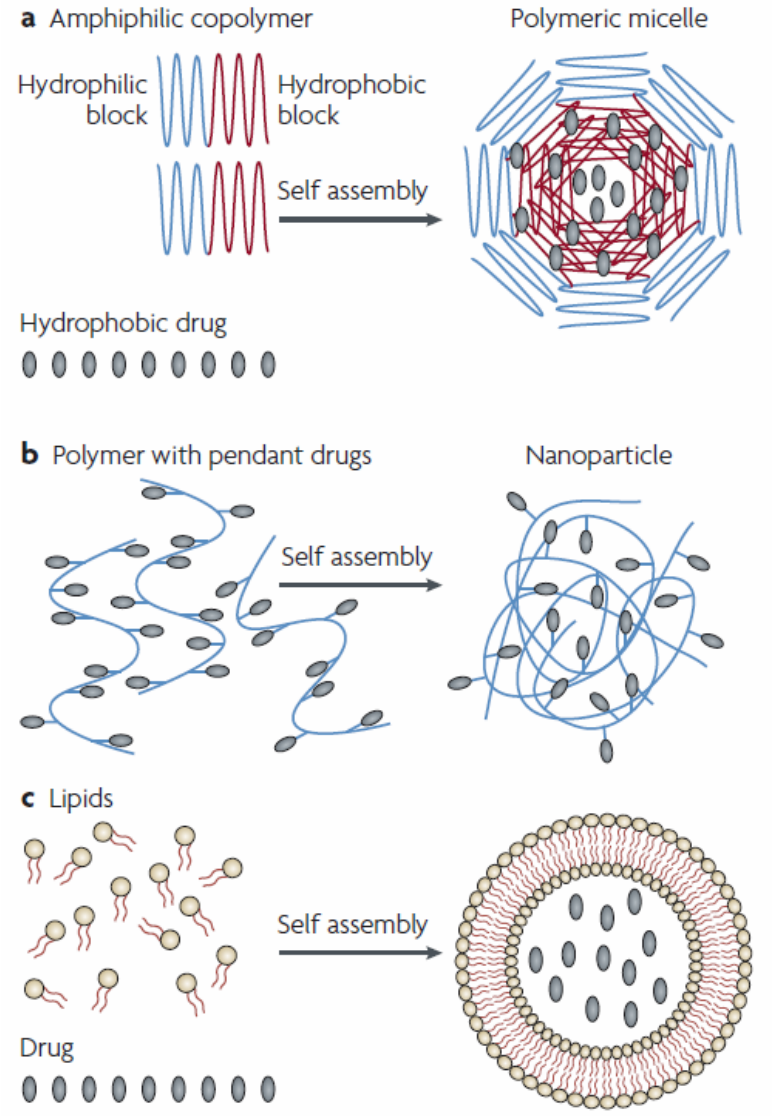

Figure 1.1 Major Types of Nanoparticles in Clinical Trials
A) Polymeric micelles that consist of block copolymers and drugs. **B)** Polymer–drug conjugate nanoparticles. **C)** Liposomal nanoparticles. Reproduced with permission.[1] 2008, Nature.

Besides Doxil and Abraxane, the field of nanoparticle-based therapeutics is currently focused on developing nanoparticles that are complexed, loaded, or functionalized with various types of therapeutic entities, including nucleic acids, small-molecule drugs (as well as combinations of small-molecule drugs), peptides, and proteins for use in the treatment of cancer **(Figure 1.1**). The benefits that are seen with the nanoparticle-based delivery of anticancer agents depend on a number of key properties, including nanoparticle size, surface properties, and functionalization.[1] Moreover, owing to the properties of nanoparticles, depending on the nanoparticle that is used, multifunctionalities can exist thereby enabling the simultaneous monitoring of nanoparticle/drug delivery or the enhancement of treatment (e.g. magnetic hyperthermia, photothermal therapy).

In terms of nanoparticle delivery to the tumor, there are currently two strategies that are being investigated – passive and active targeting. In the case of passive targeting, it has been reported that nanoparticle-based cancer therapeutics should be 10–100 nm in diameter. This lower boundary is defined by the sieving coefficient of the glomerular capillary wall, where the cutoff for kidney elimination is 10 nm.[11] On the other hand, the upper bound is still being investigated. Passive targeting is based on the well-known fact that the tumor vasculature is leaky to macromolecules. For instance, it has been shown that the lymph system is poorly operational in mouse tumor models and, as such, macromolecules (e.g. on the order of hundreds of nanometers) can leak from tumor blood vessels and accumulate at the site of the tumor - a phenomenon that has been dubbed the enhanced permeability and retention (EPR) effect.[12] While this has primarily been shown

in mouse models, evidence suggests that the EPR effect is also applicable to human tumors albeit it should be mentioned that this topic is still hotly debated. Studies using animal models have suggested that neutral or slightly negatively charged nanoparticles that are less than 150 nm in diameter can move through the tumor.[13] Moreover, recent studies have shown that slightly positive nanoparticles that are between 50-100 nm in diameter can penetrate throughout tumors.[14] As such, slightly positively or slightly negatively charged nanoparticles that are 10–100 nm in diameter should be able to penetrate tumors following intravenous injection (i.v.).

Nanoparticle functionalization is also a critical parameter that must be taken into consideration in order to enhance delivery to the tumor both in terms of active targeting as well as to enhance the stability and circulation time of the nanoparticles once they have been injected into the body. For active targeting, nanoparticles can be functionalized with various types of surface ligands (e.g. small molecules, antibodies, peptides, and proteins) that allow the nanoparticles to specifically bind to cancer cells. This can not only enhance the accumulation of the nanoparticles on the surface of the cancer cells but can also enhance tumor cell uptake via receptor-mediated endocytosis and other uptake mechanisms.[15] For instance, transferrin (Tf) is a 80 kDa glycoprotein that is typically responsible for the delivery of iron to cells. In the case of cancer, the transferrin receptor (TfR) has been shown to be highly expressed on many cancer cells.[16] As such, the incorporation of Tf on the surface of the nanoparticles allows for preferential uptake in the tumor over normal cells. Moreover, the ultimate fate of nanoparticles within the body is determined by the interactions that occur between the nanoparticles and their local environment. To this end, nanoparticles can be sterically stabilized and their surface

charge can be modulated to enhance stability and circulation time. In particular, nanoparticles are most commonly functionalized with polyethylene glycol (PEG), which is a stealth polymer that has been shown to suppress nonspecific interactions with the body (e.g. decreases interactions with blood components (opsonization) that can activate the complement system),[17] and can be endowed with either a slightly negative or slightly positive charge in order to minimize overall nanoparticle–nanoparticle and nanoparticle–environment interactions and to promote tumor/cell uptake. In particular, it has been identified that there are many negatively charged components/molecules on the inner surface of blood vessels and on the surface of cells. As such, they repel negatively charged nanoparticles. On the other hand, as the surface charge of the nanoparticle becomes larger, scavenging by macrophage increases, resulting in a greater risk of clearance by the reticuloendothelial system. As such, steric stabilization and careful control of the surface charge is needed to minimize nonspecific interactions, which minimizes nanoparticle losses, thereby maximizing accumulation at the tumor. However, the complete prevention of nonspecific interactions is currently impossible, so the strategy is to minimize interactions and, as such, minimize losses as much as possible.[1]

Overall, nanotechnology, especially nanoparticles, offers an excellent opportunity to enhance our ability to treat cancers. While most work has focused on developing nanoparticle-based platforms for drug delivery there is a huge opportunity to improve nanoparticle-based therapies owing to the multifunctionalities that nanoparticles possess (e.g. imaging and novel treatment modalities). In the following sections, we will focus on the use of magnetic nanoparticles for drug delivery as well as the multifunctionalities that

they possess, including magnetic field-facilitated delivery, magnetic resonance imaging (MRI) contrast, and magnetic hyperthermia.

1.2. Magnetic Nanoparticles for Cancer Therapy

Magnetic nanoparticles (MNPs) represent a major class of nanoparticle that holds great potential for various biomedical applications (**Figure 1.2**), including cancer, owing to their unique ability to interact with and be manipulated by magnetic fields. In particular, cancer applications of MNPs have primarily focused on their use as MRI contrast agents for cancer diagnosis and treatment monitoring[18] as well as the use of MNPs as potentially novel cancer therapies such as for the induction of magnetic hyperthermia and as a vehicle for controlled drug delivery.[19] Owing to its multifunctionalities, MNPs can also be designed to combine several therapeutic functionalities (e.g. drug delivery with hyperthermia) or therapeutic and diagnostic functions (e.g. drug delivery or hyperthermia with MRI).[20] In this section, we will begin by giving a brief overview of the current methods used to synthesize and characterize MNPs. Following, the use of MNPs as hyperthermia agents as well as drug delivery vehicles will be discussed in detail. Finally, the use of MNPs for other applications such as MRI contrast will be briefly mentioned.

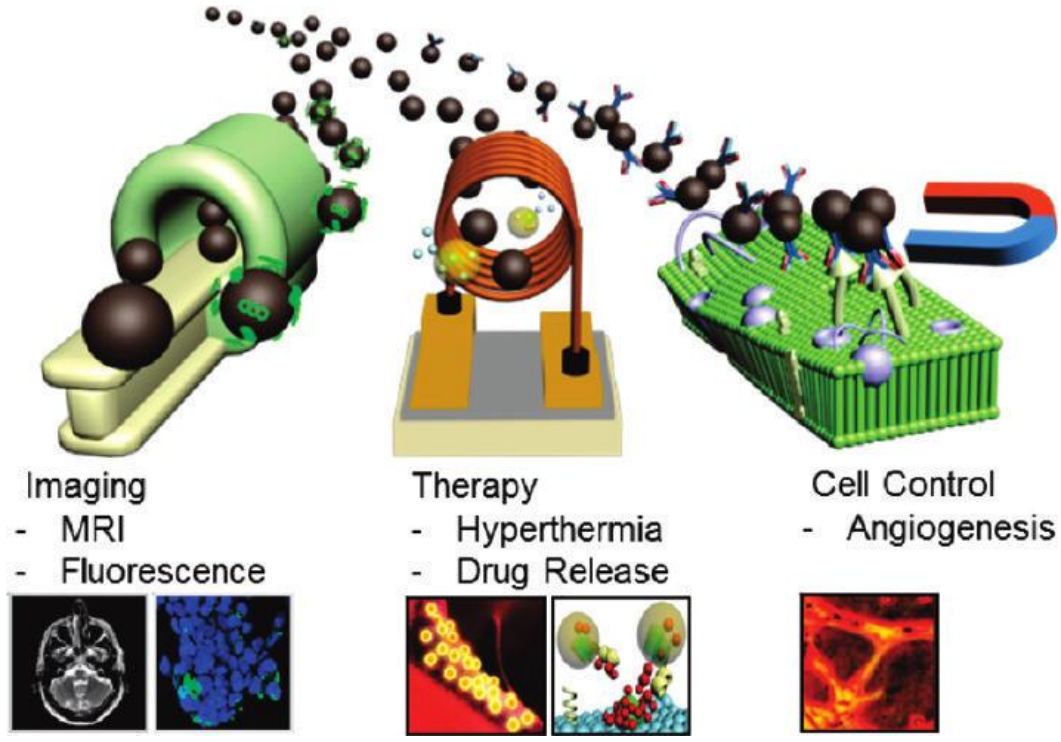

Figure 1.2 Magnetic Nanoparticles for Biomedical Applications
MNPs represent a versatile platform that can be used for targeted imaging, therapy (E.g. drug release and hyperthermia), and cell control. Reproduced with permission.[21] 2011, American Chemistry Society.

1.2.1. Synthesis and Characterization of Magnetic Nanoparticles

Various types of MNPs have been evaluated for use in biomedical applications in order to exploit their advantageous properties, which include their enhanced magnetic moments and their superparamagnetic characteristics. MNPs that are used for biomedical applications are typically superparamagnetic and are composed of a MNP core with a biocompatible shell or surface coating that provides stabilization under physiological conditions as well as additional functionalities (e.g. to enhance cell uptake/cell targeting or drug loading). In particular, superparamagnetism is a type of magnetism that is found in ferromagnetic or ferrimagnetic nanoparticles. For biomedical applications, superparamagnetic nanoparticles are preferred over ferri- and ferromagnetic nanoparticles

because they lose their magnetization once the magnetic field is removed (**Figure 1.3**).[20] Moreover, the modular design of these MNPs allows for multifunctionalities, which can be used for simultaneous drug delivery, magnetic hyperthermia, and imaging. To this end, as with other nanomaterial-based systems, the composition, size, and surface functionalization plays a critical role in not only optimizing and tuning the magnetic properties of the MNPs but also in determining their potential for different biomedical applications.

1.2.1.1. Synthesis of Magnetic Nanoparticles

MNPs are typically composed of magnetic elements, which include iron, cobalt, nickel, and their oxides (e.g. iron oxide), and can be synthesized using various processes that range from wet chemistry-based methods to more advanced techniques such as laser pyrolysis and chemical vapor deposition.[22] In particular, the most common methods that are used to synthesize MNPs, include co-precipitation, thermal decomposition, and hydrothermal synthesis.[23]

Co-precipitation is a simple and convenient method that can be used to synthesize Fe_3O_4 or Fe_2O_3 iron oxide nanoparticles from Fe^{2+}/Fe^{3+} salt solutions. In particular, this can be accomplished in the presence of a base at room temperature or higher that is under an inert atmosphere. The morphology (e.g. size and shape) and composition of the resulting MNPs depends significantly on the salt that is used (e.g. chlorides, nitrates, and sulfates), the ionic strength of the solution, the ratio of Fe^{2+}/Fe^{3+}, and the pH and reaction temperature used. However, once the synthetic conditions are optimized, the quality of the MNPs that are produced using this method is highly reproducible. Moreover, the

magnetic saturation values of the MNPs that are synthesized using co-precipitation are typically 30–50 emu g^{-1}.[23]

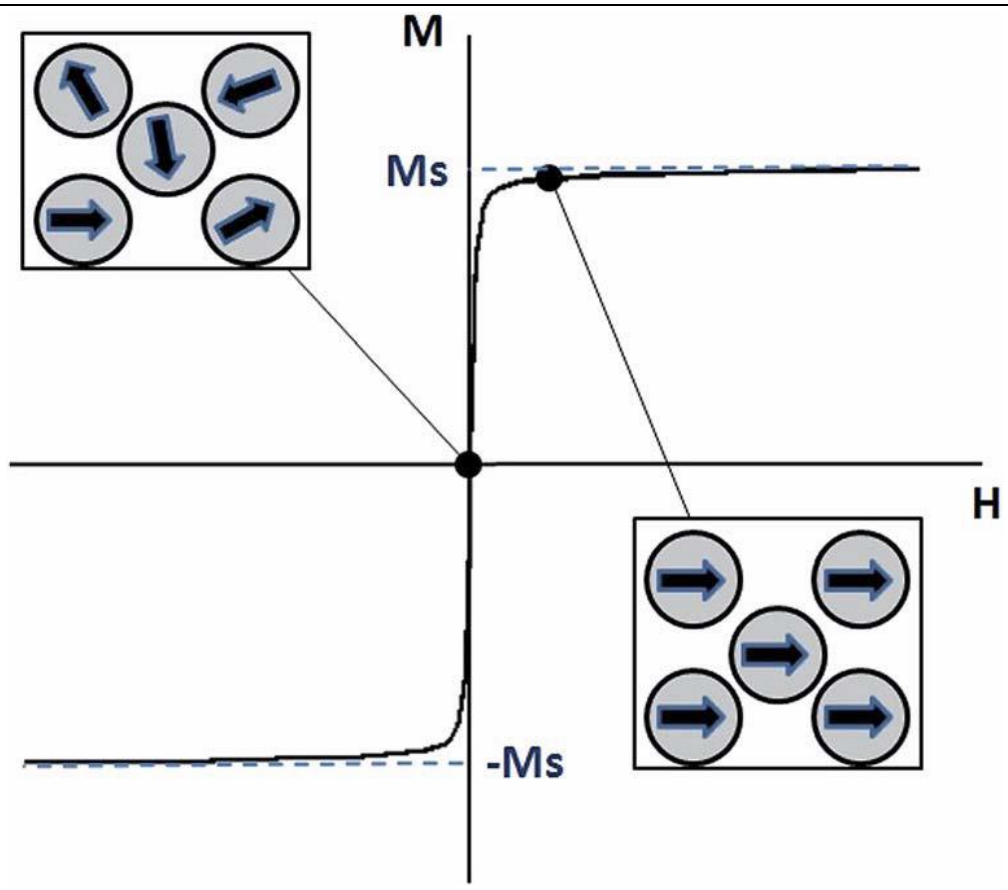

Figure 1.3 Superparamagnetic Behavior of MNPs
Reproduced with permission.[20] 2014, The Royal Society of Chemistry.

Monodisperse magnetic nanocrystals that have a smaller size than what can be obtained using co-precipitation can be synthesized using thermal decomposition. To this end, organometallic compounds are decomposed using high-boiling organic solvents that contain stabilizing surfactants.[24] In terms of the size and morphology of the MNPs that are synthesized, the ratio of the starting reagents (e.g. organometallic compounds, solvent, and surfactant) as well as the reaction temperature and time that is used play a crucial role achieving precise control over size and morphology of the resulting MNPs.

Finally, hydrothermal conditions can be used to form MNPs. This method utilizes a mixture of metal solids, an ethanol–linoleic acid liquid phase, and a water–ethanol solution.[25] Although the underlying mechanism of hydrothermal synthesis is not fully understood at this time, this multicomponent approach provides a powerful method that can be used to direct the formation of the desired MNPs. Overall, co-precipitation is the preferred route for MNP synthesis owing to its simplicity. However, on the other hand, thermo decomposition provides precise control over size and morphology.[23]

Metal-Doped Magnetic Nanoparticles

Fe_3O_4 MNPs are one of the most important and commonly used MNPs for biomedical applications.[26] However, Fe_3O_4 MNPs are constrained by their low magnetization as well as their poor dispersibility and stability.

The magnetization and dispersibility of these MNPs can be improved through metal element doping and surface modification, respectively. This is especially important for biomedical applications. Metal-doped iron oxides (MFe_2O_4), where the doping metal (M) consists of +2 cations of Co, Fe, Mn or Ni, can be fabricated by various methods and can be used to tune and improve the magnetic properties of the doped iron oxide MNPs.[27] For instance, the synthesis and characterization of MFe_2O_4, MNPs (e.g. $CoFe_2O_4$, $FeFe_2O_4$, and $NiFe_2O_4$ MNPs) was recently reported. In this case, the authors used a high-temperature reaction that occurred between metal chlorides and iron tris-2,4-pentadioate.[28] By comparing the various metal-doped MNPs that were prepared, it was reported that the MFe_2O_4 nanoparticles are highly biocompatible *in vitro* and that they possess significantly higher magnetic susceptibilities than conventional magnetite

nanoparticles. As such, this suggests that they may be used for subsequent biomedical applications such as for ultrasensitive MR imaging.

Similarly, Zn is also one of the most commonly used elements to dope into Fe_3O_4 MNPs. In particular, it has been found that doping MNPs with other metals such as Zn^{2+} or Mn^{2+} can greatly enhance the magnetization of the resulting MNPs, which is critical for downstream applications (e.g. a 4- to 14-fold increase in MRI contrast, which can be used to monitor stem cell migration, and a 4-fold enhancement in hyperthermic effect for the treatment of cancer).[29]

Magnetic Core-Shell Nanoparticles

Shells can be added to MNPs to form magnetic core-shell nanoparticles (MCNPs). This is primarily used to maintain the long-term stability of these particles while preventing agglomeration or precipitation. However, the use of different shells can also provide additional multifunctionalities (e.g. imaging or drug loading). In particular, a number of shells have been investigated over the years, including surfactants and polymers, precious metals, silica, and carbon.[23]

The surface of MNPs can be passivated using surfactants or polymers in order to avoid agglomeration. To this end, electrostatic repulsion and steric repulsion are typically used and can act as a means to not only disperse the MNPs but also to stably maintain them in a colloidal state. Moreover, a single or double layer of surfactants or polymers can be chemically bonded or physically adsorbed onto the surface of the MNPs,[30] resulting in the presence of repulsive forces that help balance the van der Waals and magnetic attractive forces. As such, the MNPs are stabilized in suspension via steric

repulsion. Disadvantages that exist with the use of surfactants or polymers include the fact that these surfactant or polymer-stabilized MNPs are not stable in air and can easily be leached by acids.[31] This can ultimately result in the loss of magnetization. Moreover, polymer coatings are unstable at high temperatures and, therefore, do not provide a high degree of protection for the underlying MNPs.

Precious metals can also be deposited on MNP cores using various methods, including microemulsion and redox transmetalation, which act to protect the MNP cores against oxidation.[32] These precious metal-coated MNPs are stable in air and can be redispersed in traditional organic solvents. Moreover, the use of a gold outer shell allows for facile subsequent surface functionalization via the use of thiol groups, improves stability owing to its low reactivity, and provides a high level of biocompatibility as well as the ability to be used for dark-field imaging.[33] However, it has also been reported that it is very difficult to directly coat MNPs with gold because the two surfaces are fundamentally dissimilar.[34]

On the other hand, a silica shell not only protects the MNP core, but can also help avoid unwanted interactions by preventing the MNP core from coming into direct contact with agents that are linked to the silica surface. For instance, the direct attachment of dye molecules to the surface of MNPs often results in quenching. As such the addition of a silica shell can prevent this quenching from occurring. Silica shells also provide several advantages because their surface is easy to modify, they are stable under aqueous conditions (e.g. at low pHs), and because, by varying the thickness of the silica shell, its interparticle interactions can be controlled. Moreover, if the MNP is coated with a mesoporous silica shell, this can allow for drug loading and release of the drug over

time.[35] However, silica is unstable when exposed to basic conditions. In addition, pores may allow oxygen or other species to diffuse.

Finally, there has been increasing interest in the use of carbon shells (e.g. carbon or graphene). This is true because carbon-based nanomaterials can provide a significantly higher degree of chemical and thermal stability as well as biocompatibility when compared to other more traditional shell materials (e.g. polymer and silica).[6] As such, carbon-coated MNPs are more thermally stable and offer additional protection against acid leaching and oxidation. In addition, carbon-coated MNPs usually remain in a metallic state, which results in a higher magnetic moment. However, despite the many advantages of carbon-coated MNPs, aggregation is a significant issue that must be overcome.[23]

1.2.1.2. Magnetic Properties of Magnetic Nanoparticles

The magnetic properties of MNPs are traditionally quantified by measuring their magnetization (M), coercivity (Hc), and magnetocrystalline anisotropy (K).[21] In particular, saturation magnetization (Ms) is defined as the maximum magnetization value of a MNP following its exposure to a magnetic field. The coercivity (Hc) is the magnetic field strength that causes the magnetization of a MNP to become zero. The coercivity of a MNP is especially important for biomedical applications where preventing aggregation and prolonging circulation is especially important. Finally, the magnetocrystalline anisotropy of a MNP is the tendency of its magnetization to align along a preferred direction of the easy axis. Specifically, the magnetocrystalline anisotropy constant (K)

correlates with the amount of energy needed to change the magnetization direction of a MNP from its easy axis to its hard axis.

Figure 1.4 summarizes the functional properties of MNPs focusing on the relationship that exists between the magnetic parameters of MNPs and their use for various applications such as their MRI, hyperthermia, and magnetofection or magnetic targeting.[21]

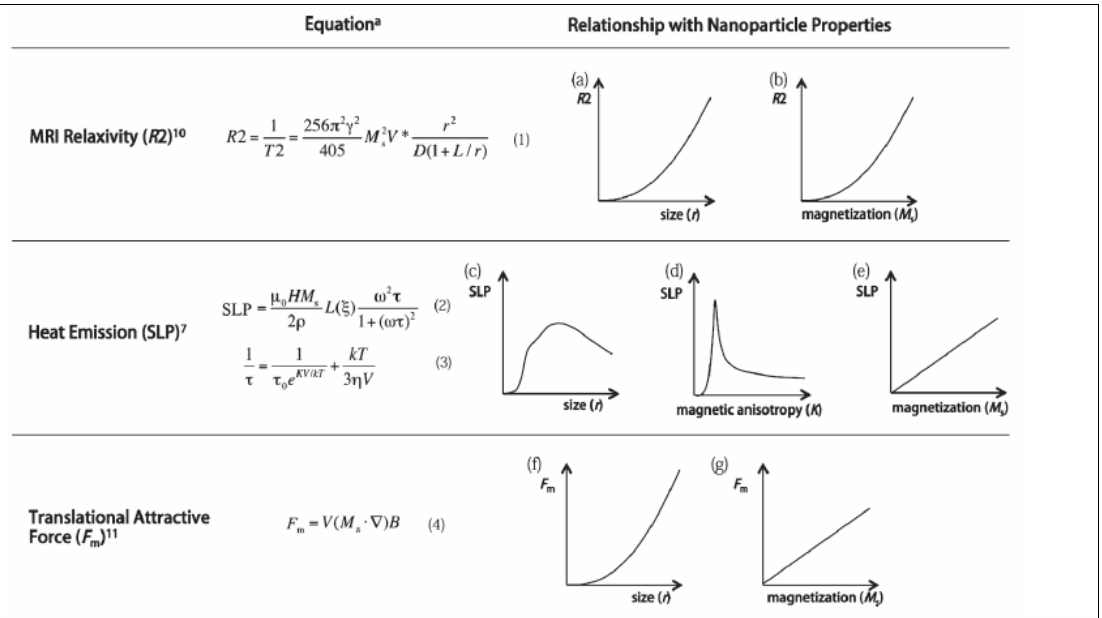

[a] $T2$, transverse relaxation time; γ, proton gyromagnetic ratio; M_S, saturation magnetization; V^*, nanoparticle volume fraction; r, nanoparticle core radius; D, diffusivity of water molecule; L, thickness of surface coating; SLP, specific loss power; μ_0, vacuum permeability; H, magnetic field strength; ρ, density of particle; $L(\xi)$, Langevin function; ω, angular frequency; τ, relaxation time; K, magnetic anisotropy constant; k, Boltzmann constant; V, particle volume; η, viscosity of solution; F_m, force experienced by a particle; B, magnetic field intensity.

Figure 1.4 Functional Properties of Magnetic Nanoparticles
Reproduced with permission. 2011,[21] American Chemistry Society.

1.2.2. Magnetic Nanoparticle-Based Magnetic Hyperthermia

Owing to the magnetic properties of MNPs, when a solution of MNPs is exposed to an alternating magnetic field (AMF), magnetic hyperthermia can be induced. In the most general sense, hyperthermia is a therapeutic procedure in which tissues are heated to temperatures above what is considered the normal physiological range.[36] Thermotherapies can be divided into two general categories based on the temperature that

is achieved: 1) moderate increases in temperature (41-46ºC) result in a hyperthermic effect that may alter/disrupt the structure of cellular components as well as the functionality of intercellular proteins leading to cellular degradation and the induction of apoptosis;[37] 2) hyperthermia treatments above 46ºC (usually 46-48ºC but can go up to 56ºC) results in thermal ablation, wherein cell carbonization occurs as well as necrosis-based death of the cells. As such, hyperthermia has been successfully applied to a number of cancer types both preclinically and clinically. These include, breast,[38] brain,[39] prostate cancers,[40] and melanoma.[41]

1.2.2.1. Mechanism of Heating

When MNPs are subjected to an AMF, the conversion of magnetic energy to thermal energy can occur following several mechanisms. In the case of superparamagnetic MNPs, these MNPs dissipate heat through relaxation losses. These losses can be devided into two categories: Néel relaxation and Brownian relaxation (**Figure 1.5**). The type of relaxation that the MNPs experience depends on the size of the MNPs as well as on the magnetic materials that are used (e.g. this affects the anisotropy constant of the MNPs).[42]

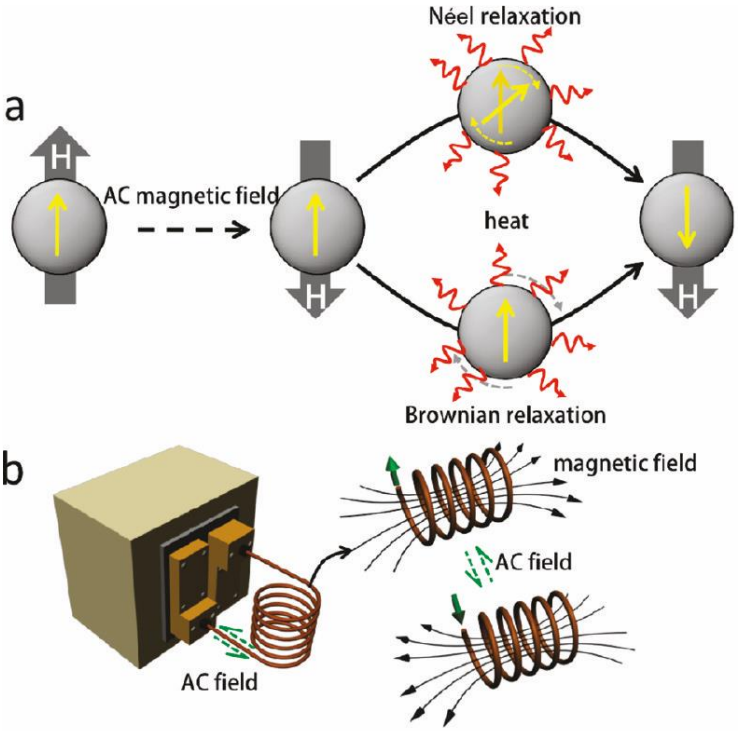

Figure 1.5 Magnetic Nanoparticle-Based Hyperthermia
A) Néel relaxation and Brownian relaxation. **B)** Apparatus for magnetic hyperthermia. Reproduced with permission.[21] 2011, American Chemistry Society.

Néel relaxation is highly size-dependent and occurs when the magnetic moment of a MNP reorients itself in the direction of an alternating magnetic field.[43] For instance, a smaller MNP needs less input energy to change the orietnation of its magnetic moment. As such, Néel relaxation plays a significant role in this case. On the other hand, Brownian relaxation results from friction that is caused by the rotation of the nanoparticle itself in the solution.[43] Brownian relaxation is also size-dependent and depends strongly on the viscosity of the solution that the MNPs are in, wherein MNPs rotate slower the higher the viscosity. Generally, Néel relaxation dominates in small MNPs while Brownian relaxation prevails as the MNPs increase in size.[43-44] For magnetic hyperthermia applications, it is better to utilize MNPs that are small enough that Néel relaxation dominates as the viscosity of the solution can change when the MNPs are internalized

into the cells. Moreover, internalization into the cell may prevent rotation of the MNPs thereby denigrating the effect of Brownian relaxation.

Quantification of the power that is dissipated when MNPs are exposed to an AMF is usually accomplished by measuring the specific absorption rate (SAR), which is expressed as W g^{-1} (also known as the specific loss power). The SAR depends on a number of parameters, including the chemical composition of the MNPs, size of the MNPs, size distribution, morphology (e.g. shape), surface functionalization, and magnetization. Moreover, the frequency and amplitude of the AMF also plays a significant role in the resulting SAR. Obtaining a high SAR and high heating potential is especially important for the clinical application of magnetic hyperthermia. This is true because the higher the SAR, the less MNP would need to be injected to obtain the same therapeutic heating effect. As such, engineering/optimizing MNPs by controlling the parameters stated above and thereby obtaining the highest SAR value possible is highly desirable.[45] Although SAR increases with increasing AMF frequency, to safely apply magnetic hyperthermia to patients, it has been found that the amplitude of the AMF should not exceed a threshold of 5×10^9 A m^{-1} s^{-1}.[46]

1.2.2.2. Magnetic Hyperthermia for Cancer

Recent studies have demonstrated that hyperthermia, which involves the localized heating of cancerous tissues to temperatures between 41-45°C, can be used as an adjuvant that enhances the effectiveness of subsequent chemotherapy or radiotherapy as demonstrated by phase III clinical trials for head and neck cancer,[47] melanoma, cervical cancer,[48] and gliomas.[49] In addition, it has been demonstrated that hyperthermia can,

itself, induce apoptosis. Though the mechanisms through which hyperthermia sensitizes tumor cells and induces apoptosis is still under investigation, it is currently attributed to a combination of four factors: i) increased blood flow to the tumor increases the effect of radiotherapy and chemotherapy (e.g. increases O_2 and drug bioavailability, respectively);[50] ii) inhibition of cellular repair mechanisms including DNA repair;[51] iii) increased permeability of the cell membrane, which helps reverse drug resistance;[52] and iv) the modulation of gene expression and key signaling pathways that result in apoptosis. For example, Vertrees *et al.* have reported that in lung cancer cells, hyperthermia results in the activation of TRAIL and FAS-L and that apoptosis mainly occurs through the up-regulation of caspase-3.[53] Hyperthermia (~42°C) has also been shown to stimulate an innate immune response via the activation of natural killer cells thereby enhancing the antitumor effect.[54, 55] For instance, Kubes *et al.* showed that, after mild local microwave hyperthermia, a large number of activated monocytes are recruited into the tumor of melanoma-bearing mice.[56] In particular, the process through which the host immune system recognizes tumor cell antigens involves the release of heat shock proteins (HSPs) from dying tumor cells, which are responsible for activating nearby monocytes and recruiting antigen-presenting cells.[57] In a typical setting, when using hyperthermia, the target region is sustained at an elevated temperature (e.g. 41-45°C) for a predetermined period of time (1-3 hours). However, these temperatures are difficult to achieve and maintain *in vivo*. Thermometry data from patients has revealed that much of the tumor only reaches a temperature of 40-41°C or less as a result of vascular drainage.[58] Moreover, it is critical to selectively heat the tumor region in order to prevent damage to normal tissues.

To this end, one of the most effective methods with which to achieve a localized hyperthermal effect is to deliver MNPs to the tumor and subsequently apply an AMF. This approach has a number of advantages over conventional hyperthermia methods such as the use of lasers, microwave radiation, radiofrequency fields, ultrasound, including: i) MNPs can readily be tuned in terms of size, structure, and surface characteristics and as a result, provide the opportunity to control the magnetic properties and to target tumors through the blood circulation,[59] ii) an AMF is a non-invasive method to generate a very localized heating, iii) MNPs offer the possibility of self-limiting the maximum achievable temperature by synthesizing MNPs with a suitable Curie temperature, iv) MNPs can afford imaging capabilities through MRI and other modalities, and v) MNPs with the proper surface modifications can be utilized as drug/gene delivery vehicles. Most of the work to date has focused on preclinical studies. For instance, Jordan and co-workers have reported that the use of dextran- or aminosilane-coated iron-oxide nanoparticles in an AMF (field strength = 0-18 kA/m and frequency = 100 kHz) could prolong the survival of a rat model of GBM 4.5-fold over controls. Histological and immunohistochemical analysis revealed that magnetic hyperthermia resulted in necrosis and a decrease in proliferation around the tumor but did not affect normal healthy cells[60]. Similarly, Zhao *et al.* demonstrated that hyperthermia induced by the exposure of magnetic iron oxide nanoparticles to an AMF could be used to treat a mouse xenograft model of human head and neck cancer.[61] Finally, Ivkov and co-workers have demonstrated the antibody-targeted application of magnetic hyperthermia.[62]

While hyperthermia and magnetic hyperthermia have shown great promise, its use in the clinic is still limited. In the case of magnetic hyperthermia, thermoseed-based

magnetic hyperthermia was first reported in 1990 for the treatment of brain tumors.[63] In this case, thermoseeds composed of a Fe-Pt alloy with a length of 15–20 mm, diameter of 1.8 mm, and Curie temperature of 68–69°C was used for seven cases of metastatic brain cancer including six cases, where hyperthermia was combined with radiation therapy (treatment time of 30–60 min, 2– 3 times a week). The treatment temperatures of the tumors were found to reach temperatures as high as 44°C–46°C during the treatment and a complete response was observed in two of the cases while a partial response was confirmed in one of the patients following treatment. Following, a larger clinical trial was conducted using thermoseeds with a Curie temperature of 68°C for the treatment of 23 cases of brain cancer, where the overall response rate was determined to be 34.8%.[64] Lastly, the only magnetic hyperthermia setup that has been developed utilizing iron oxide nanoparticles can be found in Berlin (**Figure 1.6**). This system was developed at the Charité Medical School, Clinic of Radiation Therapy, and was initially used for the treatment of prostate cancers. Moreover, in 2011, clinical trials were conducted in Berlin, where 12 nm iron oxide nanoparticles were used to treat 66 patients with recurrent brain cancers.[65] The clinical trial determined that magnetic hyperthermia followed by radiotherapy was able to provide a median survival time of 13.4 months in 59 patients with glioblastoma, which was significantly better than the 6.2 month survival time of the control group.

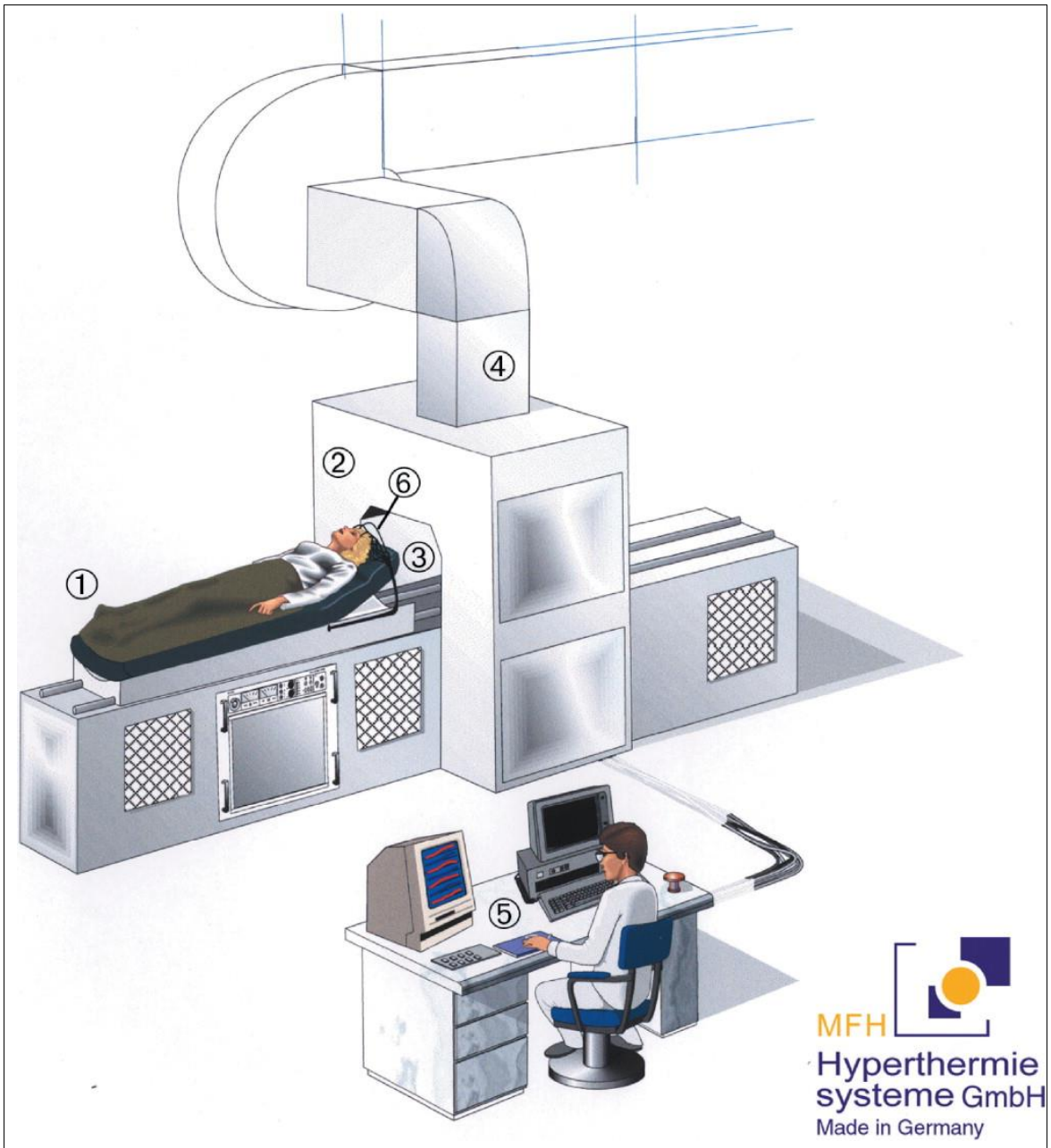

Figure 1.6 Prototype of a Magnetic Hyperthermia Therapy System
Consists of a patient couch (1) with a ferrite-core applicator (2) and an adjustable aperture (3). The system is air cooled (4). All parameters are monitored and controlled at the control unit (5). The temperature is measured invasively with temperature probes (6). Reproduced with permission.[65a] 2001, Elsevier.

1.2.3. Magnetic Nanoparticles for Drug Delivery

For MNP-based drug delivery, therapeutic molecules are usually linked to the MNP surface or encapsulated/complexed with polymer-coated MNPs. Alternatively, the MNPs can possess a mesoporous silica shell, which can be used to load hydrophobic small molecule drugs as well as other therapeutic moieties. These drug loaded MNPs can then be delivered to the tumor via passive targeting, active targeting, as well as magnetic field-facilitated delivery/targeting, wherein an exterior magnetic is used to target the MNPs.

1.2.3.1. Targeting Magnetic Nanoparticles to the Tumor

As mentioned previously, nanoparticles are typically targeted to tumors using two mechanisms: 1) passive targeting via the EPR effect or 2) active targeting. Briefly, solid tumors are characterized by an abnormal vascular architecture and poor lymphatic clearance.[66] As such, this enhances vascular permeability to macromolecules (e.g. correctly-sized nanoparticles). This greatly depends not only on the size of the MNPs (e.g. should be between 50 and 200 nm) but also on the coating/functionalization that is used. On the other hand, MNPs can also be functionalized with a variety of targeting ligands (e.g. small molecules, antibodies, peptides, and proteins) that allow the MNPs to specifically bind to cancer cells just as with any other type of nanoparticle. This can not only enhance accumulation of the nanoparticles on the surface of the cancer cells but can also enhance tumor cell uptake of the MNPs via receptor-mediated endocytosis and other cell uptake mechanisms.[15]

In addition to the EPR effect and active targeting strategies, MNPs offer the possibility of magnetic field-facilitated delivery/targeting. *In vitro*, magnetic field-facilitated delivery, which is also known as magnetofection, has been shown to greatly facilitate the uptake of MNPs that are complexed with a variety of cargoes (e.g. siRNA, DNA, small molecule drugs).[67] More importantly, *in vivo*, magnetic field-facilitated delivery can allow for the systemic administration of MNPs that are then directed towards a specific location in the human body using an applied magnetic field (e.g. static magnet). For this procedure, the drug-loaded MNPs can be injected *in vivo* and then specifically targeted to the correct site using static external magnets, where the gradient helps capture MNPs at the targeted site. This strategy is effective strategy when the target is close to the surface of the body. However, the magnetic field strength decreases rapidly with distance. To circumvent this limitation, some studies have demonstrated the implantation of magnetic within the body near the target site.[68] Although MNP applications have advance considerably, to date, there are still minimal clinical studies utilizing MNPs for other applications besides MRI contrast. In particular, a number of issues remain to be resolved, including the large-scale synthesis of stable MNPs, MNP biocompatibility, drug loading, and etc.[23,69]

1.2.3.2. Magnetic Nanoparticle-Based Cancer Drug Delivery

Despite the great promise that MNPs hold for cancer drug delivery, their primary use in the clinic has been as MRI contrast agents. For cancer drug delivery, a few clinical trials have utilized MNPs and magnetic targeting to date. In particular, the first Phase I clinical trial was performed in 1996 by Lubbe *et al.*[70] In this study, epirubicin was

complexed to MNPs via electrostatic interaction. In particular, of the 14 patients that were enrolled in the study, epirubicin was found to be effectively targeted to the tumor using magnetic targeting in 6 patients while the remaining MNPs were found to accumulate in the liver. Koda *et al*. performed a second MNP clinical trial in 2002,[71] wherein 32 hepatocellular carcinoma patients were treated with MNPs coupled with doxorubicin hydrochloride. These MNP-drug complexes were targeted via an external magnetic field and particle localization was monitored using MRI. Of these 32 patients, the tumor was effectively targeted in 30 patients. More importantly, of the 20 patients that were followed, the size of 15 of the tumors remained the same or became smaller and only 5 increased in size. Finally, in 2004, a third clinical trial also focused on hepatocellular carcinomas and found that MNPs coupled with doxorubicin could be magnetically targeted to the tumor sites with a 64 and 91% decrease in tumor volume.[72]

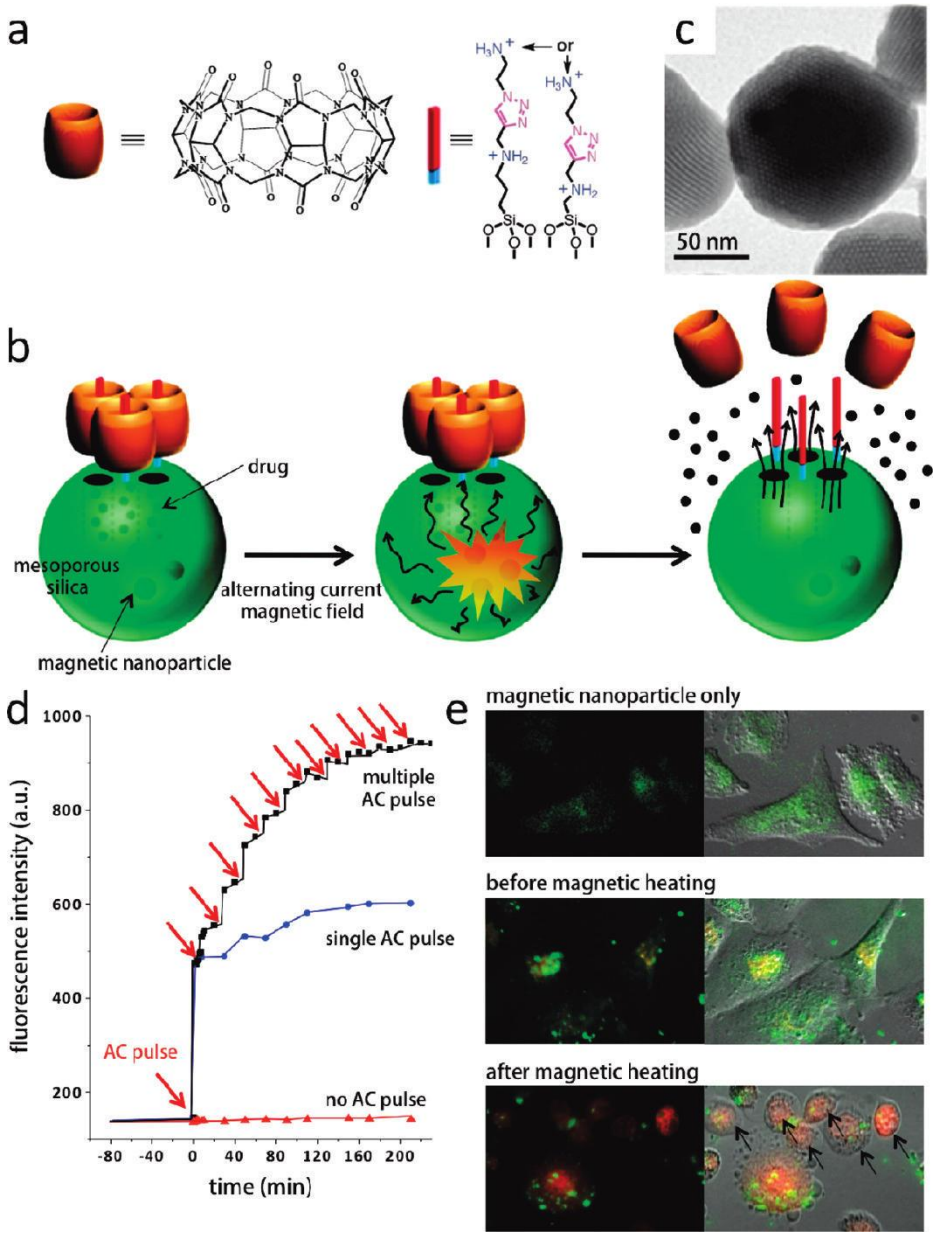

Figure 1.7. Magnetically Triggered Drug Release from MNPs
A) Chemical structure of the capping molecule. **B)** Schematic demonstrating remote-controlled drug release from MNPs. **C)** TEM image of $ZnFe_2O_4$ MNPs encapsulated in a mesoporous silica shell. **D)** Drug release profile during AMF (applied at red arrows). **E)** MDA-MB-231 cells treated with MNPs only and drug-loaded MNP. Reproduced with permission.[21] 2011, American Chemical Society.

More recently, research has focused on utilizing the advantageous magnetic properties of MNPs to further enhance cancer drug delivery. For instance, the magnetic

hyperthermia can be used as a remote-controlled trigger for drug release. Specifically, 15 nm $(Zn_{0.4}Fe_{0.6})Fe_2O_4$ nanoparticles with a high SLP value were coated with a mesoporous silica shell whose pores were blocked with molecular valves.[73] In particular, the molecular valve, which consisted of a thread and a capping molecule (cucurbit[6]uril), was used to close the silica pores and prevent unwanted drug release (**Figure 1.7**). When an external AMF was applied, heat was generated resulting in pressure in the porous nanoparticles, which causes molecular valves to be removed and the release of the drug (**Figure 1.7**).

Lastly, MNPs can also be used for gene delivery. For example, Lee *et al.* developed $MnFe_2O_4$ MNPs that were complexed with siRNA, a fluorescent dye, PEG, and RGD targeting peptide.[74] Specifically, RGD has been shown to target integrins, which are overexpressed in some cancer endothelial cells. siRNA was bound to the MNPs using a disulfide bond, which is enzymatically cleaved once uptaken. Moreover, the nanoparticles can be monitored via MRI and fluorescence imaging. In contrast, gene upregulation can also be achieved using MNP-based delivery. For instance, adenovirus,[75] can be coupled with MNPs to successfully deliver a gene, which was again confirmed using MRI and fluorescence imaging.

1.3. Engineering Stem Cells for Cancer Therapy

Cellular therapies are based on the direct injection of dissociated cells or tissues into patients and have shown great potential for use in biomedical applications.[76] This concept is not fundamentally new, as it has been more than half a century since cellular therapies were first introduced in the form of bone marrow (BM) and organ transplants.[77]

However, recent breakthroughs in genetic engineering and gene/drug delivery are now allowing for safer and more precise cellular manipulation thereby improving the feasibility and potential applicability of cellular therapies in the clinic.

Currently, various cell types are being investigated for cell-based therapies, including differentiated, undifferentiated progenitor, and stem cells, wherein each cell type presents its own unique advantages and disadvantages. For instance, significant progress has been made in the development of immune cell therapies for the clinical treatment of cancer. Immune cell therapies currently come in three forms. In the first form, tumor-infiltrating lymphocytes (TILs) are collected from the patient's tumor.[78] Following laboratory-based selection and expansion, the cells are activated by cytokines and introduced back into the patient. This approach is based on the fact that though TILs already have the ability to target tumor cells, they are not present at sufficiently high numbers to effectively destroy the tumor. As such, clinical trials have demonstrated that the introduction of a large number of activated TILs can help overcome these barriers resulting in shrinkage or destruction of the tumors. Another form of immune cell therapy that is being studied and tested in the clinic is chimeric antigen receptor (CAR) T-cell therapy.[79] In this case, T cells are harvested from the patient and genetically modified to express a CAR, which allows the CAR-modified T cells to target cancer cells. As such, the CAR T-cells are able to bind to the surface of the cancer cells, become activated, and attack the cancer cells resulting in tumor shrinkage and/or destruction. Finally, most recently, efforts have also focused on developing dendritic cell-based therapies for the treatment of cancers.[80] In this case, dendritic cells are obtained from the patient using mononuclear cell collection or a similar technique. The dendritic cells are then

treated/exposed to a targeted protein that is overexpressed by the tumor. As such, when the dendritic cells are reintroduced in the patient, they can stimulate a T-cell cytotoxic response to the targeted protein-overexpressing cancer cells. However, in general, the clinical application of differentiated cells is hindered by the practical difficulties that are associated with obtaining large cell populations, their lack of self-renewal capability, and poor engraftment upon transplantation.[81]

Stem cells, on the other hand, can be distinguished from all other cell types by their unique ability to continuously self-renew and differentiate into intermediate and mature cells of a variety of lineages. In addition, they are relatively easy to isolate when compared to mature cells and exhibit the ability to migrate to sites of damage and disease *in vivo*.[82] Finally, stem cells can often contribute directly to therapy owing to their intrinsic secretion of therapeutic and/or beneficial factors such as anti-inflammatory cytokines or angiogenic factors.[83] While the transplantation of unadulterated stem cells has shown great potential for the treatment of a variety of diseases and disorders,[76c,84] recent efforts have increasingly focused on engineering stem cells to expand and control their innate functions. Specifically, the act of engineering stem cells can be defined as the modification of stem cells to control their behavior for a particular purpose **(Figure 1.8)**. This encompasses the genetic modification of stem cells as well as the use of stem cells for gene delivery, nanoparticle delivery/loading, and even small molecule drug delivery. Currently, biomedical applications of engineered stem cells have primarily focused on regenerative medicine. In particular, studies have concentrated on engineering stem cells for the regeneration of cardiac, neural, and orthopedic tissues.[76c,85] For instance, engineered neural stem cells (NSCs) can be transplanted following central nervous

system (CNS) injuries such as spinal cord injury to promote neuronal cell survival and recovery or to guide NSC differentiation. Similarly, genetically-modified stem cells are being developed for the treatment of more specialized genetic diseases including those related to immune deficiencies.[86] Finally, there has recently been increasing interest in engineering stem cells as potent cancer therapies, where stem cells can be used as the vehicle for gene therapy or for targeted chemotherapeutic delivery, owing to the demonstrated ability of stem cells to home to and infiltrate the tumor microenvironment.[87]

In this section, we will briefly discuss the strategies that have been developed to engineer stem cells, followed by a review of their application to cancer therapy. The images and text used in this section was adapted, at least in part, from a Review paper published by the author in Advanced Healthcare Materials.[88]

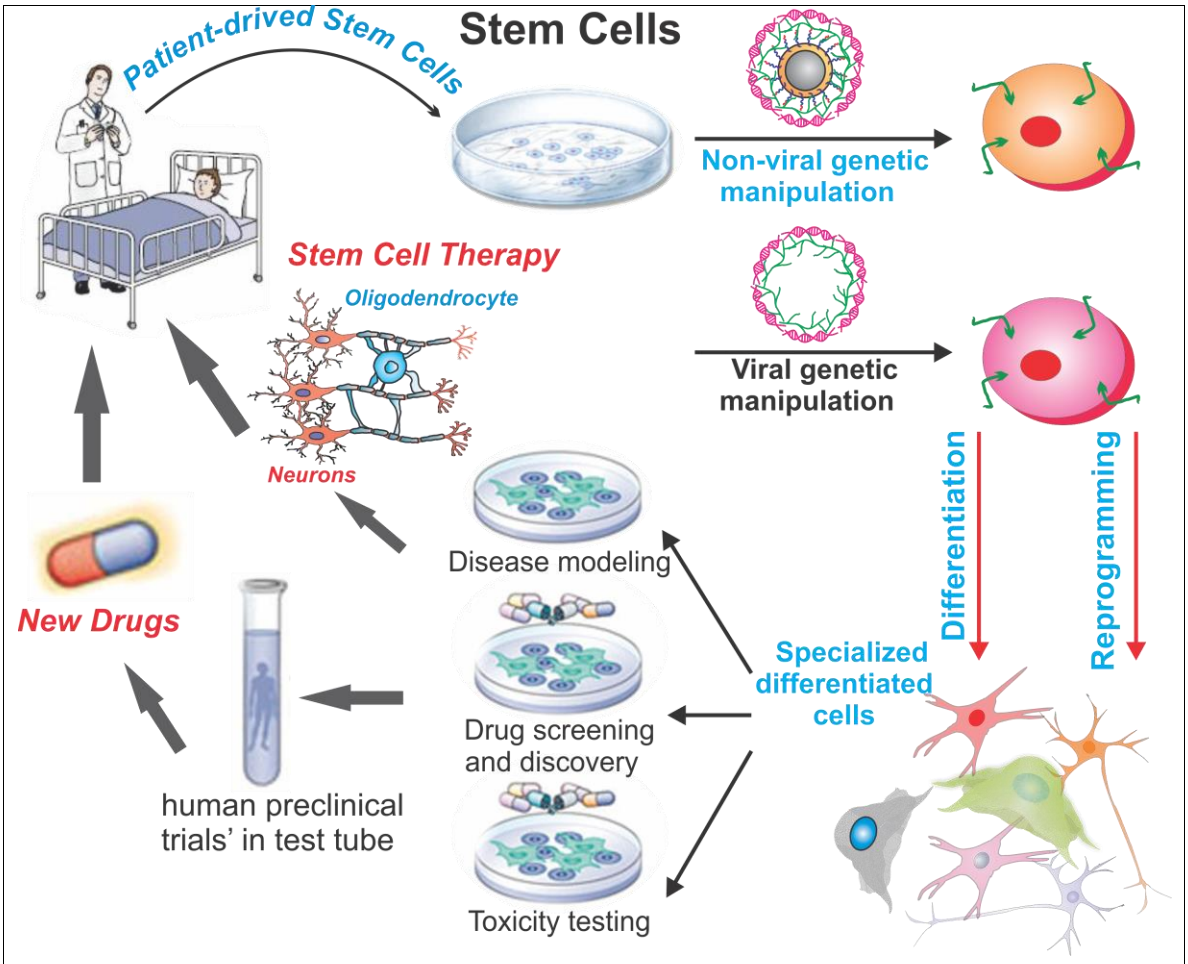

Figure 1.8. Engineering Stem Cells for Biomedical Applications
Stem cells can be obtained from various sources, engineered using non-viral and non-viral methods, and then reintroduced back into the patients' body. These engineered stem cells can take on a number of forms. For instance, engineered stem cells encompass the genetic modification of stem cells as well as the use of stem cells for gene delivery, nanoparticle delivery and loading, and even small molecule drug delivery. Reproduced with permission.[88] 2015, Wiley.

1.3.1. Stem Cell Sources

There are currently a number of stem cell sources that are being investigated for use in cancer applications, including adult stem cells, embryonic stem cells (ESCs), and induced pluripotent stem cells (iPSCs), where each has its own advantages and disadvantages. For example, adult stem cells are a readily available source that are free from ethical concerns, are less likely to form teratomas than other stem cell sources, and

can be collected from the patient, modified, and then reintroduced into the patient. On the other hand, ESCs are pluripotent cells that can be extracted from the inner cell mass of early embryos. ESCs can give rise to almost all cell lineages and, as such, are the most promising cell source for regenerative medicine. However, there are ethical issues related to their isolation. As a result, the development of iPSCs, which share many properties with ESCs but without the associated ethical concerns, also shows great promise. Unfortunately, ESCs and iPSCs have both shown the potential for teratoma formation, thereby greatly compromising their current clinical utility.

In this subsection, we will focus on adult stem cell sources with a discussion of their individual advantages and disadvantages and their current unadulterated use (e.g. without any modification) in cellular transplantation applications. For a more in-depth look at stem cell sources for biomedical applications, there are also various reviews available.[76a,89]

1.3.1.1. Adult Stem Cells

Most biomedical applications use adult stem cells. To understand the underlying reason, here, we will discuss the use of adult stem cells as a source for stem cell therapy in greater detail. Adult stem cells, also known as somatic stem cells, have been found in numerous tissues and are responsible for the maintenance and repair of the tissue in which they originate. Adult stem cell-based therapies have been successful for several decades, with the first hematopoietic stem cell (HSC) transplantation occurring over 50 years ago.[90] Adult stem cells are multipotent and have the ability to differentiate into a number of lineages depending on their source tissue. For example, adult mesenchymal

stem cells (MSCs) can readily differentiate into lineages of the mesoderm including muscle, bone, tendons, cartilage, and fat. The three main sources of stem cells that will be discussed in this subsection include: 1) NSCs, 2) HSCs, and 3) MSCs.

Neural Stem Cells

NSCs, or neural stem/precursor cells (NSPCs), are a heterogeneous population of self-renewing multipotent cells that can be found in the developing and adult CNS.[89c] NSCs were first identified in the rat brain in the 1960s as proliferating neural cells.[91] Since then, NSCs have been isolated from the embryo as well as from the adult CNS. In particular, NSCs can be collected from the ganglionic eminence of embryos as well as from both the subventricular zone (SVZ) of the lateral ventricles and the subgranular zone (SGZ) of the hippocampal dentate gyrus (DG) in adults.[92] In terms of their differentiation, NSCs can differentiate into astrocytes, oligodendrocytes, as well as various types of neurons (e.g. dopaminergic). *In vivo* studies have demonstrated that transplanted NSCs can become incorporated into various brain regions, where they primarily differentiate into neurons and glia.[93] This lack of oligodendrocyte differentiation *in vivo* has been attributed to the low oligodendroglial differentiation efficiency of NSCs.[94] As such, NSCs represent a good source of stem cells for various biomedical applications, although concerns do exist owing to their limited availability and the difficult nature of their isolation.

Stem cell therapies using NSCs have primarily focused on the replacement of neurons for various nervous system disorders including Parkinson's disease, Huntington's disease, and spinal cord injury (SCI), which is currently being validated

using numerous experimental models and a few clinical trials.[89c] In terms of the experimental models, successes have been reported. However, a number of issues remain to be addressed including whether or not the transplanted NSCs can reach the target organ as well as whether, once at the target organ, the NSCs can differentiate into the appropriate lineage in sufficiently large numbers to give functional benefits. Moreover, our understanding of the *in vivo* differentiation process is still in its infancy. Though, it is clear that the disease microenvironment presents a complex combination of signals to the NSCs, which significantly differs from normal conditions, and, as such, may not be conducive to the survival and differentiation of NSCs into the intended lineage.[95] Furthermore, in the case of oligodendrocyte regeneration, NSC transplantation alone is unable to induce sufficient oligodendrocyte differentiation, which further confounds the use of NSCs for stem cell therapies. As such, there is significant room for investigation and improvement, which may be addressed using an engineered stem cell approach.

Hematopoietic Stem Cells

HSC transplantation is the most widely used stem cell therapy in the clinic today. It was originally developed for two purposes: 1) to treat individuals with inherited anemia or immune deficiencies by replacing the abnormal hematopoietic cells with cells from a healthy individual, and 2) to allow for the delivery of myeloablative doses of radiation and/or chemotherapy to cancer patients.[96] While effective, HSC transplantations come with a number of risks, with the most common being graft-versus-host disease (GVHD).[97]

There are three primary sources of HSCs: 1) BM, which is considered the classical source of HSCs, 2) peripheral blood, and 3) cord blood. The main differences between these sources are their reconstitutive and immunogenic potential. The first cell-surface marker that was used to enrich for human HSCs was CD34, a ligand for L-selectin.[98] In particular, *in vitro* assays have revealed that almost all $CD34^+$ cells have multi-potency or oligo-potency, but also that the population is very heterogeneous. In terms of the percentage of $CD34^+$ cells that can be collected from the different cell sources, typically, the number of circulating $CD34^+$ cells is held at a steady state of 0.06% while 1.1% of the cells in the BM are $CD34^+$. As such, BM is the best source of HSCs and is the primary source used clinically.[99]

Besides the applications described above, HSC transplantation is being investigated for a number of disorders including immunological and genetic blood diseases. For instance, immunosuppression followed by the transplantation of $CD34^+$ HSCs has recently been investigated in Phase I/II clinical trials for the treatment of multiple sclerosis in order to reconstitute the immune system following the removal of active autoreactive T cells.[100] Similarly, HSC transplantation has shown promise for rheumatoid arthritis as well as Crohn's Disease.[101] Lastly, HSC therapies are in clinical trials for sickle cell disease, where it has been demonstrated that curative levels of T cell chimerism (>50%) using HLA-matched sibling allogenic $CD34^+$ HSC transplantations can be achieved.[102]

While HSC therapies have shown promising results in experimental models and in clinical trials, autologous HSC transplantation is not possible in every case, especially for genetic diseases. In addition, allogenic transplantation comes with significant risks of

GVHD. As such, engineered HSCs may provide additional benefits such as genetically repairing autologous HSCs, which can then be transplanted to treat diseases such as Wiskott-Aldrich syndrome or muscular dystrophy as will be discussed in more detail later.

Mesenchymal Stem Cells

MSCs, which are also referred to as mesenchymal stromal cells, are a subset of non-hematopoietic adult stem cells that originate from the mesoderm. Like other adult stem cells, they possess self-renewal capabilities and can differentiate into multiple lineages. In particular, MSCs can not only differentiate into mesoderm lineages, such as chondrocytes, osteocytes and adipocytes, but also ectodermic cells (e.g. neuronal cells) and endodermic cells (e.g. pancreatic cells).[103] Importantly, MSCs exist in almost all tissues. For instance, they can be isolated from the BM, adipose tissue, the umbilical cord, liver, muscle, and lung.

To identify MSCs, there is a general consensus that human MSCs do not express the hematopoietic markers CD45, CD34 and CD14 or the co-stimulatory molecules CD80, CD86 and CD40. Instead, they express variable levels of CD105 (also known as endoglin), CD73 (ecto-5'-nucleotidase), CD44, CD90 (THY1), CD71 (transferrin receptor), the ganglioside GD2, and CD271 (low-affinity nerve growth factor receptor). Moreover, they are recognized by the monoclonal antibody STRO-1. In particular, it is thought that the observed variation in marker expression levels arise from differences in tissue source and culture conditions.[83a]

As a result of the ease with which MSCs can be harvested as well as their multilineage differentiation capabilities, MSCs are currently the most widely used source for stem cell-based research and therapy. Numerous clinical trials using MSCs alone (e.g. without genetic manipulation) have been performed, with the primary applications being tissue repair and the therapy of immune disorders. In particular, MSCs have demonstrated reparative effects, where they are believed to be responsible for growth, wound healing, and the replacement of cells from everyday wear as well as from pathological conditions.[76a] For instance, MSC transplantation has been shown to improve numerous musculoskeletal injuries and diseases including the regeneration of periodontal tissue defects, diabetic critical limb ischemia, bone damage caused by osteonecrosis, and burn-induced skin defects.[104] Besides musculoskeletal tissue repair, preclinical studies have also demonstrated that MSCs can effectively treat myocardial infarction as well as brain and spinal cord injuries.[105] On the other hand, MSCs also exhibit the capacity to regulate the immune response for the treatment of immune disorders. For example, MSC transplantation can reverse GVHD in patients receiving BM transplantation.[106] Similarly, the transplantation of both autologous and allogeneic MSCs was able to suppress inflammation and reduce damage to the kidneys and bowel in patients with Crohn's disease.[107] It has also been reported that MSC transplantation can improve multiple sclerosis, amyotrophic lateral sclerosis, and stroke through their immunomodulatory effects.[108] Most importantly, MSCs for the treatment of GVHD and Crohn's disease is currently the only stem cell-based drug approved by the FDA.[109] While already promising, similar to NSCs and HSCs, MSCs are great candidates for stem cell

engineering, which can improve their survival and differentiation capacity thereby greatly enhancing the potential of MSCs for clinical applications.

Overall, adult stem cells are currently the most preferred cell type for downstream stem cell and engineered stem cell therapies as they are the most readily available and well established. Numerous studies and clinical trials have demonstrated that a large stem cell population can be obtained and expanded from patients (e.g. allogeneic source) and, following reintroduction into the patient, are less likely to form teratomas when compared to other stem cell sources upon long-term follow up. Finally, these cells are free from the ethical and moral issues associated with ESCs.

1.3.2. Methods to Engineer Stem Cells

The development of recombinant DNA technology in the 1970s marked the beginning of an exciting new era for biology. Molecular biologists gained the ability to manipulate DNA molecules, making it possible to study genes and harness them for the development of novel medicines and biotechnologies, which include engineering stem cells. However, to achieve the desired effects in engineered stem cells, the therapeutic genes must be carried by safe and effective vectors that can not only deliver genes specifically to the target cells but also sustain their expression thereafter. Other properties that these vectors should possess include: 1) high transfection efficiency, 2) long-term stability without integration into the host genome, 3) ability to spatiotemporally express appropriate levels of the therapeutic gene, and 4) not stimulate the host's immune system or induce cellular transformation.[110]

For this purpose, both viral and non-viral vectors have been developed. Non-viral vectors, such as lipid-based and polymer-based vectors as well as other nanoparticles, have the advantage of being nonpathogenic and having high loading capacities but are generally associated with low transfection efficiencies. On the other hand, viral vectors such as retroviruses, lentiviruses, adenoviruses, and adenovirus-associated vectors are much more efficient, resulting in numerous preclinical and clinical gene therapy studies. Viral vectors differ in their immunogenicity, packaging capacity, ability to transduce dividing and nondividing cells, ability to insert into the host genome, and their ease of manufacturing.[111] However, serious issues arise with their biosafety. As such, careful consideration must be taken when deciding which vectors to use for engineered stem cell applications. In this section, we will cover the techniques that have been most commonly used to genetically engineer stem cells with particular focus on viral and non-viral gene delivery methods.

1.3.2.1 Viral Gene Therapy

Currently, the most efficient and common method of introducing genes into stem cells is by means of viral vectors. However, the chief concerns associated with this approach involve frequent transgene silencing and the fact that integration of the transgene into the host genome can activate nearby oncogenes, leading to the selection of subclones with abnormal growth behaviors.[112] Moreover, viral vectors are severely hampered by their immunogenicity. While a number of excellent reviews covering the progress and challenges faced by viral vectors for gene therapy are available,[113] in this section, we will briefly highlight the various viral vectors that have been applied to

engineer stem cells. Specifically, we will focus on: 1) retroviral, 2) lentiviral, 3) adenoviral, and 4) adeno-associated viral vectors.

Retroviral Vector

Retroviral vectors were the first class of viral vector to be developed and have, historically, been the most widely used in clinical trials.[113b] Specifically, they are single-stranded RNA viruses that replicate in the host cell through reverse transcription, thereby producing DNA from its RNA genome.[114] Moreover, retroviruses have the ability to integrate into the host genome via an integrase enzyme.[115] However, it has been found that retroviral vectors are produced at relatively low titers, require proviral integration into the host chromosome for transduction, and can usually only infect dividing cells. As a result, these properties restrict most retroviral vector applications to *ex vivo* gene transfer approaches, which is not necessarily a significant limitation for the purpose of engineering stem cells.

For the purpose of engineering stem cells, retroviral vectors have traditionally been the vector of choice for the *ex vivo* transduction of HSCs and they offer two main advantages. First, they are non-immunogenic in nature. Second, and more importantly, they can offer constitutive transgene expression owing to their ability to integrate into the host genome. As a result, the genetically engineered stem cells can be used to treat various diseases. On the other hand, retroviral vectors are hampered by a number of significant limitations. Specifically, the use of retroviral vectors results in arbitrary integration of the inserted DNA into the host genome. This could modulate endogenous gene expression via insertional mutagenesis of a proto-oncogene or tumor suppressor

resulting in carcinogenesis of the engineered stem cells.[113b] As a result, in recent years, there has been a decline in the use of retroviral vectors for clinical trials (currently, only 19.7% of trials used retroviral vectors compared to 28% and 22.8% in 2004 and 2007, respectively).[113c]

Lentiviral Vectors

Lentiviral vectors, such as the human immunodeficiency virus (HIV), are specialized members of the retroviral family. Like retroviral vectors, lentiviral vectors can integrate into the genome of the host cell. However, unlike other retroviruses, lentiviral vectors have the advantage of being able to transduce non-dividing cells. As such, these vectors are one of the most efficient viral methods for gene delivery.

In terms of engineering stem cells, one of the key rationales for using lentiviral vectors is their ability to transduce stem cells with a high efficiency after only a short *ex vivo* infection, which can favor the maintenance of stem cell properties. For example, this has been demonstrated in HSCs.[116] Moreover, lentiviruses are known to be less genotoxic than other retroviral vectors.[117] However, the potential for carcinogenesis, as induced by insertional mutation, is still a major hurdle for the clinical application of lentiviral vectors. For instance, a clinical trial using a lentiviral vector expressing β-globin to transduce hematopoietic progenitor cells was conducted for the treatment of a patient with β-thalassemia-based anemia.[118] In this patient, following engineered stem cell transplantation, 10% of the erythroid cells contained the vector, but in 3% of cells the vector had integrated into the high mobility group AT-hook 2 (HMGA2) gene, which has previously been linked to cellular de-differentiation and metastasis of solid tumors.[119]

Fortunately, at 33 months, this patient had no evidence of malignancy. Lastly, besides the potential for carcinogenesis, stem cells display low permissivity to the vector, thereby potentially requiring cytokine stimulation in order to increase transduction efficiency.[116]

Adenoviral Vectors

Adenoviral vectors are non-enveloped icosahedral viruses that are composed of a nucleocapsid and a double-stranded linear DNA genome.[120] Adenoviral vectors have a number of advantages, which make them attractive for stem cell engineering. Specifically, the 36 kb genome of the adenoviral vector provides ample space for the insertion of large sequences.[113a] Moreover, adenoviral vectors have high transduction efficiency in both dividing and nondividing cells allowing for the collection of high titers with relative ease. Finally, the vector remains episomal and, as such, does not integrate into the host genome. As a result, the number of clinical trials using adenoviral vectors is growing with 23.3% of clinical trials using adenoviral vectors as of 2012.[113c]

For stem cell applications, these properties may be particularly useful as the transient expression of the transduced gene can help prevent overgrowth of the transplanted stem cells (e.g. for tissue regeneration). However, there are also significant barriers that adenoviral vectors must first overcome before they can be useful in the clinic. For example, they are limited by their large size as well as their great immunogenicity.[121] Moreover, although recombinant adenoviral vectors were the first to result in high levels of systemic gene transfer in mammals, when delivered systemically they can induce severe toxicity at the dosage levels that are required for efficacy, especially in humans. To address this, second- and third-generation vectors contain

additional deletions of the viral genes thereby reducing toxicities. However, even when all of the viral genes are deleted using a helper-dependent packaging system,[122] the vectors are not completely devoid of toxicity and transduction with these vectors can result in large changes in endogenous gene expression profiles.[123]

Adeno-Associated Viral Vectors

Adeno-associated viral vectors are derived from the parvovirus family and are small viruses with a single-stranded DNA genome that requires a helper virus for replication and completion of their life cycle.[124] When compared to adenoviral and other viral vectors, adeno-associated vectors are characterized by a number of advantages such as the ability to infect both dividing and non-dividing cells. In addition, the vector is largely episomal (>99%) and the < 1% that isn't, predictably integrates into human chromosome 19.[125] Finally, it is not currently related to any human disease and it has a lower immunogenicity.

As a result of these properties, adeno-associated viral vectors are currently the vector of choice for clinical viral transduction (4.9% in 2012, which continues to grow).[113c] Previous studies have demonstrated that these vectors can mediate 10 to 100-fold higher levels of transgene expression both *in vitro* and *in vivo* compared to other vectors. However, because of their small size (2.4 - 4 kb), they can only accommodate small genes thereby limiting their therapeutic usefulness.[126] Moreover, despite their lower immunogenicity, one study reported the formation of hepatocellular carcinoma as a result of adeno-associated viral vector integration near a miRNA locus that is known to be involved in tumorigenesis.[127] On the other hand, and more significantly, a clinical trial

conducted by Nathwani and colleagues demonstrated that adenovirus-associated viral vector-mediated gene transfer in Hemophilia B did not result in any acute or long-lasting toxicity but follow-up with a larger number of patients and for longer periods of time is necessary before a full evaluation of the usefulness of adeno-associated viral vectors can be made.[128]

In stem cells, studies have demonstrated that adeno-associated viruses can be used to transduce stem cells that originate from the muscle and brain.[129] However, the efficiency is significantly reduced when compared to the transduction of mature cells. For example, in muscle, Arnet *et al*. found that adeno-associated viral vectors were able to transduce proliferating myoblasts in culture with reduced efficiency relative to postmitotic myocytes and myotubes.[130] In addition, quiescent satellite cells were refractory to transduction *in vivo* in adult mice. On the other hand, for HSCs, some investigators have claimed that HSCs were impervious to adeno-associated viral transduction while others have reported that these vectors were capable of transducing HSCs but only at high vector-to-cell ratios.[129] Either way, despite their low transduction efficiency, recent efforts have focused on using directed evolution to enhance the utility of adeno-associated viruses for stem cell applications. To this end, Asuri and coworkers generated an adeno-associated virus variant with high gene delivery efficiencies (~50%) to human pluripotent stem cells and a considerable increase in gene-targeting frequencies (up to 0.12%).[131]

1.3.2.2 Non-Viral Delivery Vehicles

Several limitations of viral vectors, such as safety concerns that include carcinogenesis, immunogenicity, broad tropism, as well as their relatively small capacity for therapeutic DNA, have prompted the development of synthetic non-viral vectors.[132] The ideal non-viral vector should be able to overcome the many barrier involved with systemic delivery, including: 1) targeted delivery, 2) efficient cell uptake and endosomal escape, and 3) the release of its cargo, all in a biocompatible manner while protecting the cargo from degradation. To this end, nanoparticles can provide a promising platform for gene delivery to stem cells.

Nanoparticles offer a number of advantages over viral vectors, including: 1) a lower immunogenicity, 2) the ability to deliver larger payloads, and 3) generally being easier to prepare/synthesize.[133] In addition, nanoparticles can be used to deliver other nucleic acids (DNA, RNA), biomolecules (e.g. peptides, proteins), small molecule drugs, and can also provide additional multifunctionalities (e.g. heating, imaging).[134] Owing to their great potential, a plethora of nanoparticle systems have been developed to overcome the physiological barriers faced by non-viral delivery methods. Specifically, these nanoparticles can be composed of various materials including metals, noble metals, semiconductors, polymers, lipids, and other inorganic materials and can have various sizes, shapes, and properties.[135] However, few of these vectors have made it through clinical trials to become FDA approved.[132] In addition, they are generally hampered by lower delivery efficiencies relative to viral vectors.[136] As such, while these vehicles possess great potential, there is still significant room for improvement before they can be widely used in the clinic. In this section, we will give a brief overview of some of the

most common nanoparticle systems that have been developed for engineering stem cells with particular focus on lipid- and polymer-based vectors as well as gold and MNPs.

Lipid-Based Vectors

Currently, the most widely used non-viral delivery vehicle consists of lipid-based vectors. Lipid-based vectors are generally characterized of by three components: a cationic head group, a hydrophobic tail, and a linker group.[133b] The liposomal delivery of DNA was first demonstrated in 1980, wherein the phospholipid phosphatidylserine was used to deliver SV40 DNA to monkey kidney cells.[137] Since then, numerous lipid-based vectors with more efficient transfection properties have been developed. Synthetic cationic lipids such as DOTMA, DOSPA, DOTAP, DMRIE and DC-cholesterol spontaneously form small, uniform liposomes that are capable of efficient encapsulation and delivery of DNA to various mammalian cells including stem cells.[132,133b,138] On the other hand, neutral lipids, such as the fusogenic phospholipid DOPE or the membrane component cholesterol, have also been utilized as a component of liposomal formulations to enhance transfection activity and nanoparticle stability.[3b] However, despite being the most widely used non-viral delivery vehicle, limitations do exist, including low efficacy owing to poor stability and rapid clearance,[139] as well as the generation of inflammatory or anti-inflammatory responses.[140]

Polymer-Based Vectors

An alternative class of non-viral vectors consists of cationic polymers, which are attractive owing to their immense chemical diversity and the relative ease with which

they can be functionalized. The most widely developed examples of polymeric vectors include poly(l-lysine) (PLL) and polyethylenimine (PEI), which have both been demonstrated to efficiently transfect stem cells.[132] Besides PLL and PEI, a number of other polymers, which have shown efficacy for stem cell transfection, are also available. For instance, PLGA is a popular choice and can be used to create nanoparticles via solvent evaporation. Finally, chitosan is another popular polymer with an intrinsically positive charge.

In particular, PLL is a homopolypeptide of the basic amino acid lysine although unmodified PLL shows marked *in vitro* cytotoxicity.[141] Moreover, in the absence of a lysosomal disruption agent such as chloroquine, PLL has fairly poor transfection ability.[133b] As a result, numerous copolymer variants of PLL with enhanced gene delivery properties have been reported.[142] One example includes PLL coated with the hydrophilic polymer polyethylene glycol (PEG), which is designed to minimize nonspecific interaction with serum components and thereby increase circulation time.[143] On the other hand, PEI and its variants are among the most studied polymeric materials for gene delivery. PEI is a polymer that has a high positive charge density, especially at reduced pH values, owing the existence of a nitrogen atom at every third position along the polymer. As a result, it has been hypothesized that this can aid in the condensation of DNA as well as enhance endosomal escape.[144] In terms of its transfection efficiency as well as its cytotoxicity, this strongly depends on the structural properties of PEI such as molecular weight and whether it is in a linear or branched form.[145] As with PLL, owing to the cytotoxicity of PEI, a range of modifications have been investigated including block co-polymers of PEG and PEI for improved stability and biocompatibility, degradable

disulphide-crosslinked PEIs for reduced toxicity, and alkylated PEI to increase transfection ability.[132]

Gold Nanoparticles

Gold nanoparticles (GNPs) are one of the most widely used nanoparticles for stem cell applications. In particular, GNPs are attractive owing to their amenability to synthesis and functionalization. Moreover, they are very inert and non-toxic. Specifically, numerous studies have demonstrated that GNPs are well tolerated by stem cells depending on how they are coated and can be used to guide stem cell differentiation by delivering nucleic acids, other biomolecules, and/or small molecule drugs.[146]

GNPs have been synthesized using an array of methods, which are mainly based on the reduction of chloroauric acid in the presence of a stabilizing agent. For example, the most commonly used method is the citrate synthesis method, which involves reduction of chloroauric acid using trisodium citrate thereby resulting into the formation of GNPs. The size of the obtained GNPs is determined mainly by the salt concentration, temperature and rate of addition of reactants resulting in a typical size range of 10–25 nm. However, a range of 1–100 nm or more can also be achieved by varying the salt concentration and temperature.[147] To utilize GNPs for drug or gene delivery, a number of functionalization have been investigated. In particular, as mentioned previously, the surface of GNPs can readily be modified using thiol-based chemistry. As such, GNPs have been stabilized via citrate as well as the more bioapplicable PEG. In addition, to allow for gene or drug delivery to stem cells, GNPs can be covalently modified with the gene or drug. Alternatively, non-covalent methods such as electrostatic interaction

between PEI and nucleic acids can also be used and has been demonstrated successfully in stem cells.[148]

Magnetic Nanoparticles

Lastly, there has been considerable interest in MNPs as multifunctional nanoplatforms for stem cell applications. In particular, MNPs have many unique properties such as high biocompatibility, facile surface modification, and magnetic properties that result in an intrinsic ability to enhance MRI contrast, induce hyperthermia,[149] and be used for magnetic targeting.[23,150] As a result, it has been demonstrated that MNPs are be biocompatible with stem cells and can actually enhance transfection efficiency via magnetically facilitated transfection (e.g. magnetofection).[151]

MNPs, such as the most common Fe_3O_4 MNPs, are typically synthesized through the co-precipitation of Fe^{2+} and Fe^{3+} ions in basic aqueous media or thermal decomposition, which results in more uniform and highly crystalline structures.[152] In addition, it has been found that doping MNPs with other metals such as Zn^{2+} or Mn^{2+} can greatly enhance the magnetization of the resulting MNPs, which is critical for downstream applications (4- to 14-fold increase in MRI contrast, which can be used to monitor stem cell migration, and 4-fold enhancement in hyperthermic effects for the treatment of cancer).[29] Generally, as with GNPs, these MNPs are coated with biocompatible polymers, such as dextran, dextran derivatives, or PEG, to confer stability in a biological system. In addition, nucleic acids, biomolecules, and small molecule drugs can be conjugated via covalent or non-covalent bonds (e.g. PEI via electrostatic interaction). As a result of their great potential, many MNP formulations are under

clinical investigation and some formulations are already FDA approved with MRI contrast being their primary area of application. Finally, investigations have recently focused on the development of magnetic core-shell nanoparticles (MCNPs) wherein the MNP is coated with a shell that provides additional functionalities such as gold or mesoporous silica (e.g. dark-field imaging and increased drug loading, respectively).[67,153] As a result, MNPs and MCNPs have particularly great potential for stem cell engineering owing to their multifunctionalities and tunability.

1.3.3. Using Engineered Stem Cells for Cancer Therapy

Recently, there has been increasing interest in the development of gene therapies as a unique strategy for the treatment of cancer. Gene therapy for cancer encompasses a wide range of treatments that have the common theme of delivering genetic materials (e.g. DNA, RNA, and RNA interference molecules) in order to modify cancer cells.[154] A wide variety of gene therapies have been tested on cancers including glioma, pancreatic cancer, lung cancer, liver cancer, and many more. Examples include the creation of cancer vaccines, targeting viruses to cancer cells for the induction of lysis and death, targeting supporting cells to cutoff the blood supply, and introducing genes into cancer cells that either cause death or restore them to a normal phenotype.[154] However, as with more conventional drugs, gene therapies are hampered by our current inability to specifically target them to the cancer. As such, combining the tumor tropism/targeting ability of stem cells with gene therapy strategies is a promising way to approach gene therapy thereby using stem cells as a delivery vehicle that can improve our ability to treat cancers. In this section, we will focus on two iterations of stem cell-based gene therapy

for the treatment of cancer, which includes the use of engineered stem cells as a targeted delivery vehicle for gene therapies (e.g. using stem cells to deliver viruses) and genetically engineered stem cells to secrete therapeutic molecules for cancer therapy.

1.3.3.1 Engineering Stem Cells as a Delivery Vehicle for Gene Therapy

Currently, one avenue of gene therapy that is being explored for the treatment of cancer is oncolytic viruses. Specifically, oncolytic viruses are viruses that are engineered to specifically replicate in and kill cancer cells while sparing healthy cells.[155] However, these viruses are quickly cleared through the bloodstream and may exhibit non-specific behaviors when directly administered.[156] Moreover, it has been demonstrated in clinical trials that engineered viruses often only affect tumor cells in close proximity to the site of injection, which significantly hampers its efficacy for metastases.[157] To address these issues, engineered stem cells that are loaded with oncolytic viruses can be used as effective targeted delivery vehicles for gene therapy. Due to their tumor-tropic properties, stem cells can carry the gene therapy vectors to tumors and sites of metastases thereby increasing the local concentration of therapeutic at the cancer site while decreasing the required dosage and subsequent side effects.[156]

To this end, multiple studies have shown that virus loaded stem cells can decrease tumor burden more effectively than direct viral injections.[158] In particular, MSCs have been the most frequently used stem cell source for this purpose with the most common demonstration being for gliomas.[158d,159] For instance, Sonabed *et al.* demonstrated that MSCs can effectively deliver oncolytic conditionally replicative adenovirus (CRAd) to glioma.[157] In particular, the promoter of CRAd's were designed to be tumor specific and,

in this case, are only activated at the tumor site by C-X-C chemokine receptor 4 (CXCR4), which has been shown to be overexpressed by gliomas.[160] To infect the MSCs with CRAd, cells were simply incubated with virus-containing medium (1,000 viral particles per cell) for 48 hours. It was found that CRAd-loaded MSCs effectively migrated *in vitro* and released CRAds that infected U87 glioma cells. More importantly, MSCs also migrated *in vivo* when injected away (5 mm) from the tumor site and delivered 46-fold more viral copies than CRAds injected alone.

Although the majority of studies using stem cells to deliver viruses have focused on MSCs, NSCs have also shown significant migratory ability for the treatment of gliomas.[87] As such, Ahmed and coworkers conducted a comparative study of NSC- and MSC-based carriers for oncolytic adenoviruses for GBM.[161] In this case, commercial stem cells were transduced with a variety of adenoviral vectors (AdWT, CRAd-CXCR4, etc.). Importantly, it was found that both cell sources had similar potential to function as cell carriers. However, the amount of virus released from NSCs was a log higher than from MSCs. As such, only virus loaded NSCs, which were administered intracranially to an orthotopic glioma model, significantly prolonged the survival of tumor bearing animals (68.7 days of survival for NSCs-injected animals vs. 44 days for MSCs). Besides glioma, Stoff-Khalili *et al.* implemented a therapy utilizing MSCs to shuttle CRAd agents to metastatic breast tumors.[162] In particular, the CRAd's promoter was tumor specific and, as with the case in glioma, were also designed to be activated at the tumor site by CXCR4, which is overexpressed by certain breast cancer cell lines.[163] The MSCs were successfully loaded with the adenovirus via diffusion during 18 hours of incubation and were subsequently trypsinized and intravenously injected. Results

indicated that mice bearing MDA-MB-231 breast cancer pulmonary metastases that were injected with the adenovirus loaded MSCs survived significantly longer than their control counterparts (approximately 3 times longer).[162] The ability of stem cells to infiltrate tumors was also hypothesized to significantly increase the tumor's exposure time to the therapy resulting in the corresponding increase in therapeutic efficiency.[164]

Lastly, Mader and colleagues demonstrated the use of engineered patient-derived MSCs as a carrier to deliver oncolytic measles virus (MV) to ovarian tumors as optimization for a Phase I clinical trial.[165] In particular, various experimental models have previously validated the use of MV and phase I clinical trials are in progress to evaluate the safety and maximal tolerated dose of oncolytic MV for cancers such as ovarian, cancer, myeloma, and glioma.[166] To further improve viral delivery to the tumor, the authors infected patient-derived MSCs with MV via centrifugation (70% infectivity with 1000 x g centrifugation for 5-10 minutes), which did not compromise cell viability. *In vivo*, no tumors were seen despite receiving up to 1.6×10^9 MSCs/kg and MSCs did not promote the growth of SKOV3 human ovarian cancer cells in mice. Using non-invasive SPECT-CT imaging, Mader *et al.* saw rapid co-localization of MV infected MSCs and SKOV3 tumors, within 5–8 minutes of intraperitoneal administration (**Figure 1.9A**). Importantly, MSCs could be pre-infected with MV, stored in liquid nitrogen, and thawed on the day of injection into mice without loss of activity. Finally, it was found that MV infected MSC, but not virus alone, significantly prolonged the survival of animals bearing measles immune ovarian cancer **(Figure 1.9B**).

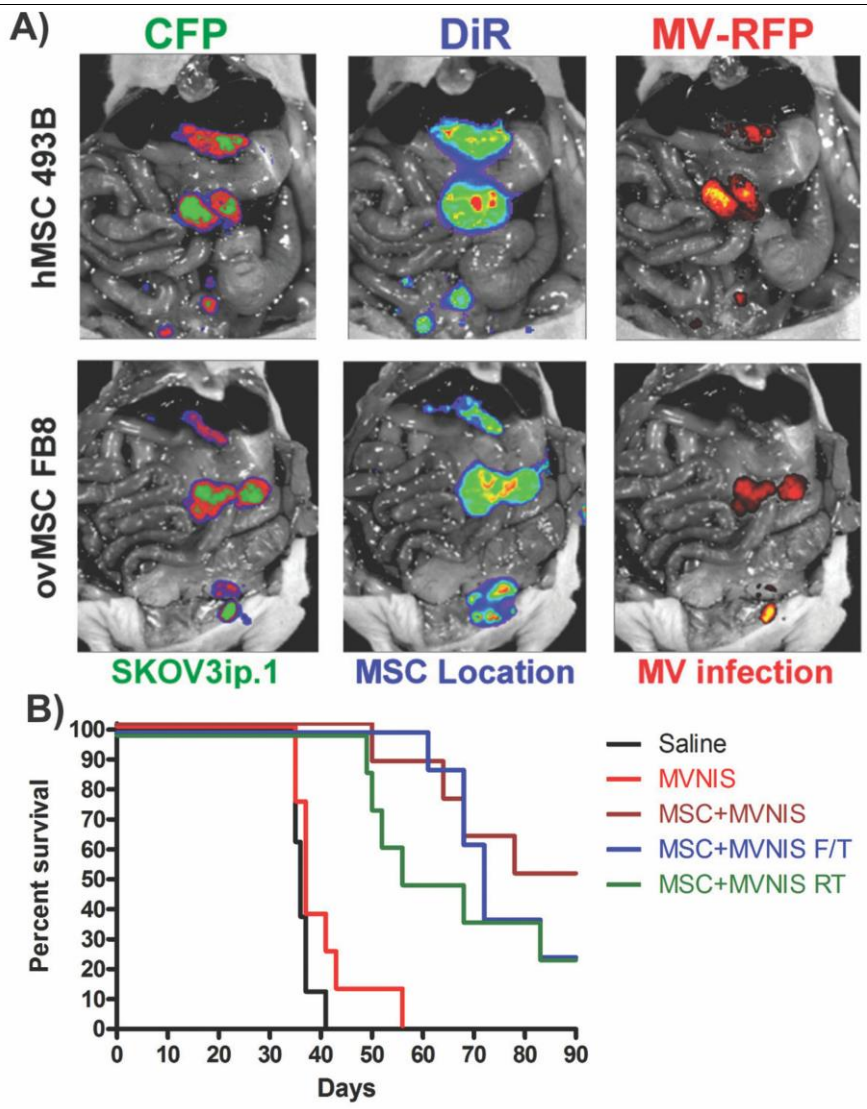

Figure 1.9 Mesenchymal Stem Cells as Virus Carriers for the Treatment of Ovarian Cancer

A) MSCs labeled with DiR and infected with measles virus expressing RFP (MV-RFP) were injected into mice bearing tumors that stably expressed CFP. Representative images from mice that received MSCs from healthy donors (MSC 493B) or ovarian cancer patients (FB8) showed co-localization of MV-infected MSCs with the tumors. **B)** Mice with tumors were passively immunized with measles immune human sera and given 10^5 TCID 50 MV-NIS or 10^5 MV-NIS infected MSCs at 7 days post-tumor implantation. RT = MSCs were given 20 Gy radiation immediately before MV-NIS infection. F/T = Frozen stock of MV infected MSCs were thawed, washed, and used immediately. Reproduced with permission.[165] Copyright 2013, BioMed Central.

1.3.3.2 Genetically Engineering Stem Cells for Cancer Therapy

Aside from delivering oncolytic viruses to cancer, stem cells can also be genetically engineered to secrete: 1) therapeutic proteins or 2) enzymes that convert a separately administered non-toxic prodrug into a cytotoxic drug. Using these approaches, engineered stem cells are capable of migrating to and continuously producing the drug or enzyme at the sites of cancer and metastases, thus bypassing restrictions such as the short half-life of drugs and the need for repeated drug dosages.[158a] For this purpose, MSCs are, again, especially attractive as candidate carriers since they are relatively easy to expand and transduce.[167] Moreover, multiple studies have already shown that genetically engineered MSCs are efficient tools for delivering anticancer agents to metastatic tumors, as we will review later in this section. In particular, this section will focus on the use of genetically engineered stem cells for: 1) the secretion of therapeutic molecules and 2) the secretion of an enzyme that can then convert a separately administered prodrug.

Secretion of Therapeutic Proteins

When genetically engineering stem cells to secrete therapeutic proteins, there are a number of candidate genes including genes encoding proteins that directly act on malignant cells as well as those that affect supporting cells (e.g. blood vessel and stroma). This is typically achieved using viral methods, as although non-viral vectors have been used and offer some advantages such as lower immunogenicity, they have a much lower efficiency.[168] In particular, direct effectors include cytokines such as interferon-β (IFN-β) and tumor necrosis factor-related apoptosis inducing ligand (TRAIL). On the other hand,

those that affect supporting cells typically target angiogenesis or induce an immune response via the secretion of interleukins.

In the case of IFN-β, high concentrations of IFN-β have been shown to inhibit cancer cell growth. However, the direct administration of IFN-β is limited by its short half-life and has been associated with excessive systemic toxicity.[169] Addressing these concerns, a number of studies have focused on using stem cells, especially MSCs, to deliver IFN-β specifically to tumors.[170] For instance, Studeny *et al.* engineered BM-derived MSCs to IFN-β via adenoviral transduction.[171] *In vivo* tests with mice carrying A375SM melanoma tumors demonstrated that the transplanted MSCs preferentially survive and proliferate in the presence of malignant cells and become incorporated into the tumor architecture as stromal fibroblasts. More importantly, the authors found that, on average, mice injected with engineered MSCs survived almost twice as long as control mice (60 days compared to control mice, which survived for only 37 days). On the other hand, the direct intravenous injection of recombinant IFN-β did not increase mice survival compared to control mice, which further supports the use of MSCs as a delivery vehicle for IFN-β. Similarly, Ren and colleagues reported that MSCs engineered with a recombinant adeno-associated virus encoding IFN-β could effectively treat prostate cancer lung metastasis.[172] Evaluation 30 and 75 days after transplantation indicated a significant reduction in tumor volume. In addition, a significant increase in the natural kill cell activity was observed following stem cell-based IFN-β therapy and systemic levels of IFN-β was not significantly elevated. Lastly, aside from MSCs, NSCs have also been used to deliver IFN-β but to a lesser extent.[173]

On the other hand, TRAIL has also been a cytokine of particular interest. TRAIL can induce apoptosis in a wide range of cancers while, generally, sparing normal healthy cells.[174] In particular, TRAIL has been shown to directly attach to death receptors (DR4 and DR5) that are preferentially expressed on tumor cells, activating pro-apoptotic proteases that result in cancer cell apoptosis.[175] However, translation of TRAIL into the clinic is confounded by its short half-life, inadequate delivery methods, and the fact that recent studies have found that TRAIL can cause some hepatotoxicity depending on the patient and drug combinations used.[176] As with IFN-β, MSCS have been shown to have the ability to deliver a secretable form of TRAIL, thereby enhancing the efficacy of TRAIL versus systemic administration of TRAIL alone. For example, engineered MSCs that secrete TRAIL have been utilized to treat *in vivo* glioma models.[177] In particular, these MSCs were transfected using a lentiviral vector and the resulting engineered MSCs secreted around 250 ng of TRAIL per every million cells over a 24-hour timespan. In addition, it was found that the engineered MSCs provided a method to facilitate the transportation of TRAIL across the BBB and continuous production of TRAIL helped mitigate the issue of TRAIL's short half-life (**Figure 1.10**).[178] Importantly, it was shown that MSCs were resistant to apoptosis from TRAIL making them viable targeting candidates.[177] As a result, the engineered MSCs exhibited significant anti-tumor effect over unengineered MSCs resulting in a significant reduction in glioma burden via the induction of apoptosis and a significant decrease in the number of proliferating tumor cells **(Figure 1.10)**.

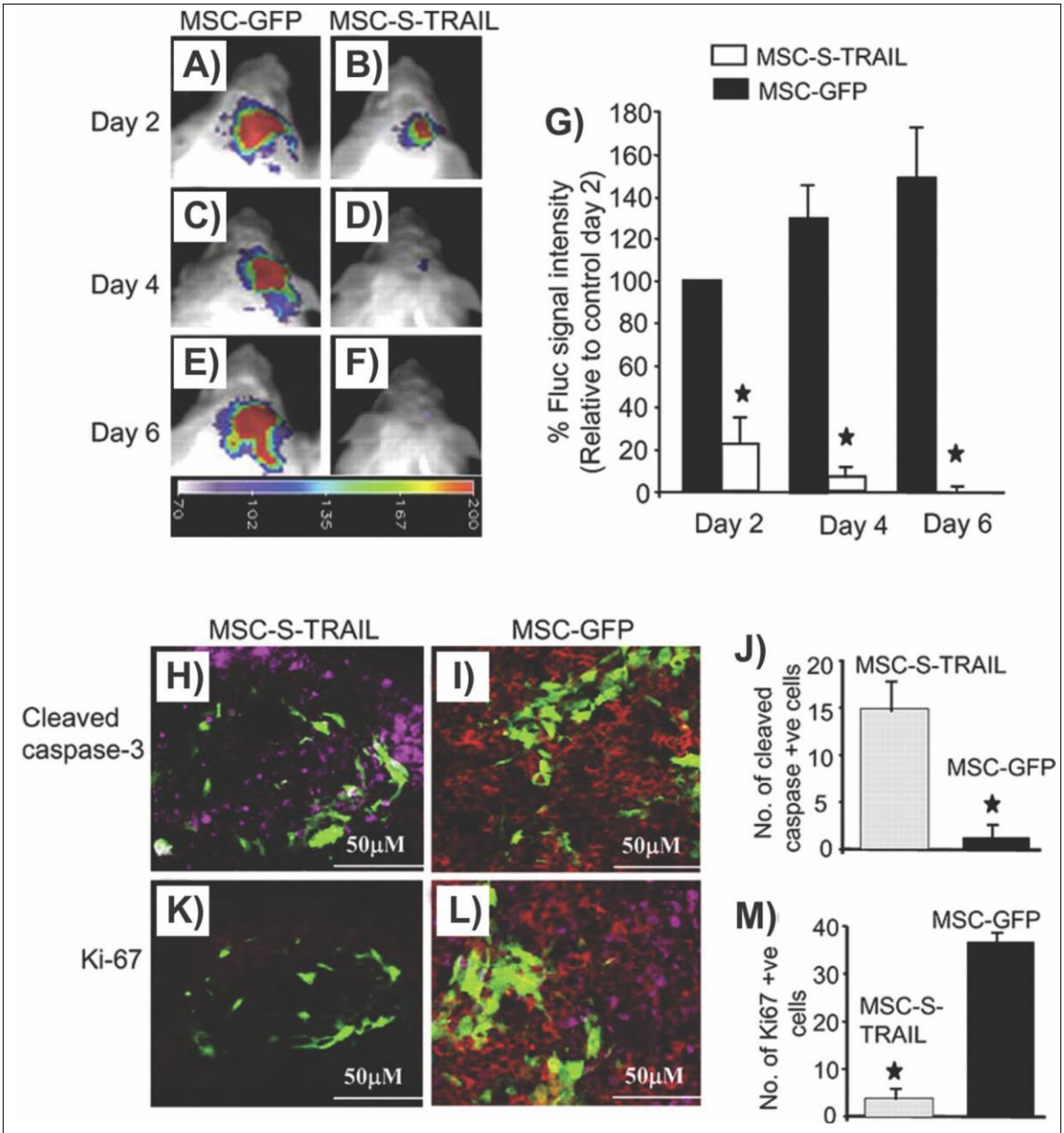

Figure 1.10 Mesenchymal Stem Cells Genetically Engineered to Secrete TRAIL to Enhance the Treatment of Glioma

A–F) Serial *in vivo* bioluminescence imaging of tumor growth following intracranial implantation of Gli36-EGFRvIII-FD glioma cells mixed with MSCs expressing S-TRAIL (MSC-S-TRAIL; B,D,F) or GFP (MSC-GFP; A,C,E). **G)** Relative mean bioluminescent signal intensities after quantification of *in vivo* images. **H–M)** Photomicrographs show the presence of cleaved caspase-3 (H) and Ki67-positive cells (K) in brain sections from MSCS-TRAIL-treated and control mice (I,L) 6 days after implantation. Plot shows the number of cleaved caspase-3 (J) and Ki67 (M) cells in MSC-S-TRAIL and MSC-GFP-treated tumors. (Green, MSCs; red, glioma cells; purple, Ki67 or cleaved caspase-3 expression). Reproduced with permission.[177] Copyright 2009, PNAS.

Besides direct effectors of cancer apoptosis, stem cells have also been engineered to express indirect effectors such as molecules that inhibit the formation of the tumor-associated vasculature (TSP1[179] or PEX) or immunomodulatory molecules (IL-12[180] and IL-18[181]). In addition, the delivery of growth factor inhibitors such as NK4 using MSCs has also been shown to significantly increase survival of mice in a lung metastasis model.[182] For instance, Kim *et al*. engineered HB1.F3 immortalized NSCs to produce PEX in order to inhibit angiogenesis for the treatment of glioma.[183] In particular, PEX is a naturally occurring fragment of human metalloproteinase-2 and acts as an inhibitor of glioma and endothelial cell proliferation, migration, and angiogenesis.[184] Following transfection of the NSCs with a plasmid for PEX via SuperFect (Qiagen) and *in vivo* injection, histologic analysis showed that engineered NSCs migrated to the tumor boundary and caused a 90% reduction of tumor volume. In particular, this reduction was associated with a significant decrease in angiogenesis (44.8%) and proliferation (23.6%), demonstrating the effectiveness of engineering NSCs to express PEX.

Immunomodulatory molecules such as IL-12 are also effective for the treatment of cancer. Typically, immunotherapies focus on utilizing our own immune systems or its components to attack cancer cells. In particular, the delivery of cytokines such as IL-12 has been shown to boost both the innate and adaptive immune response against tumors. However, cytokines such as IL-12 are hindered by poor *in vivo* distribution and are associated with serious and even life-threatening consequences as well as marginal clinical responses in most patients.[185] To improve this, MSCs were transduced with an adenovirus expressing IL-12 and the antitumor effect of these engineered MSCs, as injected via different routes, was evaluated in solid and metastatic melanoma.[186] As

expected, it was reported that the engineered MSCs were more efficient than adenovirus alone as a cytokine gene delivery vehicle. Moreover, when comparing intratumoral, subcutaneous, and intravenous injection of engineered MSCs, intratumoral injection was found to be the best approach to induce a strong tumor-specific T-cell response that correlated with anti-metastatic effects as well as the inhibition of solid tumor growth. Though, interestingly, intravenous injection of engineered MSCs actually induced earlier and higher peak levels of cytokines than other routes demonstrating that this is not an indicator of subsequent antitumor effects.

Secretion of Enzymes for the Conversion of Prodrugs

Prodrugs are another viable candidate for stem cell delivery. Prodrugs are compounds that are normally nontoxic. Instead, they are designed to respond to tumor specific enzymes, which then convert the prodrug into its toxic form.[187] Thus, prodrugs can provide a more targeted approach towards cancer therapy as greater concentrations of the cytotoxic form of the prodrug will be located at sites of cancer rather than in healthy tissues.[188] Moreover, prodrugs exhibit the bystander effect owing to the diffusion of the activated prodrug agent further enhancing the efficacy of the prodrug.[189] As such, three major suicide gene systems are currently used. Cytosine deaminase (CD) converts 5-fluorocytosine (5-FC) to the toxic antimetabolite 5-fluorouracil. The herpes simplex virus thymidine kinase (HSV-tk) converts ganciclovir (GCV) to GCV-monophosphate, which is further phosphorylated to GCV-triphosphate thereby potently blocking DNA synthesis. Finally, carboxylesterase (CE) converts the prodrug irinotecan (CPT-11) to the potent topoisomerase inhibitor SN-38.[190]

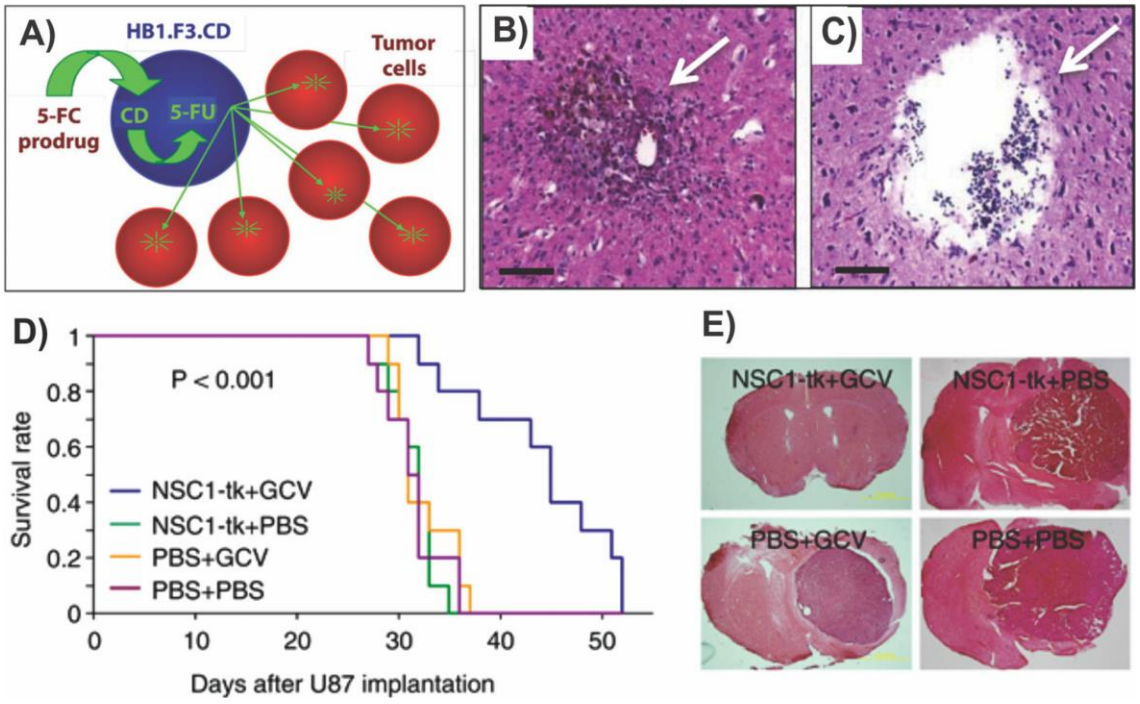

Figure 1.11 Engineering Stem Cells to Secrete Enzymes for the Conversion of Prodrugs
A) Diagram of CD-expressing NSCs localized to tumor cells, and CD conversion of 5-FC to 5-FU, which readily diffuses out of the NSCs to selectively kill the surrounding tumor cells. **B,C)** H&E-stained brain tumor sections from U251 glioma–bearing mice that received HB1.F3.CD NSCs only (B) or HB1.F3.CD NSCs in combination with 5-FC (C). White arrows indicate tumor region. Reproduced with permission.[191] Copyright 2013, Science. **D)** Brain injection of NSC1-tk cells coupled with GCV treatment prolonged the life of mice inoculated with U87 glioma cells. Statistical analysis was performed using the log rank test. **E)** Representative pictures of brain sections show the tumor size of different groups. NSC1-tk brain injection followed by GCV i.p. injection appears to shrink the tumor. Reproduced with permission.[192] Copyright 2012, Nature.

While promising, the efficacy of prodrugs can be further improved using stem cell-based delivery thereby enhancing targeting and infiltrating. Moreover, an added benefit of stem cell-mediated prodrug delivery is that the stem cells are eliminated after conversion of the prodrug, thereby abolishing any concern over its long-term fate. Using the CD–5-FC system, engineered MSCs and NSCs have been shown to effectively treat tumors of the brain.[192-193] [194] For instance, Aboody and colleagues engineered

immortalized NB1.F3 NSCs to express CD via a retroviral vector for the treatment of glioblastoma (**Figure 1.11A**).[191] They found that these engineered NSCs retained their tumor tropism following intracerebral injection even in orthotopic glioblastoma bearing mice pretreated with radiation or dexamethasone, which mimics clinically relevant adjuvant therapies. Importantly, it was reported that the average tumor volume was one-third that of the average volume in control mice **(Figure 1.11B and C**). Moreover, no toxicity associated with conversion of 5-fluorocytosine to 5-fluorouracil was detected and there was no evidence of tumorigenesis attributable to the NSCs. Similarly, Wang and coworkers also engineered NB1-F3 cells to express CD and demonstrated their ability to target and disseminate therapeutic agent to medulloblastoma thereby resulting in a 76% reduction of tumor volume compared to unengineered controls.[195]

On the other hand, the HSV-tk system, which relies on the formation of gap junctions between the stem cell and surrounding target cells for an efficient bystander effect using the prodrug GCV, has shown efficacy in several cancer models including those of the brain, breast, and prostate.[196] For example, Yang and colleagues engineered iPSC-derived NSCs using recombinant baculovirus vectors containing the herpes HSV-tk gene expression cassette to treat metastatic breast cancer.[192,197] In particular, they demonstrated that after tail vein injection, the engineered iPSC-derived NSCs displayed robust migratory capacity even outside the CNS in both immunodeficient and immunocompetent mice and homed in on established orthotopic 4T1 mouse mammary tumors. Moreover, the engineered iPSC-derived NSCs were able to effectively inhibit the growth of orthotopic 4T1 breast tumors as well as the metastatic spread of the cancer

cells, leading to prolonged survival of the tumor-bearing mice (median survival of 39 days, which was significantly greater than controls) (**Figure 1.11D and E**).

Finally, NSCs engineered using the CE–CPT-11 system have proven to be effective in the treatment of preclinical models of brain, lung, and ovarian cancers.[198] For instance, Kim *et al.* engineered immortalized HB1.F3 NSCs to express CE using a retroviral vector to enhance the treatment of ovarian cancer.[195,199] In this study, the authors reported that the engineered NSCs retained their ability to migrate to ovarian tumors and greatly inhibited cancer cell proliferation. Interestingly, the authors compared engineered stem cells using the CD-5-FC system to engineered NSCs expressing CE for the CE-CPT-11 system and found that the CE approach seems to be more promising than the CD approach because the CE approach decreased proliferation with a lower engineered NSC cell number and at a lower concentration of CPT-11 when compared to the concentration of cells and prodrug needed for the CD approach.

1.4. Overview of the Dissertation

Overall, it has been demonstrated that MNPs hold tremendous potential for various biomedical applications, including cancer diagnosis and treatment, owing to their unique ability to interact with and be manipulated by magnetic fields. In particular, cancer applications of MNPs have primarily focused on their use as MRI contrast agents, drug delivery vehicles, and as agents for the induction of magnetic hyperthermia. From the onset of this thesis, I was highly interested in utilizing the multifunctionalities of MNPs to overcome the two major problems with cancer therapy – namely, chemoresistance and the lack of tumor targeting. For this purpose, I have developed two

orthogonal approaches that utilize the multifunctional properties of MNPs to overcome these challenges. Specifically, I focused on the development and advancement of novel MNP-based combination therapies, wherein MNPs are used for the dual purpose of not only acting as a delivery vehicle but also as an agent for magnetic hyperthermia.

In the first half of this thesis, novel MNP and magnetic core-shell nanoparticle (MCNP)-based combination therapies are developed to enhance the treatment of cancer by sensitizing cancer cells to subsequent therapies. In particular, MNPs are first developed for the dual purpose of delivering microRNA and inducing magnetic hyperthermia for the treatment of brain cancer. We demonstrate that the combination of lethal-7a microRNA (let-7a), which targets a number of survival pathways, can sensitize cancer cells to subsequent magnetic hyperthermia. Moreover, we demonstrate the use of MCNPs that are composed of a magnetic core and a mesoporous silica shell for the simultaneous delivery of let-7a and doxorubicin, wherein let-7a was found to sensitize breast cancer cells to subsequent chemotherapy.

In the second half of this thesis, we develop a stem cell-based gene therapy to take advantage of the innate ability of stem cells to target cancers. For this purpose, MCNPs are reported for the dual purpose of delivering and activating a heat-inducible gene vector that encodes TNF-related apoptosis-inducing ligand (TRAIL) in adipose-derived mesenchymal stem cells (AD-MSCs) for the treatment of cancer. These engineered AD-MSCs were observed to retain their innate ability to proliferate, differentiate, and home to tumors, making them ideal cellular carriers for cancer therapy. Moreover, mild magnetic hyperthermia resulted in the selective expression of TRAIL in the engineered AD-MSCs

and, as such, induced significant ovarian cancer cell death highlighting the robustness of our remotely-controlled stem cell-based gene therapy.

Overall, this thesis demonstrates two multifunctional MNP-based approaches for cancer therapy: 1) combined MNP-based delivery of microRNA and magnetic hyperthermia to sensitize cancers to subsequent chemotherapy and 2) MNP-based activation of heat-inducible genes in stem cells for the targeted treatment of cancer.

Chapter 2 :

Combined Magnetic Nanoparticle-Based microRNA and Hyperthermia Therapy to Enhance the Treatment of Cancer

The text and images used in this chapter have been previously published, at least in part, in Small as an original manuscript (Yin PT, Shah BP, Lee KB. Small, 2014. 10(20): p. 4106-12.) and Perry Yin was the first author.

2.1. Introduction

In recent years, mild hyperthermia (40-45°C) has been increasingly investigated as an adjuvant that can effectively sensitize tumors to chemotherapy and radiotherapy as well as induce apoptosis.[200] In particular, magnetic hyperthermia, wherein the exposure of magnetic nanoparticles (MNPs) to an alternating magnetic field (AMF) results in the induction of hyperthermia via Neel and Brownian relaxation, represents a novel and attractive approach that can overcome the technical challenges that exist with other methods used to induce hyperthermia – mainly the difficulty of actually achieving the intended therapeutic temperature in the tumor region while sparing surrounding healthy tissue. As such, by delivering the MNPs explicitly to the tumor either through intratumoral or targeted intravenal injection, a highly localized hyperthermia can be achieved for the selective heating of tumors while sparing the surrounding healthy tissues.[201]

In terms of its molecular mechanism of action, the treatment of a tumor with magnetic hyperthermia results in the synthesis of heat shock proteins (HSPs), which can

subsequently beget an anti-tumor immune response. For example, following the induction of magnetic hyperthermia in sarcoma-bearing mice, HSPs are typically expressed on the surface of malignant cells but not on normal cells.[202] As a result, these HSP-expressing malignant cells are more susceptible to lysis by natural killer effector cells. However, it is also a well-known fact that the fundamental function of HSPs is to protect cellular proteins from degradation. Moreover, HSPs have been shown to promote cell survival and inhibit apoptosis (**Figure 2.1**).[203] As such, HSP expression resulting from magnetic hyperthermia actually hinders MNP-mediated cell death. For instance, it has been demonstrated that the activation of HSPs preserves tumor cell viability and can impart tumor cells with resistance to chemotherapy and radiotherapy.[204] These effects occur through numerous signaling pathways that are involved in therapeutic resistance including the activation of DNA repair mechanisms (via the BRCA family),[205] the regulation of apoptosis (via the Akt/PI3K pathway),[206] and the modulation of p53 function, which has been shown to hold true for a broad range of neoplastic tissues.[206a,207]

As a result, a number of therapeutics are currently being investigated for their ability to target HSP-related pathways. For example, the proteasome inhibitor, bortezimab, targets the NF-kB pathway, which is in part regulated by HSP70 and HSP90.[208] There are also agents directed at the HSP90 and mTOR/HIF pathways, including the inhibitor geldanamycin.[209] For instance, Yoo *et al.* developed resistance-free apoptosis-inducing magnetic nanoparticles (RAIN) composed of MNPs that release geldanamycin to inhibit HSP90 and induce magnetic hyperthermia upon exposure to an AMF.[210] While promising, each individual of the HSP family (e.g. HSP27, HSP70, HSP72, HSP90) has numerous subsequent targets whose pathways have significant

degeneracy.[207b] Therefore, to maximize the therapeutic potential of magnetic hyperthermia for the treatment of cancer, there is a clear need to simultaneously target the multiple key downstream effectors of HSPs that promote cell survival and inhibit apoptosis following treatment.

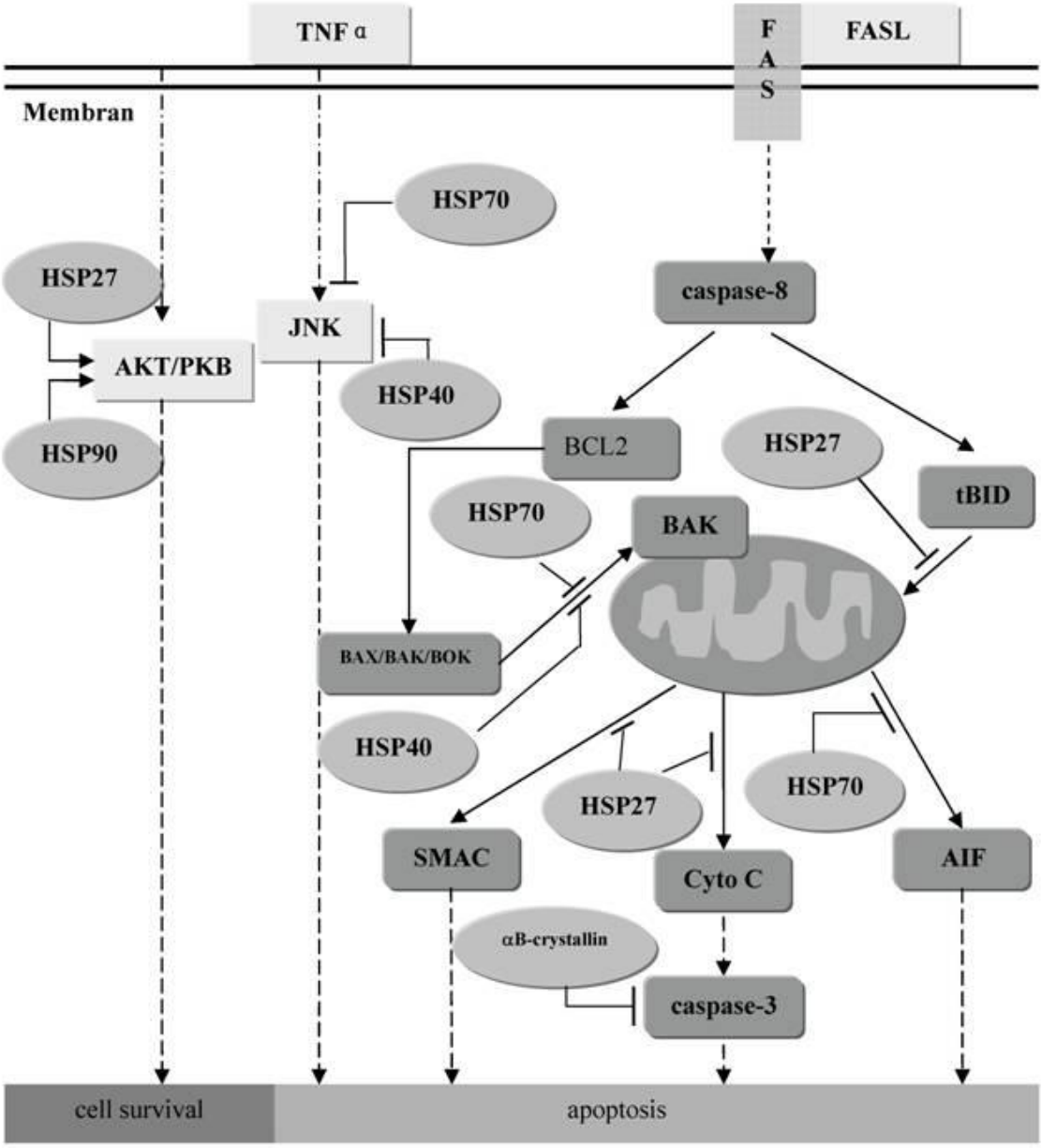

Figure 2.1. Heat Shock Protein Pathway
The heat shock protein family acts to promote cell survival and inhibit apoptosis. Reproduced with permission.[203] 2007, Ivyspring International Publisher.

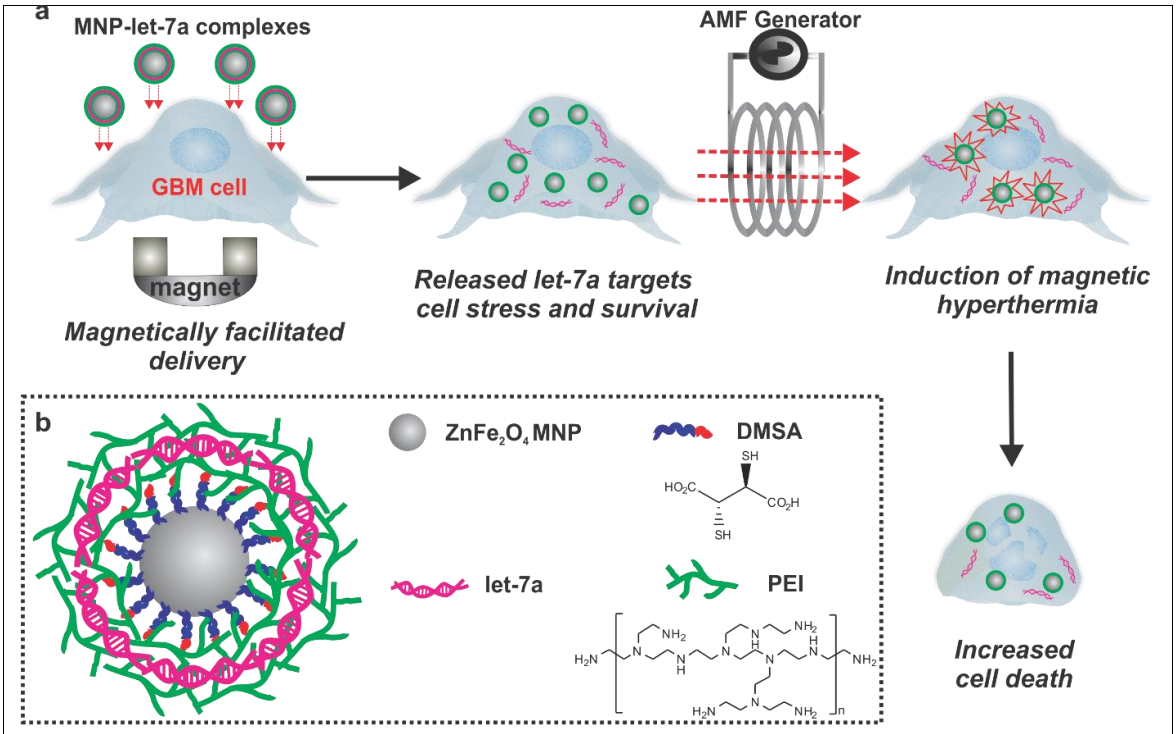

Figure 2.2 Magnetic Nanoparticle-Based microRNA and Hyperthermia Therapy to Enhance the Treatment of Brain Cancer
A) MNP complexes are first delivered to GBM cells, which is enhanced by magnetofection. Once inside the cell, let-7a miRNA is released thereby targeting downstream effectors of HSPs. This sensitizes the cancer cells to subsequent magnetic hyperthermia enhancing apoptosis. **B)** MNPs will be complexed with let-7a miRNA using 10 kDa branched PEI via a layer-by-layer approach.

In this chapter, we report the novel application of highly magnetic zinc-doped iron oxide nanoparticles ($ZnFe_2O_4$) for the dual purpose of delivering a microRNA (miRNA) that targets multiple downstream pathways modulated by HSPs and inducing magnetic hyperthermia to enhance the treatment of cancer cells (**Figure 2.2**). Specifically, in this study, glioblastoma multiforme (GBM) brain cancer cells were used as a model system. miRNAs are small endogenous noncoding RNA molecules that interact with target messenger RNAs (mRNAs) to down-regulate or inhibit translation.[211] The function of miRNAs in cancer formation and treatment is well established.[212] However, the unique feature that makes miRNA particularly suitable to be combined with magnetic

hyperthermia is their ability to have multiple, possibly hundreds of, targets.[213] Moreover, these targets are often on the same or similar pathways. Therefore, the delivery of a single miRNA can potentially have a greater, more cumulative effect on HSPs and their downstream effectors than delivering other types of therapeutic molecules such as small interfering RNA (siRNA) molecules or drugs, which can only modulate single HSP-related targets.[214] To this end, we are interested in delivering lethal-7a miRNA (let-7a), which is known to be a tumor suppressor that inhibits malignant growth by targeting factors such as the BRCA family,[215] RAS,[216] IGF1R,[217] HMGA2,[217] and c-Myc,[218] which overlap with a number of key downstream effectors of HSPs (**Figure 2.3**).[219] Moreover, let-7a has been reported to be down-regulated in a number of cancer types including cancers of the lung,[220] prostate,[221] breast,[222] and brain, where let-7a is decreased by over 3-fold compared to healthy surrounding tissue.[223] As such, we hypothesized that the MNP-mediated delivery of let-7a should act synergistically with magnetic hyperthermia to enhance hyperthermia-mediated apoptosis by targeting multiple key HSP-related pathways including DNA repair and cell survival (via IGF1R and RAS) mechanisms. Please note that the materials, images, and text that are used in this chapter have been published, at least in part, in Small as an original manuscript.[149]

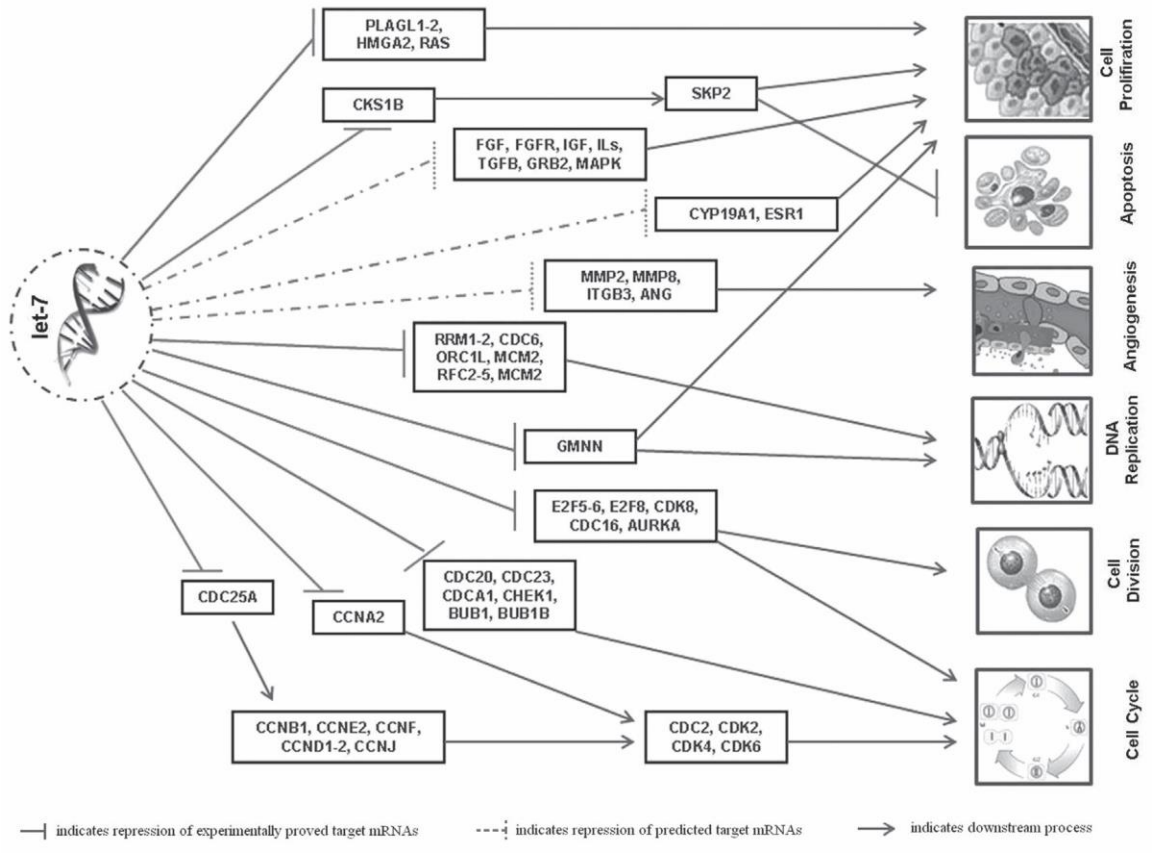

Figure 2.3 let-7 Targets
Let-7 targets a number of pathways in cancer and stem cell biology. All together, let-7 targets cell proliferation, apoptosis, angiogenesis, DNA republication, cell division, and cell cycle. Reproduced with permission.[224] 2010, Multimed.

2.2. Results and Discussion

2.2.1. Synthesis and Characterization of Magnetic Nanoparticles

For the MNP-based combined miRNA and magnetic hyperthermia therapy, we utilized zinc doped iron oxide ($ZnFe_2O_4$) nanoparticles. These MNPs have previously been shown to have a significantly higher magnetic susceptibility and hence, can afford improved magnetic properties while requiring a much lower dose when compared to conventional Fe_2O_3 or Fe_3O_4 nanoparticles.[29] As such, we first synthesized $ZnFe_2O_4$ MNPs with a doping percentage of $(Zn_{0.4}Fe_{0.6})Fe_2O_4$ via the thermal decomposition of a

mixture of metal precursors (zinc chloride, ferrous chloride, and ferric acetylacetonate) in the presence of oleic acid using a previously reported protocol that was modified by our group.[29,67] The resulting highly monodisperse and hydrophobic $ZnFe_2O_4$ MNPs were then made water-soluble via ligand exchange with 2, 3-dimercaptosuccinic acid (DMSA).[225]

Transmission electron microscopy (TEM) analysis revealed that the overall diameter of the $ZnFe_2O_4$ MNPs was 22.92 ± 3.7 nm (**Figure 2.4**). A high-resolution TEM image shows the monocrystalline structure of the MNPs with a lattice fringe that was measured to be 0.296 nm (**Inset of Figure 2.4**), which is characteristic of the (220) planes of the spinel and is in agreement with previous reports.[112,113] In terms of the water soluble MNPs, it was found that the DMSA coated MNPs had a hydrodynamic size of 30.1 ± 2.8 nm (polydispersity index [PDI] = 0.192) as measured by dynamic light scattering (DLS) and a zeta potential of -23.3 ± 1.3 mV. Moreover, with regard to their magnetic properties, the MNPs were characterized by a specific absorption rate (SAR) of 341 W/g, which was determined using an AMF with an amplitude of 5 kA/m and a frequency of 225 kHz. This SAR is consistent with data reported in the literature for similar $ZnFe_2O_4$ MNPs.[226] In comparison, we found that conventional Fe_3O_4 MNPs (7 nm diameter) have a SAR of 28.46 W/g, which is also in agreement with values that have been reported (10-40 W/g).[227] As such, our monodisperse water soluble $ZnFe_2O_4$MNPs are characterized by expectedly superior magnetic properties thereby allowing for the use of significantly lower doses when compared to conventional MNPs.

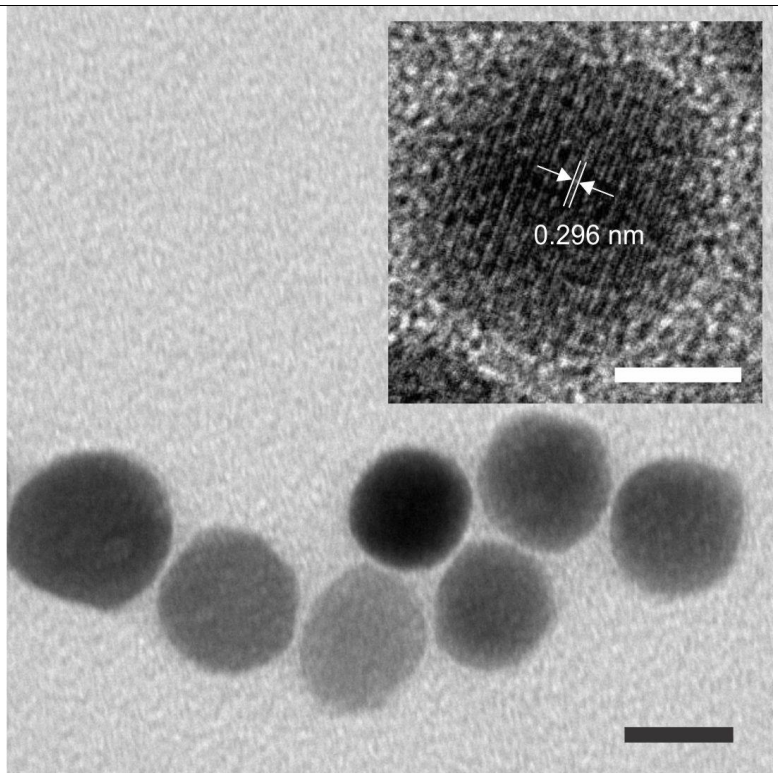

Figure 2.4 Transmission Electron Micrographs of the MNPs
TEM micrograph of the MNPs (scale bar = 20 nm). Inset: High resolution TEM micrograph of the MNPs showing the lattice fringes (scale bar = 10 nm).

2.2.2. Efficient microRNA Delivery Using Magnetic Nanoparticles

To prepare the aforementioned $ZnFe_2O_4$ MNPs for miRNA delivery, the negatively charged water-soluble MNPs were coated with a 10 kDa branched cationic polymer, polyethyleneimine (PEI), which affords the MNPs with an overall positive charge. PEI is a polymer that is partially protonated under physiological conditions, thus allowing for the formation of complexes in the presence of nucleic acids.[228] PEIs have been used extensively to deliver plasmids and other DNA and RNA molecules including siRNA and miRNA.[228-229] Specifically, it has been demonstrated that PEI complexes are uptaken into the cell through caveolae- or clathrin-dependent routes and are able to facilitate release from the endosome with high efficiency via the "proton sponge

effect."[230] Moreover, previous studies have shown that a direct relationship exists between the molecular weight of PEI and cytotoxicity.[231] Therefore, to minimize cytotoxicity while maximizing transfection efficiency we used 10 kDa branched PEI (**Figure 2.5A**). In particular, to deliver miRNAs efficiently using our MNPs, we developed a two-step layer-by-layer process (**Figure 2.5B**). First, the PEI-coated MNPs (1 μg/mL) were incubated with miRNA in an 80 mM NaCl solution to minimize the size of the complex. Afterwards, an outer coat of PEI was added to provide additional protection for the miRNA as well as to facilitate cell uptake and endosomal escape. We observed that the size of the MNP complexes increased to a final diameter of 76.91 ± 11 nm (PDI = 0.242) for the layer-by-layer MNP-PEI/miRNA/PEI complex and had a positive zeta potential of +23.7 ± 1.7 mV. Moreover, a reversal of the zeta potential was observed after the deposition of each layer (**Figure 2.5B**). A more detailed description of the optimization process can be found in the Materials and Methods section (**Figure 2.5**).

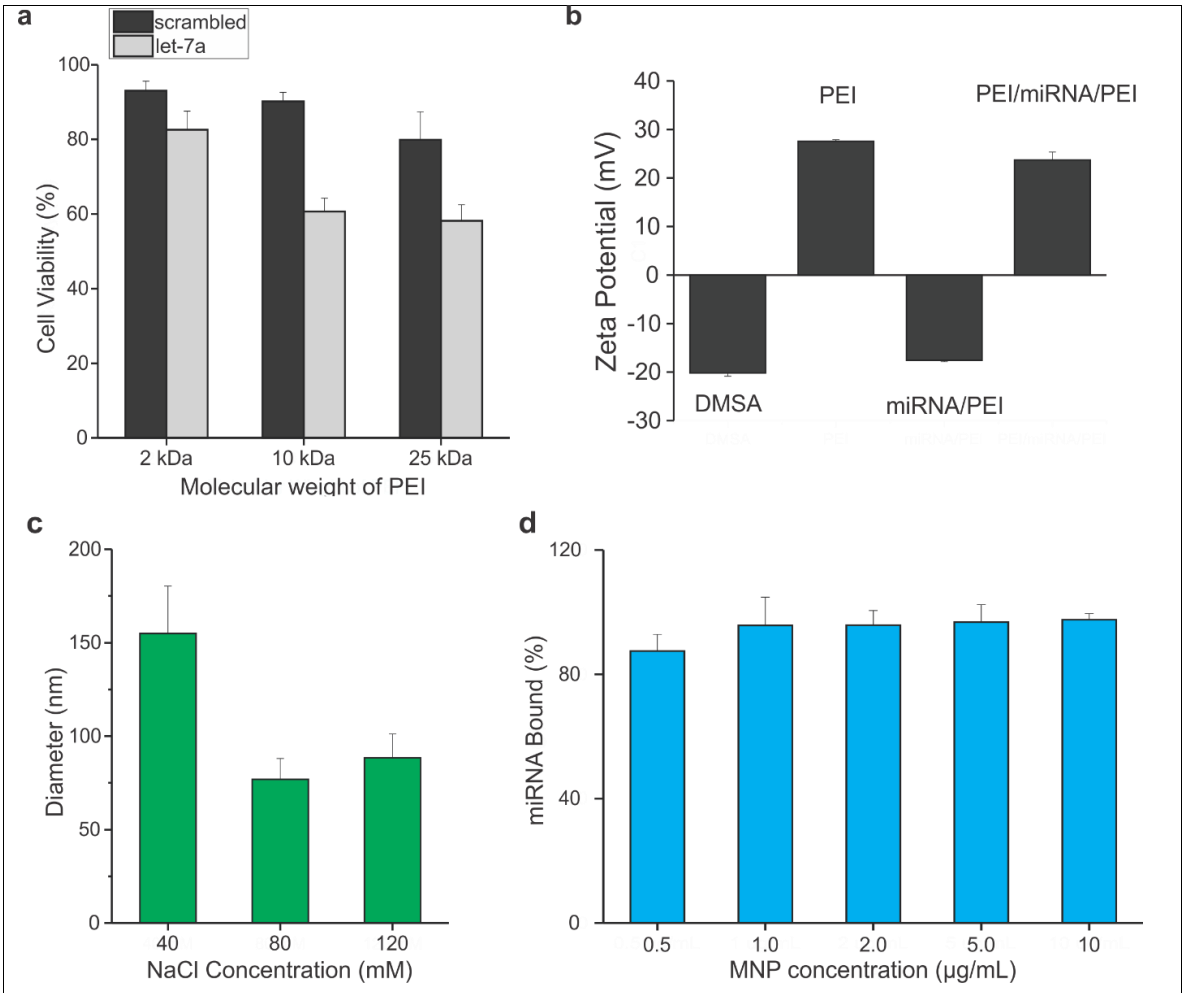

Figure 2.5 Optimization of Magnetic Nanoparticle Complex Formation
A) To determine the optimal molecular weight of PEI for miRNA delivery, we coated out MNPs with 2 kDa, 10 kDa, and 25 kDa, following the same protocol. We found that while 2 kDa PEI coated MNPs had the lowest cytotoxicity, 10 kDa had a significantly higher transfection efficiency. **B)** A reversal in the zeta potential is observed after the addition of each layer. **C)** To determine the NaCl concentration that should be used in the solution during complexing, 3 different NaCl concentrations were tested. Afterwards, the overall diameter of the complexes was measured using DLS. The results demonstrate that 80 mM NaCl solution worked best for layer-by-layer complex formation. **D)** To determine the minimum concentration of MNP that was needed to bind 100% of the miRNA, a PicoGreen dye was used. It was found that 1 µg/mL MNP was sufficient to bind nearly 100% of the miRNA.

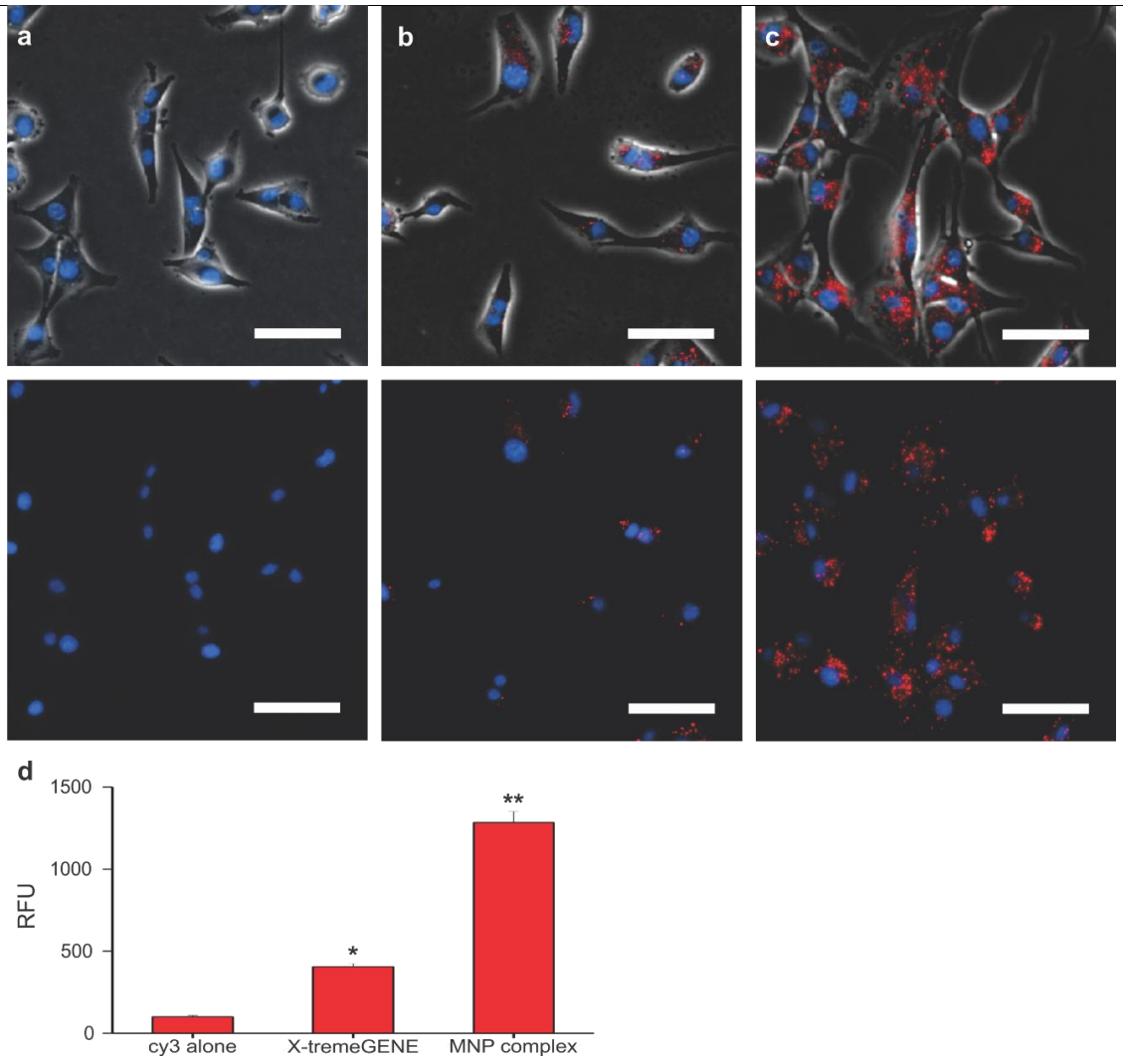

Figure 2.6. Cell Uptake of Magnetic Nanoparticles Complexes
A) U87-EGFRvIII GBM cells do not uptake Cy3-labeled scrambled miRNA (100 nM) in the absence of transfection agents. **B)** Uptake of Cy3-labeled scrambled miRNA after transfection using a commercially available transfection agent (e.g. X-tremeGENE) following the manufacturer's protocol. **C)** GBM cells readily uptake MNPs complexed with 100 nM Cy3-labeled scrambled miRNA (scale bar = 50 μm). Blue = Hoechst stained nuclei, red = cy3-labeled scrambled miRNA. Top image in each column represents phase merged with the fluorescence images. **D)** Quantification of the fluorescence intensity illustrates that miRNA uptake is significantly greater for MNP-based delivery compared to Cy3 alone or X-tremeGENE mediated transfection (*$p < 0.05$, **$p < 0.01$).

To assess the efficiency of cellular uptake, we performed fluorescence microscopy on GBM cells (U87-EGFRvIII) that were transfected with MNP-

PEI/miRNA/PEI complexes (**Figure 2.6**). In this case, the MNP complexes were assembled using 100 nM Cy3-labeled scrambled precursor miRNA (Ambion) and delivery was enhanced by magnetofection, a well-established method that allows for the rapid accumulation of MNPs and their payloads upon exposure to an external magnetic field.[67,232] Twenty-four hours after transfection, we visualized and quantified the efficiency of uptake (Cy3 positive cells divided by the total number of cells). We found that the GBM cells were able to efficiently uptake the MNP-PEI/Cy3-miRNA/PEI complexes without the use of transfection agents or active uptake methods such as electroporation (98% efficiency). Moreover, compared to commercially available transfection agents (X-tremeGENE®), the fluorescence intensity of Cy3-miRNA uptaken after magnetofection using our layer-by-layer MNP complexes was significantly greater (**Figure 2.6**).

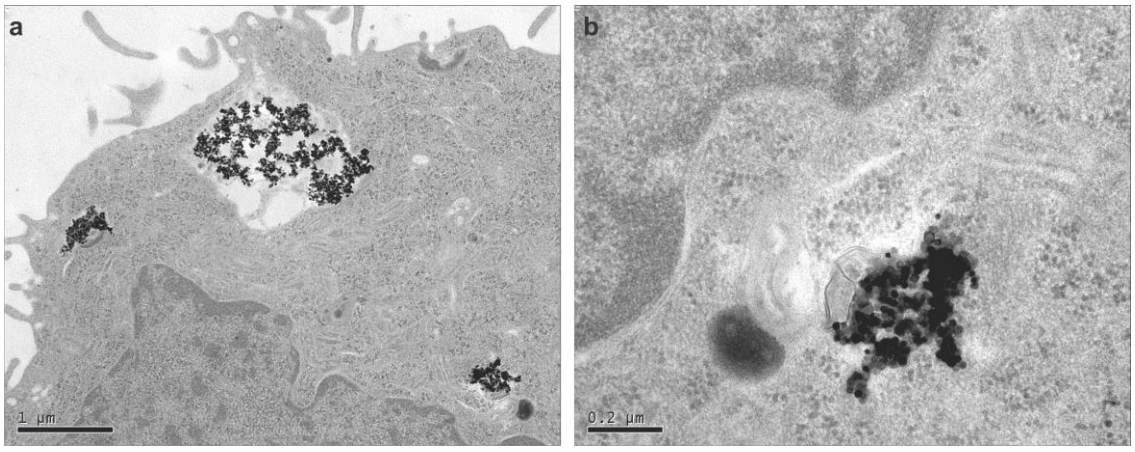

Figure 2.7 Cell Uptake of MNPs
A) A cross-sectional TEM micrograph of a GBM cell further confirms that MNP complexes (black clusters) are able to enter the cell (scale bar = 1 µm). **B)** MNP complexes at higher magnification (scale bar = 0.2 µm).

To further confirm MNP uptake, cross-sectional cellular images were obtained using TEM (**Figure 2.7**). Specifically, TEM confirms that MNPs were successfully

endocytosed and were able to enter the cell. Finally, in contrast to other cationic transfection methods, which can result in severe damage to cell membranes resulting in low cell viabilities,[233] the MNP complexes and the process of magnetofection caused little to no cell death (92% cell viability) owing to the much lower concentration and shorter time of incubation that is necessary. As such, this demonstrates that these complexes can be used for extended incubation and downstream applications such as magnetic hyperthermia or imaging (**Figure 2.8**).

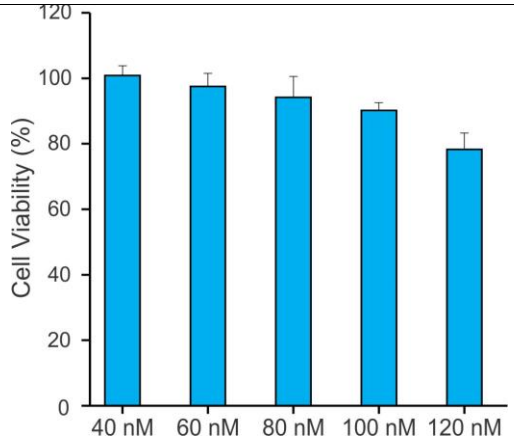

Figure 2.8 Biocompatibility of the MNP complexes
MNP-PEI/scrambled miRNA/PEI were delivered to U87-EGFRvIII GBM cells in increasing concentrations and delivery was enhanced using magnetofection (10 min). The MNP complexes are well tolerated by the cells as determined via MTS assay 48 hours after transfection.

2.2.3. Magnetic Nanoparticle-Mediated Delivery of let-7a microRNA to Brain Cancer Cells

miRNAs are small 20-24 nucleotide long RNAs, each of which has the potential to post-transcriptionally down-regulate a specific set of target genes. As mentioned previously, let-7a is known to target a number of genes involved in cell survival (PI3K via IGF1R),[206c,d] proliferation (RAS, HMGA2),[216-217] DNA repair (BRCA1, BRCA2),[215] and cell cycle (AURKA, CDK4) (**Figure 2.9A**).[215] However, this has not been confirmed

in GBM cells. To confirm this in GBM, we first delivered 70-nucleotide precursor let-7a miRNA (100 nM) to U87-EGFRvIII GBM cells using our optimized MNP-based delivery conditions and quantified the mRNA expression levels of selected let-7a targets, as it has been reported that mammalian miRNAs primarily regulate target genes by decreasing mRNA levels.[234] Specifically, using quantitative PCR (qPCR) measurements made from total RNA, we observed at least 40% down-regulation ($p < 0.05$) of all target gene transcripts (KRAS, NRAS, c-MYC, and IGF1R) relative to U87-EGFRvIII cells treated with scrambled miRNA (100 nM) as delivered by our MNPs (**Figure 2.9B**). This is also supported by Lee *et al.*, who reported that let-7 can inhibit proliferation in GBM cells (e.g. U251 and U87) via the down regulation of NRAS and KRAS.[235] These results not only confirm that let-7a targets the desired genes in GBM cells but also that the function and target-specificity of let-7a is retained upon cellular uptake/endosomal escape.

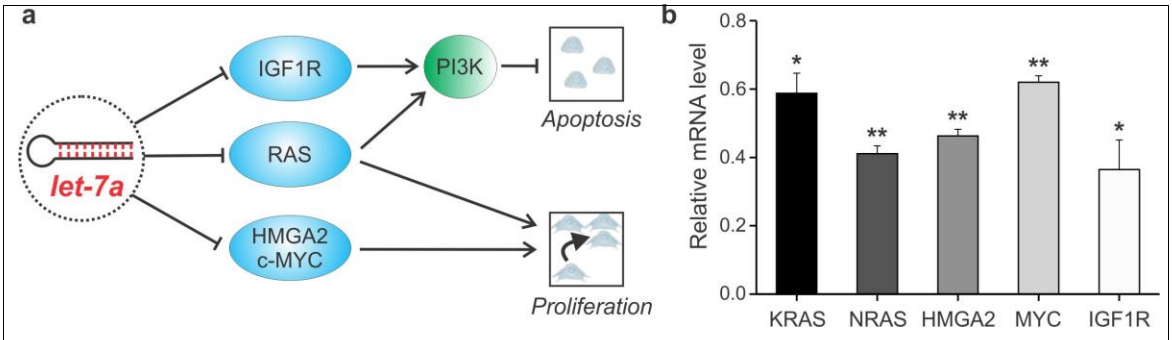

Figure 2.9 let-7a Targets in GBM
A) The delivery of let-7a can inhibit targets such as IGF1R, RAS, HMGA2, and c-MYC, which typically promote proliferation and cell survival while inhibiting apoptosis. **B)** The delivery of let-7a to U87-EGFRvIII GBM cells significantly down-regulates expected targets of let-7a compared to scrambled miRNA controls as determined by qPCR (*$p < 0.05$, **$p < 0.01$).

Next, to induce apoptosis and evaluate the therapeutic potential of let-7a, we modulated intracellular levels of this miRNA. Transient transfection of let-7a using our

MNPs resulted in a significant decrease in the viability of GBM cells. Specifically, we observed that 48 hours after the MNP-mediated delivery of let-7a, GBM cell viability decreased significantly compared to scrambled miRNA controls in a dose-dependent fashion (**Figure 2.10A**). Using 100 nM miRNA as the optimal concentration for the remainder of the studies, apoptosis levels in the GBM cells were evaluated using Annexin-V/propidium iodide staining and qPCR of caspase-3 expression. In particular, FACS analysis of Annexin-V/propidium iodide stained cells demonstrated that significantly more cells underwent apoptosis after treatment with let-7a (**Figure 2.10B**) compared to scrambled miRNA controls. Similarly, the expression of caspase-3 was up regulated by 30% ($p < 0.05$) after treatment with let-7a as compared to scrambled miRNA control (**Figure 2.10C**).

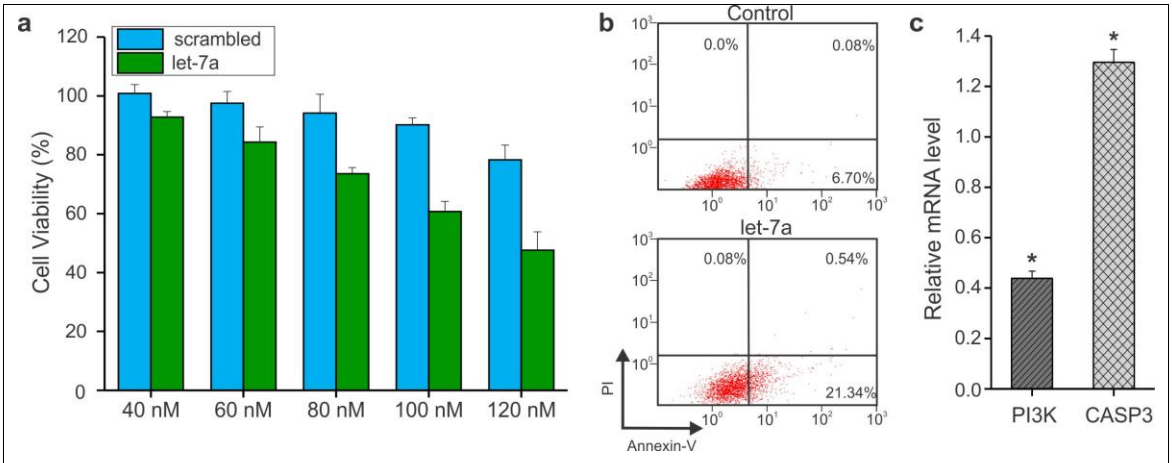

Figure 2.10 MNP-Based let-7a Delivery
A) Cell viability as quantified by MTS assay 48 hours after initial transfection with let-7a. Samples were normalized to untreated controls. **B)** FACS analysis of Annexin-V and propidium iodide stained cells. **C)** qPCR of downstream targets of let-7a compared to scrambled miRNA controls (*$p < 0.05$).

In terms of the effect that let-7a delivery has on key signaling pathways, we observed that the delivery of let-7a to GBM cells resulted in a significant decrease in the

expression of PI3K (56% decrease, $p < 0.05$), which typically promotes cell survival and inhibits apoptosis.[236] As PI3K is downstream of let-7a targets including RAS and IGF1R (**Figure 2.9A**),[237] this result suggests that let-7a induces apoptosis in GBM cells via the targeting of RAS and IGF1R. Finally, we investigated the efficacy of let-7a delivery to other GBM cell lines (U87-WT, U87-EGFR) as well as normal brain cells (astrocytes) (**Figure 2.11**). We found that let-7a appears to be most effective in U87-EGFRvIII cells compared to U87-WT and U87-EGFR cells possibly because the U87-EGFRvIII cell line overexpresses EGFRvIII, which is upstream of PI3K and is targeted by let-7a.[217] Moreover, we observed that let-7a does not induce cytotoxicity in normal brain cells (astrocytes), which is expected as non-cancer cells should have much higher endogenous levels of let-7a compared to brain cancer cells.[223] Taken together, these studies indicate that not only does let-7a retain its functionality after delivery using MNPs but it also exhibits significant toxicity in GBM cells while sparing normal cells.

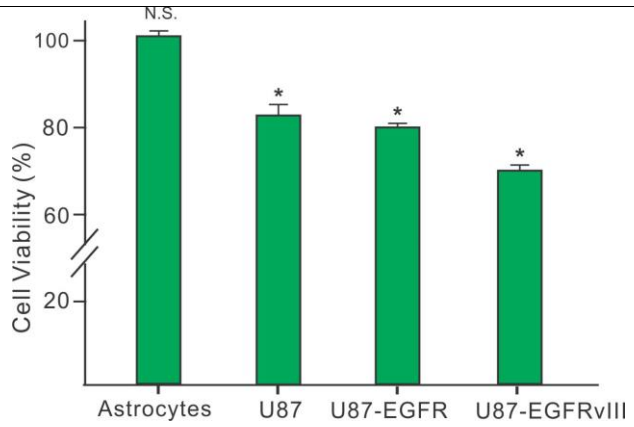

Figure 2.11 Efficacy of let-7a Delivery to Other GBM Cell Lines
Cell viability of normal and glioblastoma multiforme cell lines after the delivery of let-7a using magnetic nanoparticles. let-7a appears to be most effective in U87-EGFRvIII cells compared to U87-WT and U87-EGFR cells. Moreover, let-7a does not induce cytotoxicity in normal brain cells (astrocytes) as astrocytes have much higher endogenous levels of let-7a compared to brain cancer cells. Each result is normalized to the MNP-based delivery of scrambled miRNA to each respective cell line (N.S. = no significance, $*p < 0.05$).

2.2.4. Induction of Magnetic Hyperthermia Using Magnetic Nanoparticles

In terms of their magnetic properties, the MNPs were characterized by a specific absorption rate (SAR) of 341 W/g, which was determined using a magnetic field with a 5 kA/m amplitude and a frequency of 225 kHz. Considering that the SAR value depends on the amplitude and frequency of the magnetic field as well as the structure (e.g. size and shape) and magnetic properties of the MNPs used, the SAR determined for the $ZnFe_2O_4$ MNPs used in this study is consistent with data reported in the literature for similar $ZnFe_2O_4$ MNPs.[226] In comparison, we found that conventional Fe_3O_4 MNPs (7 nm diameter) have a SAR of 28.46 W/g, which is also in agreement with values that have been reported (10-40 W/g).[227] As such, our monodisperse water soluble $ZnFe_2O_4$ MNPs are characterized by expectedly superior magnetic properties thereby allowing for the use of significantly lower doses when compared to conventional MNPs.

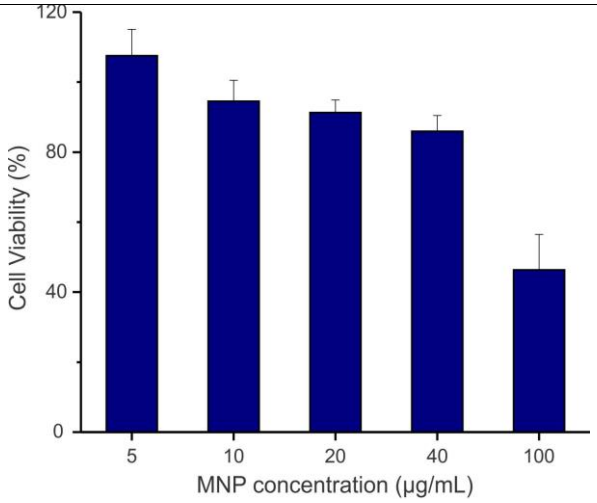

Figure 2.12 Magnetic Nanoparticle Biocompatibility
Cell viability measured using MTS 48 hours after the delivery of increasing concentrations of MNPs. Note: 10 μg/mL was used for magnetic hyperthermia.

To evaluate the ability of our MNP complexes to induce magnetic hyperthermia, we delivered MNP-PEI (10 μg/mL, **Figure 2.12**) to U87-EGFRvIII cells. Twenty-four hours after treatment, the MNP-PEI transfected cells were trypsinized and exposed to an AMF (5 kA/m, 225 kHz). We found that the therapeutic effect of magnetic hyperthermia was dose-dependent with the lowest cell viability (63.14%) being achieved after 45 minutes of exposure to an AMF (**Figure 2.13A**). Moreover, an increase in the level of apoptosis was observed as quantified via Annexin-V/PI staining (**Figure 2.13B**) and the mRNA expression level of caspase-3 (2 fold increase) when compared to control cells transfected with MNPs but not exposed to an AMF (**Figure 2.13C**). Finally, to determine the approximate temperature that was achieved at this MNP concentration, we monitored the temperature of the solution containing GBM cells that had been transfected with 10 μg/mL of MNPs using a fiber optic temperature probe. We observed that after 45 minutes of exposure to an AMF, an approximate temperature of 44.1°C was reached (**Figure 2.13D**).

To study the effect that hyperthermia has on the expression of HSPs and the activation of their downstream effectors, we confirmed that magnetic hyperthermia significantly increases the expression of HSPs including HSP70 (4.1 fold, $p < 0.005$), HSP72 (5.4 fold, $p < 0.001$), and HSP90 (2.9 fold, $p < 0.05$), which have all been implicated in cancer progression and chemoresistance (**Figure 2.13C**).[238] Moreover, downstream effectors of these HSPs such as IGF1R, RAS, and PI3K, which are well-known to inhibit apoptosis and promote cell survival, are also significantly activated ($p < 0.01$) when compared to controls that have not been exposed to magnetic hyperthermia (**Figure 2.13E**). As such, while MNP-mediated magnetic hyperthermia does induce

significant toxicity in GBM cells, the activation of pathways that promote cell survival and inhibit apoptosis is also apparent suggesting that the inhibition of these multiple key downstream effectors can potentially improve the therapeutic effects of MNP-mediated magnetic hyperthermia.

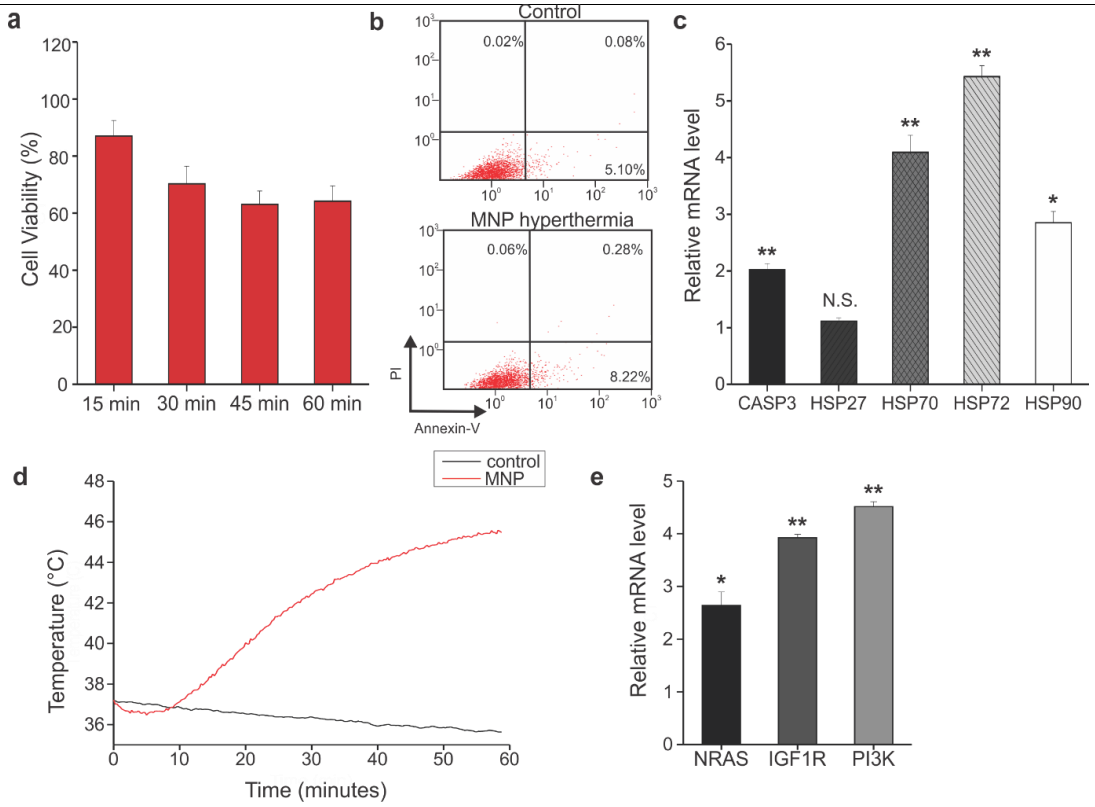

Figure 2.13 Magnetic Nanoparticle-Based Magnetic Hyperthermia.
A) MTS assay following the induction of magnetic hyperthermia (10 µg/mL MNP) in U87-EGFRvIII GBM cells. Conditions were assayed 48 hours after transfection and normalized to MNP controls (without exposure to AMF). **B)** FACS analysis of Annexin-V and propidium iodide stained cells with and without treatment. **C)** qPCR illustrates that, following magnetic hyperthermia, caspase-3 is significantly up regulated as are HSPs. Results were normalized to MNP controls without magnetic hyperthermia (*$p < 0.05$, **$p < 0.01$, N.S. = no significance). **D)** The temperature of the solution was monitored using a fiber optic temperature probe (Lumasense) over the course of magnetic hyperthermia. Control consisted of the same conditions but without MNPs. **E)** qPCR shows up regulation of let-7a targets following magnetic hyperthermia. Again, results were normalized to MNP controls in the absence of magnetic hyperthermia (*$p < 0.01$, **$p < 0.001$).

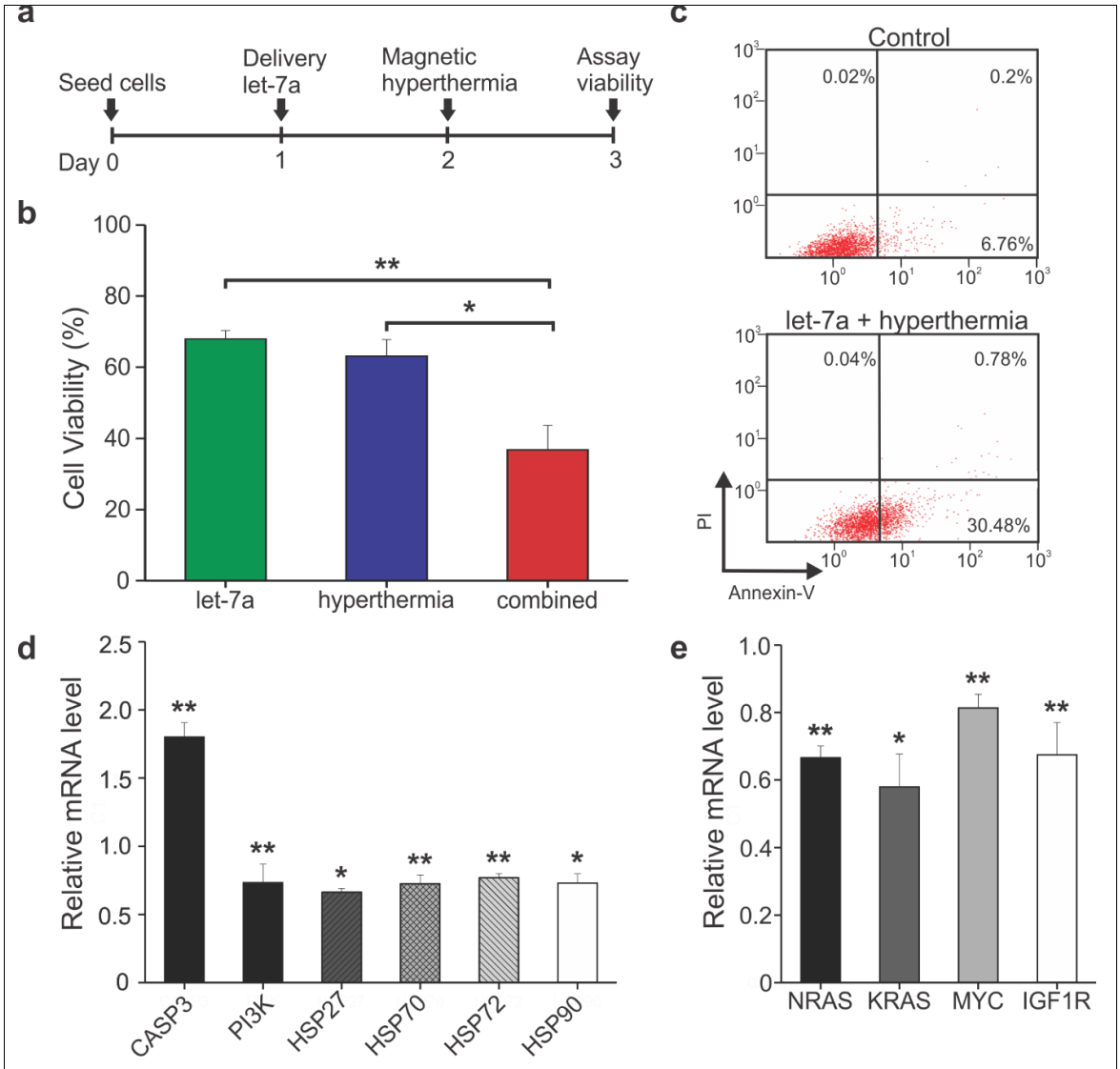

Figure 2.14. Combined Magnetic Nanoparticle-Based let-7a Delivery and Magnetic Hyperthermia Therapy.
A) Timeline of combined treatment. **B)** Cell viability following combined let-7a delivery and magnetic hyperthermia as quantified by MTS assay (*$p < 0.05$, **$p < 0.01$). **C)** FACS analysis of combination treated cells compared to controls. **D)** Combined let-7a delivery and magnetic hyperthermia results in up regulation of caspase-3 and a decrease in PI3K as well as HSPs as determined by qPCR (*$p < 0.05$, **$p < 0.01$). **E)** qPCR analysis of let-7a targets following combined therapy (*$p < 0.05$, **$p < 0.01$). qPCR results were normalized to MNP-PEI/miRNA/PEI complex controls delivering scrambled miRNA without exposure to magnetic hyperthermia.

2.2.5. MNP-Based Combined microRNA Delivery and Magnetic Hyperthermia

To treat GBM more effectively, we hypothesized that the MNP-based combined miRNA and magnetic hyperthermia therapy would enhance the therapeutic effects of let-7a delivery or magnetic hyperthermia alone. To test this hypothesis, we delivered MNP-PEI/miRNA/PEI complexes to U87-EGFRvIII cells. Twenty-four hours after treatment, the cells were trypsinized and exposed to an AMF. This treatment sequence, as depicted in **Figure 2.14A**, was chosen because an independent study demonstrated it to be the optimal treatment time for combined therapy (**Figure 2.15**). This is expected as the maximal effects of magnetic hyperthermia are typically seen within 24 hours whereas miRNAs such as let-7a act over 48-72 hours. Overall, combined MNP-based let-7a delivery and magnetic hyperthermia exhibited an additive effect resulting in a cell viability as low as 34% (**Figure 2.14B**), which is significantly lower than either let-7a treatment (69.8%, $p < 0.01$) or magnetic hyperthermia alone (63.14%, $p < 0.05$). Moreover, a significant increase in apoptosis levels was observed as quantified via Annexin-V/PI staining (**Figure 2.14C**) and the mRNA expression of caspase-3 (80% increase) when compared to either let-7a treatment or magnetic hyperthermia alone (**Figure 2.14D**).

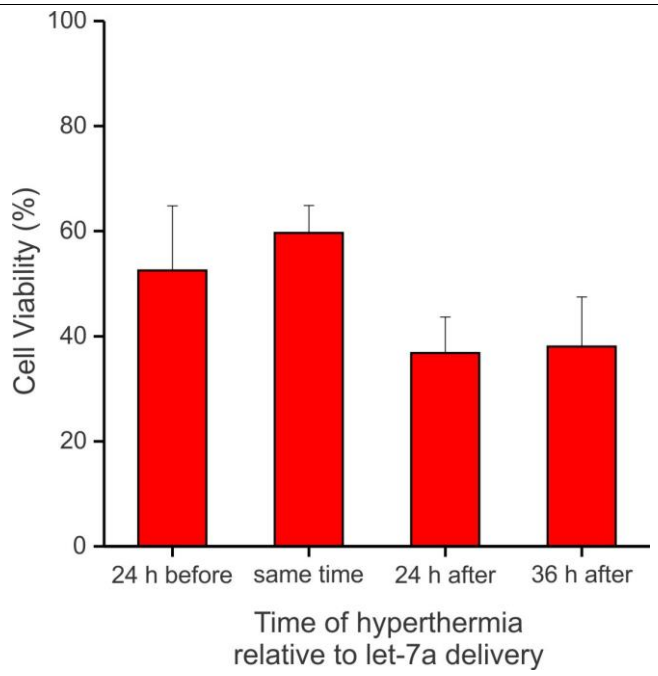

Figure 2.15 Optimization of Magnetic Hyperthermia Conditions
To determine the sequence with which to induce magnetic hyperthermia after the delivery of let-7a, different time points were tested. Viability was quantified 48 hours after the delivery of let-7a using MTS.

To further demonstrate the potential of our combined MNP-based let-7a delivery and magnetic hyperthermia therapy, we utilized a tumor spheroid monoculture assay as an intermediate between *in vitro* monolayer-based models and future *in vivo* studies. Specifically, unlike classical monolayer-based models, tumor spheroid models are able to mirror the three-dimensional (3D) context of *in vivo* tumors to a high degree and can provide more therapeutically relevant results. In particular, we observed that upon exposure to combined therapy using the same conditions as those used in monolayer cell cultures, we saw a similar additive effect resulting in tumor spheroid cell viability as low as 47% (**Figure 2.16**). As expected of a 3D environment, although still effective, combined therapy was not as effective as in monolayer cultures across all conditions (e.g. let-7a alone, magnetic hyperthermia alone, and combined therapy). Finally, as a

preliminary *in vivo* study, we performed a biodistribution study wherein MNP complexes (25 and 50 mg MNP/kg of body weight) functionalized with poly(ethylene glycol) (PEG; molecular weight = 2,000) and targeted via anti-CD44 antibodies were injected (tail-vein injection) into nu/nu mice implanted with subcutaneous SUM159 xenografts. We found that the animals tolerated both doses well and that the MNPs were able to localize/target the tumors within one week of injection (**Figure 2.17**). While more detailed *in vivo* studies remain to be performed, our findings taken together with previous evidence demonstrating the effectiveness of let-7 alone *in vivo*[235] and magnetic hyperthermia alone *in vivo*[201,239] suggests that combined MNP-based let-7a delivery and magnetic hyperthermia will be able to act as an effective treatment *in vivo*.

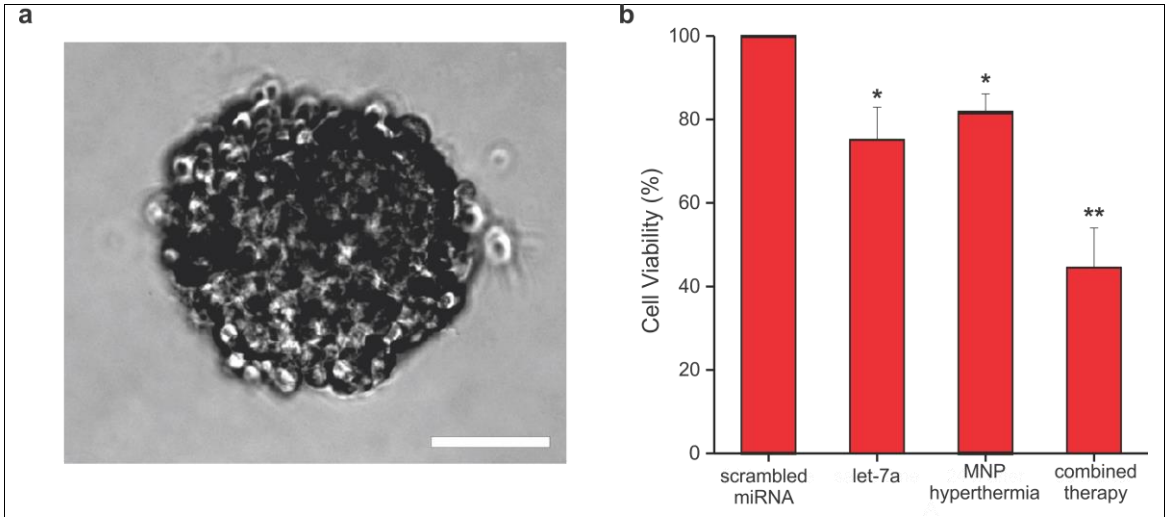

Figure 2.16 Tumor Spheroid Monoculture Assay
A) Tumor spheroid monocultures were formed from U87-EGFRvIII cells using the hanging drop technique (20,000 cells in 20 ul droplets, scale bar = 50 μm). **B)** 24 hours after spheroid formation, individual spheroids were transferred to 24-well plates and exposed to the varying treatment conditions (same as those utilized in the monolayer cell culture condition). Cell viability following combined let-7a delivery and magnetic hyperthermia as quantified by MTS assay demonstrates that combined therapy remains effective even on tumor spheroids albeit expectedly less effective compared to monolayer cultures. Conditions were normalized to scrambled microRNA as delivered by MNPs (*$p < 0.05$, **$p < 0.01$).

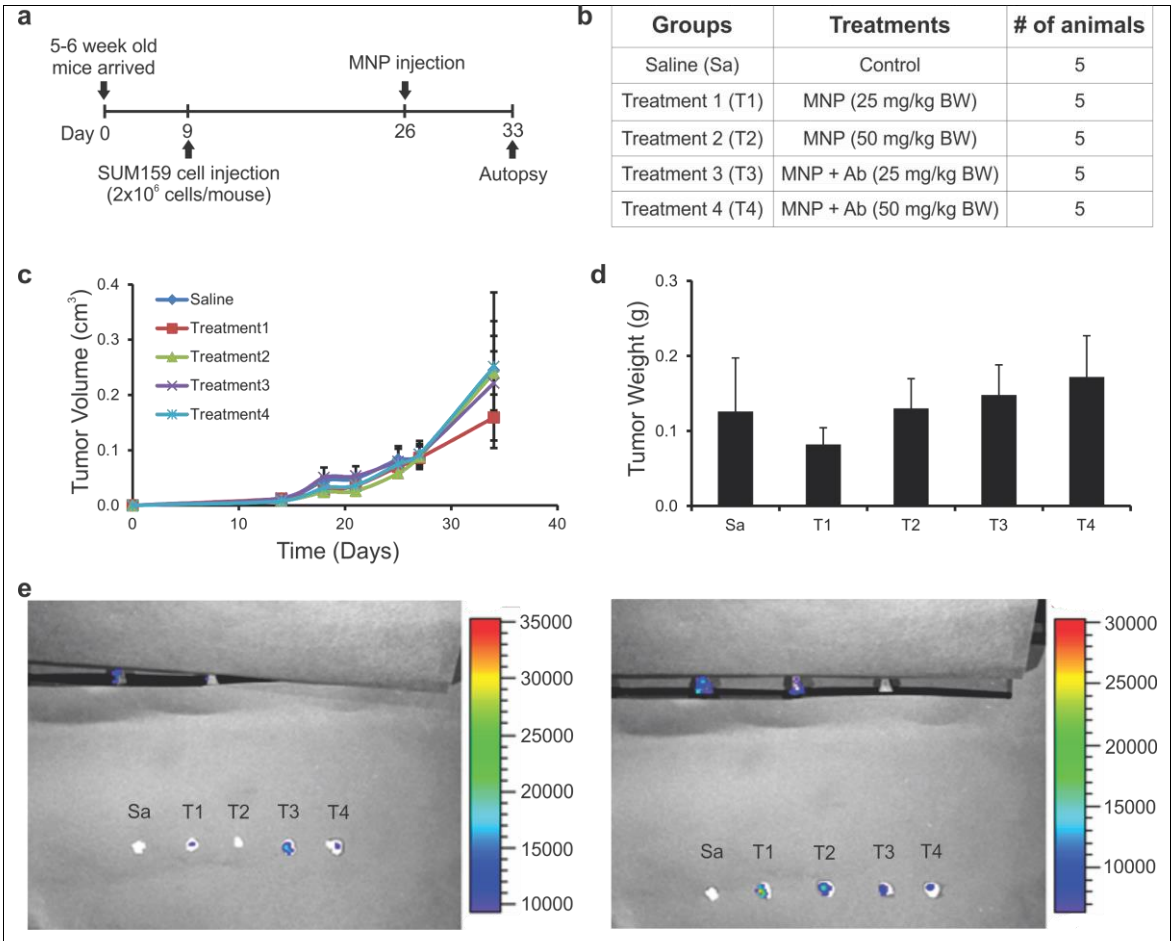

Figure 2.17 *In Vivo* Biodistribution of Magnetic Nanoparticle Complexes
A) 2 x 10^6 SUM159 breast cancer cells were subcutaneously inoculated into the dorsal part of 5-6 week old nu/nu mice. Tumors were allowed to develop for 2 weeks after which cy3-conjugated MNPs that were coated with PEI-PEG and targeted via anti-CD44 antibody were injected via tail vein injection (25 and 50 mg/kg of body weight). Images were taken over the following week and mice were euthanized one week after MNP injection. **B)** Table explaining the different treatment groups. There were 5 groups with 5 animals in each group. **C)** Tumor volume was monitored over the entire study **D)** Tumor weight was also quantified after tumor collection. **E)** Representative images taken using an IVIS system confirm that the cy3-conjugated MNPs (with and without targeting) were able to localize within the tumor within 1 week after MNP injection.

Finally, to examine the molecular mechanisms by which MNP-based combined let-7 and magnetic hyperthermia therapy can increase cell death in GBM cells, we investigated its target genes focusing on those related to HSPs as well as cell survival and proliferation (**Figure 2.14D**). Specifically, we observed that PI3K expression was

significantly down regulated (23% decrease, $p < 0.001$) whereas caspase-3 was significantly up regulated (80% increase, $p < 0.001$) when magnetic hyperthermia was combined with let-7a delivery (**Figure 2.14D**). Moreover, the expression of HSPs was also significantly down regulated (>20%, $p < 0.02$) when compared to magnetic hyperthermia treated control cells. In terms of let-7a targets, the expression of RAS, IGF1R, and MYC were down regulated significantly after exposure to combined therapy (**Figure 2.14E**). These results suggest that the down regulation of pathways including IGF1R and RAS, which directly activate PI3K,[237] by let-7a may lead to a greater increase in caspase-3 mediated apoptosis than would otherwise be possible with magnetic hyperthermia or let-7a delivery alone. Moreover, it has been shown that the inhibition of PI3K can also down regulate HSPs,[239] which is supported by the down regulation of HSP that is observed in our results (**Figure 2.14D**), further pushing GBM cells towards apoptosis following combined therapy. Together, these results suggest that the MNP-based combination of let-7a delivery followed by magnetic hyperthermia may significantly enhance the treatment of GBM.

2.3. Conclusions

In summary, we have successfully demonstrated the effective MNP-based delivery of miRNA to cancer cells as well as the novel combined MNP-based miRNA and magnetic hyperthermia therapy to enhance apoptosis in cancer cells. As mentioned previously, to maximize the therapeutic effects of hyperthermia, a number of therapeutics have been developed to target HSP-mediated pathways including the HSP70 and HSP90 inhibitor, bortezimab[208] and geldanamycin, which targets HSP90.[209] While promising,

each individual of the HSP family (e.g. HSP27, HSP70, HSP72, HSP90) has numerous subsequent targets.[207b] As such, in this study we sought to deliver a miRNA (let-7a), which simultaneously targets multiple key downstream effectors of HSPs on a MNP platform that also acts as an excellent magnetic hyperthermia agent to enhance apoptosis in brain cancer cells. The results indicate that combined MNP-based let-7a delivery and magnetic hyperthermia showed an additive effect resulting in significantly more apoptosis in brain cancer cells than either let-7a treatment or magnetic hyperthermia alone. Moreover, our results suggest that the targeting of pathways such as IGF1R and RAS by let-7a may lead to an increase in caspase-3 mediated apoptosis. Finally, besides enhancing the effects of magnetic hyperthermia, combined MNP-based let-7a delivery and magnetic hyperthermia can also offer a number of other advantages. First, the use of MNPs allows for enhancement of transfection using magnetofection as well as magnetic targeting. Second, treatment can potentially be monitored via magnetic resonance imaging (MRI) owing to the use of MNPs. Finally, we believe this treatment strategy can enhance the therapeutic potential of magnetic hyperthermia and by choosing cancer-specific miRNAs, can even be applied to enhance the treatment of other cancers and cancer stem cells including, but not limited to, breast and prostate cancers. In the future, we plan to improve targeting and biocompatibility by the addition of targeting ligands (e.g. iRGD) and polyethylene glycol (PEG), respectively.

2.4. Materials and Methods

2.4.1. Nanoparticle Synthesis

The synthesis of $ZnFe_2O_4$ magnetic nanoparticles (MNPs) has previously been reported and modified by our group.[67,240] Typically, 300 mg $ZnCl_2$, 400 g $FeCl_2$, and 3.5 g $Fe(acac)_3$ were mixed in 50 mL of tri-octylamine. Next, 1.2 mL oleic acid was added and refluxed at 300°C in a 250 mL three necked round bottom flask. After one hour, the reaction was cooled to room temp and ethanol was used to precipitate the MNPs. Then, the MNPs were purified by repeated centrifugation and sonication. Afterwards, the nanoparticles were dried under a vacuum overnight. To convert the hydrophobic MNPs into hydrophilic MNPs, ligand exchange was carried out using 2, 3 -dimercaptosuccinic acid (DMSA).[28a,225] In a typical experiment, 5 g of DMSA was dissolved in chloroform and added to a solution containing 40 mg of oleic acid/oleyl amine coated MNPs in toluene. The resulting mixture/solution was allowed to react for 24 hrs at room temperature with continuous stirring. The nanoparticles were then collected by centrifugation and dried under vacuum. The dried nanoparticles were then re-dispersed in DPBS (pH 7.4), to obtain an aqueous solution of MNPs with the desired concentration.

2.4.2. Formation of Magnetic Nanoparticle-PEI/miRNA/PEI complexes

To prepare the aforementioned $ZnFe_2O_4$ MNPs for microRNA (miRNA) delivery, the negatively charged water-soluble MNPs were coated with a branched cationic polymer, polyethyleneimine (PEI), which affords the MNPs with an overall positive charge. PEI is a polymer that is partially protonated under physiological conditions, thus allowing for the formation of complexes in the presence of nucleic acids.[228] PEIs have

been used extensively for the delivery of plasmids and other DNA and RNA molecules including small interfering RNA (siRNA) and miRNA.[228-229] Specifically, uptake of PEI-based complexes occurs through caveolae- or clathrin-dependent routes and PEI is able to facilitate release from the endosome with high efficiency via the "proton sponge effect."[230]

To obtain PEI coated MNPs, the water soluble MNPs were first diluted to 0.1 mg/mL using DPBS. Afterwards, excess 10 kDa branched PEI (Sigma Aldrich) was added drop wise (1 mg/mL). This molecular weight (MW) and structure of PEI was chosen based on previous reports.[241] After overnight spinning, the MNP-PEI was filtered (EMD Millipore, 10,000 MW) to remove excess PEI. To complex the PEI coated MNPs with miRNA, MNP-PEI were diluted in 80 mM NaCl solution and 100 nM miRNA was added to the solution. Specifically, the NaCl solution was necessary to overcome repulsive forces and to wrap the miRNA and PEI polymer around the small MNPs.[242] It should also be noted that all miRNAs were purchased from Ambion in the pre-miRNA form (~70 nucleotides): Pre-miR miRNA Precursor let-7a (PM10050), Pre-miR miRNA Precursor Negative Control #1 (AM17110), and Cy3 dye-labeled Pre-miR Negative Control #1 (AM17120). After 20 minutes of complex formation at room temperature, 1 uL of 1 mg/mL PEI was added and the samples were incubated for an additional 20 minutes. After the incubation was completed, the samples were once again filtered using a centrifugal filter unit (EMD Millipore, 10,000 MW) to remove excess PEI. To determine the initial concentration of MNP-PEI that needed to be added to complex 100 nM of miRNA, complexes with increasing concentrations of MNP-PEI were incubated with 100 nM miRNA. Afterwards, 100 μL of solution was transferred to a 96-well

(black-walled, clear-bottom, non-adsorbing) plate. 100 μL of diluted PicoGreen dye (1:200 dilution in Tris-EDTA (TE) buffer) was added to each well. Following 10 minutes of incubation at room temp, fluorescence measurements were obtained using a M200 Pro Multimode Detector (Tecan USA Inc, NC, USA), at an excitation and emission wavelength of 485 and 535 nm, respectively. Background fluorescence was subtracted by measuring a solution containing only buffer and PicoGreen dye. Similarly, to determine the concentration of NaCl solution used in complexing, complexes were prepared as described above utilizing different concentrations of NaCl solution (40, 80, 120 mM) and the size of the complexes was determined using dynamic light scattering (DLS).

2.4.3. Nanoparticle Complex Characterization

Dynamic light scattering (DLS) and Zeta Potential analyses were performed using a Malvern Instruments Zetasizer Nano ZS-90 instrument (Southboro, MA). Nanoparticle/miRNA complexes (miRNA concentration = 100 nM) were prepared using water. DLS measurements were performed at a 90° scattering angle at room temp. Zeta potential was collected at room temp and the zeta potentials of three sequential measurements were collected.

2.4.4. Transfection of Cell Lines with Magnetic Nanoparticle Complexes

Twenty-four hours before the magnetofection of MNP complexes, 30,000 brain cancer cells were seeded into each well of a 12-well plate (80% confluency). MNP-PEI/miRNA/PEI complexes were formed as described above. Thereafter the MNP complexes were mixed with Opti MEM (Life Technologies) and added to each well to

attain the desired final concentration of miRNA/well. Subsequently, the cell culture plates were placed on an Nd-Fe-B magnetic plate (OZ Biosciences, France) for 10 minutes (as optimized from previous reports).[67] The culture plates were then placed back into the incubator for 5 hrs. Afterwards, the cells were washed once with DPBS and fresh growth medium was added. The growth mediums for the cell lines (obtained from ATCC) used in the study are as follows: U87-EGFRvIII (DMEM supplemented with 10% FBS, 1% Penicillin-Streptomycin, 1% Glutamax, and hygromycin B as a selection marker) as well as U87-WT, U87-EGFR, and Astrocytes (DMEM supplemented with 10% FBS, 1% Penicillin-Streptomycin).

2.4.5. Magnetic Hyperthermia

24 hours after the cells were seeded as described above, 10 μg/mL of PEI-MNPs were prepared in Opti MEM (Life Technologies) and added to each well. Following, the cell culture plates were exposed to magnetofection for 10 minutes and then placed back into the incubator for 5 hrs. Afterwards, the cells were washed with DPBS and fresh growth medium was added. To perform magnetic hyperthermia, 24 hours after transfection, cells were washed with DPBS, trypsinized, and then exposed to an alternating magnetic field (5 kA/m, 225 kHz). Thereafter, fresh media was added to the treated cells, which were then plated back into 12-well plates.

2.4.6. Combined MNP-Based miRNA Delivery and Magnetic Hyperthermia

MNP- PEI/let-7a/PEI complexes were delivered to U87-EGFRvIII GBM cells 24 hrs after seeding. Next, cells were trypsinized and exposed to an alternating magnetic

field to induce magnetic hyperthermia 24 hrs after transfection and cell viability was quantified 48 hrs after initial transfection.

2.4.7. Cell Viability Assays

The cell viability was determined by MTS assay using the standard protocol that was described by the manufacturer. All measurements were made 48 hrs after initial transfection. All experiments were conducted by averaging triplicates. Absorbance at 490 nm was measured and the control (untreated) cells were normalized as 100% viable. To assay apoptosis using Annexin V-FLUOS and Propidium Iodide staining (Roche), 48 hrs after initial transfection, 10^6 cells were suspended in 1 mL of PBS with 10% FBS. After centrifugation, cells were resuspended in 100 µl Annexin V Binding Buffer (ice-cold) and Annexin V-FLUOS and Propidium Iodide (PI) were added following the manufacturers protocol. Samples were incubated in the dark for 15 minutes at room temp. Lastly, 400 µl of additional ice-cold Annexin V Binding Buffer was added and the samples were kept on ice until the analysis was performed using flow cytometry.

2.4.8. qPCR Analysis

To quantify the effect that miRNA delivery had, we quantified the mRNA expression levels, as it has been reported that mammalian miRNAs primarily regulate target genes by decreasing mRNA levels.[234] Total RNA was extracted 48 hrs after initial transfection using Trizol Reagent (Life Technologies) and the expression level of mRNA of the target genes (Table 1) were analyzed using quantitative PCR (qPCR). In particular, 1 µg of total RNA was used to generate cDNA using the Superscript III First-Strand

Synthesis System (Life Technologies). mRNA expression was then quantified using specific primers for each target mRNA. qPCRs were performed on a StepOnePlus Real-Time PCR System (Applied Biosystems) using SYBR Green PCR Master Mix (Applied Biosystems). The Ct values that were obtained were normalized to GAPDH. Standard cycle conditions were used with a primer melting temperature of 60°C. Primers are listed in Table 1. All primers were obtained from the PrimerBank database.[243]

2.4.9. Tumor Spheroid Monoculture Assay

Tumor spheroid monocultures of U87-EGFRvIII cells were formed using the hanging drop method. Specifically, adherent U87-EGFRvIII cell cultures were first grown to 90% confluence after which they were rinsed with PBS and tryspinized (0.05% trypsin-1 mM EDTA). Trypsinization was halted using complete medium and the cell suspension was centrifuged at 200 XG for 5 minutes. Afterwards, the supernatant was discarded and the pellet was resuspended in 1 mL of media. Cells were counted using a hemacytometer and the cell concentration was adjusted to 1 x 10^6 cells/mL. To form hanging drops, the lid of a 6 cm cell culture dish was removed and 20 ul drops of cell suspension were placed on the bottom of the lid. The lid was then inverted into a PBS-filled bottom chamber and incubated at 37°C for 24 hours. Finally, after 24 hours, each spheroid was transferred to separate wells of a 24-well plate.

2.4.10. Animal Studies

5-6 week old nu/nu mice were used for the *in vivo* experiments. SUM159 breast cancer cells were cultured under standard conditions. 2 x 10^6 SUM159 breast cancer cells

were subcutaneously inoculated into the dorsal part of the mice. Tumors were allowed to develop for 2 weeks after which MNPs (25 and 50 mg/kg of body weight) were injected via tail vein injection. Specifically, MNPs (DMSA-capped) were conjugated with PEI (10 kDa, branched) via electrostatic interaction. Afterwards, the amine groups of the PEI were conjugated with the carboxyl group of poly(ethylene glycol) (PEG; MW = 2,000; COOH-PEG-COOH) using EDC coupling. The other carboxyl group was conjugated with anti-CD44, again, using EDC coupling. Finally, cy3-NHS was conjugated onto the nanoparticles (NHS binds to the amine groups of PEI). Images were taken up to a week after injection (IVIS system) after which, the mice were euthanized and the tumors were harvested. All *in vivo* animal procedures were approved by the Laboratory Animal Services at Rutgers University.

Table 1. Table of Primers Used for qPCR

	Forward Primer	Reverse Primer
AURKA	TTCAGGACCTGTTAAGGCTACA	CGAGAACACGTTTTGGACCTC
AURKB	CGCAGAGAGATCGAAATCCAG	AGTTGTAGAGACGCAGGATGTT
BRCA1	GGCTATCCTCTCAGAGTGACATTT	GCTTTATCAGGTTATGTTGCATGG
BRCA2	CTAATTAACTGTTCAGCCCAGT	CTAGAACATTTCCTCAGAATTGTC
CASP3	AGAACTGGACTGTGGCATTGA	GCTTGTCGGCATACTGTTTCAG
CDK4	AGAGTGTGAGAGTCCCCAATG	CGCCTCAGTAAAGCCACCT
GRB2	CTGGGTGGTGAAGTTCAATTCT	GTTCTATGTCCCGCAGGAATATC
HRAS	GACGTGCCTGTTGGACATC	CTTCACCCGTTTGATCTGCTC
HSP27	TGGACCCCACCCAAGTTTC	CGGCAGTCTCATCGGATTTT
HSP70	TTTTACCACTGAGCAAGTGACTG	ACAAGGAACCGAAACAACACA
HSP72	TGCTGATCCAGGTGTACGAG	CGTTGGTGATGGTGATCTTG
HSP90	AGGTGTTTATACGGGAGCTGA	GCATTGGTCTGCAAGTGAATCTC
HMGA2	CAGCAGCAAGAACCAACCG	GGTCTTCCCCTGGGTCTCTTA
IGF1R	CTCCTGTTTCTCTCCGCCG	ATAGTCGTTGCGGATGTCGAT
KRAS	AGCGTCACTGGCACTTTCAAA	CACCCACATAGAAGACCTGGT
MYC	CTCCTCACAGCCCACTGGTC	CTTGGCAGCAGGATAGTCCTTC
NRAS	TGAGAGACCAATACATGAGGACA	CCCTGTAGAGGTTAATATCCGCA
P53	TTTGCGTGTGGAGTATTTGGAT	CAACCTCAGGCGGCTCATA
PI3K	GAAACAAGACGACTTTGTGACCT	CTTCACGGTTGCCTACTGGT

Chapter 3 :

Multifunctional Magnetic Nanoparticle-Based microRNA and Doxorubicin Therapy to Enhance the Treatment of Cancer

3.1. Introduction

Cancer is a complex disease that is characterized by the existence of a multitude of genetic and epigenetic alterations, which combine to promote cellular abnormalities like aggressive growth and resistance to apoptosis.[244] For instance, breast cancer, which is the most diagnosed cancer in women and the second most frequent cancer worldwide, is typically divided into histological subtypes based on the expression of specific receptors such as the estrogen receptor (ER), progesterone receptor (PR), and HER2 receptor or the absence of all of them (e.g. triple negative breast cancer).[245] The conventional treatment for breast cancer depends on the subtype that is present, but typically includes surgical resection of the tumor followed by adjuvant radiotherapy and chemotherapy. For instance, the most frequently used chemotherapy regimens for breast cancers are anthracyclines (doxorubicin)[246] and taxanes (paclitaxel and docetaxel).[247] However, current strategies to treat breast cancers often cannot account for the vast degree of heterogeneity that exists within the tumor. Moreover, breast cancer cells often acquire chemoresistance, resulting in a failure to eradicate the entire tumor and recurrence, especially in patients with triple negative breast cancer.

One way that cancer cells acquire drug resistance is through the overexpression of drug transporters, which reduce intracellular drug levels to a sublethal threshold (**Figure**

3.1). There are also a number of other mechanisms through which the tumor can operate in order to achieve chemoresistance. For instance, the tumor cells may acquire mutations in the drug target and in DNA repair mechanisms. Moreover, alternative signaling pathways may be activated in tumor cells resulting in cell survival and allowing tumor cells to evade cell death. Therefore, there is a need for novel multifunctional approaches that can simultaneously regulate a broad set of deregulated genes thereby promoting apoptosis and sensitizing cancer cells to subsequent chemotherapy.[248]

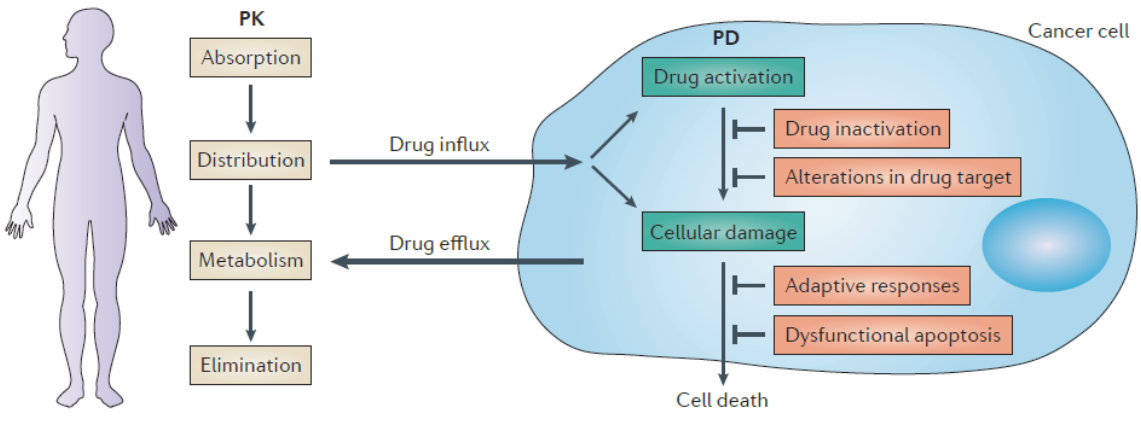

Figure 3.1 General Principles of Drug Resistance
Drug resistance can be divided into pharmacokinetic (PK) and pharmacodynamics (PD) principles. PK factors include poor drug absorption, distribution, metabolism, and elimination within the body. PD factors include poor drug influx or excessive efflux into the cell. It also includes drug inactivation and changes in the drug target. Finally, the upregulation of prosurvival pathways and inhibition of apoptosis are common. Reproduced with permission.[248] 2013, Nature.

microRNAs (miRNAs) are small (20–22 nucleotides) noncoding RNA molecules that bind mRNAs in a completely or partially complementary fashion, resulting in the degradation or translation inhibition of the mRNA targets.[249] miRNAs have already been demonstrated to play a significant role in development as well as in stem cell biology and studies have shown that miRNA up or down-regulation significantly affects cancer development and progression.[249b,250] For example, let-7a, which is reduced in brain,

breast, lung, and ovarian cancers, is a tumor suppressor that inhibits cancer cell growth by inhibiting RAS and HMGA2.[224] Therefore, miRNA delivery represents a promising strategy for the treatment of cancers such as those of the breast. Yet, although miRNA-based treatment modalities have great clinical potential, possible synergies with currently available chemotherapies remain poorly explored and their clinical application is greatly obstructed by our inability to delivery it efficiently.

In this chapter, we report the novel use of multifunctional magnetic core-shell nanoparticles (MCNPs), composed of a highly magnetic zinc-doped iron oxide nanoparticle ($ZnFe_2O_4$) core and a biocompatible mesoporous silica shell (mSi), as a vehicle for the simultaneous delivery of a let-7a microRNA and doxorubicin chemotherapy to breast cancer cells (**Figure 3.2**). While let-7a has primarily been shown to inhibit malignant growth by targeting RAS and HMGA2, it is also known to have functions in DNA repair/replications (e.g. BRCA1 and BRCA2), cell cycle, and has even been shown to regulate multidrug resistance genes/drug efflux pumps (e.g. MDR1 and ABCG2).[251] As such, in this study, using triple-negative breast cancer (e.g. MDA-MB-231) as a model system, we hypothesized that the delivery of a let-7a mimic as a replacement therapy, could sensitize breast cancer cells to subsequent DNA-intercalating chemotherapies such as doxorubicin (DOX). Moreover, the multifunctionalities of our MCNPs allows for monitoring of drug delivery via MRI as well as the induction of magnetic hyperthermia via exposure to an alternating magnetic field (AMF) to further sensitize cancer cells to subsequent chemotherapy.[19a,20] Overall, we have developed a multifunctional platform that provides an attractive means with which to enhance our ability to not only to monitor and deliver therapeutics, but also sensitize cancer cells to

treatment via the combination of microRNA replacement therapy and magnetic hyperthermia all in a single platform.

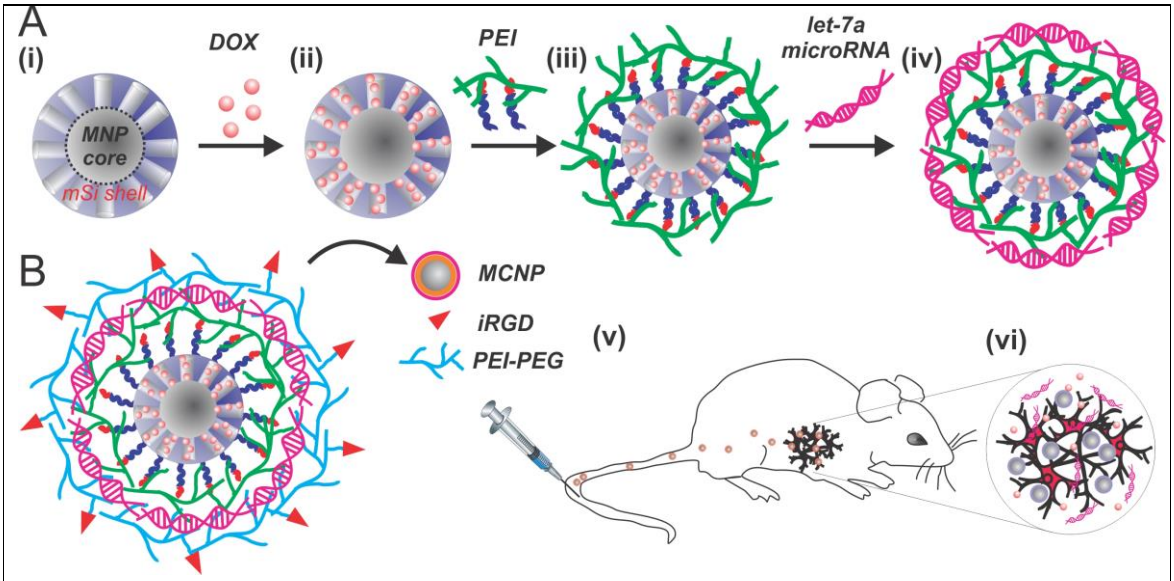

Figure 3.2 Magnetic Core-Shell Nanoparticle-Based Delivery of microRNA and Doxorubicin to Enhance the Treatment of Cancer
A) MCNPs composed of a $ZnFe_2O_4$ magnetic nanoparticle (MNP) core and a mesoporous silica (mSi) shell **(i)** are loaded with doxorubicin (DOX) (**ii**). Following, they are functionalized with polyethyleneimine (PEI) to allow for complexing with microRNA (e.g. mature let-7a) **(iii-iv)**. For *in vivo* treatment of breast cancer, MCNPs were injected either via tail vein injection or intramurally **(v)**. Once the MCNPs have been uptaken, the microRNA and DOX is released over time **(vi)** resulting in enhanced treatment of the cancer cells. **B)** To enhance stability/dispersity and cell uptake as well as to allow for tumor targeting, we used a layer-by-layer strategy where the outer layer consisted of PEI-PEG and iRGD was used to specifically target the MCNPs to breast cancer cells *in vitro* and *in vivo*.

3.2. Results and Discussion

3.2.1. Synthesis and Characterization of the Magnetic Core-Shell Nanoparticles

For the purpose of simultaneously delivering let-7a microRNA and doxorubicin chemotherapy, we synthesized multifunctional MCNPs with a zinc-doped iron oxide ($ZnFe_2O_4$) core. These cores have previously been shown to have a significantly higher

saturation magnetization when compared to conventional Fe_2O_3 or Fe_3O_4 magnetic nanoparticles (MNPs).[29] As such, we first synthesized $ZnFe_2O_4$ cores with a doping percentage of $(Zn_{0.4}Fe_{0.6})Fe_2O_4$ via the thermal decomposition of a mixture of metal precursors (zinc chloride, ferrous chloride, and ferric acetylacetonate) in the presence of oleic acid and oleylamine using a previously reported protocol that was modified by our group.[29,67] Following core synthesis, an inert mSi shell was formed around the MNP cores via the condensation of TEOS in the presence of a CTAB micelle template.[252] TEM revealed that the diameter of the cores was 18.93 ± 1.6 nm and that the MNP cores were uniformly coated with a 33.91 ± 3.8 nm thick mSi shell. As a result, the overall diameter of the as-synthesized MCNPs was 88.03 ± 8.22 nm (**Figure 3.3A**). In addition, the pores were estimated to be approximately 3 nm in diameter based on HR-TEM (**Inset of Figure 3.3A**) as well as previous reports.[252] For more detailed characterization, HR-TEM revealed the monocrystalline structure of the MNP cores with a lattice fringe that was measured to be 4.8 Å, which is characteristic of the (111) plane of the spinel.[29,67] Finally, FTIR analysis was used to confirm that the CTAB template had been extracted and removed from the pores of the mSi shell (**Figure 3.3C**).

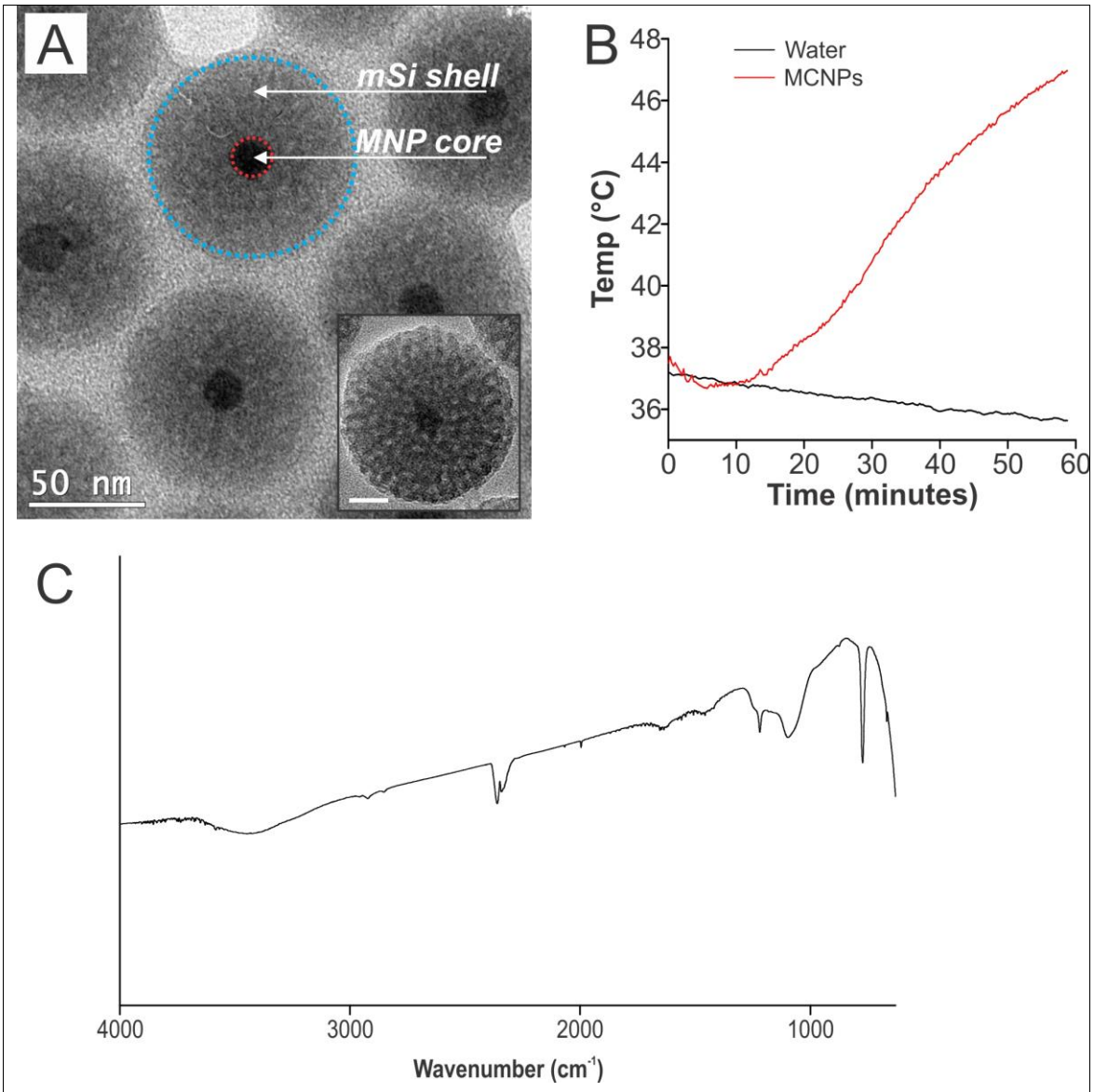

Figure 3.3 Characterization of the MCNPs
A) HR-TEM image of the MCNPs. Inset: Higher magnification HR-TEM image of the MCNPs shows that the pores are about 3 nm in size. Scale bar of inset = 20 nm. **B)** The MCNPs (25 µg/mL) can be heated to temperatures as high as 47°C after exposure to an alternating magnetic field (5 kA/m, 225 kHz) for one hour. **C)** Fourier-transform infrared spectra (FTIR) analysis was carried out to confirm the complete removal of CTAB. CTAB typically shows two intense peaks at 2,800–3,200 cm^{-1}, which correspond to the symmetric (2,849 cm^{-1}) and asymmetric (2,918 cm^{-1}) stretching vibrations of the methylene chains. These peaks were absent from the MCNPs, indicating the complete removal of CTAB from the MCNPs.

The MCNPs were also characterized by excellent magnetic properties that can be used to enhance MRI contrast as well as to induce magnetic hyperthermia. In particular, the MCNPs were characterized by a specific absorption rate (SAR) of 564 W/g, which was determined using an AMF with an amplitude of 5 kA/m and a frequency of 225 kHz. This SAR is consistent with data reported in the literature for similar $ZnFe_2O_4$ MNPs.[149,226] Moreover, we demonstrated that these MCNPs (25 µg/mL) could reach temperatures as high as 47°C within an hour of exposure to the AMF (**Figure 3.3B**) and that we could maintain a mild hyperthermia temperature of 43-45°C following periodic exposure to the AMF. As such, we were able to synthesize monodisperse water-soluble MCNPs with a narrow size distribution and, more importantly, these MCNPs had excellent magnetic properties for magnetic hyperthermia even after the addition of an mSi shell.

3.2.2. Loading and Release of Doxorubicin from the MCNPs

To efficiently deliver DOX over time, DOX was loaded in the pores of the mSi shell of the MCNPs. For this purpose, the pores of the mSi shell were first functionalized with methyl phosphonate ($-PO_3^-$) groups using the post-grafting method, from a previously described protocol that was modified by our group.[253] In particular, this has previously been shown to enhance the loading of doxorubicin as well as prolong doxorubicin release from mSi via electrostatic interactions.[253a] Briefly, the as-synthesized MCNPs were subjected to the post-grafting of trihydroxysilylpropyl methylphosphonate (THMP). To confirm that the surface of the MCNPs were functionalized with $-PO_3^-$ the zeta potential of the MCNPs was measured. It was found that the zeta potential of the -

PO_3^- -modified MCNPs decreased after functionalization, which agrees with previous reports.[253a]

Next, to load the MCNPs with DOX, the -PO_3^- -modified MCNPs were added to a concentrated solution of DOX and stirred at room temperature overnight. The mixture was then centrifuged to collect the DOX-loaded MCNPs. The loading content was found to be 11.1% and the DOX-loaded and had a release profile that reached its maximum over one week, which is significantly higher than plain MCNPs that were not modified with -PO_3^- and is also in agreement with previous reports.[253a]

Following, to prepare the aforementioned MCNPs for cell uptake and microRNA delivery, the MCNPs were coated with branched polyethylenimine (PEI, MW = 10 kDa) via electrostatic interactions in the presence of NaCl to afford the MCNPs with an overall positive charge. As a result, this would facilitate MCNP complexation with negatively-charged microRNA and induce endosomolysis within the cytoplasm.[254] Previous studies have shown that a direct relationship exists between the molecular weight of PEI and cytotoxicity.[145a] Therefore, to minimize cytotoxicity while maximizing transfection efficiency, we used 10 kDa branched PEI, which has previously been demonstrated to be biocompatible.[149,255] The resulting water soluble PEI-coated MCNPs (MCNP-PEI) had a hydrodynamic size of 117.2 ± 37 nm (polydispersity index [PDI] = 0.177) as measured by dynamic light scattering (DLS) and a zeta potential of +44.23 ± 0.72 mV. In particular, it was found that the MCNP-PEI was highly biocompatible and that delivery of MCNP-PEI to MDA-MB-231 breast cancer cells was biocompatible even up to levels as high as 200 μg/mL with 100 μg/mL having a cell viability of over 95% (**Figure 3.4A**). As such, 100 μg/mL was used for all remaining studies. Moreover, delivery of DOX-

loaded MCNPs resulted in a dose-dependent decrease in cell viability, wherein 100 μg/mL of DOX-loaded MCNP decreased cell viability by over 80% (**Figure 3.4B**). Finally, using qPCR measurements made from total RNA, we observed that DOX treatment activates caspase-3-mediated apoptosis and also results in the up-regulation of ABCG2 (drug efflux pump), which agrees with previous reports (**Figure 3.4C**).[256]

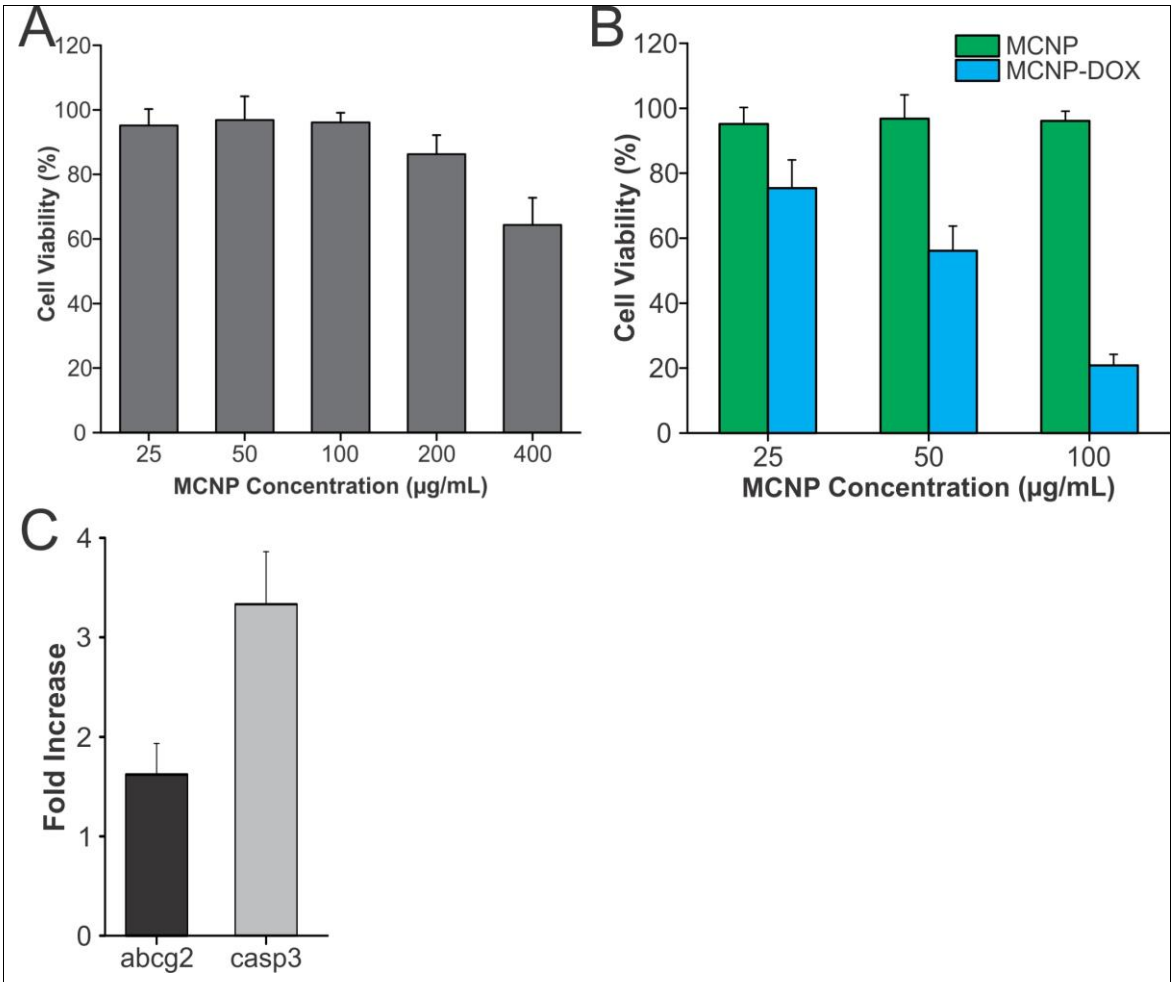

Figure 3.4 MCNP-PEI Biocompatibility and DOX Release
A) Increasing concentrations of MCNP-PEI were delivered to MDA-MB-231 breast cancer cells and delivery was enhanced using magnetofection (10 min). The MCNP complexes were well tolerated by the cells as determined via MTS assay 48 hours after transfection even at concentrations as high as 100 μg/mL. **B)** Increasing concentrations of DOX-loaded MCNPs were also delivered to MDA-MB-231 breast cancer cells and cell viability was again determined via MTS assay 48 hours after transfection. **C)** qPCR analysis following treatment with DOX-loaded MCNPs.

3.2.3. MCNP-Based let-7a microRNA Delivery

To deliver miRNAs efficiently using our MNPs, we developed a two-step layer-by-layer process (**Figure 3.2B**). First, the PEI-coated MNPs (1 μg/mL) were incubated with miRNA (100 nM as was optimized form our previous study) in an 80 mM NaCl solution. Afterwards, an outer coat of PEI was added to provide additional protection for the miRNA as well as to facilitate cell uptake and endosomal escape. We observed that the size of the MNP complexes increased to a final diameter of approximately 150 nm for the layer-by-layer MNP-PEI/miRNA/PEI complex and had a positive zeta potential. A more detailed description of the optimization process for MNP complex formation can be found in the Materials and Methods section.

As mentioned previously, let-7a is known to target a number of genes involved in cell survival (PI3K via IGF1R),[206c,d] proliferation (RAS, HMGA2),[216-217] and DNA repair (BRCA1, BRCA2).[215] For breast cancer, previous studies have shown that let-7 primarily acts to inhibit proliferation and self-renewal through the down-regulation of H-RAS and HMGA2.[257] As such, we used our MCNPs to delivered let-7a alone to MDA-MB-231 cells and evaluated their therapeutic potential. We observed that 48 hours after the MNP-mediated delivery of let-7a, breast cancer cell viability decreased significantly compared to control. Moreover, using quantitative PCR (qPCR) measurements made from total RNA, we confirmed that let-7a acts primarily through the down regulation of H-RAS and HMGA2, wherein H-RAS and HMGA2 were down regulated by over 80%. Finally, we observed at least 40% down-regulation of all target gene transcripts (ABCG2 and KRAS) relative to MDA-MB-231 cells treated with scrambled miRNA (100 nM) as delivered by our MNPs. As such, this suggests that let-7a, which targets DNA repair mechanisms and

drug efflux pumps, may be combined with DNA-intercalating drugs such as DOX to induce a synergistic effect.

3.2.4. MCNP-Based Tumor Targeting

To achieve MCNP-based tumor targeting, we functionalized our MCNPs with a combination of polyethylene glycol (PEG) and iRGD (CRGDKGPCD).[258] PEG is a stealth polymer that suppresses nonspecific interactions with the body (e.g. decreased interactions with blood components (opsonization) that activate the complement system),[17] and is endowed with either a slightly negative or slightly positive charge in order to minimize overall nanoparticle–nanoparticle and nanoparticle–environment interactions. On the other hand, iRGD is a peptide that can facilitate cell and tissue penetration.[259]

To initially test our MCNP-PEI-PEG-iRGD system, we labeled the targeted MCNPs with FITC via a covalent linker. Following, the FITC-labeled, targeted MCNPs were delivered to two cell lines: MCF-7 breast cancer cells, which have previously been shown to have low integrin levels, and MDA-MB-231 breast cancer cells, which are much more aggressive/invasive and highly express integrins.[260] In particular, following the same protocol as was used previously (e.g. transfection was enhanced via exposure to 10 minutes of magnetofection),[149] the FITC-labeled, targeted MCNPs were initially delivered to MCF-7 and MDA-MB-231 breast cancer cells *in vitro*. The cells were washed 5 hours after transfection and then imaged after 24 hours via fluorescence microscopy. By visualizing the fluorescence of FITC (**Figure 3.5**), it was observed that the FITC-labeled, targeted MCNPs were efficiently uptaken into MDA-MB-231 cells

while a minimal amount was uptaken into MCF-7 cells, which also agrees with the literature.[260]

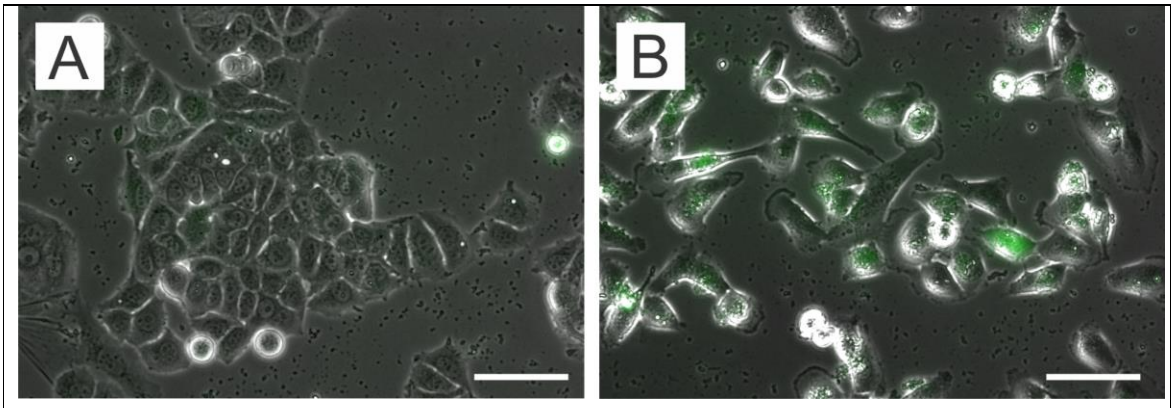

Figure 3.5 *In Vitro* Targeting of MCNPs
A) MCNP-PEI-PEG-iRGD (50 µg/mL) that were labeled with FITC were delivered to MCF-7 breast cancer cells, which have been shown to have low integrin levels. As a result, there was minimal uptake of MCNP-PEI-PEG-iRGD in these cells. **B)** MCNP-PEI-PEG-iRGD (50 µg/mL) that were labeled with FITC were also delivered to MDA-MB-231 breast cancer cells, which have been shown to have high integrin levels. As a result, there was significant uptake of MCNP-PEI-PEG-iRGD in these cells as can be seen by presence of fluorescence within the cells. Scale bar = 50 µm

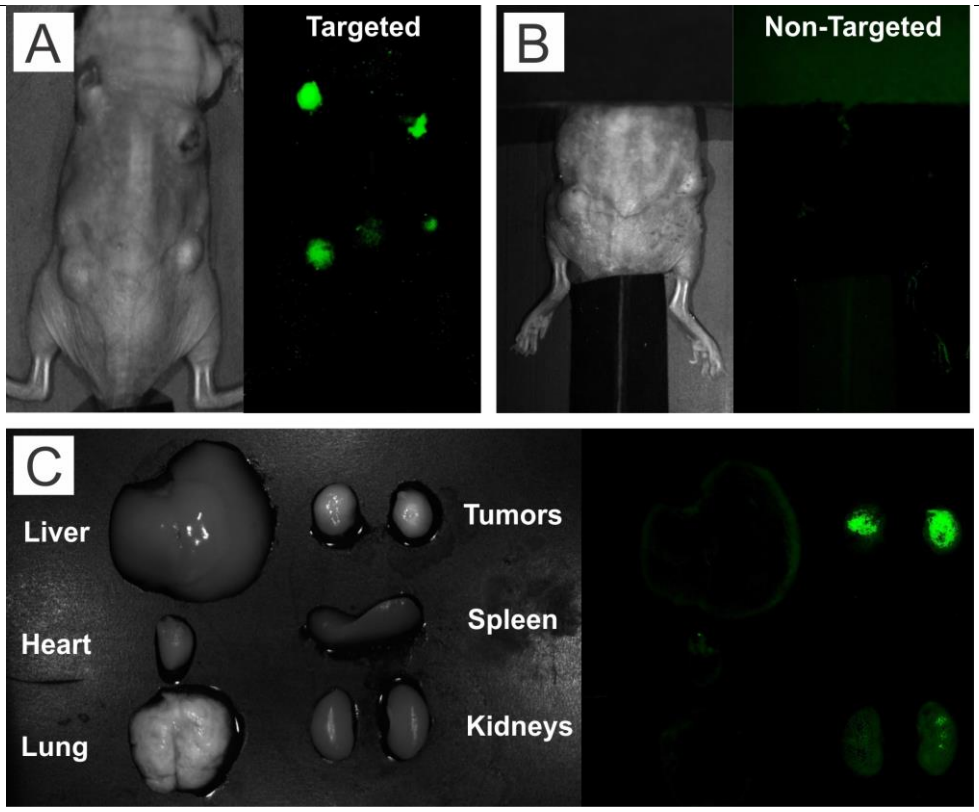

Figure 3.6 *In Vivo* Targeting of MCNPs
A-B) FITC-labeled, targeted (A) and non-targeted (B) MCNPs were injected via tail vein injection (1 mg/kg) into BALB/c nude mice with MDA-MB-231 tumors (4 tumors each). Images were taken over a week using an IVIS to monitor fluorescence. As can be seen, only the targeted MCNPs localized at the sites of the tumors. **C)** Tumors and organs were imaged *ex vivo* using an IVIS. It was found that FITC-labeled, targeted MCNPs primarily accumulate at the tumors as well as the kidneys.

Next, we tested the tumor targeting of these MCNP-PEI-PEG-iRGD nanoparticles *in vivo*. For this purpose, four MDA-MB-231 tumors were established in each BALB/c nude mouse via subcutaneous injection in the left and right shoulders and left and right flanks. Again, the same FITC-labeled, targeted MCNPs were used and FITC-labeled MCNPs that were not targeted were used as a control. In this case, the FITC-labeled, targeted and nontargeted MCNPs were injected via tail vein injection (1 mg/kg). Images were taken over a week using an IVIS to monitor fluorescence. As can be seen, only the targeted MCNPs localized at the sites of the tumors (**Figure 3.6A and B**). Finally, at the

conclusion of the week, the animals were euthanized and the tumors and other organs were removed. The tumors and organs were then imaged *ex vivo* using an IVIS. In this way, it was determined that the FITC-labeled, targeted MCNPs primarily accumulate at the tumors. However, some FITC-labeled, targeted MCNPs were also seen in the kidneys (**Figure 3.6C**).

3.2.5. Combined MCNP-Based let-7a and Doxorubicin Delivery

Finally, we tested the ability of our MCNPs to simultaneously deliver DOX and let-7a microRNA. For this purpose, we first loaded the MCNPS with DOX, which was then followed by complexation with let-7a microRNA. Using the optimized DOX delivery conditions and let-7a delivery conditions that were optimized previously, we delivered DOX-loaded and let-7a-complexed MCNPs to MDA-MB-231 cells. Cell viability was then assayed 48 hours after initial transfection. In this way, we observed a dose-dependent decrease in cell viability of the MDA-MB-231 breast cancer cells with 100 μg/mL of this combination therapy decreasing the cell viability by over 90%, which is significantly greater than either treatment modality alone (**Figure 3.7**).

To investigate the underlying mechanism of this synergy, qPCR was performed for MDA-MB-231 cells that had been exposed to both DOX and let-7a. In this way, it was determined that the combination of DOX and let-7a resulted in significant down-regulation of proliferation (e.g. via H-RAS), drug efflux pumps (e.g. via ABCG2), and cell cycle (e.g. via HMGA2).

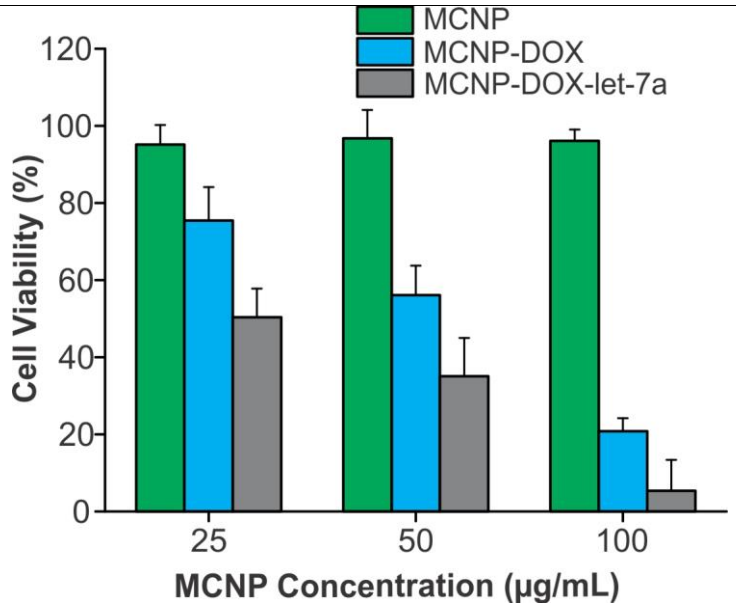

Figure 3.7 MCNP-Based Doxorubicin and let-7a Delivery
Using the optimized DOX delivery conditions and let-7a delivery conditions, DOX-loaded and let-7a-complexed MCNPs were delivered to MDA-MB-231 cells. Cell viability was then assayed 48 hours after initial transfection. In this way, we observed a dose-dependent decrease in cell viability of the MDA-MB-231 breast cancer cells with 100 µg/mL of this combination therapy decreasing the cell viability by over 90%, which is significantly greater than either treatment modality alone.

3.3. Conclusions

In summary, we have successfully demonstrated that the novel combination of DOX and microRNA can act as a potent therapy for cancer. For this purpose, we developed MCNPs consisting of a highly magnetic core and a biocompatible mesoporous silica shell. As such, DOX could be loaded in the pores of the mesoporous silica shell while let-7a microRNA was complexed on the surface through electrostatic interaction. We found that treatment of triple-negative breast cancer cells (e.g. MDA-MB-231) with our combination therapy resulted in a synergistic decrease in cell viability, wherein 100 µg/mL of this combination therapy decreased the cell viability by over 90%, which is significantly greater than either treatment modality alone.

From our preliminary analysis of the underlying mechanism, we believe that this unique combination acts primarily through the down-regulation of drug efflux pumps, DNA repair mechanisms, and tumor proliferation. In particular, let-7a microRNA has the ability to simultaneous down-regulate multiple gene targets, including members of the RAS family, HMGA2, ABCG2, and BRCA2. As a result, this sensitizes triple-negative breast cancer cells to the slow release of DOX from the pores of our MCNPs.

In the future, we plan to study the underlying mechanism in more detail as well as conduct *in vivo* studies to evaluate its preclinical efficacy. Moreover, owing to the magnetic properties that MCNPS possess, we seek to demonstrate the utility of these MCNPS not only for the simultaneous delivery of DOX and let-7a microRNA but also for other functions such as magnetic hyperthermia, which can sensitize cancer cells to subsequent combination therapy, as well as MRI contrast to monitor drug delivery.

3.4. Materials and Methods

3.4.1. Nanoparticle Synthesis and Characterization

The synthesis of $ZnFe_2O_4$ magnetic nanoparticles (MNPs) has previously been reported and modified by our group.[29,67,149,153,261] Briefly, 1.35 mmol, 0.3 mmol, and 0.7 mmol of $Fe(acac)_3$, $ZnCl_2$, and $FeCl_2$, respectively, were mixed into a round bottom flask with 20 mL of tri-n-octylamine, 6 mmol of both oleic acid and oleylamine, and 10 mmol of 1,2 hexadecanediol. The reaction mixture was then heated up to 200°C for 2 hrs. From here, the mixture was heated to 305°C for 2 hrs and the nanoparticles were purified by repeatedly washing with ethanol.

To coat the MNP cores with a mSi shell, a modified procedure from what was reported by Hyeon *et al.* was used.[252] 5 mg of the alkyl-capped MNP cores dispersed in chloroform were sonicated using a probe type sonicator in a 0.1 M aqueous cetyltrimethylammonium bromide (CTAB) solution. Upon evaporation of chloroform, the CTAB capped MNP cores were diluted to 50 mL with water and the pH of this mixture was adjusted to ~ 11 using a 2M NaOH solution. This reaction mixture was heated to 70°C and, under vigorous stirring, 0.4 mL of tetraethylorthosilicate (TEOS) in 2.4 mL of ethyl acetate was added. After the addition of TEOS, the reaction was allowed to continue for 4 hrs. The MCNPs were collected and washed several times with ethanol. To remove the template, the nanoparticles were heated to 60°C in an ammonium nitrate solution. The extracted MCNPs were again washed with ethanol. Finally, the MCNPs were characterized by high-resolution Transmission electron microscopy (HR-TEM) and Fourier-transform infrared spectra (FTIR).

To characterize the magnetic properties of the nanoparticles, the resulting MCNPs (25 µg/mL in H_2O) were exposed to an AMF (5 kA/m, 225 kHz) using a solid-state induction heating system (Superior Induction Company) for one hour. The temperature of the solution was monitored using a fiber optic temperature probe (LumaSense Technologies). To calculate the specific absorption rate (SAR), the following equation was used:

$$SAR\ (W/g)\ = C\left(\frac{dT}{dt}\right)\left(\frac{m_s}{m_m}\right)$$

where C is the specific heat capacity, m_s is the mass of the solution, m_m is the mass of the magnetic nanoparticles, T is the temperature, and t is the time.[262]

3.4.2. DOX Loading of the MCNPs

The MCNPs were functionalized with $–PO_3^-$ using a post-grafting method that was modified by our group.[263] For this purpose, MCNPs were dispersed in ethanol. Organic silanes were then added and the mixture was stirred at 80°C for 6 h. Afterwards, the precipitate was collected via centrifugation, washed with ethanol, and then dried under a vacuum. The obtained modified MCNPs were then post-grafted with THMP to obtain the MCNPs functionalized with $–PO_3^-$.

The MCNPs are dispersed in a water/DOX solution (DOX is at a final concentration of 1 mg/mL) such that the final particle concentration is 1 mg/mL. The solution is then stirred overnight for DOX loading. Next, Mn=10,000 and Mw=25,000 KDa PEI (100 mg/mL stock) is added such that the final PEI concentration is 10 mg/mL and NaCl is added such that the final concentration of NaCl is 1 mM. Following, the solution is stirred for at least half hour and then purified by spinning down at 10,000 for 10 min. This is performed twice and then the DOX-loaded MCNP-PEI is dispersed in PBS and used immediately.

3.4.3. Formation of MCNP-PEI/miRNA/PEI complexes

To prepare the aforementioned MCNPs for microRNA (miRNA) delivery, the negatively charged water-soluble MCNPs were coated with a branched cationic polymer, polyethyleneimine (PEI), which affords the MCNPs with an overall positive charge. PEI is a polymer that is partially protonated under physiological conditions, thus allowing for the formation of complexes in the presence of nucleic acids.[228] PEIs have been used extensively for the delivery of plasmids and other DNA and RNA molecules including

small interfering RNA (siRNA) and miRNA.[228-229] Specifically, it has been demonstrated that PEI-based complexes are able to enter the cell through caveolae- or clathrin-dependent routes and are able to facilitate release from the endosome with high efficiency via the "proton sponge effect."[230]

To obtain PEI coated MCNPs, the water soluble MCNPs were first diluted to 0.1 mg/mL using DBPS. Afterwards, excess 10 kDa branched PEI (Sigma Aldrich) was added drop wise (1 mg/mL). This molecular weight (MW) and structure of PEI was chosen based on previous reports.[241] After spinning overnight, the PEI coated MCNPs were filtered (EMD Millipore, 10,000 MW) to remove excess PEI. To complex the PEI coated MCNPs with miRNA, MCNP-PEI were diluted in 80 mM NaCl solution and 100 nM miRNA was added to the solution. Specifically, the NaCl solution was necessary to overcome repulsive forces and to wrap the miRNA and PEI polymer around the small MCNPs.[242] It should also be noted that all miRNAs were purchased from Ambion in the pre-miRNA form (~70 nucleotides): Pre-miR miRNA Precursor let-7a (PM10050), Pre-miR miRNA Precursor Negative Control #1 (AM17110), and Cy3 dye-labeled Pre-miR Negative Control #1 (AM17120). After 20 minutes of complex formation at room temperature, 1 uL of 1 mg/mL PEI was added and the samples were incubated for an additional 20 minutes. After the incubation was completed, the samples were once again filtered using a centrifugal filter unit (EMD Millipore, 10,000 MW) to remove excess PEI. To determine the initial concentration of MCNP-PEI that needed to be added to complex 100 nM of miRNA, complexes with increasing concentrations of MCNP-PEI were incubated with 100 nM miRNA. Afterwards, 100 μL of solution was transferred to a 96-well (black-walled, clear-bottom, non-adsorbing) plate. 100 μL of diluted PicoGreen

dye (1:200 dilution in Tris-EDTA (TE) buffer) was added to each well. Following 10 minutes of incubation at room temp, fluorescence measurements were obtained using a M200 Pro Multimode Detector (Tecan USA Inc, NC, USA), at an excitation and emission wavelength of 485 and 535 nm, respectively. Background fluorescence was subtracted by measuring a solution containing only buffer and PicoGreen dye. Similarly, to determine the concentration of NaCl solution used in complexing, complexes were prepared as described above utilizing different concentrations of NaCl solution (40, 80, 120 mM) and the size of the complexes was determined using dynamic light scattering (DLS).

3.4.4. Nanoparticle Complex Characterization

Dynamic light scattering (DLS) and Zeta Potential analyses were performed using a Malvern Instruments Zetasizer Nano ZS-90 instrument (Southboro, MA). Nanoparticle/miRNA complexes (miRNA concentration = 100 nM) were prepared using water. DLS measurements were performed at a 90° scattering angle at room temp. Zeta potential was collected at room temp and the zeta potentials of three sequential measurements were collected.

3.4.5. Preparing the MCNPs for Tumor Targeting

The synthesis of PEI-PEG-iRGD conjugates was described previously and modified by our group.[264] Briefly, iRGD was first dissolved in DMF with excess TEA. NHS-PEG-VS was also dissolved in DMF. Immediately after, the NHS-PEG-VS mixed with iRGD. After incubating at room temp for 2 hours, cold ether was added. Afterwards

the precipitate was dried under a vacuum and it was then dissolved in sodium carbonate (pH = 9) and filtered. Then, iRGD -PEG-VS was mixed with PEI sodium carbonate (pH=9) and incubated overnight at room temp. PEI-g-PEG-iRGD was obtained by dialysis.

3.4.6. Transfection of Cell Lines with MCNP Complexes

Twenty-four hours before the magnetofection of MCNP complexes, 30,000 breast cancer cells were seeded into each well of a 12-well plate (80% confluency). MCNP-PEI/miRNA/PEI complexes were formed as described above. Thereafter the MCNP complexes were mixed with Opti MEM (Life Technologies) and added to each well to attain the desired final concentration of miRNA/well. Subsequently, the cell culture plates were placed on an Nd-Fe-B magnetic plate (OZ Biosciences, France) for 10 minutes (as optimized from previous reports).[67] The culture plates were then placed back into the incubator for 5 hrs and afterwards, the cells were washed with DPBS and fresh growth medium was added. The growth mediums for the cell lines (obtained from ATCC) used in the study are as follows: DMEM supplemented with 10% FBS, and 1% Penicillin-Streptomycin.

3.4.7. Magnetic Hyperthermia

24 hours after the cells were seeded as described above, MCNP-PEI were prepared in Opti MEM (Life Technologies) and added to each well. Following, the cell culture plates were exposed to magnetofection for 10 minutes and then placed back into the incubator for 5 hrs. Afterwards, the cells were washed with DPBS and fresh growth

medium was added. To perform magnetic hyperthermia, 24 hours after transfection, cells were washed with DPBS, trypsinized, and then exposed to an alternating magnetic field (5 kA/m, 225 kHz). Thereafter, fresh media was added to the treated cells, which were then plated back into 12-well plates.

3.4.8. Cell Viability Assays

The cell viability was determined using MTT assay following the standard protocol that was provide by the manufacturer. All measurements were made 48 hrs after initial transfection. All experiments were conducted by averaging triplicates. Absorbance at 490 nm was measured and the control (untreated) cells were normalized as 100% viable.

3.4.9. PCR Analysis

Total RNA was extracted 48 hrs after initial transfection using Trizol Reagent (Life Technologies) and the expression level of mRNA of the target genes (Table 2) were analyzed using quantitative PCR (qPCR). In particular, 1 μg of total RNA was used to generate cDNA using the Superscript III First-Strand Synthesis System (Life Technologies). mRNA expression was then quantified using specific primers for each target mRNA. qPCRs were performed on a StepOnePlus Real-Time PCR System (Applied Biosystems) using SYBR Green PCR Master Mix (Applied Biosystems). The Ct values that were obtained were normalized to GAPDH. Standard cycle conditions were used with a primer melting temperature of 60°C. Primers are listed in Table 2. All primers were obtained from the PrimerBank database.[243]

Table 2. Table of Primers Used for qPCR

	Forward Primer	Reverse Primer
ABCG2	ACGAACGGATTAACAGGGTCA	CTCCAGACACACCACGGAT
BRCA2	CTAATTAACTGTTCAGCCCAGT	CTAGAACATTTCCTCAGAATTGTC
CASP3	AGAACTGGACTGTGGCATTGA	GCTTGTCGGCATACTGTTTCAG
HRAS	GACGTGCCTGTTGGACATC	CTTCACCCGTTTGATCTGCTC
GAPDH	CATGTTCCAATATGATTCCACC	GATGGGATTTCCATTGATGAC
HMGA2	CAGCAGCAAGAACCAACCG	GGTCTTCCCCTGGGTCTCTTA

3.4.10. Animal Studies

6- to 8-week-old BALB/c nude mice were purchased from RaonBio (Kayonggido, Yonginsi, South Korea). For subcutaneous tumor injection, 5.0×10^6 MDA-MB-231 cells were mixed with matrigel and subcutaneously injected in the right and left flanks and right and left shoulders. Treatments were injected either via i.v. injection or through intratumoral injection.

In vivo imaging system (IVIS) spectrum (PerkinElmer, Waltham, MA, USA) was used to monitor the fluorescence emitted from the FITC-labeled MCNPs. For *ex vivo* imaging, the tumors and other organs (heart, kidney, liver, lung, and spleen) were dissected using an IVIS spectrum. The fluorescence images were then analyzed (Living Image software for IVIS Spectrum/200, ver. 4.1, Waltham, MA, USA).

Chapter 4 :

Stem Cell-Based Gene Therapy Activated Using Magnetic Hyperthermia to Enhance the Treatment of Cancer

The text and images used in this chapter have been previously published, at least in part, in Biomaterials as an original manuscript (Yin PT, Shah S, Pasquale NJ, Garbuzenko OB, Minko T, and Lee KB. Biomaterials, 2016. 81: p. 46-57.) and Perry Yin was the first author.

4.1. Introduction

Ovarian cancer currently ranks fifth in cancer mortalities among women and is the leading cause of death from gynecological malignancies.[265] The conventional mode of therapy for this cancer consists of cytoreductive surgery, followed by adjuvant platinum/taxane-based chemotherapy.[266] However, while most ovarian cancer patients exhibit initial sensitivity to chemotherapy, over 70% of these patients are diagnosed at an advanced stage, when the tumors have already metastasized throughout the peritoneal cavity.[267] As a consequence, the majority of ovarian cancer patients experience recurrence within 18-24 months of treatment and only 20% of them survive longer than 5 years after their initial diagnosis.[268]

To enhance the treatment of advanced cancers, such as advanced ovarian cancer, mesenchymal stem cell (MSC)-based therapies have emerged as an attractive alternative that can overcome the limited tumor-targeting ability of conventional treatments.[269] MSCs have the intrinsic ability to self-renew and differentiate into multiple lineages

including osteoblasts, chondrocytes, and adipocytes.[270] More importantly, several groups have demonstrated that these stem cells have the innate ability to migrate to tumors including ovarian tumors/metastases, even following systemic administration.[271] While the exact mechanism is still being elucidated, this tumor tropism has prompted the development of stem cell-based gene therapies, wherein MSCs are genetically engineered to express therapeutic molecules and therefore, act as targeted delivery vehicles to enhance our ability to treat metastatic cancers.[272]

To this end, a number of therapeutic molecules have been investigated, including direct effectors of apoptosis, such as the cytokines, interferon-β (IFN-β)[273] and tumor necrosis factor-related apoptosis inducing ligand (TRAIL),[274] as well as more indirect immunomodulatory molecules like interleukin 12 (IL-12).[275] Of these, TRAIL is a particularly attractive therapeutic candidate owing to its ability to selectively induce apoptosis in cancer cells, but not in most normal cells (**Figure 4.1**).[276] For example, Mueller *et al.* reported that multipotent MSCs that were genetically engineered to express TRAIL were able to induce apoptosis and inhibit the growth of colorectal carcinomas *in vivo* with no serious observable side effects.[277] Similarly, Loebinger and colleagues demonstrated that MSCs engineered to produce and deliver TRAIL could induce apoptosis in lung, breast, squamous, and cervical cancer cells.[274] Importantly, these engineered MSCs were able to significantly reduce tumor growth in a subcutaneous breast cancer xenograft and could home to and reduce lung metastasis. However, while TRAIL has largely been demonstrated to be biocompatible with normal cells, there have been a number of reports indicating potential hepatotoxicity upon treatment with TRAIL, thereby greatly dampening its clinical potential.[176,278] As such, to limit these potentially

detrimental side effects and in order for stem cell therapies to reach their full potential, there remains a pressing need for approaches that can allow for the precise spatiotemporal control of therapeutic gene activation such that the engineered stem cells only express their therapeutic payload once they have reached the targeted tumor sites.

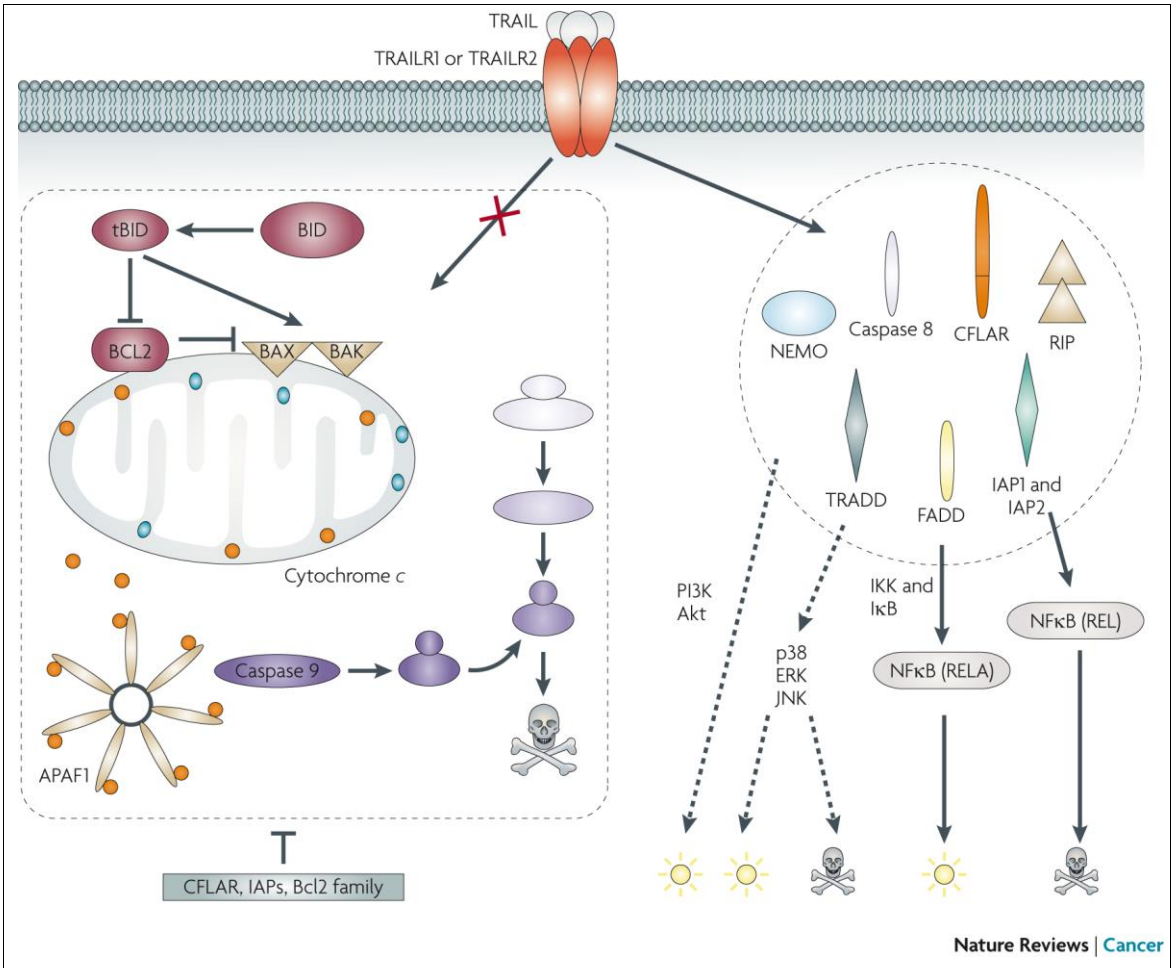

Figure 4.1 Tumor Necrosis Factor-Related Apoptosis Inducing Ligand (TRAIL) Pathway
TRAIL activates the caspase cascade as well as other apoptotic pathways such as PI3K–Akt, NFkappaB, and MAPK pathways. Reproduced with permission.[279] 2008, Nature.

In this chapter, we report the novel application of magnetic core-shell nanoparticles (MCNPs), composed of a highly magnetic zinc-doped iron oxide ($ZnFe_2O_4$) core and a biocompatible mesoporous silica (mSi) shell, for the dual purpose of

delivering and activating a heat-inducible gene vector that encodes a secretable form of TRAIL in MSCs (**Figure 4.2**). For this purpose, we developed a plasmid with the heat shock protein 70B' (HSP70B') promoter (**Figure 4.2B**), which has previously been demonstrated to be more heat-specific than other heat shock promoters.[280] As such, the MSCs can first be engineered with MCNPs that are complexed with the heat-inducible TRAIL plasmid *in vitro*. Afterwards, following *in vivo* injection and migration of the engineered MSCs to the targeted tumor sites, TRAIL expression can be specifically activated via the induction of mild magnetic hyperthermia (~41°C). In this report, we demonstrated the efficient and biocompatible uptake of MCNP-plasmid complexes into MSCs. In particular, we observed that the engineering process had no significant effects on MSC proliferation or differentiation. Moreover, the engineered MSCs retained their tumor tropism towards disseminated peritoneal ovarian cancer xenografts. Importantly, we demonstrated that mild magnetic hyperthermia, via exposure of the engineered MSCs to an alternating magnetic field (AMF), could be used to specifically raise the intracellular temperature to ~41°C, which resulted in the selective expression of TRAIL in the engineered MSCs. As a result, significant ovarian cancer cell apoptosis and death was observed *in vitro* and *in vivo*. Overall, by combining the tumor tropism of MSCs with the spatiotemporal MCNP-based delivery and activation of TRAIL expression, this platform provides an attractive means with which to enhance our control over the activation of stem cell-based gene therapies. Please note that the materials, images, and text that are used in this chapter have been published, at least in part, in Biomaterials as an original manuscript.[281]

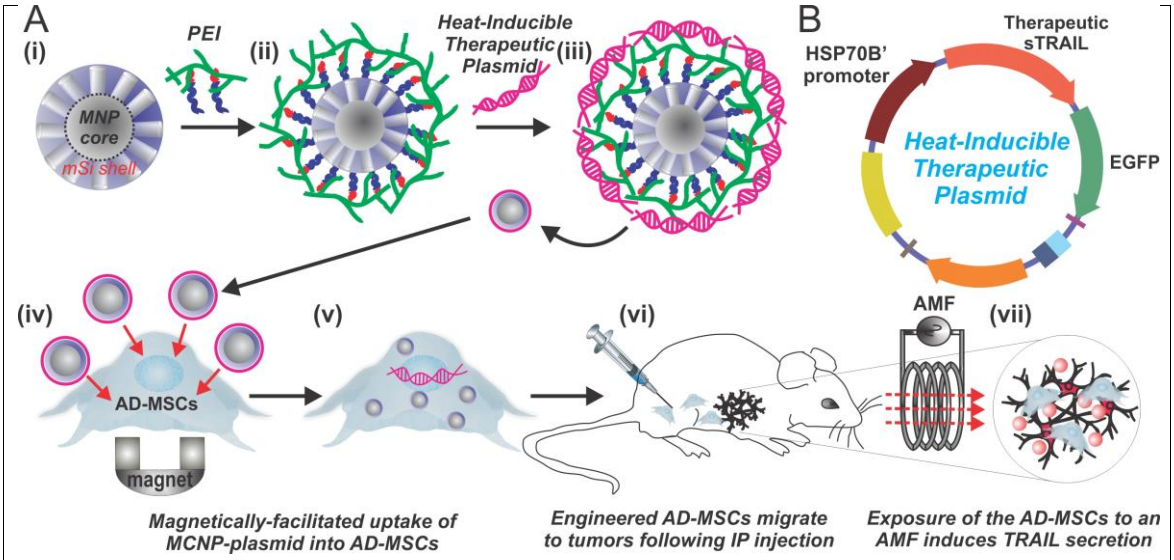

Figure 4.2 Mild Magnetic Hyperthermia-Activated Stem Cell-Based Gene Therapy A) MCNPs composed of a $ZnFe_2O_4$ magnetic nanoparticle (MNP) core and a mesoporous silica (mSi) shell **(i)** are functionalized with polyethyleneimine (PEI) to allow for complexing with a heat-inducible therapeutic plasmid **(iii)**. The MCNPs enhance delivery of the heat-inducible plasmid into the adipose-derived mesenchymal stem cells (AD-MSCs) via magnetically-facilitated uptake **(iv-v)**. These engineered AD-MSCs can then be injected *in vivo* **(vi)**, where they innately home to the tumors/metastases. Finally, mild magnetic hyperthermia, via exposure of the MCNPs to an alternating magnetic field (AMF), can be used to specifically activate the heat-inducible secretion of therapeutic TRAIL from the AD-MSCs **(vii)**. **B)** The heat-inducible plasmid is composed of a HSP70B' promoter and a secreted form of TRAIL (sTRAIL) that is fused to an EGFP reporter.

4.2. Results and Discussion

4.2.1. Synthesis and Characterization of the Magnetic Core-Shell Nanoparticles

For the dual purpose of delivering a heat-inducible therapeutic plasmid to the stem cells as well as spatiotemporally activating the plasmid via mild magnetic hyperthermia, we synthesized MCNPs with a zinc-doped iron oxide ($ZnFe_2O_4$) core. These cores have previously been shown to have a significantly higher saturation magnetization when compared to conventional Fe_2O_3 or Fe_3O_4 magnetic nanoparticles (MNPs).[29] As such, we first synthesized $ZnFe_2O_4$ cores with a doping percentage of $(Zn_{0.4}Fe_{0.6})Fe_2O_4$ via the

thermal decomposition of a mixture of metal precursors (zinc chloride, ferrous chloride, and ferric acetylacetonate) in the presence of oleic acid and oleylamine using a previously reported protocol that was modified by our group.[29,67] Following core synthesis, an inert mSi shell was formed via the condensation of TEOS in the presence of a CTAB micelle template.[252] TEM revealed that the diameter of the cores was 18.93 ± 1.6 nm and that the MNP cores were uniformly coated with a 33.91 ± 3.8 nm thick mSi shell. As a result, the overall diameter of the as-synthesized MCNPs was 88.03 ± 8.22 nm (**Figure 4.3A**). For more detailed characterization, HR-TEM revealed the monocrystalline structure of the MNP cores with a lattice fringe that was measured to be 4.8 Å (**Figure 4.3B**), which is characteristic of the (111) plane of the spinel.[29,67] Finally, FTIR analysis was used to confirm that the CTAB template had been extracted and removed from the pores of the mSi shell (**Figure 4.3C**). In addition, the pores were estimated to be approximately 3 nm in diameter based on HR-TEM (**Figure 4.3D**) as well as previous reports.[252]

To prepare the aforementioned MCNPs for plasmid delivery, the MCNPs were coated with branched polyethylenimine (PEI, MW = 10 kDa) via electrostatic interactions in the presence of NaCl to afford the MCNPs with an overall positive charge. As a result, this would facilitate MCNP complexation with negatively-charged plasmid DNA and induce endosomolysis within the cytoplasm.[254] To minimize cytotoxicity while maximizing transfection efficiency, we used 10 kDa branched PEI, which has previously been demonstrated to be biocompatible with stem cells.[149,255] The resulting water soluble PEI-coated MCNPs (MCNP-PEI) had a hydrodynamic size of 117.2 ± 37 nm

(polydispersity index [PDI] = 0.177) as measured by dynamic light scattering (DLS) and a zeta potential of +44.23 ± 0.72 mV (**Figure 4.4**).

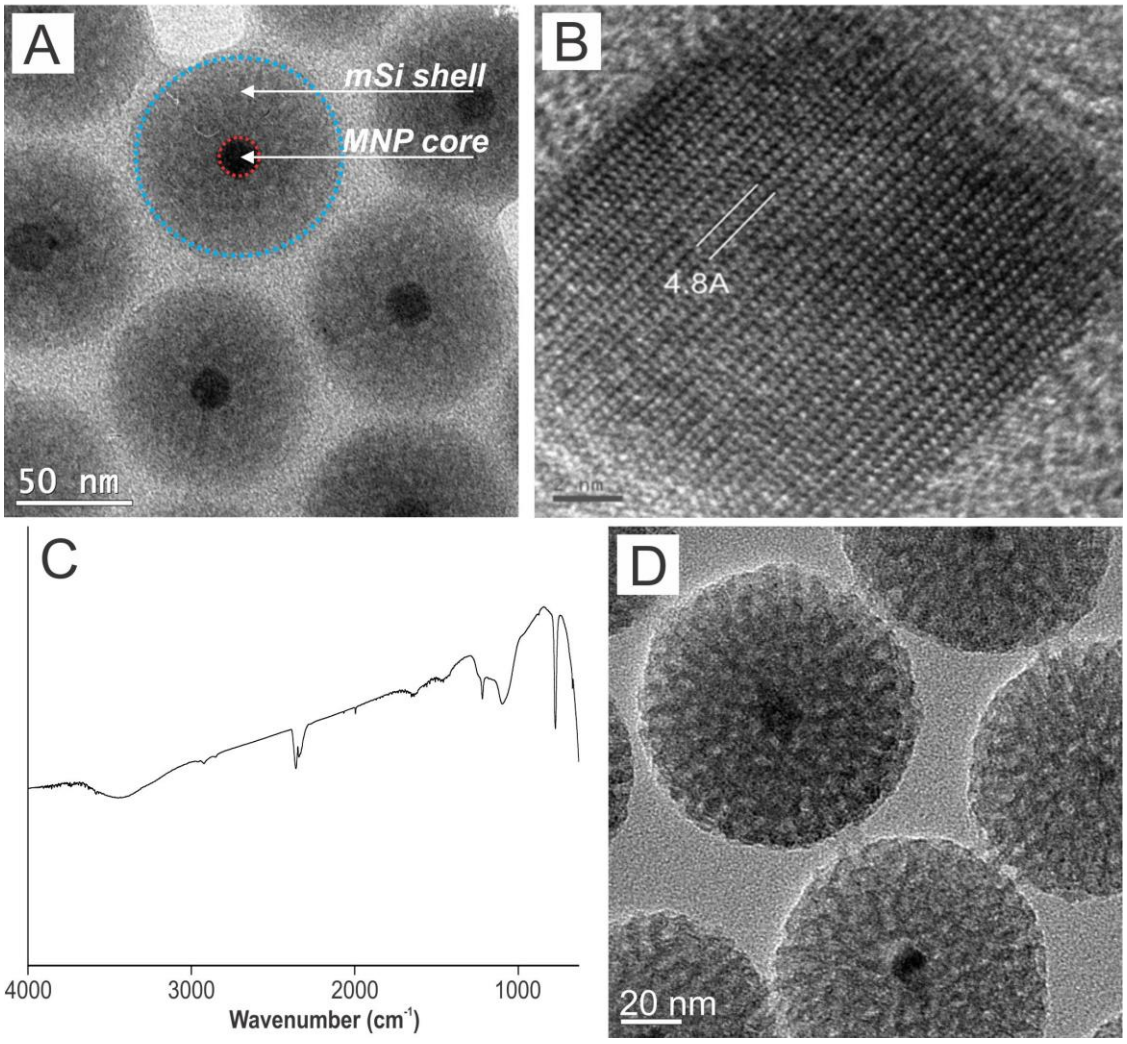

Figure 4.3 Characterization of the MCNPs
A) HR-TEM image of the MCNPs. **B)** HR-TEM revealed the monocrystalline structure of the MNP cores with a lattice fringe that was measured to be 4.8Å, which is characteristic of the (111) planes of the spinel. Scale bar = 2 nm. **C)** Fourier-transform infrared spectra (FTIR) analysis was carried out to confirm the complete removal of CTAB. CTAB typically shows two intense peaks at 2,800–3,200 cm^{-1}, which correspond to the symmetric (2,849 cm^{-1}) and asymmetric (2,918 cm^{-1}) stretching vibrations of the methylene chains. These peaks were absent from the MCNPs, indicating the complete removal of CTAB from the MCNPs. **D)** Higher magnification HR-TEM image of the MCNPs shows that the pores are about 3 nm in size.

A

	Size (nm)	Zeta Potential (mV)
MCNP	88.03±8.2	-
MCNP-PEI	117.2±37	+44.23±0.72
MCNP-PEI/Plasmid	197.5±38	+17.8±5.11

B

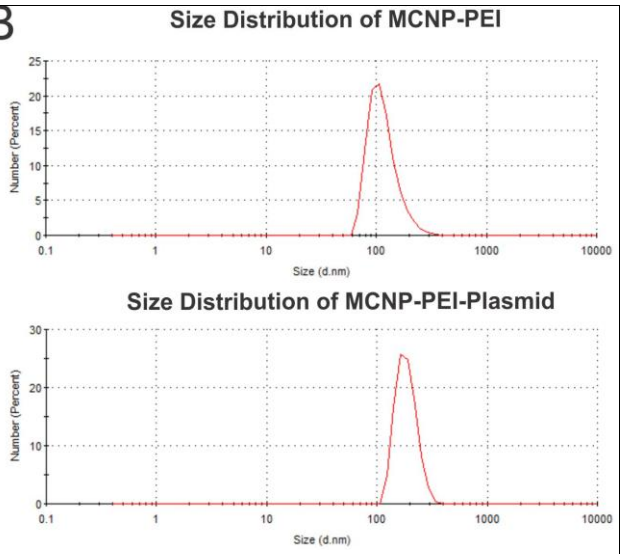

Figure 4.4 Characterization of the MCNP-PEI
A) Size was determined using TEM and dynamic light scattering (DLS). Moreover, the Zeta potential was confirmed. The values in the chart are given as mean ± standard deviation. **B)** Size distribution of the MCNP-PEI and MCNP-PEI/plasmid complexes as determined using DLS.

Finally, the MCNPs were characterized by a specific absorption rate (SAR) of 564 W/g, which was determined using an AMF with an amplitude of 5 kA/m and a frequency of 225 kHz. This SAR is consistent with data reported in the literature for similar $ZnFe_2O_4$ MNPs.[149,226] Moreover, we demonstrated that these MCNPs (25 µg/mL) could reach temperatures as high as 47°C within an hour of exposure to the AMF (**Figure 4.5A**) and that we could maintain a mild hyperthermia temperature of 41-43°C following periodic exposure to the AMF (5 minutes on, 5 minutes off, **Figure 4.5B**). As such, we were able to synthesize monodisperse water-soluble MCNPs with a narrow size distribution and, more importantly, these MCNPs had excellent magnetic properties for magnetic hyperthermia even after the addition of an mSi shell.

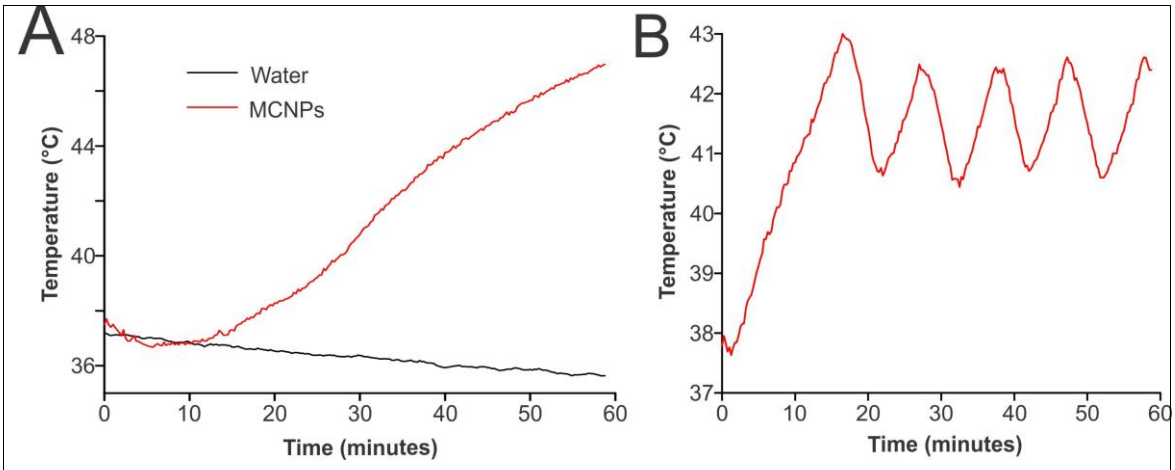

Figure 4.5 MCNP-Based Magnetic Hyperthermia
A) The MCNPs (25 µg/mL) can be heated to temperatures as high as 47°C after exposure to an alternating magnetic field (5 kA/m, 225 kHz) for one hour. **B)** By initially exposing 50 µg/mL of MCNP to an alternating magnetic field (AMF, 5 kA/m) for 20 minutes, a temperature of 43°C can be reached. Afterwards, if the AMF is periodically turned on and off (5 minutes on, 5 minutes off), an average temperature of approximately 41.5°C can be achieved and maintained.

4.2.2. Heat-Inducible Plasmid Construction.

Next, in order to attain control over the secretion of TRAIL from the engineered stem cells using mild magnetic hyperthermia, we constructed a heat-inducible TRAIL plasmid using the HSP70B' promoter (HSP-sTRAIL plasmid, **Figure 4.6A**). To this end, we first cloned the recombinant gene that encodes a secreted form of the human TRAIL protein into the pEGFNP-N1 backbone (Clonetech), thereby creating a secretable TRAIL-EGFP fusion that was constitutively active due to its CMV promoter (sTRAIL-EGFP plasmid, **Figure 4.6A(i)**). Specifically, this recombinant TRAIL gene was composed of the soluble form of the human Flt3L gene (hFlex) at its 5' end and the human TRAIL gene at its 3' end with an isoleucine zipper at the N-terminal of TRAIL, which was previously shown to significantly enhance the trimerization of the fusion protein as well as its anti-tumor activity.[282] Following insertion of the recombinant

TRAIL gene into pEGFP-N1, the CMV promoter of the resultant sTRAIL-EGFP plasmid was replaced with a HSP70B' promoter (**Figure 4.6A(ii)**) to enable strict remote control of gene expression using MCNP-mediated mild magnetic hyperthermia, thereby forming the final HSP-sTRAIL plasmid construct. In particular, the human HSP70B' promoter has previously been shown to exhibit highly specific heat inducibility with low background activity when compared to other heat shock promoters (e.g. HSP70),[283] which can be activated by a number of stresses besides heat (e.g. heavy metal-induced oxidative stress).[280] To confirm the successful construction of the plasmid, all steps were evaluated via restriction enzyme analysis and DNA sequencing (data not shown).

Following plasmid construction, we determined whether the recombinant plasmids could produce the TRAIL protein. For this purpose, we performed a simple proof-of-concept study by delivering the constitutively active sTRAIL-EGFP plasmid into A2780 ovarian cancer cells. About 48 hours after initial transfection, total RNA was collected and reverse transcription PCR (RT-PCR) was performed (**Figure 4.6B**). From these results, we confirmed that TRAIL is produced, whereas it is not present in control samples, which consisted of cells that had been transfected with an EGFP plasmid. Lastly, we confirmed that heat could be used to specifically induce TRAIL expression in cells transfected with the HSP-sTRAIL plasmid. For this purpose, 24 hours after initial transfection, the cells were subjected to mild hyperthermia (41°C) for one hour via exposure to a water bath. Then, 48 hours after initial transfection, fluorescence microscopy images of the cells transfected with the heat-inducible HSP-sTRAIL plasmid with and without exposure to mild hyperthermia were taken to visualize the expression of the TRAIL-EGFP fusion (**Figure 4.6C**). These images clearly demonstrate that

engineered cells only express EGFP when exposed to mild hyperthermia. As confirmation, RNA was also collected from samples with and without exposure to mild hyperthermia. qPCR analysis of these samples demonstrated that following mild hyperthermia at 41°C for one hour, TRAIL expression was significantly increased (3-fold, $p < 0.05$) compared to samples that were not exposed to mild hyperthermia (**Figure 4.6D**). Altogether, these results confirm that the constructed HSP-sTRAIL plasmid can induce the expression of TRAIL in a heat-specific manner.

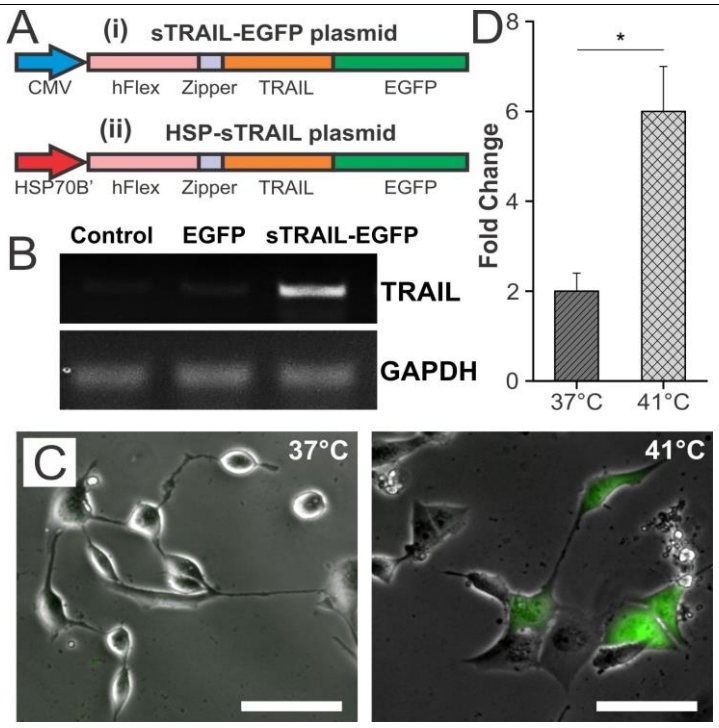

Figure 4.6 Characterization of the Heat-Inducible Plasmid
A) Schematic depicting the sTRAIL-EGFP plasmid (i), which expresses a sTRAIL-EGFP fusion that is constitutively activate, and the HSP-sTRAIL plasmid (ii), which expresses the same sTRAIL-EGFP fusion under the control of a heat-inducible HSP70B' promoter. **B)** RT-PCR demonstrating the successful synthesis of the sTRAIL-EGFP plasmid, which was transfected into A2780 ovarian cancer cells. **C)** Proof-of-concept demonstrating that the HSP-sTRAIL plasmid can be specifically activated by heat (1 hour at 41°C in a water bath) as seen via fluorescence imaging due to fusion of TRAIL with EGFP. Scale bar = 50 µm. **D)** Confirmation of heat-specific TRAIL activation was obtained using qPCR (*$p < 0.05$) and was normalized to transfected cells that were incubated at 37°C. GAPDH was used as the housekeeping gene.

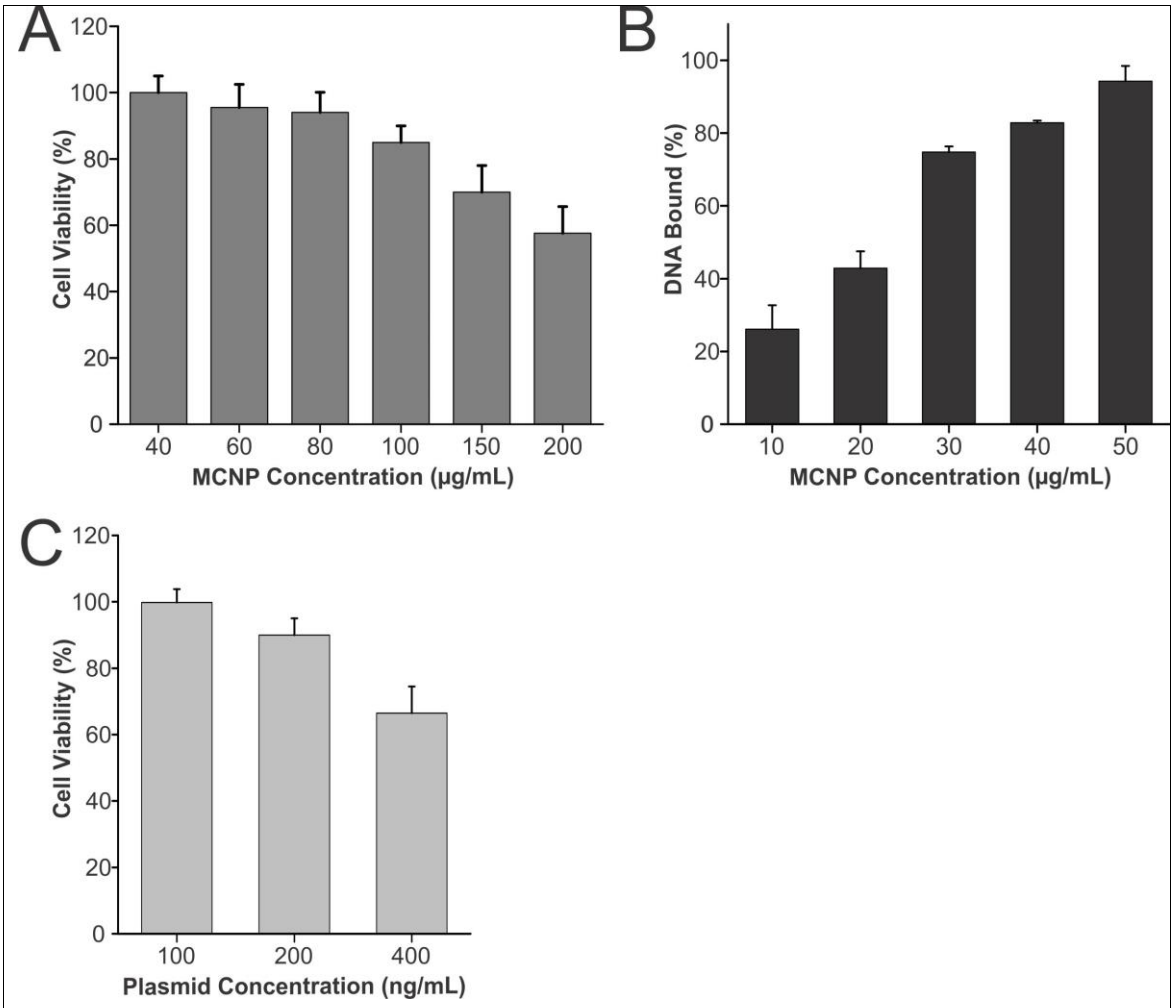

Figure 4.7 Biocompatibility of the MCNP-PEI/Plasmid Complexes
A) Increasing concentrations of MCNP-PEI were delivered to A2780 ovarian cancer cells and delivery was enhanced using magnetofection (10 min). The MCNP complexes were well tolerated by the cells as determined via MTS assay 48 hours after transfection even at concentrations as high as 100 µg/mL. **B)** Picogreen assay was used to determine that 50 µg/mL of MCNP-PEI could complex all of the 200 ng/mL of plasmid. **C)** To determine the maximal concentration of plasmid that can be delivered, we complexed 50 µg/mL of MCNP-PEI with increasing concentrations of plasmid. In particular, we confirmed that 200 ng/mL was optimal for use with the remainder of our studies.

4.2.3. Engineering MSCs with the MCNP-PEI/Plasmid Complexes.

Following plasmid construction and initial proof-of-concept studies, we sought to optimize the MCNP-based transfection into stem cells. For this purpose, we engineered adipose-derived MSCs (AD-MSCs) with our MCNP-PEI/plasmid complexes as AD-

MSCs represent a readily available source of adult stem cells that have the ability to differentiate into multiple lineages.[103b] Before engineering the AD-MSCs, we initially transfected the AD-MSCs with MCNP-PEI alone to determine the optimal concentration of MCNP-PEI that can be delivered while minimizing cytotoxicity. We observed that the delivery of MCNP-PEI alone had minimal cytotoxicity even at concentration as high as 100 μg/mL (~85% cell viability 48 hours after transfection, **Figure 4.7A**). As such, we used 50 μg/mL for future steps as this concentration induced almost no cytotoxicity (~95% cell viability) while also exhibiting robust heating capabilities. Next, to complex the PEI-coated MCNPs with the HSP-sTRAIL plasmid, we mixed the two components together and incubated them at room temperature for 20 minutes. Final characterization of these MCNP-PEI/plasmid complexes demonstrated that the size of the MCNP-PEI/plasmid complexes, as measured by DLS, increased to a final diameter of 197.5 ± 38 nm (PDI = 0.410) and retained a positive zeta potential of +17.8 ± 5.11 mV (**Figure 4.4C**).

Subsequently, to engineer the AD-MSCs with our MCNP-PEI/plasmid complexes, we delivered MCNP-PEI/plasmid complexes wherein 50 μg/mL of MCNP were complexed with increasing concentrations of HSP-sTRAIL plasmid to determine the maximal amount of plasmid that could be delivered with our MCNPs without significantly affecting AD-MSC viability. From this optimization process, we determined that a plasmid concentration of 200 ng/mL was optimal. Moreover, it was found that this amount of plasmid could be completely complexed using 50 μg/mL of MCNP as determined via Picogreen assay, which is a dye that binds to free double-stranded DNA (**Figure 4.7B**). Using the optimized complexing and transfection conditions, the AD-

MSCs maintained a cell viability of ~90% following the engineering process (**Figure 4.7C**). To characterize the affect that engineering had on AD-MSC proliferation in more detail, we performed immunocytochemistry for Ki-67 (**Figure 4.8A**), which is a mitotic marker that is expressed during all phases of the cell cycle except during G_0. It was observed that approximately 20% of the AD-MSCS expressed Ki-67 and that there was no statistically significant difference between the number of Ki-67 expressing engineered AD-MSCs and unengineered AD-MSC controls (**Figure 4.8B**).

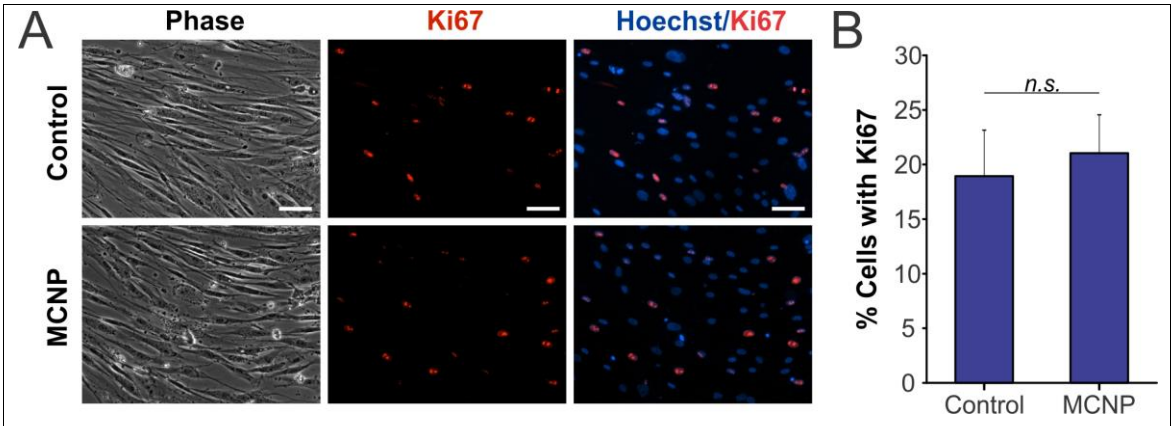

Figure 4.8 Proliferation of AD-MSCs Engineered with MCNP-PEI/Plasmid Complexes
A) The proliferation of unengineered (control) and engineered (MCNP-PEI/plasmid) AD-MSCs was evaluated using Ki-67 (red). The nuclei were stained with Hoechst (blue). Scale bar = 50 µm. **B)** Approximately 20% of the AD-MSCS expressed Ki-67 and there was no statistically significant difference between the two groups ($p > 0.05$).

4.2.4. Characterizing the Engineered AD-MSCs.

After engineering the AD-MSCs with MCNP-PEI/plasmid complexes, we next sought to determine whether the act of engineering the AD-MSCs negatively affected their ability to differentiate and, more importantly, to migrate to cancers *in vivo*. AD-MSCs are multipotent cells that have been shown to readily differentiate along osteogenic, chondrogenic, and adipogenic lineages. Therefore, to confirm that the process

of engineering did not compromise the ability of the AD-MSCs to differentiate, we compared the ability of engineered and unengineered control AD-MSCS to differentiate along an osteogenic lineage. Briefly, to induce differentiation along this lineage, the engineered or unengineered AD-MSCs were exposed to osteogenic differentiation media for three weeks.[284] After this differentiation period, osteogenic differentiation was quantified via Alizarin Red S (ARS) staining, which is typically used to evaluate calcium deposited by cells in culture, and qPCR. ARS staining revealed calcium-rich deposits in both engineered and unengineered osteogenic AD-MSCs (**Figure 4.9A**). Quantification suggested that the osteogenic differentiation capability was unaffected by the act of engineering as there was no statistically significant difference between the quantity of calcium deposited by engineered AD-MSCs and unengineered AD-MSC controls (**Figure 4.9B**). Further confirming these results, we performed qPCR on key osteogenic genes including osteonectin (ON), bone alkaline phosphate (BAP), osteocalcin (OCN), and osteopontin (OPN). As expected, all four genes were highly expressed when normalized to non-differentiated control AD-MSCs (**Figure 4.9C**) and no significant difference was found between the engineered osteogenic AD-MSCs and the unengineered osteogenic AD-MSCs.

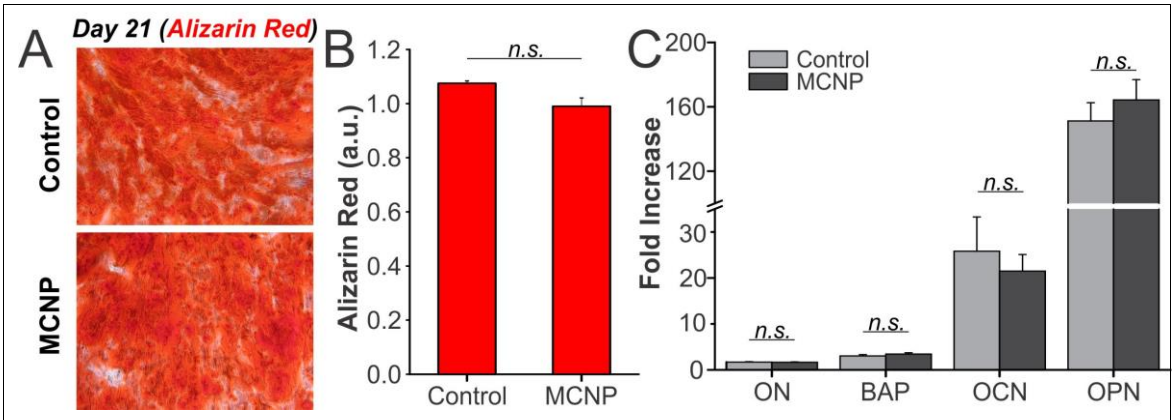

Figure 4.9 Differentiation of AD-MSCs Engineered with MCNP-PEI/Plasmid Complexes
A) To evaluate osteogenic differentiation, engineered or unengineered AD-MSCs were differentiated for three weeks. Osteogenesis was then quantified via Alizarin Red staining. **B)** Quantification of staining suggested that there was no statistically significant difference between the two groups ($p > 0.05$). **C)** qPCR of key osteogenic genes demonstrated that all four genes were highly expressed over non-differentiated control and that no significant difference was found between the engineered and unengineered AD-MSCs ($p > 0.05$). GAPDH was used as the housekeeping gene.

Next, we confirmed that the act of engineering the AD-MSCs did not negatively affect their ability to migrate to ovarian tumors *in vivo* (**Figure 4.10A**). To this end, we established a metastatic model of ovarian cancer wherein two million A2780 ovarian cancer cells were injected intraperitoneally (i.p.) into female nude mice (**Figure 4.10A(i)**). To confirm that the engineered AD-MSCs could co-localize with ovarian tumors, the mice, which had disseminated peritoneal A2780 tumors, were injected with half a million engineered AD-MSCs or unengineered AD-MSC controls i.p. at 7 days post-tumor implantation (**Figure 4.10A(ii)**). Mice were then harvested after an additional 7 days (**Figure 4.10A(iii)**). Multimodality imaging was used to identify the various components; luciferase was used to identify the A2780 ovarian cancer cells (**Figure 4.10B**) and a lipophilic DiD dye was used to label the engineered and unengineered AD-MSCs. From **Figure 4.10C and Figure** 4.10**D**, it can be observed that, after the tumors

were collected (week 3), the DiD-labeled engineered AD-MSCs (**Figure 4.10C**) co-localized with the luciferase labeled A2780 cells (**Figure 4.10D**) within one week of AD-MSC injection (**Figure 4.11**). Importantly, it can be seen that there was no significant difference between the co-localization of engineered AD-MSCs and unengineered AD-MSC controls. As such, these results suggest that the engineered AD-MSCs can act as an effective delivery vehicle for gene therapy.

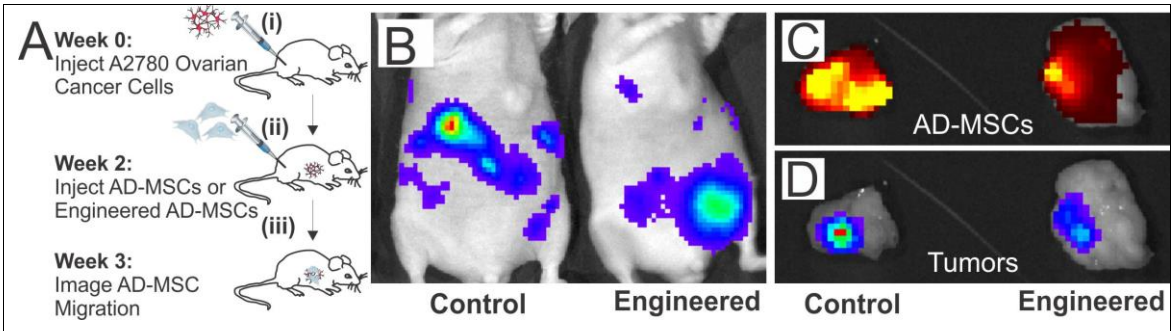

Figure 4.10 Migration of AD-MSCs Engineered with MCNP-PEI/Plasmid Complexes
A) Timeline of the studies used to evaluate the tumor homing ability of the engineered and unengineered AD-MSCs. **B)** Luciferase was used to identify the A2780 cells. Luminescence imaging shows the establishment of disseminated A2780 tumors. The luminescence intensity goes from blue to red, wherein blue is the weakest and red is the strongest. **C)** One week after the injection of AD-MSCs, tumors were collected. Fluorescence imaging shows the DiD-labeled engineered and unengineered AD-MSCs. The fluorescence intensity goes from dark red to yellow, wherein dark red is the weakest and yellow is the strongest. **D)** Luminescence imaging of the conglomerated tumors demonstrates that the AD-MSCs are able to colocalize with the tumors.

4.2.5. Mild Magnetic Hyperthermia-Activated TRAIL Expression from AD-MSCs Can Effectively Induce Apoptosis in Ovarian Cancer Cells.

Previous studies have demonstrated that TRAIL-expressing MSCs can induce cancer cell apoptosis and decrease the development of tumors and metastases *in vivo*.[274] In these experiments, the TRAIL expression was either constitutively active or conditionally activated with the addition of doxycycline. However, while TRAIL is

largely biocompatible with normal cells, as mentioned previously, there have been reports demonstrating potential hepatotoxicity in preclinical models when treated with recombinant TRAIL.[176,278]

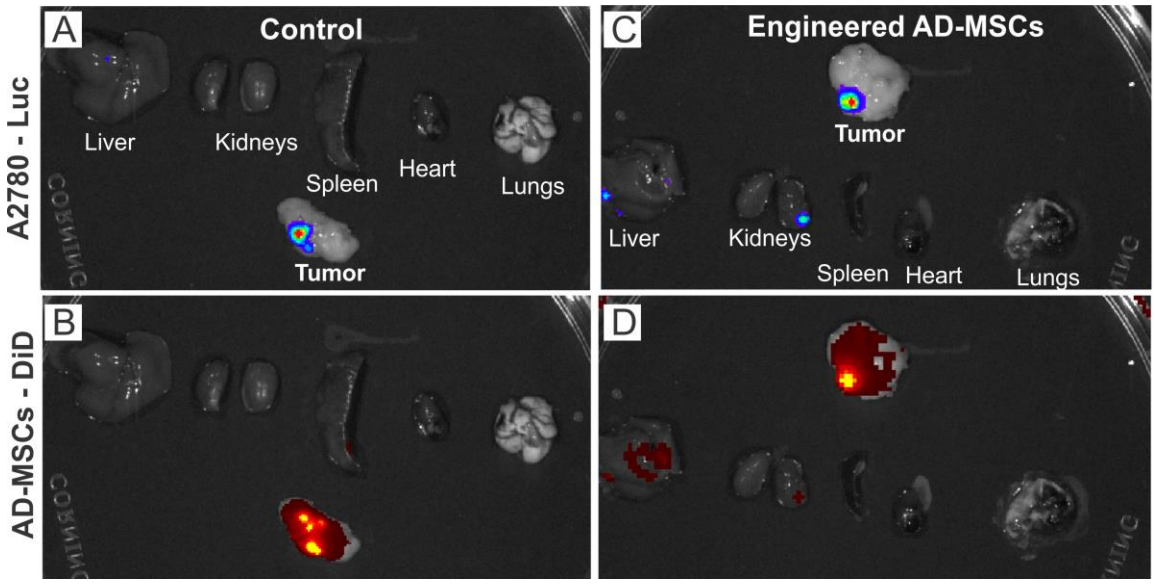

Figure 4.11 Tumor Homing of the Engineered and Unengineered AD-MSCs
1 week after the injection of engineered or unengineered AD-MSCs, animals were sacrificed and organs and tumors were collected. **A)** Luminescence image showing A2780 ovarian cancer cells. **B)** Fluorescence image showing co-localization of DiD-labeled unengineered AD-MSCs controls with the tumors and not in other organs. **C)** Luminescence image showing A2780 ovarian cancer cells. **D)** Fluorescence image showing co-localization of DiD-labeled engineered AD-MSCs controls with the tumors and not in other organs.

Addressing this major limitation, we engineered AD-MSCs with MCNP-PEI/plasmid complexes, where the plasmid was the heat-inducible HSP-sTRAIL, in order to gain spatiotemporal control over therapeutic gene expression. Having already determined that mild hyperthermia (induced using a water bath) could be used to activate this plasmid, we next sought to induce TRAIL expression from the engineered AD-MSCs using mild magnetic hyperthermia, which can be induced remotely and non-invasively by

exposing the engineered AD-MSCs to an AMF. To this end, we employed the experimental design illustrated in **Figure 4.12A**. In particular, 24 hours after transfection of the AD-MSCs with MCNP-PEI/plasmid complexes, we exposed the cells to an AMF (same conditions as described previously) to maintain a temperature of approximately 41°C for one hour (**Figure 4.12B**). About 72 hours after initial transfection, we collected the conditioned media from the engineered AD-MSCs, which contains TRAIL that was secreted from the engineered AD-MSCs, and added it (60:40 ratio with normal A2780 growth media) to the A2780 ovarian cancer cells. Following an additional incubation of 48 hours, its therapeutic efficacy was evaluated. Importantly, our first observation was that mild magnetic hyperthermia alone did not significantly affect AD-MSC viability, which agrees with previously published results on the effects of heat on stem cell viability (**Figure 4.12C**).[285] In terms of its therapeutic efficacy, A2780 ovarian cancer cells treated with conditioned media from the engineered AD-MSCs that were exposed to mild magnetic hyperthermia showed a remarkable decrease in cell viability (40% decrease) when compared to those treated with conditioned media from engineered AD-MSCs controls that had not been exposed to mild magnetic hyperthermia (**Figure 4.12D**).

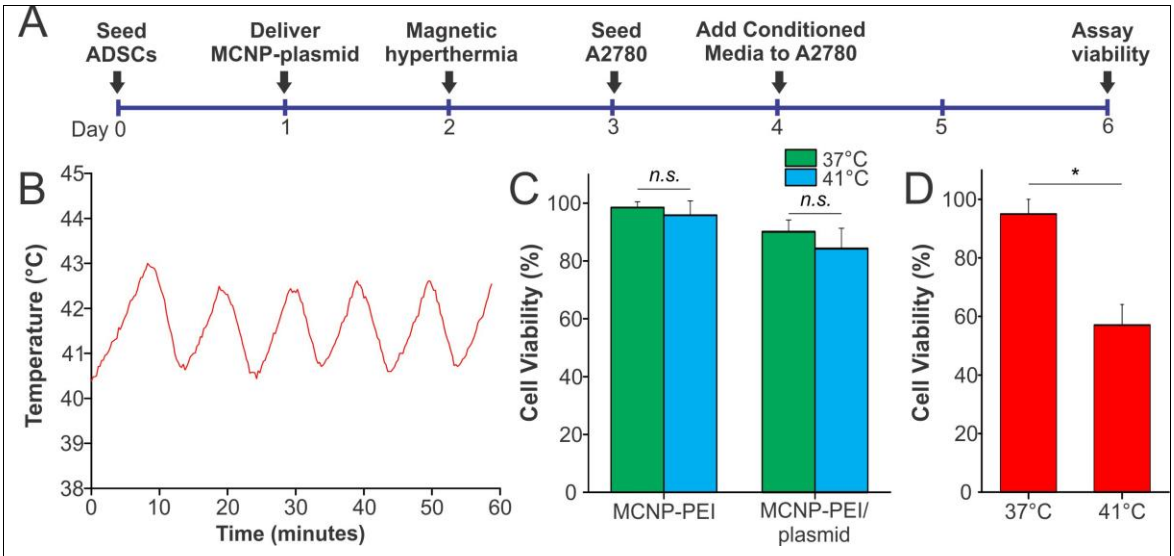

Figure 4.12 Engineered AD-MSCs Can Effectively Induce Apoptosis When Exposed to Heat

A) Timeline of the *in vitro* study. **B)** Mild magnetic hyperthermia with an average temperature of 41.5°C was maintained for one hour by periodically exposing the engineered AD-MSCs to an AMF (5 minutes on, 5 minutes off). **C)** Mild magnetic hyperthermia alone did not significantly affect AD-MSC viability. Moreover, the process of engineering the AD-MSCs with MCNP-PEI/plasmid complexes did not significantly affect cell viability. **D)** To test therapeutic efficacy, A2780 ovarian cancer cells were treated with conditioned media from the engineered AD-MSCs that were exposed to mild magnetic hyperthermia. A2780 cells showed a remarkable decrease in cell viability when compared to those treated with conditioned media from engineered AD-MSCs that had not been exposed to mild magnetic.

To confirm that this loss in viability was a function of the mild magnetic hyperthermia-activated secretion of TRAIL from the engineered AD-MSCs, the underlying mechanism was explored. It is well-established that TRAIL primarily induces apoptosis by binding to death receptor 4 (DR4) and death receptor 5 (DR5), which we confirmed to be expressed in A2780 ovarian cancer cells via qPCR (**Figure 4.13A**).[279] As such, we first investigated the contribution of the death receptors to the observed decrease in cell viability by treating the A2780 cells with monoclonal antibodies blocking DR4 and/or DR5 selectively prior to exposure to conditioned media from the engineered AD-MSCs that were exposed to mild magnetic hyperthermia. We found that blocking DR4

alone (82.7% cell viability), DR5 alone (75.7% cell viability), and both DR4 and DR5 (87.7% cell viability) were able to abrogate the effect of the conditioned media (**Figure 4.13B**). This agrees with our qPCR (**Figure 4.13A**) and previous results from the literature,[286] which show/state that DR4 is expressed at higher levels than DR5. Moreover, upon immunodepletion of TRAIL from conditioned media of engineered AD-MSCs that were exposed to mild magnetic hyperthermia using magnetic nanoparticles functionalized with anti-TRAIL antibody, it was observed that the apoptotic effect of the AD-MSC conditioned media was reversed (90.1% cell viability). Next, as it has been reported that TRAIL acts primarily through the activation of caspase-8 and subsequent activation of caspase-3,[287] we confirmed that A2780 ovarian cancer cells that have been exposed to conditioned media from the engineered AD-MSCs that were exposed to mild magnetic hyperthermia exhibited significant activation of caspases when compared to those treated with conditioned media from engineered AD-MSCs controls that had not been exposed to mild magnetic hyperthermia (**Figure 4.13C**). Lastly, we demonstrated that specific inhibition of caspase-8 (85.2% cell viability) and non-specific inhibition of caspases (97.9% cell viability) were able to neutralize the effect of the conditioned media (**Figure 4.13D**). As such, these results confirm that the observed decrease in A2780 cell viability is due to the mild magnetic hyperthermia-activated secretion of TRAIL from the engineered AD-MSCs.

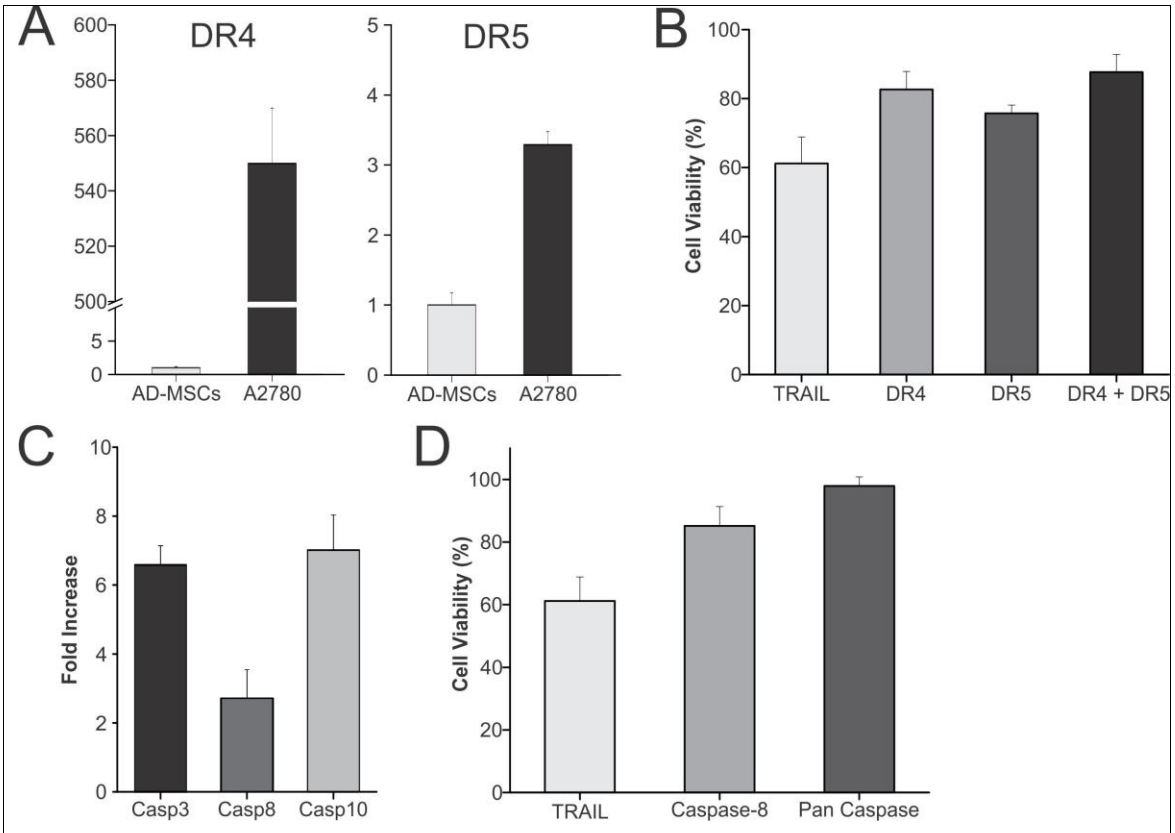

Figure 4.13 Mechanistic Studies
A) qPCR shows that DR4 and DR5 are both innately expressed at much higher levels in A2780 ovarian cancer cells as compared to AD-MSCs. The results were normalized to AD-MSCs. GAPDH was used as the housekeeping gene. **B)** Blocking DR4 and/or DR5 with monoclonal antibodies could reverse the apoptotic effect of mild magnetic hyperthermia-activated secretion of TRAIL from the engineered AD-MSCs on A2780 cells. A2780 cell viability was measured 24 hours after treatment. **C)** To confirm the mechanism of action, qPCR for caspases, which are downstream of TRAIL, was performed. **D)** Inhibition of caspase-8 and non-specific inhibition of caspases could also neutralize the effect of mild magnetic hyperthermia-activated secretion of TRAIL from the engineered AD-MSCs on A2780 cells. A2780 cell viability was again measured 24 hours after treatment.

Finally, we have also conducted *in vivo* studies, wherein engineered AD-MSCs were delivered into a metastatic ovarian cancer mouse model via i.p. injection. Our results suggest that engineered AD-MSCs, which secrete TRAIL, are efficacious and can significantly decrease tumor volume when compared to unengineered AD-MSC controls as well as treatment with a single dose of recombinant TRAIL (5 mg/kg via i.p. injection)

over a two-week period (**Figure 4.14A**). Specifically, we found that even after a single dose of half a million engineered AD-MSCS (sTRAIL-EGFP plasmid), the overall tumor volume, as measured by luminescence intensity, decreased by over 50% (**Figure 4.14B**). On the other hand, treatment with a single dose of recombinant TRAIL (5 mg/kg) did not decrease tumor size. Instead, the size of the tumor in mice that were treated with a single dose of recombinant TRAIL remained nearly constant over the two-week period. This agrees with previous reports from the literature as recombinant TRAIL is limited by its short half-life. As such, treatment with recombinant TRAIL typically requires high doses (1 – 10 mg/kg) that are injected daily.[288]

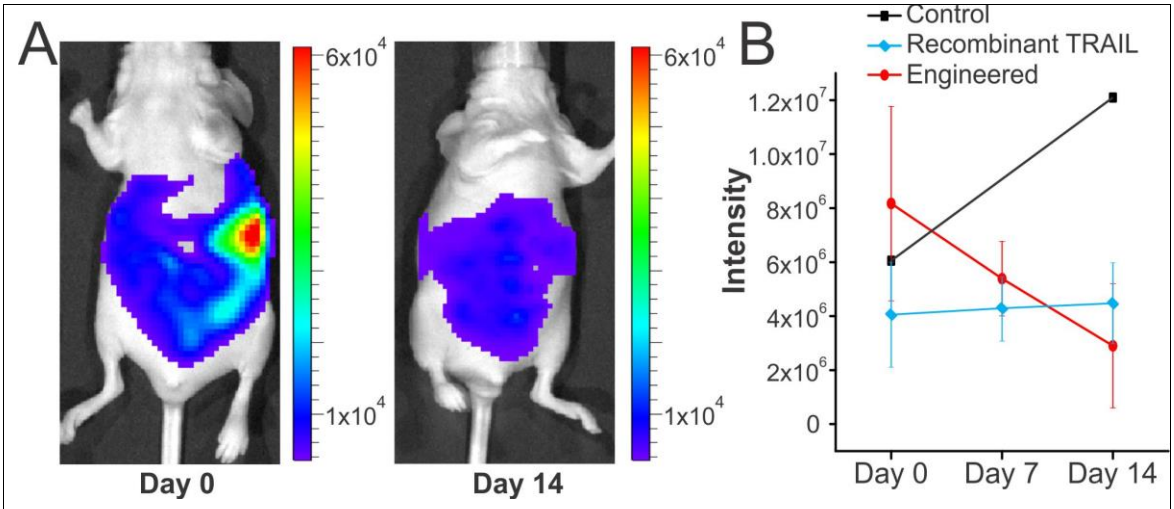

Figure 4.14 *In Vivo* Efficacy of the Engineered AD-MSCs.
A) To evaluate *in vivo* efficacy, we injected half a million AD-MSCS engineered with MCNP-PEI/plasmid complex, wherein the plasmid was sTRAIL-EGFP. Unengineered AD-MSCs and a single dose of recombinant TRAIL (5 mg/kg) were injected as controls. Tumor volume was followed over two weeks, we found that the size of the tumors decreased significantly (max value at day 0 was 6 x 10^4 whereas the max value on day 14 was 8 x 10^3) when treated with the engineered AD-MSCs. **B)** Quantification of luminescence intensity shows that the engineered AD-MSCs are significantly better than treatment with a single dose of recombinant TRAIL.

4.3. Conclusions

In this work, a stimuli-responsive stem cell-based gene therapy was developed to enhance the treatment of ovarian cancer. In particular, MCNPs were used for the dual purpose of delivering a heat-inducible plasmid encoding TRAIL and remotely activating TRAIL secretion in the engineered AD-MSCs via mild magnetic hyperthermia. As such, by combining the tumor tropism of the AD-MSCs with the spatiotemporal MCNP-based delivery and activation of TRAIL expression, this platform provides an attractive means with which to enhance our control over the activation of stem cell-based gene therapies. Importantly, we demonstrated that the process of engineering the AD-MSCs did not significantly affect their innate proliferation, differentiation, and tumor homing capabilities. Moreover, mild magnetic hyperthermia resulted in the selective expression of TRAIL in the engineered MSCs, thereby inducing significant ovarian cancer cell apoptosis and death *in vitro* and *in vivo*.

Previous studies have demonstrated that mild hyperthermia can be used to activate genes.[289] However, these reports have primarily focused on simple proof-of-concept studies wherein reporter genes were activated in cancer cells. For instance, Ortner *et al*. used iron oxide nanoparticles to deliver a heat-inducible luciferase or GFP plasmid to Human embryonic kidney 293 (HEK293) cells.[289b] In particular, they demonstrated that they could regulate reporter gene expression *in vitro* using magnetic hyperthermia. On the other hand, Yamaguchi *et al*. demonstrated a heat-inducible system for cancer treatment, wherein magnetic nanoparticles were used to deliver a heat-inducible plasmid encoding tumor necrosis factor alpha (TNF-α).[289a] In this case, these magnetic nanoparticle-plasmid complexes were delivered directly to the human lung

adenocarcinoma cells (A549) in order to induce apoptosis of the lung adenocarcinoma cells. Using this system, the authors were able to control the expression of TNF-α in the transfected cancer cells both *in vitro* and *in vivo* using magnetic hyperthermia, thereby demonstrating a local and effective cancer therapy.

While promising, these previous demonstrations are still plagued by the difficulty of actually delivering the magnetic nanoparticles and plasmids to the tumor *in vivo*. As such, they would be unable to target cancers in distinct parts of the body where the cancer has metastasized and, as a result, would be extremely difficult to translate to the clinic. Moreover, the cell lines used in these previous studies are relatively easy to transfect. Addressing these challenges, we have demonstrated an advanced heat-activated gene therapies in this report, wherein we engineered stem cells in order to take advantage of their innate tumor targeting ability. In particular, we are the first to report the use of mild magnetic hyperthermia to remotely activate a heat-inducible gene in stem cells. In the future, we envision that the biocompatible mSi shell of the MCNP can be filled with chemotherapy in order to enhance the effect of TRAIL. For instance, while the delivery of TRAIL has already been shown to be effective against cancer cells that have acquired resistance to conventional chemotherapy via p53 inactivation, tumor cells have also developed a number of mechanisms with which to escape TRAIL-induced apoptosis.[265] To this end, numerous studies have identified novel combinations that could be used with TRAIL to enhance its therapeutic efficacy. For instance, Kelly *et al*. has demonstrated that the pretreatment of prostate cancer cells with doxorubicin can increase their sensitivity to TRAIL.[290]

In conclusion, we have successfully combined synthetic biology with nanotechnology, wherein mild magnetic hyperthermia was used to specifically activate genes in stem cells. Owing to the great potential of stem cells, the implications of this study go well beyond cancer applications, and can potentially be used for a host of applications that range from the stimuli-guided differentiation of stem cells for the treatment of injuries such as spinal cord or traumatic brain injury to other diseases such as those involving inflammation, wherein stem cells can be engineered to conditionally secrete anti-inflammatory molecules. As such, we have demonstrated a stimuli-responsive stem cell-based gene therapy using multifunctional MCNPs, which could have great potential for both cancer and other regenerative applications.

4.4. Materials and Methods

4.4.1. Nanoparticle Synthesis and Characterization

The synthesis of $ZnFe_2O_4$ magnetic nanoparticles (MNPs) has previously been reported and modified by our group.[29,67,149,153,261] Briefly, 1.35 mmol, 0.3 mmol, and 0.7 mmol of $Fe(acac)_3$, $ZnCl_2$, and $FeCl_2$, respectively, were mixed into a round bottom flask with 20 mL of tri-n-octylamine, 6 mmol of both oleic acid and oleylamine, and 10 mmol of 1,2 hexadecanediol. The reaction mixture was then heated up to 200°C for 2 hrs. From here, the mixture was heated to 305°C for 2 hrs and the nanoparticles were purified by repeatedly washing with ethanol.

To coat the MNP cores with a mSi shell, a modified procedure from what was reported by Hyeon *et al.* was used.[252] 5 mg of the alkyl-capped MNP cores dispersed in chloroform were sonicated using a probe type sonicator in a 0.1 M aqueous

cetyltrimethylammonium bromide (CTAB) solution. Upon evaporation of chloroform, the CTAB capped MNP cores were diluted to 50 mL with water and the pH of this mixture was adjusted to ~ 11 using a 2M NaOH solution. This reaction mixture was heated to 70°C and, under vigorous stirring, 0.4 mL of tetraethylorthosilicate (TEOS) in 2.4 mL of ethyl acetate was added. After the addition of TEOS, the reaction was allowed to continue for 4 hrs. The MCNPs were collected and washed several times with ethanol. To remove the template, the nanoparticles were heated to 60°C in an ammonium nitrate solution. The extracted MCNPs were again washed with ethanol. Finally, the MCNPs were characterized by high-resolution Transmission electron microscopy (HR-TEM) and Fourier-transform infrared spectra (FTIR).

To characterize the magnetic properties of the nanoparticles, the resulting MCNPs (25 µg/mL in H_2O) were exposed to an AMF (5 kA/m, 225 kHz) using a solid-state induction heating system (Superior Induction Company) for one hour. The temperature of the solution was monitored using a fiber optic temperature probe (LumaSense Technologies). To calculate the specific absorption rate (SAR), the following equation was used:

$$SAR\ (W/g)\ = C\left(\frac{dT}{dt}\right)\left(\frac{m_s}{m_m}\right)$$

where C is the specific heat capacity, m_s is the mass of the solution, m_m is the mass of the magnetic nanoparticles, T is the temperature, and t is the time.[262]

4.4.2 Construction of the Plasmids

To construct the plasmids, we first cloned the recombinant gene that encodes a secreted form of the human TRAIL protein into the pEGFNP-N1 backbone (Clonetech)

thereby creating a secretable TRAIL-EGFP fusion that is constitutively active (e.g. via CMV promoter) to allow for monitoring (sTRAIL-EGFP plasmid). In particular, the secreted form of TRAIL was kindly provided by Drs. Leaf Huang (Department of Biomedical Engineering, University of North Carolina at Chapel Hill) and Yukai He (Cancer Center, Georgia Health Sciences University).[282] This recombinant TRAIL gene (sTRAIL) was composed of the soluble form of the human Flt3L gene (hFlex) at the 5' end and the human TRAIL gene at the 3' end (aa residues 95-281) with an isoleucine zipper at the N-terminal of TRAIL, which was previously shown to significantly enhance trimerization of the fusion protein as well as its anti-tumor activity.[282] As such, the cDNA for sTRAIL was amplified using PCR by employing the 5' and 3' primers 5'-CGGCCGCTCGAGATGACAGTGCTGGCGCCA-3' and 5'-CGCCGCAAGCTTTTAGCCAACTAAAAAGGC-3', respectively. In this way, the 5' end of the PCR product contained the XhoI restriction site and the 3' end of the PCR product contained the HindIII site. This 1 kb PCR product was digested with XhoI/HindIII and then cloned into pEGFNP-N1 to create the sTRAIL-EGFP fusion. The plasmid was denoted sTRAIL-EGFP. Similarly, HSP70B' was ordered from Addgene (Plasmid #19486).[291] The cDNA for the HSP70B' promoter was amplified using PCR by employing the 5' and 3' primers 5'-GACAATTAATACCATGCAGGCCCCACGGGAGCT-3' and 5'-CGGCGCTCGAGTCAATCAACCTCCTCAATGA-3', respectively. In this way, the 5' end of the PCR product contained the AseI restriction site and the 3' end of the PCR product contained the XhoI site. This 200 bp PCR product was digested with AseI/XhoI and then cloned into the sTRAIL-EGFP plasmid thereby creating the final HSP-sTRAIL

plasmid. The open reading frames of the fusion proteins were confirmed by DNA sequencing (Macrogen).

4.4.3 Formation of MCNP-PEI/Plasmid Complexes

To prepare the aforementioned MCNPs for plasmid delivery, the negatively charged MCNPs were coated with a branched cationic polymer, polyethyleneimine (PEI), which affords the MNPs with an overall positive charge. PEI is a polymer that is partially protonated under physiological conditions, thus allowing for the formation of complexes in the presence of nucleic acids.[228] PEIs have been used extensively for the delivery of plasmids and nucleic acids including small interfering RNAs (siRNAs) and microRNAs.[228-229] Specifically, it has been demonstrated that PEI-based complexes are able to enter the cell through caveolae- or clathrin-dependent routes and are able to facilitate release from the endosome with high efficiency via the "proton sponge effect."[230]

To obtain PEI-coated MCNPs, the MCNPs, dispersed in a minimal amount of ethanol, were added to a stirring solution containing excess PEI (MW=25,000; Mn=10,000) and 20 mM NaCl. This PEI molecular weight (MW) and structure was chosen based on previous reports.[241] After spinning overnight, the PEI-coated MCNPs were filtered (EMD Millipore, 10,000 MW). To complex the PEI coated MCNPs with plasmid, MCNP-PEI were diluted in a 20 mM NaCl solution and plasmid was added to the solution. Complexing was allowed to occur for 20 minutes.

To determine the initial concentration of MCNP-PEI that needed to be added to complex 200 ng/mL of plasmid, complexes with increasing concentrations of MCNP-PEI

were incubated with 200 ng/mL of plasmid. Afterwards, 100 μL of solution was transferred to a 96-well (black-walled, clear-bottom, non-adsorbing) plate. 100 μL of diluted PicoGreen dye (1:200 dilution in Tris-EDTA (TE) buffer) was added to each well. Following 10 minutes of incubation at room temp, fluorescence measurements were obtained using a M200 Pro Multimode Detector (Tecan USA Inc, NC, USA), at an excitation and emission wavelength of 485 and 535 nm, respectively. Background fluorescence was subtracted by measuring a solution containing only buffer and PicoGreen dye.

Dynamic light scattering (DLS) and Zeta Potential analyses were performed using a Malvern Instruments Zetasizer Nano ZS-90 instrument (Southboro, MA). Nanoparticle/miRNA complexes (miRNA concentration = 100 nM) were prepared using water. DLS measurements were performed at a 90° scattering angle at room temp. Zeta potential was collected at room temp and the zeta potentials of three sequential measurements were collected.

4.4.4. Transfecting Cells with MCNP-PEI/Plasmid Complexes

Twenty-four hours before the magnetofection of MCNP complexes, A2780 ovarian cancer (ATCC) or human adipose-derived mesenchymal stem cells (AD-MSCs from Lonza [catalog # PT-5006]) were seeded into each well of a 12-well plate (80% confluency). MNP-PEI/plasmid complexes were formed as described above. Thereafter, the MCNP complexes were mixed with Opti MEM (Life Technologies) and added to each well to attain the desired final concentration of plasmid/well. Subsequently, the cell culture plates were placed on a static Nd-Fe-B magnetic plate (OZ Biosciences, France)

for 10 minutes (as optimized from previous reports).[67] The culture plates were then placed back into the incubator for 5 hrs and afterwards, the cells were washed with DPBS and fresh growth medium was added. The growth mediums for the cell lines (obtained from ATCC or Lonza) used in the study are as follows: A2780 (DMEM supplemented with 10% FBS, 1% Penicillin-Streptomycin, and 1% Glutamax) and AD-MSCs (Lonza ADSC Basal Medium [Catalog # PT-3273] with ADSC-GM SQ kit [Catalog # PT-4503]).

4.4.5. Magnetic Hyperthermia

Twenty-four hours after transfection, cells were washed with DPBS, trypsinized, and exposed to an AMF (5 kA/m, 225 kHz). In particular, to achieve a constant temperature of ~41℃, the cells were initially exposed to an AMF for 20 minutes to achieve a temperature of ~43 ℃. Afterwards, the cells were periodically exposed to the AMF (5 minutes on, 5 minutes off) to maintain the temperature at ~41℃. Finally, fresh growth media was added to the treated cells and they were plated back into 12-well plates.

4.4.6. Cell Viability Assays

The cell viability was determined using MTT assay following the standard protocol that was provide by the manufacturer. All measurements were made 48 hrs after initial transfection. All experiments were conducted by averaging triplicates. Absorbance at 490 nm was measured and the control (untreated) cells were normalized as 100% viable.

4.4.7. Mild Magnetic Hyperthermia-Activated TRAIL Expression from AD-MSCs to Induce Apoptosis in Ovarian Cancer Cells.

24 hours after the transfection of AD-MSCs with MCNP-PEI/plasmid complexes (50 μg/mL MCNP, 200 ng/mL of plasmid), we exposed the cells to an AMF (same conditions as described previously) to maintain a temperature of approximately 41℃ for one hour. About 72 hours after initial transfection, we collected the conditioned media from the engineered AD-MSCs, which contains TRAIL that was secreted from the engineered AD-MSCs, and added it (60:40 ratio with normal A2780 growth media) to the A2780 ovarian cancer cells. Following an additional incubation of 48 hours, its therapeutic efficacy was evaluated using MTT assay.

4.4.8. Cell Differentiation

To confirm that the MSCs could still differentiate, we performed osteogenic differentiation. To this end, AD-MSCs were incubated in CEM until they were confluent. Afterwards, osteogenic differentiation medium was then added (IMDM supplemented with 9 % FBS, 9 % HS, 2 mM L-glutamine, 100 U/mL penicillin, 100 μg/mL streptomycin, 50 ng/mL L-thyroxine (Sigma Aldrich), 20 mM β-glycerol phosphate, (Sigma Aldrich), 100 nM dexamethansone (Sigma Aldrich), and 50 μM ascorbic acid (Sigma Aldrich)). This medium was changed every 3-4 days. After 21 days of differentiation, cells were fixed in 10% formalin, rinsed with DPBS and Alizarin Red S assay was used to assess calcium deposition. In particular, DPBS was removed and the Alizarin Red solution (40mM, pH 4.2) was added to each well and kept for 30 min with

gentle shaking. The pH of the Alizarin Red solution was carefully adjusted using a pH meter (Accumet Basic, AB15, Fisher Scientific, USA). The solution was then removed and cells were washed with DI water five times. Following, the calcium-stained cells were imaged using an optical microscope (Eclipse Ti-U, Nikon, Japan). To quantitative these results, cells were destained using 10% cetylpyridinium chloride (CPC) in 10 mM sodiumphosphate (pH 7.0) for 30 minutes at room temperature. Finally, the concentration Alizarin Red S was determined by measuring its absorbance at 562 nm on a multiplate reader (Tecan, Switzerland).

4.4.9. Immunocytochemistry

Cell cultures were fixed with 4% formaldehyde (ThermoScientific) for 15 min, blocked for 1 hr with 5% normal goat serum (NGS, Life Technologies), and permeabilized with 0.3% Triton X-100 when staining for intracellular markers (Ki-67). The primary antibody for Ki-67 (1:400, Cell Signaling, catalog # 9449S) was incubated overnight at 4°C. Alexa Fluor 546-conjugated secondary antibodies were used to detect the primary antibodies (1:200, Molecular Probes) and Hoechst 33342 (1:100, Life Technologies) was used as a nuclear counterstain. The substrates were mounted on glass slides using ProLong® Gold antifade (Life Technologies) and were then imaged using a Nikon TE2000 Fluorescence Microscope.

4.4.10. PCR Analysis

Total RNA was extracted 48 hrs after initial transfection using Trizol Reagent (Life Technologies) and the expression level of mRNA of the target genes (Table 3) were

analyzed using quantitative PCR (qPCR). In particular, 1 μg of total RNA was used to generate cDNA using the Superscript III First-Strand Synthesis System (Life Technologies). mRNA expression was then quantified using specific primers for each target mRNA. qPCRs were performed on a StepOnePlus Real-Time PCR System (Applied Biosystems) using SYBR Green PCR Master Mix (Applied Biosystems). The Ct values that were obtained were normalized to GAPDH. Standard cycle conditions were used with a primer melting temperature of 60°C. Primers are listed in Table 3. All primers were obtained from the PrimerBank database.[243]

Table 3. Table of Primers Used for qPCR.

	Forward Primer	Reverse Primer
GAPDH	CATGTTCCAATATGATTCCACC	GATGGGATTTCCATTGATGAC
DR4	GCGGGGAGGATTGAACCAC	CGACGACAAACTTGAAGGTCTT
DR5	GCCCCACAACAAAAGAGGTC	AGGTCATTCCAGTGAGTGCTA
CASP3	AGAACTGGACTGTGGCATTGA	GCTTGTCGGCATACTGTTTCAG
CASP8	CATCCAGTCACTTTGCCAGA	GCATCTGTTTCCCCATGTTT
CASP10	GCTTCCCAAAACTGAAATGACC	CCTTGATACGACTCGGCTTCC

4.4.11. Mechanistic Studies

For the blocking experiments, A2780 ovarian cancer cells were incubated in growth medium containing 10 ug/mL of the respective blocking antibodies for 1 hour before the addition of conditioned media from the engineered AD-MSCs (60:40 ratio with normal A2780 growth media). In particular, mouse monoclonal TRAIL-R1/DR4 (Enzo Life Sciences) and mouse monoclonal TRAIL-R2/DR5 (Enzo Life Sciences) antibodies were used for these experiments. Cell viability was then evaluated 24 hrs after the addition of conditioned media using MTT assay.

To inhibit caspases, the pan-caspase inhibitor, Z-VAD-FMK (Enzo Life Sciences), and the caspase-8 inhibitor, Z-IETD-FMK (Enzo Life Sciences), were used. For Z-VAD-FMK, a 10 mM stock solution of the inhibitor was prepared using DMSO and the final concentration of the inhibitor and DMSO that the A2780 ovarian cancer cells were exposed to was 20 µM and 0.1%, respectively. For Z-IETD-FMK, a 10 mM stock solution of the inhibitor was prepared using DMSO and the final concentration of the inhibitor and DMSO that the A2780 ovarian cancer cells were exposed to was 2 µM and 0.1%, respectively. The A2780 ovarian cancer cells were treated with the inhibitors at the same time as the addition of the conditioned media (60:40 ratio with normal A2780 growth media). Cell viability was then evaluated 24 hrs after the addition of conditioned media and inhibitors using MTT assay.

For TRAIL immunoprecipitation, MCNPS were conjugated with TRAIL monoclonal antibodies (Santa Cruz Biotechnology). For this purpose, the MCNPs were first functionalized with primary amines via the grafting of aminopropyltriethoxysilane (APTES). This was performed by refluxing up to 50 mg of MCNPs in 40 mL of toluene with 20 uL of APTES overnight under dry conditions. The resulting amine-functionalized MCNPs were then washed several times with ethanol and resupended in DMF. The TRAIL antibody (30 uL of 0.1 mg/mL solution) was activated with EDC/NHS coupling in 250 uL of DMF. Then, 1 mg of MCNPs dispersed in 250 uL of DMF was added to the activated TRAIL antibody and allowed to stir overnight. The resulting particles were washed several times with water and finally resuspended in DPBS. To perform MCNP-based immunoprecipitations, 200 µl of the antibody-conjugated MCNPs (1 mg/mL) was added to 500 µl of conditioned media and incubated on ice for 30 min. To separate the

nanoparticles from the conditioned media, a magnet was placed on the side of the tube for 5 minutes and the supernatant was carefully collected and transferred to a new tube. The supernatant was then added to A2780 cells (60:40 ratio with normal A2780 growth media) and cell viability was evaluated 24 hrs later using MTT assay.

4.4.12. Animal Studies

Human ovarian cancer cells (A2780) expressing the luciferase enzyme were purchased from Cell Biolabs, Inc (San Diego, CA). The cells were cultured in DMEM with L-glutamine (Lonza, Walkersvile, MD) supplemented with 10% fetal bovine serum (Invitrogen, Carlsbad, CA), and 1% penicillin-streptomycin (Gibco, Grand Island, NY).

6-8 weeks old Athymic nu/nu mice (NCRNU-M, CrTac: NCr-Foxn1nu) were obtained from Taconic (Hudson, NY, USA). All of the mice were maintained in cages under pathogen-free conditions in the animal facilities of Rutgers, The State University of New Jersey and the research has been reviewed and approved by the Institutional Animal Care and Use Committee. Orthotopic (intraperitoneal) ovarian cancer model was created by intraperitoneally injecting 2 x 10^6 ovarian cancer cells (A2780) labeled with luciferase into the mice. Luciferase transfected cancer cells were visualized using an IVIS system (Xenogen, Alameda, CA). To this end, Luciferin (150 mg/kg) was administered intraperitoneally 10 min prior to imaging. For imaging, mice were anesthetized with isoflurane (4% initially and 1–2% for maintenance) using a XGI-8 Gas Anesthesia System (Xenogen, Alameda, CA) as previously described.[292]

After allowing up to 2 weeks for the tumors to develop, AD-MSCs were administered. For AD-MSC injection, AD-MSCs were engineered with MCNP-

PEI/plasmid complexes as described above. 24 hours after transfection, Vybrant DiD Cell-labeling solution was used (Molecular Probes, Catalog # V-22887) to label the cells prior to administration to animals. Specifically, staining media was prepared by adding 5 µL of the supplied DiD solution for every 1 mL of normal growth media required. The media from the engineered or unengineered AD-MSCs were then removed and replaced with staining media. AD-MSCs were incubated with staining media for 30 minutes. Afterwards, the labeled AD-MSCs were washed three times with DPBS, trypsinized, and then resuspended such that there were 5×10^5 cells per 300 µL DPBS. As such, each animal received an intraperitoneal injection of 5×10^5 cells in 300 µL of DPBS. As a control, a single dose of 200 µL (5 mg/kg) of recombinant TRAIL (ProSpec) in DPBS was injected intraperitoneally on day 0. Tumor volume of all animals was then monitored over two weeks by monitoring tumor luminescence. Please note that each group in each experiment had at least three mice.

Chapter 5 :

Conclusions and Perspectives

Parts of the text used in this chapter have been previously published, at least in part, in Small as an original manuscript (Yin PT, Shah BP, Lee KB. Small, 2014. 10(20): p. 4106-12.) and Perry Yin was the first author.

As can be seen from the earlier chapters, nanotechnology, and especially MNPs, have tremendous potential for use in various biomedical applications such as for the treatment of cancer. Previous biomedical demonstrations using MNPs have focused on their use as MRI contrast agents, magnetic hyperthermia agents, as well as for cancer drug delivery, wherein an exterior magnetic field can be used to enhance uptake/targeting of the MNPs. This thesis has demonstrated a few examples wherein multimodal or multifunctional MNPs were developed for combined therapies to overcome the major limitations that exist with current treatments – namely, their lack of tumor tropism and the existence of chemoresistance. In particular, as a summary, MNPs offer a number of advantages, which we have demonstrated in this thesis. First, the use of MNPs allows for the enhancement of transfection using magnetofection as well as magnetic targeting. Second, MNPs can be used for the delivery of multiple therapeutics (e.g. small molecule drugs, nucleic acids). Third, MNPs provide a powerful platform for the induction of heat, which can not only be used directly for the treatment of cancer but can also be used to manipulate gene expression in stem cells. Fourth, though it was not shown in this work, treatment can potentially be monitored via magnetic resonance imaging (MRI) owing to

the use of MNPs. To conclude this thesis, a brief summary of each chapter will be presented below.

In chapter 2, we successfully demonstrated the effective MNP-based delivery of miRNA to cancer cells as well as the novel combined MNP-based miRNA and magnetic hyperthermia therapy to enhance apoptosis in brain cancer cells. As mentioned previously, to maximize the therapeutic effects of hyperthermia, a number of therapeutics have been developed to target HSP-mediated pathways including the HSP70 and HSP90 inhibitor, bortezimab[208] and geldanamycin, which targets HSP90.[209] While promising, each individual of the HSP family (e.g. HSP27, HSP70, HSP72, HSP90) has numerous subsequent targets.[207b] As such, we sought to deliver a miRNA (let-7a), which simultaneously targets multiple key downstream effectors of HSPs on a MNP platform that also acts as an excellent magnetic hyperthermia agent to enhance apoptosis in brain cancer cells. The results indicate that combined MNP-based let-7a delivery and magnetic hyperthermia showed an additive effect resulting in significantly more apoptosis in brain cancer cells than either let-7a treatment or magnetic hyperthermia alone. Moreover, our results suggest that the targeting of pathways such as IGF1R and RAS by let-7a may lead to an increase in caspase-3 mediated apoptosis.

In chapter 3, we have successfully demonstrated that the novel combination of DOX and microRNA can act as a potent therapy for breast cancer. For this purpose, we developed MCNPs consisting of a highly magnetic core and a biocompatible mesoporous silica shell. As such, DOX could be loaded in the pores of the mesoporous silica shell while let-7a microRNA was complexed on the surface through electrostatic interaction. We found that treatment of triple-negative breast cancer cells (e.g. MDA-MB-231) with

our combination therapy resulted in a synergistic decrease in cell viability, wherein 100 µg/mL of this combination therapy decreased the cell viability by over 90%, which is significantly greater than either treatment modality alone. Moreover, from our preliminary analysis of the underlying mechanism, we believe that this unique combination acts primarily through the down-regulation of drug efflux pumps, DNA repair mechanisms, and tumor proliferation. In particular, let-7a microRNA has the ability to simultaneous down-regulate multiple gene targets, including members of the RAS family, HMGA2, ABCG2, and BRCA2. As a result, this sensitizes triple-negative breast cancer cells to the slow release of DOX from the pores of our MCNPs.

In chapter 4, a stimuli-responsive stem cell-based gene therapy was developed to enhance the treatment of ovarian cancer and overcome challenges with tumor targeting. In particular, MCNPs were used for the dual purpose of delivering a heat-inducible plasmid encoding TRAIL and remotely activating TRAIL secretion in the engineered AD-MSCs via mild magnetic hyperthermia. As such, by combining the tumor tropism of the AD-MSCs with the spatiotemporal MCNP-based delivery and activation of TRAIL expression, this platform provides an attractive means with which to enhance our control over the activation of stem cell-based gene therapies. Importantly, we demonstrated that the process of engineering the AD-MSCs did not significantly affect their innate proliferation, differentiation, and tumor homing capabilities. Moreover, mild magnetic hyperthermia resulted in the selective expression of TRAIL in the engineered MSCs, thereby inducing significant ovarian cancer cell apoptosis and death *in vitro* and *in vivo*.

We believe the treatment strategies that were developed in this work can significantly enhance the treatment of cancer. In particular, as it is well known that

cancers are heterogeneous, treatment strategies must be multimodal in nature. To this end, based on the studies in Chapters 2 and 3 we envision that as we gain a better understanding of the underlying mechanisms of cancer as well as the biology of microRNAs, we can choose cancer-specific microRNAs that can be used to enhance the treatment of cancers and even cancer stem cells either by itself or in combination with conventional therapies. Moreover, the application of hyperthermia and magnetic targeting can be used to not only enhance the effect of microRNA but also to sensitize cancers to conventional small molecule drugs thereby overcoming chemoresistance. As for the study performed in Chapter 4, this technology provides a truly novel platform that has vast potential. While the focus of Chapter 4 was on the development of a vehicle that can home to tumors for cancer therapy (e.g. TRAIL delivery), the therapeutic molecule can be replaced with any gene. Moreover, the promoter can be replaced for use with other stimuli (e.g. light). As such, this stem cell-based stimuli-responsive gene expression system can be applied not only to cancer but also to various other application such as spinal cord injury, where NSCs can be injected into the body, innately migrate to the site of injury, and be induced to differentiate into neurons or oligodendrocytes (e.g. via an external stimuli) only once the NSCs have reached the site of injury.

In conclusion, this work develops two approaches using multifunctional MNPs to overcome chemoresistance and enhance tumor tropism. Importantly, this work has the potential of being extended to clinical applications on its own or in combination with the other therapeutic strategies that are currently being employed. As such, I hope that the research I have conducted in this thesis helps to advance the use of MNPs toward the

clinic and further the fields of nanotechnology and nanomedicine for the treatment of solid tumors.

References

(1) Davis, M. E.; Chen, Z. G.; Shin, D. M. *Nature reviews. Drug discovery* **2008**, *7*, 771.

(2) Roduner, E. *Chemical Society reviews* **2006**, *35*, 583.

(3) (a) Mulder, W. J.; Strijkers, G. J.; van Tilborg, G. A.; Griffioen, A. W.; Nicolay, K. *NMR in biomedicine* **2006**, *19*, 142(b) Li, W. J.; Szoka, F. C. *Pharm Res* **2007**, *24*, 438.

(4) Kumari, A.; Yadav, S. K.; Yadav, S. C. *Colloids and surfaces. B, Biointerfaces* **2010**, *75*, 1.

(5) Mody, V. V.; Siwale, R.; Singh, A.; Mody, H. R. *Journal of pharmacy & bioallied sciences* **2010**, *2*, 282.

(6) Yin, P. T.; Shah, S.; Chhowalla, M.; Lee, K. B. *Chemical reviews* **2015**, *115*, 2483.

(7) Kango, S.; Kalia, S.; Celli, A.; Njuguna, J.; Habibi, Y.; Kumar, R. *Prog Polym Sci* **2013**, *38*, 1232.

(8) Brown, J. M.; Giaccia, A. J. *Cancer research* **1998**, *58*, 1408.

(9) Danhier, F.; Feron, O.; Preat, V. *J Control Release* **2010**, *148*, 135.

(10) (a) Wang, R. B.; Billone, P. S.; Mullett, W. M. *Journal of Nanomaterials* **2013**(b) Rink, J. S.; Plebanek, M. P.; Tripathy, S.; Thaxton, C. S. *Curr Opin Oncol* **2013**, *25*, 646.

(11) Venturoli, D.; Rippe, B. *Am J Physiol-Renal* **2005**, *288*, F605.

(12) Tanaka, T.; Shiramoto, S.; Miyashita, M.; Fujishima, Y.; Kaneo, Y. *Int J Pharm* **2004**, *277*, 39.

(13) Nomura, T.; Koreeda, N.; Yamashita, F.; Takakura, Y.; Hashida, M. *Pharm Res* **1998**, *15*, 128.

(14) Hu-Lieskovan, S.; Heidel, J. D.; Bartlett, D. W.; Davis, M. E.; Triche, T. J. *Cancer research* **2005**, *65*, 8984.

(15) Bazak, R.; Houri, M.; El Achy, S.; Kamel, S.; Refaat, T. *J Cancer Res Clin* **2015**, *141*, 769.

(16) Steegmann-Olmedillas, J. L. *Clin Transl Oncol* **2011**, *13*, 71.

(17) Knop, K.; Hoogenboom, R.; Fischer, D.; Schubert, U. S. *Angew Chem Int Edit* **2010**, *49*, 6288.

(18) Huang, C.; Neoh, K. G.; Wang, L. A.; Kang, E. T.; Shuter, B. *J Mater Chem* **2010**, *20*, 8512.

(19) (a) Banobre-Lopez, M.; Teijeiro, A.; Rivas, J. *Reports of practical oncology and radiotherapy : journal of Greatpoland Cancer Center in Poznan and Polish Society of Radiation Oncology* **2013**, *18*, 397(b) McBain, S. C.; Yiu, H. H. P.; Dobson, J. *Int J Nanomed* **2008**, *3*, 169.

(20) Hervault, A.; Thanh, N. T. *Nanoscale* **2014**, *6*, 11553.

(21) Yoo, D.; Lee, J. H.; Shin, T. H.; Cheon, J. *Accounts Chem Res* **2011**, *44*, 863.

(22) Hyeon, T. *Chemical Communications* **2003**, 927.

(23) Lu, A. H.; Salabas, E. L.; Schuth, F. *Angew Chem Int Edit* **2007**, *46*, 1222.

(24) Park, J.; An, K.; Hwang, Y.; Park, J. G.; Noh, H. J.; Kim, J. Y.; Park, J. H.; Hwang, N. M.; Hyeon, T. *Nature materials* **2004**, *3*, 891.

(25) Wang, X.; Zhuang, J.; Peng, Q.; Li, Y. *Nature* **2005**, *437*, 121.

(26) Laurent, S.; Forge, D.; Port, M.; Roch, A.; Robic, C.; Vander Elst, L.; Muller, R. N. *Chemical reviews* **2008**, *108*, 2064.

(27) Willard, M. A.; Kurihara, L. K.; Carpenter, E. E.; Calvin, S.; Harris, V. G. *Int Mater Rev* **2004**, *49*, 125.

(28) (a) Lee, J. H.; Huh, Y. M.; Jun, Y. W.; Seo, J. W.; Jang, J. T.; Song, H. T.; Kim, S.; Cho, E. J.; Yoon, H. G.; Suh, J. S.; Cheon, J. *Nat Med* **2007**, *13*, 95(b) Lee, S.; Kim, S.; Choo, J.; Shin, S. Y.; Lee, Y. H.; Choi, H. Y.; Ha, S.; Kang, K.; Oh, C. H. *Analytical chemistry* **2007**, *79*, 916.

(29) Jang, J. T.; Nah, H.; Lee, J. H.; Moon, S. H.; Kim, M. G.; Cheon, J. *Angew Chem Int Edit* **2009**, *48*, 1234.

(30) Shen, L. F.; Laibinis, P. E.; Hatton, T. A. *Langmuir* **1999**, *15*, 447.

(31) Farrell, D.; Majetich, S. A.; Wilcoxon, J. P. *J Phys Chem B* **2003**, *107*, 11022.

(32) (a) Park, J. I.; Cheon, J. *J Am Chem Soc* **2001**, *123*, 5743(b) Lyon, J. L.; Fleming, D. A.; Stone, M. B.; Schiffer, P.; Williams, M. E. *Nano Lett* **2004**, *4*, 719.

(33) Gorin, D. A.; Portnov, S. A.; Inozemtseva, O. A.; Luklinska, Z.; Yashchenok, A. M.; Pavlov, A. M.; Skirtach, A. G.; Mohwald, H.; Sukhorukov, G. B. *Physical chemistry chemical physics : PCCP* **2008**, *10*, 6899.

(34) (a) Yu, H.; Chen, M.; Rice, P. M.; Wang, S. X.; White, R. L.; Sun, S. *Nano letters* **2005**, *5*, 379(b) Wang, L. Y.; Luo, J.; Maye, M. M.; Fan, Q.; Qiang, R. D.; Engelhard, M. H.; Wang, C. M.; Lin, Y. H.; Zhong, C. J. *J Mater Chem* **2005**, *15*, 1821.

(35) Zhao, W.; Gu, J.; Zhang, L.; Chen, H.; Shi, J. *Journal of the American Chemical Society* **2005**, *127*, 8916.

(36) Deatsch, A. E.; Evans, B. A. *Journal of Magnetism and Magnetic Materials* **2014**, *354*, 163.

(37) Harmon, B. V.; Takano, Y. S.; Winterford, C. M.; Gobe, G. C. *International journal of radiation biology* **1991**, *59*, 489.

(38) Alphandery, E. *Journal of Cancer* **2014**, *5*, 472.

(39) (a) Muller, S. *Nanomedicine : nanotechnology, biology, and medicine* **2009**, *5*, 387(b) Mahmoudi, K.; Hadjipanayis, C. G. *Frontiers in chemistry* **2014**, *2*, 109.

(40) Johannsen, M.; Thiesen, B.; Wust, P.; Jordan, A. *International journal of hyperthermia : the official journal of European Society for Hyperthermic Oncology, North American Hyperthermia Group* **2010**, *26*, 790.

(41) Balivada, S.; Rachakatla, R. S.; Wang, H.; Samarakoon, T. N.; Dani, R. K.; Pyle, M.; Kroh, F. O.; Walker, B.; Leaym, X.; Koper, O. B.; Tamura, M.; Chikan, V.; Bossmann, S. H.; Troyer, D. L. *BMC cancer* **2010**, *10*, 119.

(42) Fortin, J. P.; Gazeau, F.; Wilhelm, C. *Eur Biophys J Biophy* **2008**, *37*, 223.

(43) Suto, M.; Hirota, Y.; Mamiya, H.; Fujita, A.; Kasuya, R.; Tohji, K.; Jeyadevan, B. *Journal of Magnetism and Magnetic Materials* **2009**, *321*, 1493.

(44) Levy, M.; Wilhelm, C.; Siaugue, J. M.; Horner, O.; Bacri, J. C.; Gazeau, F. *Journal of physics. Condensed matter : an Institute of Physics journal* **2008**, *20*, 204133.

(45) (a) Sharifi, I.; Shokrollahi, H.; Amiri, S. *Journal of Magnetism and Magnetic Materials* **2012**, *324*, 903(b) Liu, X. L.; Fan, H. M.; Yi, J. B.; Yang, Y.; Choo, E. S. G.; Xue, J. M.; Di Fan, D.; Ding, J. *J Mater Chem* **2012**, *22*, 8235.

(46) Hergt, R.; Dutz, S. *Journal of Magnetism and Magnetic Materials* **2007**, *311*, 187.

(47) Valdagni, R.; Amichetti, M. *International journal of radiation oncology, biology, physics* **1994**, *28*, 163.

(48) van der Zee, J.; Gonzalez Gonzalez, D.; van Rhoon, G. C.; van Dijk, J. D.; van Putten, W. L.; Hart, A. A. *Lancet* **2000**, *355*, 1119.

(49) Sneed, P. K.; Stauffer, P. R.; McDermott, M. W.; Diederich, C. J.; Lamborn, K. R.; Prados, M. D.; Chang, S.; Weaver, K. A.; Spry, L.; Malec, M. K.; Lamb, S. A.; Voss, B.; Davis, R. L.; Wara, W. M.; Larson, D. A.; Phillips, T. L.; Gutin, P. H. *International journal of radiation oncology, biology, physics* **1998**, *40*, 287.

(50) Song, C. W. *Cancer research* **1984**, *44*, 4721s.

(51) Dahm-Daphi, J.; Brammer, I.; Dikomey, E. *International journal of radiation biology* **1997**, *72*, 171.

(52) Konings, A. W.; Ruifrok, A. C. *Radiation research* **1985**, *102*, 86.

(53) Vertrees, R. A.; Das, G. C.; Coscio, A. M.; Xie, J.; Zwischenberger, J. B.; Boor, P. J. *Molecular carcinogenesis* **2005**, *44*, 111.

(54) Hildebrandt, B.; Wust, P.; Ahlers, O.; Dieing, A.; Sreenivasa, G.; Kerner, T.; Felix, R.; Riess, H. *Critical reviews in oncology/hematology* **2002**, *43*, 33.

(55) Colombo, M.; Carregal-Romero, S.; Casula, M. F.; Gutierrez, L.; Morales, M. P.; Bohm, I. B.; Heverhagen, J. T.; Prosperi, D.; Parak, W. J. *Chemical Society reviews* **2012**, *41*, 4306.

(56) Multhoff, G. *International journal of hyperthermia : the official journal of European Society for Hyperthermic Oncology, North American Hyperthermia Group* **2002**, *18*, 576.

(57) Ito, A.; Matsuoka, F.; Honda, H.; Kobayashi, T. *Cancer gene therapy* **2003**, *10*, 918.

(58) Peer, A. J.; Grimm, M. J.; Zynda, E. R.; Repasky, E. A. *Immunol Res* **2010**, *46*, 137.

(59) Moroz, P.; Jones, S. K.; Gray, B. N. *International journal of hyperthermia : the official journal of European Society for Hyperthermic Oncology, North American Hyperthermia Group* **2002**, *18*, 267.

(60) Jordan, A.; Scholz, R.; Maier-Hauff, K.; van Landeghem, F. K. H.; Waldoefner, N.; Teichgraeber, U.; Pinkernelle, J.; Bruhn, H.; Neumann, F.; Thiesen, B.; von Deimling, A.; Felix, R. *J Neuro-Oncol* **2006**, *78*, 7.

(61) Zhao, Q.; Wang, L.; Cheng, R.; Mao, L.; Arnold, R. D.; Howerth, E. W.; Chen, Z. G.; Platt, S. *Theranostics* **2012**, *2*, 113.

(62) Ivkov, R.; DeNardo, S. J.; Daum, W.; Foreman, A. R.; Goldstein, R. C.; Nemkov, V. S.; DeNardo, G. L. *Clinical cancer research : an official journal of the American Association for Cancer Research* **2005**, *11*, 7093s.

(63) Kida, Y.; Ishiguri, H.; Ichimi, K.; Kobayashi, T. *No shinkei geka. Neurological surgery* **1990**, *18*, 521.

(64) Kobayashi, T.; Kida, Y.; Tanaka, T.; Hattori, K.; Matsui, M.; Amemiya, Y. *J Neurooncol* **1991**, *10*, 153.

(65) (a) Jordan, A.; Scholz, R.; Maier-Hauff, K.; Johannsen, M.; Wust, P.; Nadobny, J.; Schirra, H.; Schmidt, H.; Deger, S.; Loening, S.; Lanksch, W.; Felix, R. *Journal of Magnetism and Magnetic Materials* **2001**, *225*, 118(b) Maier-Hauff, K.; Ulrich, F.; Nestler, D.; Niehoff, H.; Wust, P.; Thiesen, B.; Orawa, H.; Budach, V.; Jordan, A. *J Neuro-Oncol* **2011**, *103*, 317.

(66) Maeda, H.; Wu, J.; Sawa, T.; Matsumura, Y.; Hori, K. *Journal of controlled release : official journal of the Controlled Release Society* **2000**, *65*, 271.

(67) Shah, B.; Yin, P. T.; Ghoshal, S.; Lee, K. B. *Angew Chem Int Edit* **2013**, *52*, 6190.

(68) Kubo, T.; Sugita, T.; Shimose, S.; Nitta, Y.; Ikuta, Y.; Murakami, T. *International journal of oncology* **2000**, *17*, 309.

(69) Frimpong, R. A.; Hilt, J. Z. *Nanomedicine (Lond)* **2010**, *5*, 1401.

(70) Lubbe, A. S.; Bergemann, C.; Riess, H.; Schriever, F.; Reichardt, P.; Possinger, K.; Matthias, M.; Dorken, B.; Herrmann, F.; Gurtler, R.; Hohenberger, P.; Haas, N.; Sohr, R.; Sander, B.; Lemke, A. J.; Ohlendorf, D.; Huhnt, W.; Huhn, D. *Cancer research* **1996**, *56*, 4686.

(71) Koda, J.; Venook, A.; Walser, E.; Goodwin, S. *Eur J Cancer* **2002**, *38*, S18.

(72) Wilson, M. W.; Kerlan, R. K.; Fidelman, N. A.; Venook, A. P.; LaBerge, J. M.; Koda, J.; Gordon, R. L. *Radiology* **2004**, *230*, 287.

(73) Thomas, C. R.; Ferris, D. P.; Lee, J. H.; Choi, E.; Cho, M. H.; Kim, E. S.; Stoddart, J. F.; Shin, J. S.; Cheon, J.; Zink, J. I. *J Am Chem Soc* **2010**, *132*, 10623.

(74) Lee, J. H.; Lee, K.; Moon, S. H.; Lee, Y.; Park, T. G.; Cheon, J. *Angewandte Chemie* **2009**, *48*, 4174.

(75) Huh, Y. M.; Lee, E. S.; Lee, J. H.; Jun, Y. W.; Kim, P. H.; Yun, C. O.; Kim, J. H.; Suh, J. S.; Cheon, J. *Adv Mater* **2007**, *19*, 3109.

(76) (a) Wei, X.; Yang, X.; Han, Z. P.; Qu, F. F.; Shao, L.; Shi, Y. F. *Acta Pharmacol Sin* **2013**, *34*, 747(b) Kim, S. U.; de Vellis, J. *J Neurosci Res* **2009**, *87*, 2183(c) Segers, V. F. M.; Lee, R. T. *Nature* **2008**, *451*, 937.

(77) (a) Thomas, E. D.; Lochte, H. L., Jr.; Lu, W. C.; Ferrebee, J. W. *The New England journal of medicine* **1957**, *257*, 491(b) Guild, W. R.; Harrison, J. H.; Merrill, J. P.; Murray, J. *Transactions of the American Clinical and Climatological Association* **1955**, *67*, 167.

(78) Gooden, M. J.; de Bock, G. H.; Leffers, N.; Daemen, T.; Nijman, H. W. *British journal of cancer* **2011**, *105*, 93.

(79) Gill, S.; June, C. H. *Immunological reviews* **2015**, *263*, 68.

(80) Palucka, K.; Banchereau, J. *Nat Rev Cancer* **2012**, *12*, 265.

(81) (a) Wang, Y. X.; Dumont, N. A.; Rudnicki, M. A. *Journal of Cell Science* **2014**(b) Roy, N. S.; Cleren, C.; Singh, S. K.; Yang, L.; Beal, M. F.; Goldman, S. A. *Nat Med* **2006**, *12*, 1259.

(82) (a) Cheng, Z. K.; Ou, L. L.; Zhou, X.; Li, F.; Jia, X. H.; Zhang, Y. G.; Liu, X. L.; Li, Y. M.; Ward, C. A.; Melo, L. G.; Kong, D. L. *Mol Ther* **2008**, *16*, 571(b) Hoehn, M.; Kustermann, E.; Blunk, J.; Wiedermann, D.; Trapp, T.; Wecker, S.; Focking, M.; Arnold, H.; Hescheler, J.; Fleischmann, B. K.; Schwindt, W.; Buhrle, C. *P Natl Acad Sci USA* **2002**, *99*, 16267.

(83) (a) Uccelli, A.; Moretta, L.; Pistoia, V. *Nat Rev Immunol* **2008**, *8*, 726(b) Rehman, J.; Li, J. L.; Orschell, C. M.; March, K. L. *Circulation* **2003**, *107*, 1164.

(84) Lindvall, O.; Kokaia, Z.; Martinez-Serrano, A. *Nat Med* **2004**, *10*, S42.

(85) (a) Muller, F. J.; Snyder, E. Y.; Loring, J. F. *Nat Rev Neurosci* **2006**, *7*, 75(b) Gafni, Y.; Turgeman, G.; Liebergal, M.; Pelled, G.; Gazit, Z.; Gazit, D. *Gene Ther* **2004**, *11*, 417.

(86) Alderuccio, F.; Nasa, Z.; Chung, J. Y.; Ko, H. J.; Chan, J.; Toh, B. H. *Mol Pharmaceut* **2011**, *8*, 1488.

(87) Ahmed, A. U.; Alexiades, N. G.; Lesniak, M. S. *Curr Opin Mol Ther* **2010**, *12*, 546.

(88) Yin, P. T.; Han, E.; Lee, K. B. *Advanced healthcare materials* **2015**.

(89) (a) Robinton, D. A.; Daley, G. Q. *Nature* **2012**, *481*, 295(b) Barker, N.; Bartfeld, S.; Clevers, H. *Cell Stem Cell* **2010**, *7*, 656(c) Martino, G.; Pluchino, S. *Nat Rev Neurosci* **2006**, *7*, 395.

(90) Jung, Y.; Bauer, G.; Nolta, J. A. *Stem cells* **2012**, *30*, 42.

(91) Altman, J.; Das, G. D. *The Journal of comparative neurology* **1965**, *124*, 319.

(92) Gage, F. H. *Science* **2000**, *287*, 1433.

(93) Zhang, S. C.; Wernig, M.; Duncan, I. D.; Brustle, O.; Thomson, J. A. *Nature biotechnology* **2001**, *19*, 1129.

(94) Svendsen, C. N.; Caldwell, M. A.; Ostenfeld, T. *Brain pathology* **1999**, *9*, 499.

(95) Ronaghi, M.; Erceg, S.; Moreno-Manzano, V.; Stojkovic, M. *Stem cells* **2010**, *28*, 93.

(96) Jenq, R. R.; van den Brink, M. R. M. *Nat Rev Cancer* **2010**, *10*, 213.

(97) Passweg, J. R.; Halter, J.; Bucher, C.; Gerull, S.; Heim, D.; Rovo, A.; Buser, A.; Stern, M.; Tichelli, A. *Swiss Med Wkly* **2012**, *142*.

(98) (a) Digiusto, D.; Chen, S.; Combs, J.; Webb, S.; Namikawa, R.; Tsukamoto, A.; Chen, B. P.; Galy, A. H. M. *Blood* **1994**, *84*, 421(b) Krause, D. S.; Fackler, M. J.; Civin, C. I.; May, W. S. *Blood* **1996**, *87*, 1.

(99) Körbling, M.; Anderlini, P. *Peripheral blood stem cell versus bone marrow allotransplantation: does the source of hematopoietic stem cells matter?*, 2001.

(100) Capello, E.; Vuolo, L.; Gualandi, F.; Van Lint, M. T.; Roccatagliata, L.; Bonzano, L.; Pardini, M.; Uccelli, A.; Mancardi, G. *Neurol Sci* **2009**, *30*, 175.

(101) (a) Szodoray, P.; Varoczy, L.; Szegedi, G.; Zeher, M. *Scand J Rheumatol* **2010**, *39*, 1(b) Trounson, A.; Thakar, R. G.; Lomax, G.; Gibbons, D. *Bmc Med* **2011**, *9*.

(102) Hsieh, M. M.; Kang, E. M.; Fitzhugh, C. D.; Link, M. B.; Bolan, C. D.; Kurlander, R.; Childs, R. W.; Rodgers, G. P.; Powell, J. D.; Tisdale, J. F. *New Engl J Med* **2009**, *361*, 2309.

(103) (a) Granero-Molto, F.; Weis, J. A.; Longobardi, L.; Spagnoli, A. *Expert Opin Biol Th* **2008**, *8*, 255(b) Salem, H. K.; Thiemermann, C. *Stem cells* **2010**, *28*, 585.

(104) (a) Lu, D. B.; Chen, B.; Liang, Z. W.; Deng, W. Q.; Jiang, Y. Z.; Li, S. F.; Xu, J.; Wu, Q. N.; Zhang, Z. H.; Xie, B.; Chen, S. H. *Diabetes Res Clin Pr* **2011**, *92*,

26(b) Yamada, Y.; Ueda, M.; Hibi, H.; Baba, S. *Int J Periodont Rest* **2006**, *26*, 363(c) Rasulov, M. F.; Vasil'chenkov, A. V.; Onishchenko, N. A.; Krasheninnikov, M. E.; Kravchenko, V. I.; Gorshenin, T. L.; Pidtsan, R. E.; Potapov, I. V. *B Exp Biol Med+* **2005**, *139*, 141.

(105) Lee, R. H.; Pulin, A. A.; Seo, M. J.; Kota, D. J.; Ylostalo, J.; Larson, B. L.; Semprun-Prieto, L.; Delafontaine, P.; Prockop, D. J. *Cell Stem Cell* **2009**, *5*, 54.

(106) Prasad, V. K.; Lucas, K. G.; Kleiner, G. I.; Talano, J. A. M.; Jacobsohn, D.; Broadwater, G.; Monroy, R.; Kurtzberg, J. *Biol Blood Marrow Tr* **2011**, *17*, 534.

(107) (a) Ciccocioppo, R.; Bernardo, M. E.; Sgarella, A.; Maccario, R.; Avanzini, M. A.; Ubezio, C.; Minelli, A.; Alvisi, C.; Vanoli, A.; Calliada, F.; Dionigi, P.; Perotti, C.; Locatelli, F.; Corazza, G. R. *Gut* **2011**, *60*, 788(b) Duijvestein, M.; Vos, A. C. W.; Roelofs, H.; Wildenberg, M. E.; Wendrich, B. B.; Verspaget, H. W.; Kooy-Winkelaar, E. M. C.; Koning, F.; Zwaginga, J. J.; Fidder, H. H.; Verhaar, A. P.; Fibbe, W. E.; van den Brink, G. R.; Hommes, D. W. *Gut* **2010**, *59*, 1662.

(108) Honmou, O.; Houkin, K.; Matsunaga, T.; Niitsu, Y.; Ishiai, S.; Onodera, R.; Waxman, S. G.; Kocsis, J. D. *Brain* **2011**, *134*, 1790.

(109) Mannon, P. J. *Expert Opin Biol Th* **2011**, *11*, 1249.

(110) Kazuki, Y.; Oshimura, M. *Mol Ther* **2011**, *19*, 1591.

(111) Robbins, P. D.; Ghivizzani, S. C. *Pharmacology & therapeutics* **1998**, *80*, 35.

(112) (a) Kustikova, O.; Fehse, B.; Modlich, U.; Yang, M.; Dullmann, J.; Kamino, K.; von Neuhoff, N.; Schlegelberger, B.; Li, Z. X.; Baum, C. *Science* **2005**, *308*, 1171(b) Vroemen, M.; Weidner, N.; Blesch, A. *Exp Neurol* **2005**, *195*, 127.

(113) (a) Kay, M. A. *Nat Rev Genet* **2011**, *12*, 316(b) Thomas, C. E.; Ehrhardt, A.; Kay, M. A. *Nat Rev Genet* **2003**, *4*, 346(c) Ginn, S. L.; Alexander, I. E.; Edelstein, M. L.; Abedi, M. R.; Wixon, J. *The journal of gene medicine* **2013**, *15*, 65.

(114) Rios, H. F.; Lin, Z.; Oh, B.; Park, C. H.; Giannobile, W. V. *J Periodontol* **2011**, *82*, 1223.

(115) Gabriel, R.; Schmidt, M.; von Kalle, C. *Current opinion in immunology* **2012**, *24*, 592.

(116) Santoni de Sio, F. R.; Cascio, P.; Zingale, A.; Gasparini, M.; Naldini, L. *Blood* **2006**, *107*, 4257.

(117) Montini, E.; Cesana, D.; Schmidt, M.; Sanvito, F.; Ponzoni, M.; Bartholomae, C.; Sergi, L. S.; Benedicenti, F.; Ambrosi, A.; Di Serio, C.; Doglioni, C.; von Kalle, C.; Naldini, L. *Nature biotechnology* **2006**, *24*, 687.

(118) Cavazzana-Calvo, M.; Payen, E.; Negre, O.; Wang, G.; Hehir, K.; Fusil, F.; Down, J.; Denaro, M.; Brady, T.; Westerman, K.; Cavallesco, R.; Gillet-Legrand, B.; Caccavelli, L.; Sgarra, R.; Maouche-Chretien, L.; Bernaudin, F.; Girot, R.; Dorazio, R.; Mulder, G. J.; Polack, A.; Bank, A.; Soulier, J.; Larghero, J.; Kabbara, N.; Dalle, B.; Gourmel, B.; Socie, G.; Chretien, S.; Cartier, N.; Aubourg, P.; Fischer, A.; Cornetta, K.; Galacteros, F.; Beuzard, Y.; Gluckman, E.; Bushman, F.; Hacein-Bey-Abina, S.; Leboulch, P. *Nature* **2010**, *467*, 318.

(119) Winslow, M. M.; Dayton, T. L.; Verhaak, R. G.; Kim-Kiselak, C.; Snyder, E. L.; Feldser, D. M.; Hubbard, D. D.; DuPage, M. J.; Whittaker, C. A.; Hoersch, S.; Yoon, S.; Crowley, D.; Bronson, R. T.; Chiang, D. Y.; Meyerson, M.; Jacks, T. *Nature* **2011**, *473*, 101.

(120) Partridge, K. A.; Oreffo, R. O. C. *Tissue Eng* **2004**, *10*, 295.

(121) Douglas, J. T. *Molecular biotechnology* **2007**, *36*, 71.

(122) Brunetti-Pierri, N.; Ng, P. *Curr Gene Ther* **2009**, *9*, 329.

(123) McCaffrey, A. P.; Fawcett, P.; Nakai, H.; McCaffrey, R. L.; Ehrhardt, A.; Pham, T. T. T.; Pandey, K.; Xu, H.; Feuss, S.; Storm, T. A.; Kay, M. A. *Mol Ther* **2008**, *16*, 931.

(124) Ramseier, C. A.; Abramson, Z. R.; Jin, Q.; Giannobile, W. V. *Dental clinics of North America* **2006**, *50*, 245.

(125) (a) Inagaki, K.; Piao, C.; Kotchey, N. M.; Wu, X.; Nakai, H. *Journal of virology* **2008**, *82*, 9513(b) Surosky, R. T.; Urabe, M.; Godwin, S. G.; McQuiston, S. A.; Kurtzman, G. J.; Ozawa, K.; Natsoulis, G. *Journal of virology* **1997**, *71*, 7951.

(126) (a) Cossu, G.; Sampaolesi, M. *Trends in molecular medicine* **2007**, *13*, 520(b) McCarty, D. M.; Monahan, P. E.; Samulski, R. J. *Gene Ther* **2001**, *8*, 1248.

(127) Donsante, A.; Miller, D. G.; Li, Y.; Vogler, C.; Brunt, E. M.; Russell, D. W.; Sands, M. S. *Science* **2007**, *317*, 477.

(128) Nathwani, A. C.; Tuddenham, E. G.; Rangarajan, S.; Rosales, C.; McIntosh, J.; Linch, D. C.; Chowdary, P.; Riddell, A.; Pie, A. J.; Harrington, C.; O'Beirne, J.; Smith, K.; Pasi, J.; Glader, B.; Rustagi, P.; Ng, C. Y.; Kay, M. A.; Zhou, J.; Spence, Y.; Morton, C. L.; Allay, J.; Coleman, J.; Sleep, S.; Cunningham, J. M.; Srivastava, D.; Basner-Tschakarjan, E.; Mingozzi, F.; High, K. A.; Gray, J. T.;

Reiss, U. M.; Nienhuis, A. W.; Davidoff, A. M. *The New England journal of medicine* **2011**, *365*, 2357.

(129) Srivastava, A. *Hum Gene Ther* **2005**, *16*, 792.

(130) Arnett, A. L. H.; Konieczny, P.; Ramos, J. N.; Hall, J.; Odom, G.; Yablonka-Reuveni, Z.; Chamberlain, J. R.; Chamberlain, J. S. *Molecular Therapy — Methods & Clinical Development* **2014**, *1*.

(131) Asuri, P.; Bartel, M. A.; Vazin, T.; Jang, J. H.; Wong, T. B.; Schaffer, D. V. *Mol Ther* **2012**, *20*, 329.

(132) Yin, H.; Kanasty, R. L.; Eltoukhy, A. A.; Vegas, A. J.; Dorkin, J. R.; Anderson, D. G. *Nat Rev Genet* **2014**, *15*, 541.

(133) (a) Pack, D. W.; Hoffman, A. S.; Pun, S.; Stayton, P. S. *Nature reviews. Drug discovery* **2005**, *4*, 581(b) Mintzer, M. A.; Simanek, E. E. *Chemical reviews* **2009**, *109*, 259.

(134) Lee, D. E.; Koo, H.; Sun, I. C.; Ryu, J. H.; Kim, K.; Kwon, I. C. *Chemical Society reviews* **2012**, *41*, 2656.

(135) Alexis, F.; Pridgen, E.; Langer, R.; Farokhzad, O. In *Drug Delivery*; Schäfer-Korting, M., Ed.; Springer Berlin Heidelberg, 2010; Vol. 197.

(136) Putnam, D. *Nat Mater* **2006**, *5*, 439.

(137) Fraley, R.; Subramani, S.; Berg, P.; Papahadjopoulos, D. *J Biol Chem* **1980**, *255*, 431.

(138) Wasungu, L.; Hoekstra, D. *J Control Release* **2006**, *116*, 255.

(139) Whitehead, K. A.; Langer, R.; Anderson, D. G. *Nature Reviews Drug Discovery* **2009**, *8*, 129.

(140) Lonez, C.; Vandenbranden, M.; Ruysschaert, J. M. *Prog Lipid Res* **2008**, *47*, 340.

(141) Choi, Y. H.; Liu, F.; Kim, J. S.; Choi, Y. K.; Park, J. S.; Kim, S. W. *J Control Release* **1998**, *54*, 39.

(142) Kim, S. W. *Cold Spring Harbor protocols* **2012**, *2012*, 433.

(143) Alexis, F.; Pridgen, E.; Molnar, L. K.; Farokhzad, O. C. *Mol Pharmaceut* **2008**, *5*, 505.

(144) Lungwitz, U.; Breunig, M.; Blunk, T.; Gopferich, A. *Eur J Pharm Biopharm* **2005**, *60*, 247.

(145) (a) Godbey, W. T.; Wu, K. K.; Mikos, A. G. *J Biomed Mater Res* **1999**, *45*, 268(b) Wightman, L.; Kircheis, R.; Rossler, V.; Carotta, S.; Ruzicka, R.; Kursa, M.; Wagner, E. *Journal of Gene Medicine* **2001**, *3*, 362.

(146) (a) Nativo, P.; Prior, I. A.; Brust, M. *Acs Nano* **2008**, *2*, 1639(b) Patel, S.; Jung, D.; Yin, P. T.; Carlton, P.; Yamamoto, M.; Bando, T.; Sugiyama, H.; Lee, K. B. *Acs Nano* **2014**, *8*, 8959(c) Ghosh, P.; Han, G.; De, M.; Kim, C. K.; Rotello, V. M. *Adv Drug Deliver Rev* **2008**, *60*, 1307.

(147) Tiwari, P. M.; Vig, K.; Dennis, V. A.; Singh, S. R. *Nanomaterials-Basel* **2011**, *1*, 31.

(148) Zhou, J. F.; Ralston, J.; Sedev, R.; Beattie, D. A. *J Colloid Interf Sci* **2009**, *331*, 251.

(149) Yin, P. T.; Shah, B. P.; Lee, K. B. *Small* **2014**, *10*, 4106.

(150) Kim, J.; Piao, Y.; Hyeon, T. *Chemical Society reviews* **2009**, *38*, 372.

(151) Sapet, C.; Laurent, N.; de Chevigny, A.; Le Gourrierec, L.; Bertosio, E.; Zelphati, O.; Beclin, C. *Biotechniques* **2011**, *50*, 187.

(152) Jun, Y. W.; Lee, J. H.; Cheon, J. *Angew Chem Int Edit* **2008**, *47*, 5122.

(153) Shah, B. P.; Pasquale, N.; De, G. J.; Tan, T.; Ma, J. J.; Lee, K. B. *Acs Nano* **2014**, *8*, 9379.

(154) Cross, D.; Burmester, J. K. *Clinical medicine & research* **2006**, *4*, 218.

(155) Aghi, M.; Martuza, R. L. *Oncogene* **2005**, *24*, 7802.

(156) Nakashima, H.; Kaur, B.; Chiocca, E. A. *Cytokine & growth factor reviews* **2010**, *21*, 119.

(157) Sonabend, A. M.; Ulasov, I. V.; Tyler, M. A.; Rivera, A. A.; Mathis, J. M.; Lesniak, M. S. *Stem cells* **2008**, *26*, 831.

(158) (a) Fritz, V.; Jorgensen, C. *Current stem cell research & therapy* **2008**, *3*, 32(b) Ahmed, A. U.; Rolle, C. E.; Tyler, M. A.; Han, Y.; Sengupta, S.; Wainwright, D. A.; Balyasnikova, I. V.; Ulasov, I. V.; Lesniak, M. S. *Mol Ther* **2010**, *18*, 1846(c) Ong, H. T.; Federspiel, M. J.; Guo, C. M.; Ooi, L. L.; Russell, S. J.; Peng, K. W.; Hui, K. M. *J Hepatol* **2013**, *59*, 999(d) Yong, R. L.; Shinojima, N.; Fueyo, J.;

Gumin, J.; Vecil, G. G.; Marini, F. C.; Bogler, O.; Andreeff, M.; Lang, F. F. *Cancer research* **2009**, *69*, 8932.

(159) Duebgen, M.; Martinez-Quintanilla, J.; Tamura, K.; Hingtgen, S.; Redjal, N.; Wakimoto, H.; Shah, K. *Journal of the National Cancer Institute* **2014**, *106*, dju090.

(160) Ulasov, I. V.; Rivera, A. A.; Sonabend, A. M.; Rivera, L. B.; Wang, M.; Zhu, Z. B.; Lesniak, M. S. *Cancer Biol Ther* **2007**, *6*, 679.

(161) Ahmed, A. U.; Tyler, M. A.; Thaci, B.; Alexiades, N. G.; Han, Y.; Ulasov, I. V.; Lesniak, M. S. *Mol Pharmaceut* **2011**, *8*, 1559.

(162) Stoff-Khalili, M.; Rivera, A.; Mathis, J. M.; Banerjee, N. S.; Moon, A.; Hess, A.; Rocconi, R.; Numnum, T. M.; Everts, M.; Chow, L.; Douglas, J.; Siegal, G.; Zhu, Z.; Bender, H.; Dall, P.; Stoff, A.; Pereboeva, L.; Curiel, D. *Breast Cancer Res Treat* **2007**, *105*, 157.

(163) Furusato, B.; Mohamed, A.; Uhlen, M.; Rhim, J. S. *Pathology international* **2010**, *60*, 497.

(164) Nakamura, K.; Ito, Y.; Kawano, Y.; Kurozumi, K.; Kobune, M.; Tsuda, H.; Bizen, A.; Honmou, O.; Niitsu, Y.; Hamada, H. *Gene Ther* **2004**, *11*, 1155.

(165) Mader, E. K.; Butler, G.; Dowdy, S. C.; Mariani, A.; Knutson, K. L.; Federspiel, M. J.; Russell, S. J.; Galanis, E.; Dietz, A. B.; Peng, K. W. *J Transl Med* **2013**, *11*.

(166) Msaouel, P.; Dispenzieri, A.; Galanis, E. *Curr Opin Mol Ther* **2009**, *11*, 43.

(167) Compte, M.; Cuesta, A. M.; Sanchez-Martin, D.; Alonso-Camino, V.; Vicario, J. L.; Sanz, L.; Alvarez-Vallina, L. *Stem cells* **2009**, *27*, 753.

(168) Hu, Y. L.; Huang, B.; Zhang, T. Y.; Miao, P. H.; Tang, G. P.; Tabata, Y.; Gao, J. Q. *Mol Pharmaceut* **2012**, *9*, 2698.

(169) Wakabayashi, T.; Natsume, A.; Hashizume, Y.; Fujii, M.; Mizuno, M.; Yoshida, J. *The journal of gene medicine* **2008**, *10*, 329.

(170) Dembinski, J. L.; Wilson, S. M.; Spaeth, E. L.; Studeny, M.; Zompetta, C.; Samudio, I.; Roby, K.; Andreeff, M.; Marini, F. C. *Cytotherapy* **2013**, *15*, 20.

(171) Studeny, M.; Marini, F. C.; Dembinski, J. L.; Zompetta, C.; Cabreira-Hansen, M.; Bekele, B. N.; Champlin, R. E.; Andreeff, M. *Journal of the National Cancer Institute* **2004**, *96*, 1593.

(172) Ren, C.; Kumar, S.; Chanda, D.; Kallman, L.; Chen, J.; Mountz, J. D.; Ponnazhagan, S. *Gene Ther* **2008**, *15*, 1446.

(173) Ehtesham, M.; Kabos, P.; Kabosova, A.; Neuman, T.; Black, K. L.; Yu, J. S. *Cancer research* **2002**, *62*, 5657.

(174) Stuckey, D. W.; Shah, K. *Trends in molecular medicine* **2013**, *19*, 685.

(175) Walczak, H.; Krammer, P. H. *Experimental cell research* **2000**, *256*, 58.

(176) Volkmann, X.; Fischer, U.; Bahr, M. J.; Ott, M.; Lehner, F.; MacFarlane, M.; Cohen, G. M.; Manns, M. P.; Schulze-Osthoff, K.; Bantel, H. *Hepatology* **2007**, *46*, 1498.

(177) Sasportas, L. S.; Kasmieh, R.; Wakimoto, H.; Hingtgen, S.; van de Water, J. A.; Mohapatra, G.; Figueiredo, J. L.; Martuza, R. L.; Weissleder, R.; Shah, K. *Proc Natl Acad Sci U S A* **2009**, *106*, 4822.

(178) (a) Kagawa, S.; He, C.; Gu, J.; Koch, P.; Rha, S. J.; Roth, J. A.; Curley, S. A.; Stephens, L. C.; Fang, B. *Cancer research* **2001**, *61*, 3330(b) Liu, L.; Eckert, M. A.; Riazifar, H.; Kang, D.-K.; Agalliu, D.; Zhao, W. *Stem Cells International* **2013**, *2013*, 7.

(179) van Eekelen, M.; Sasportas, L. S.; Kasmieh, R.; Yip, S.; Figueiredo, J. L.; Louis, D. N.; Weissleder, R.; Shah, K. *Oncogene* **2010**, *29*, 3185.

(180) (a) Gao, P.; Ding, Q.; Wu, Z.; Jiang, H. W.; Fang, Z. J. *Cancer Lett* **2010**, *290*, 157(b) Ryu, C. H.; Park, S. H.; Park, S. A.; Kim, S. M.; Lim, J. Y.; Jeong, C. H.; Yoon, W. S.; Oh, W. I.; Sung, Y. C.; Jeun, S. S. *Hum Gene Ther* **2011**, *22*, 733(c) Hong, X.; Miller, C.; Savant-Bhonsale, S.; Kalkanis, S. N. *Neurosurgery* **2009**, *64*, 1139.

(181) Xu, G.; Jiang, X. D.; Xu, Y.; Zhang, J.; Huang, F. H.; Chen, Z. Z.; Zhou, D. X.; Shang, J. H.; Zou, Y. X.; Cai, Y. Q.; Kou, S. B.; Chen, Y. Z.; Xu, R. X.; Zeng, Y. J. *Cell biology international* **2009**, *33*, 466.

(182) Kanehira, M.; Xin, H.; Hoshino, K.; Maemondo, M.; Mizuguchi, H.; Hayakawa, T.; Matsumoto, K.; Nakamura, T.; Nukiwa, T.; Saijo, Y. *Cancer gene therapy* **2007**, *14*, 894.

(183) Kim, S. K.; Cargioli, T. G.; Machluf, M.; Yang, W.; Sun, Y.; Al-Hashem, R.; Kim, S. U.; Black, P. M.; Carroll, R. S. *Clinical cancer research : an official journal of the American Association for Cancer Research* **2005**, *11*, 5965.

(184) Bello, L.; Lucini, V.; Carrabba, G.; Giussani, C.; Machluf, M.; Pluderi, M.; Nikas, D.; Zhang, J.; Tomei, G.; Villani, R. M.; Carroll, R. S.; Bikfalvi, A.; Black, P. M. *Cancer research* **2001**, *61*, 8730.

(185) Car, B. D.; Eng, V. M.; Lipman, J. M.; Anderson, T. D. *Toxicologic pathology* **1999**, *27*, 58.

(186) Seo, S. H.; Kim, K. S.; Park, S. H.; Suh, Y. S.; Kim, S. J.; Jeun, S. S.; Sung, Y. C. *Gene Ther* **2011**, *18*, 488.

(187) Hamstra, D. A.; Rehemtulla, A. *Hum Gene Ther* **1999**, *10*, 235.

(188) Xu, G.; McLeod, H. L. *Clinical cancer research : an official journal of the American Association for Cancer Research* **2001**, *7*, 3314.

(189) Friedlos, F.; Court, S.; Ford, M.; Denny, W. A.; Springer, C. *Gene Ther* **1998**, *5*, 105.

(190) Robert, H.; Bahuaud, J.; Kerdiles, N.; Passuti, N.; Capelli, M.; Pujol, J. P.; Hartman, D.; Locker, B.; Hulet, C.; Hardy, P.; Coudane, H.; Rochverger, A.; Francheschi, J. P.; Arthroscopie, S. F. *Rev Chir Orthop* **2007**, *93*, 701.

(191) Aboody, K. S.; Najbauer, J.; Metz, M. Z.; D'Apuzzo, M.; Gutova, M.; Annala, A. J.; Synold, T. W.; Couture, L. A.; Blanchard, S.; Moats, R. A.; Garcia, E.; Aramburo, S.; Valenzuela, V. V.; Frank, R. T.; Barish, M. E.; Brown, C. E.; Kim, S. U.; Badie, B.; Portnow, J. *Science translational medicine* **2013**, *5*, 184ra59.

(192) Zhao, Y.; Lam, D. H.; Yang, J.; Lin, J.; Tham, C. K.; Ng, W. H.; Wang, S. *Gene Ther* **2012**, *19*, 189.

(193) Kosaka, H.; Ichikawa, T.; Kurozumi, K.; Kambara, H.; Inoue, S.; Maruo, T.; Nakamura, K.; Hamada, H.; Date, I. *Cancer gene therapy* **2012**, *19*, 572.

(194) Altaner, C.; Altanerova, V.; Cihova, M.; Ondicova, K.; Rychly, B.; Baciak, L.; Mravec, B. *Int J Cancer* **2014**, *134*, 1458.

(195) Kim, S. K.; Kim, S. U.; Park, I. H.; Bang, J. H.; Aboody, K. S.; Wang, K. C.; Cho, B. K.; Kim, M.; Menon, L. G.; Black, P. M.; Carroll, R. S. *Clinical cancer research : an official journal of the American Association for Cancer Research* **2006**, *12*, 5550.

(196) (a) Martinez-Quintanilla, J.; Bhere, D.; Heidari, P.; He, D.; Mahmood, U.; Shah, K. *Stem cells* **2013**, *31*, 1706(b) Ryu, C. H.; Park, K. Y.; Kim, S. M.; Jeong, C. H.; Woo, J. S.; Hou, Y.; Jeun, S. S. *Biochemical and biophysical research communications* **2012**, *421*, 585(c) Lee, W. Y.; Zhang, T.; Lau, C. P.; Wang, C. C.; Chan, K. M.; Li, G. *Cytotherapy* **2013**, *15*, 1484.

(197) Yang, J.; Lam, D. H.; Goh, S. S.; Lee, E. X.; Zhao, Y.; Tay, F. C.; Chen, C.; Du, S. H.; Balasundaram, G.; Shahbazi, M.; Tham, C. K.; Ng, W. H.; Toh, H. C.; Wang, S. *Stem cells* **2012**, *30*, 1021.

(198) (a) Hong, S. H.; Lee, H. J.; An, J.; Lim, I.; Borlongan, C.; Aboody, K. S.; Kim, S. U. *Cancer gene therapy* **2013**, *20*, 678(b) Gutova, M.; Shackleford, G. M.; Khankaldyyan, V.; Herrmann, K. A.; Shi, X. H.; Mittelholtz, K.; Abramyants, Y.; Blanchard, M. S.; Kim, S. U.; Annala, A. J.; Najbauer, J.; Synold, T. W.; D'Apuzzo, M.; Barish, M. E.; Moats, R. A.; Aboody, K. S. *Gene Ther* **2013**, *20*, 143.

(199) Kim, K. Y.; Kim, S. U.; Leung, P. C. K.; Jeung, E. B.; Choi, K. C. *Cancer Sci* **2010**, *101*, 955.

(200) Wust, P.; Hildebrandt, B.; Sreenivasa, G.; Rau, B.; Gellermann, J.; Riess, H.; Felix, R.; Schlag, P. M. *Lancet Oncol* **2002**, *3*, 487.

(201) Kumar, C. S. S. R.; Mohammad, F. *Adv Drug Deliver Rev* **2011**, *63*, 789.

(202) (a) Multhoff, G.; Botzler, C.; Wiesnet, M.; Muller, E.; Meier, T.; Wilmanns, W.; Issels, R. D. *International journal of cancer. Journal international du cancer* **1995**, *61*, 272(b) Multhoff, G.; Botzler, C.; Wiesnet, M.; Eissner, G.; Issels, R. *Blood* **1995**, *86*, 1374.

(203) Luo, G. R.; Chen, S.; Le, W. D. *International journal of biological sciences* **2007**, *3*, 20.

(204) Jolly, C.; Morimoto, R. I. *Journal of the National Cancer Institute* **2000**, *92*, 1564.

(205) (a) Ciocca, D. R.; Clark, G. M.; Tandon, A. K.; Fuqua, S. A.; Welch, W. J.; McGuire, W. L. *Journal of the National Cancer Institute* **1993**, *85*, 570(b) Fuqua, S. A.; Oesterreich, S.; Hilsenbeck, S. G.; Von Hoff, D. D.; Eckardt, J.; Osborne, C. K. *Breast cancer research and treatment* **1994**, *32*, 67(c) Landriscina, M.; Amoroso, M. R.; Piscazzi, A.; Esposito, F. *Gynecologic oncology* **2010**, *117*, 177.

(206) (a) Gibbons, N. B.; Watson, R. W. G.; Coffey, R. N. T.; Brady, H. P.; Fitzpatrick, J. M. *Prostate* **2000**, *45*, 58(b) Creagh, E. M.; Sheehan, D.; Cotter, T. G. *Leukemia* **2000**, *14*, 1161(c) Garrido, C.; Solary, E. *Cell Death Differ* **2003**, *10*, 619(d) Takayama, S.; Reed, J. C.; Homma, S. *Oncogene* **2003**, *22*, 9041.

(207) (a) Levine, A. J.; Momand, J.; Finlay, C. A. *Nature* **1991**, *351*, 453(b) Ciocca, D. R.; Calderwood, S. K. *Cell Stress Chaperon* **2005**, *10*, 86.

(208) Minnnaugh, E. G.; Xu, W. P.; Vos, M.; Yuan, X. T.; Isaacs, J. S.; Bisht, K. S.; Gius, D.; Neckers, L. *Mol Cancer Ther* **2004**, *3*, 551.

(209) Miyata, Y. *Curr Pharm Design* **2005**, *11*, 1131.

(210) Yoo, D.; Jeong, H.; Noh, S. H.; Lee, J. H.; Cheon, J. *Angew Chem Int Edit* **2013**, *52*, 13047.

(211) He, L.; Hannon, G. J. *Nat Rev Genet* **2004**, *5*, 522.

(212) Calin, G. A.; Croce, C. M. *Nat Rev Cancer* **2006**, *6*, 857.

(213) Bartel, D. P. *Cell* **2009**, *136*, 215.

(214) Bader, A. G.; Brown, D.; Winkler, M. *Cancer research* **2010**, *70*, 7027.

(215) Johnson, C. D.; Esquela-Kerscher, A.; Stefani, G.; Byrom, N.; Kelnar, K.; Ovcharenko, D.; Wilson, M.; Wang, X. W.; Shelton, J.; Shingara, J.; Chin, L.; Brown, D.; Slack, F. J. *Cancer Res* **2007**, *67*, 7713.

(216) Johnson, S. M.; Grosshans, H.; Shingara, J.; Byrom, M.; Jarvis, R.; Cheng, A.; Labourier, E.; Reinert, K. L.; Brown, D.; Slack, F. J. *Cell* **2005**, *120*, 635.

(217) Zhu, H.; Shyh-Chang, N.; Segre, A. V.; Shinoda, G.; Shah, S. P.; Einhorn, W. S.; Takeuchi, A.; Engreitz, J. M.; Hagan, J. P.; Kharas, M. G.; Urbach, A.; Thornton, J. E.; Triboulet, R.; Gregory, R. I.; Altshuler, D.; Daley, G. Q.; Consortium, D.; Investigators, M. *Cell* **2011**, *147*, 81.

(218) Sampson, V. B.; Rong, N. H.; Han, J.; Yang, Q. Y.; Aris, V.; Soteropoulos, P.; Petrelli, N. J.; Dunn, S. P.; Krueger, L. J. *Cancer Res* **2007**, *67*, 9762.

(219) Roush, S.; Slack, F. J. *Trends Cell Biol* **2008**, *18*, 505.

(220) Takamizawa, J.; Konishi, H.; Yanagisawa, K.; Tomida, S.; Osada, H.; Endoh, H.; Harano, T.; Yatabe, Y.; Nagino, M.; Nimura, Y.; Mitsudomi, T.; Takahashi, T. *Cancer Res* **2004**, *64*, 3753.

(221) Jiang, J. M.; Lee, E. J.; Gusev, Y.; Schmittgen, T. D. *Nucleic Acids Res* **2005**, *33*, 5394.

(222) Sempere, L. F.; Christensen, M.; Silahtaroglu, A.; Bak, M.; Heath, C. V.; Schwartz, G.; Wells, W.; Kauppinen, S.; Cole, C. N. *Cancer Res* **2007**, *67*, 11612.

(223) Lavon, I.; Zrihan, D.; Granit, A.; Einstein, O.; Fainstein, N.; Cohen, M. A.; Cohen, M. A.; Zelikovitch, B.; Shoshan, Y.; Spektor, S.; Reubinoff, B. E.; Felig, Y.; Gerlitz, O.; Ben-Hur, T.; Smith, Y.; Siegal, T. *Neuro-Oncology* **2010**, *12*, 422.

(224) Barh, D.; Malhotra, R.; Ravi, B.; Sindhurani, P. *Current oncology* **2010**, *17*, 70.

(225) Guo, S. T.; Huang, Y. Y.; Jiang, Q. A.; Sun, Y.; Deng, L. D.; Liang, Z. C.; Du, Q. A.; Xing, J. F.; Zhao, Y. L.; Wang, P. C.; Dong, A. J.; Liang, X. J. *Acs Nano* **2010**, *4*, 5505.

(226) Zelis, P. M.; Pasquevich, G. A.; Stewart, S. J.; van Raap, M. B. F.; Aphesteguy, J.; Bruvera, I. J.; Laborde, C.; Pianciola, B.; Jacobo, S.; Sanchez, F. H. *J Phys D Appl Phys* **2013**, *46*.

(227) Drake, P.; Cho, H. J.; Shih, P. S.; Kao, C. H.; Lee, K. F.; Kuo, C. H.; Lin, X. Z.; Lin, Y. J. *J Mater Chem* **2007**, *17*, 4914.

(228) Boussif, O.; Lezoualch, F.; Zanta, M. A.; Mergny, M. D.; Scherman, D.; Demeneix, B.; Behr, J. P. *P Natl Acad Sci USA* **1995**, *92*, 7297.

(229) (a) Urban-Klein, B.; Werth, S.; Abuharbeid, S.; Czubayko, F.; Aigner, A. *Gene Ther* **2005**, *12*, 461(b) Babar, I. A.; Cheng, C. J.; Booth, C. J.; Liang, X. P.; Weidhaas, J. B.; Saltzman, W. M.; Slack, F. J. *P Natl Acad Sci USA* **2012**, *109*, E1695.

(230) Behr, J. P. *Chimia* **1997**, *51*, 34.

(231) Werth, S.; Urban-Klein, B.; Dai, L.; Hobel, S.; Grzelinski, M.; Bakowsky, U.; Czubayko, F.; Aigner, A. *J Control Release* **2006**, *112*, 257.

(232) Plank, C.; Zelphati, O.; Mykhaylyk, O. *Adv Drug Deliver Rev* **2011**, *63*, 1300.

(233) Lv, H. T.; Zhang, S. B.; Wang, B.; Cui, S. H.; Yan, J. *J Control Release* **2006**, *114*, 100.

(234) Guo, H. L.; Ingolia, N. T.; Weissman, J. S.; Bartel, D. P. *Nature* **2010**, *466*, 835.

(235) Lee, S. T.; Chu, K.; Oh, H. J.; Im, W. S.; Lim, J. Y.; Kim, S. K.; Park, C. K.; Jung, K. H.; Lee, S. K.; Kim, M.; Roh, J. K. *J Neuro-Oncol* **2011**, *102*, 19.

(236) Datta, S. R.; Brunet, A.; Greenberg, M. E. *Gene Dev* **1999**, *13*, 2905.

(237) Bielen, A.; Perryman, L.; Box, G. M.; Valenti, M.; de Haven Brandon, A.; Martins, V.; Jury, A.; Popov, S.; Gowan, S.; Jeay, S.; Raynaud, F. I.; Hofmann, F.; Hargrave, D.; Eccles, S. A.; Jones, C. *Mol Cancer Ther* **2011**, *10*, 1407.

(238) (a) Hermisson, M.; Strik, H.; Rieger, J.; Dichgans, J.; Meyermann, R.; Weller, M. *Neurology* **2000**, *54*, 1357(b) Ito, A.; Shinkai, M.; Honda, H.; Yoshikawa, K.;

Saga, S.; Wakabayashi, T.; Yoshida, J.; Kobayashi, T. *Cancer Immunol Immun* **2003**, *52*, 80.

(239) Silva, A. C.; Oliveira, T. R.; Mamani, J. B.; Malheiros, S. M. F.; Malavolta, L.; Pavon, L. F.; Sibov, T. T.; Amaro, E.; Tannus, A.; Vidoto, E. L. G.; Martins, M. J.; Santos, R. S.; Gamarra, L. F. *Int J Nanomed* **2011**, *6*, 591.

(240) Jang, J. T.; Nah, H.; Lee, J. H.; Moon, S. H.; Kim, M. G.; Cheon, J. *Angewandte Chemie* **2009**, *48*, 1234.

(241) Hobel, S.; Aigner, A. *Wires Nanomed Nanobi* **2013**, *5*, 484.

(242) Elbakry, A.; Zaky, A.; Liebkl, R.; Rachel, R.; Goepferich, A.; Breunig, M. *Nano Lett* **2009**, *9*, 2059.

(243) (a) Spandidos, A.; Wang, X.; Wang, H.; Seed, B. *Nucleic acids research* **2010**, *38*, D792(b) Spandidos, A.; Wang, X.; Wang, H.; Dragnev, S.; Thurber, T.; Seed, B. *BMC genomics* **2008**, *9*, 633(c) Wang, X.; Seed, B. *Nucleic acids research* **2003**, *31*, e154.

(244) Marusyk, A.; Almendro, V.; Polyak, K. *Nat Rev Cancer* **2012**, *12*, 323.

(245) (a) Carey, L. A.; Dees, E. C.; Sawyer, L.; Gatti, L.; Moore, D. T.; Collichio, F.; Ollila, D. W.; Sartor, C. I.; Graham, M. L.; Perou, C. M. *Clinical cancer research : an official journal of the American Association for Cancer Research* **2007**, *13*, 2329(b) Voduc, K. D.; Cheang, M. C.; Tyldesley, S.; Gelmon, K.; Nielsen, T. O.; Kennecke, H. *Journal of clinical oncology : official journal of the American Society of Clinical Oncology* **2010**, *28*, 1684.

(246) Hortobagyi, G. N. *The New England journal of medicine* **1998**, *339*, 974.

(247) (a) Gradishar, W. J. *Breast cancer : basic and clinical research* **2012**, *6*, 159(b) Crown, J.; O'Leary, M.; Ooi, W. S. *The oncologist* **2004**, *9 Suppl 2*, 24.

(248) Holohan, C.; Van Schaeybroeck, S.; Longley, D. B.; Johnston, P. G. *Nat Rev Cancer* **2013**, *13*, 714.

(249) (a) Ha, M.; Kim, V. N. *Nature reviews. Molecular cell biology* **2014**, *15*, 509(b) Lin, S.; Gregory, R. I. *Nat Rev Cancer* **2015**, *15*, 321(c) He, L.; Hannon, G. J. *Nat Rev Genet* **2004**, *5*, 522.

(250) Davis-Dusenbery, B. N.; Hata, A. *Genes & cancer* **2010**, *1*, 1100.

(251) Boyerinas, B.; Park, S. M.; Murmann, A. E.; Gwin, K.; Montag, A. G.; Zillhardt, M.; Hua, Y. J.; Lengyel, E.; Peter, M. E. *Int J Cancer* **2012**, *130*, 1787.

(252) Kim, J.; Kim, H. S.; Lee, N.; Kim, T.; Kim, H.; Yu, T.; Song, I. C.; Moon, W. K.; Hyeon, T. *Angew Chem Int Edit* **2008**, *47*, 8438.

(253) (a) Chang, B. S.; Guo, J.; Liu, C. Y.; Qian, J.; Yang, W. L. *J Mater Chem* **2010**, *20*, 9941(b) Horcajada, P.; Ramila, A.; Gerard, F.; Vallet-Regi, M. *Solid State Sciences* **2006**, *8*, 1243.

(254) Liu, Y.; Shipton, M. K.; Ryan, J.; Kaufman, E. D.; Franzen, S.; Feldheim, D. L. *Anal Chem* **2007**, *79*, 2221.

(255) Delyagina, E.; Schade, A.; Scharfenberg, D.; Skorska, A.; Lux, C.; Li, W. Z.; Steinhoff, G. *Nanomedicine-Uk* **2014**, *9*, 999.

(256) (a) Kennedy, R. D.; Quinn, J. E.; Mullan, P. B.; Johnston, P. G.; Harkin, D. P. *Journal of the National Cancer Institute* **2004**, *96*, 1659(b) Donmez, Y.; Gunduz, U. *Biomedicine & pharmacotherapy = Biomedecine & pharmacotherapie* **2011**, *65*, 85.

(257) Yu, F.; Yao, H.; Zhu, P.; Zhang, X.; Pan, Q.; Gong, C.; Huang, Y.; Hu, X.; Su, F.; Lieberman, J.; Song, E. *Cell* **2007**, *131*, 1109.

(258) Sancey, L.; Garanger, E.; Foillard, S.; Schoehn, G.; Hurbin, A.; Albiges-Rizo, C.; Boturyn, D.; Souchier, C.; Grichine, A.; Dumy, P.; Coll, J. L. *Mol Ther* **2009**, *17*, 837.

(259) Sugahara, K. N.; Teesalu, T.; Karmali, P. P.; Kotamraju, V. R.; Agemy, L.; Girard, O. M.; Hanahan, D.; Mattrey, R. F.; Ruoslahti, E. *Cancer Cell* **2009**, *16*, 510.

(260) (a) Desgrosellier, J. S.; Cheresh, D. A. *Nat Rev Cancer* **2010**, *10*, 9(b) Moore, K. M.; Thomas, G. J.; Duffy, S. W.; Warwick, J.; Gabe, R.; Chou, P.; Ellis, I. O.; Green, A. R.; Haider, S.; Brouilette, K.; Saha, A.; Vallath, S.; Bowen, R.; Chelala, C.; Eccles, D.; Tapper, W. J.; Thompson, A. M.; Quinlan, P.; Jordan, L.; Gillett, C.; Brentnall, A.; Violette, S.; Weinreb, P. H.; Kendrew, J.; Barry, S. T.; Hart, I. R.; Jones, J. L.; Marshall, J. F. *Journal of the National Cancer Institute* **2014**, *106*.

(261) Sun, S.; Zeng, H.; Robinson, D. B.; Raoux, S.; Rice, P. M.; Wang, S. X.; Li, G. *J Am Chem Soc* **2004**, *126*, 273.

(262) Kallumadil, M.; Tada, M.; Nakagawa, T.; Abe, M.; Southern, P.; Pankhurst, Q. A. *J Magn Magn Mater* **2009**, *321*, 1509.

(263) Chen, W.; Yuan, Y.; Cheng, D.; Chen, J.; Wang, L.; Shuai, X. *Small* **2014**, *10*, 2678.

(264) (a) Yin, P. T.; Shah, S.; Pasquale, N. J.; Garbuzenko, O. B.; Minko, T.; Lee, K.-B. *Biomaterials* **2016**, *81*, 46(b) Kim, W. J.; Yockman, J. W.; Lee, M.; Jeong, J. H.; Kim, Y.-H.; Kim, S. W. *J Control Release* **2005**, *106*, 224.

(265) Khaider, N. G.; Lane, D.; Matte, I.; Rancourt, C.; Piche, A. *Am J Cancer Res* **2012**, *2*, 75.

(266) Bevis, K. S.; Buchsbaum, D. J.; Straughn, J. M. *Gynecol Oncol* **2010**, *119*, 157.

(267) Aletti, G. D.; Gallenberg, M. M.; Cliby, W. A.; Jatoi, A.; Hartmann, L. C. *Mayo Clin Proc* **2007**, *82*, 751.

(268) McGuire, W. P.; Hoskins, W. J.; Brady, M. F.; Kucera, P. R.; Partridge, E. E.; Look, K. Y.; ClarkePearson, D. L.; Davidson, M. *New Engl J Med* **1996**, *334*, 1.

(269) Peer, D.; Karp, J. M.; Hong, S.; FaroKHzad, O. C.; Margalit, R.; Langer, R. *Nat Nanotechnol* **2007**, *2*, 751.

(270) Pittenger, M. F.; Mackay, A. M.; Beck, S. C.; Jaiswal, R. K.; Douglas, R.; Mosca, J. D.; Moorman, M. A.; Simonetti, D. W.; Craig, S.; Marshak, D. R. *Science* **1999**, *284*, 143.

(271) (a) Spaeth, E. L.; Marini, F. C. *Methods in molecular biology* **2011**, *750*, 241(b) Ponte, A. L.; Marais, E.; Gallay, N.; Langonne, A.; Delorme, B.; Herault, O.; Charbord, P.; Domenech, J. *Stem cells* **2007**, *25*, 1737(c) Yagi, H.; Soto-Gutierrez, A.; Parekkadan, B.; Kitagawa, Y.; Tompkins, R. G.; Kobayashi, N.; Yarmush, M. L. *Cell Transplant* **2010**, *19*, 667(d) Coffelt, S. B.; Marini, F. C.; Watson, K.; Zwezdaryk, K. J.; Dembinski, J. L.; LaMarca, H. L.; Tomchuck, S. L.; Bentrup, K. H. Z.; Danka, E. S.; Henkle, S. L.; Scandurro, A. B. *P Natl Acad Sci USA* **2009**, *106*, 3806.

(272) (a) Gao, Z. B.; Zhang, L. N.; Hu, J.; Sun, Y. J. *Nanomed-Nanotechnol* **2013**, *9*, 174(b) Dwyer, R. M.; Khan, S.; Barry, F. P.; O'Brien, T.; Kerin, M. J. *Stem cell research & therapy* **2010**, *1*.

(273) Ling, X.; Marini, F.; Konopleva, M.; Schober, W.; Shi, Y.; Burks, J.; Clise-Dwyer, K.; Wang, R. Y.; Zhang, W.; Yuan, X.; Lu, H.; Caldwell, L.; Andreeff, M. *Cancer microenvironment : official journal of the International Cancer Microenvironment Society* **2010**, *3*, 83.

(274) Loebinger, M. R.; Eddaoudi, A.; Davies, D.; Janes, S. M. *Cancer research* **2009**, *69*, 4134.

(275) Ehtesham, M.; Kabos, P.; Kabosova, A.; Neuman, T.; Black, K. L.; Yu, J. S. *Cancer research* **2002**, *62*, 5657.

(276) Walczak, H.; Miller, R. E.; Ariail, K.; Gliniak, B.; Griffith, T. S.; Kubin, M.; Chin, W.; Jones, J.; Woodward, A.; Le, T.; Smith, C.; Smolak, P.; Goodwin, R. G.; Rauch, C. T.; Schuh, J. C. L.; Lynch, D. H. *Nature medicine* **1999**, *5*, 157.

(277) Mueller, L. P.; Luetzkendorf, J.; Widder, M.; Nerger, K.; Caysa, H.; Mueller, T. *Cancer Gene Ther* **2011**, *18*, 229.

(278) Lawrence, D.; Shahrokh, Z.; Marsters, S.; Achilles, K.; Shih, D.; Mounho, B.; Hillan, K.; Totpal, K.; DeForge, L.; Schow, P.; Hooley, J.; Sherwood, S.; Pai, R.; Leung, S.; Khan, L.; Gliniak, B.; Bussiere, J.; Smith, C. A.; Strom, S. S.; Kelley, S.; Fox, J. A.; Thomas, D.; Ashkenazi, A. *Nature medicine* **2001**, *7*, 383.

(279) Johnstone, R. W.; Frew, A. J.; Smyth, M. J. *Nat Rev Cancer* **2008**, *8*, 782.

(280) Rohmer, S.; Mainka, A.; Knippertz, I.; Hesse, A.; Nettelbeck, D. M. *The journal of gene medicine* **2008**, *10*, 340.

(281) Yin, P. T.; Shah, S.; Pasquale, N.; Garbuzenko, O. B.; Minko, T.; Lee, K. B. *Biomaterials* **2015**.

(282) Wu, X.; He, Y.; Falo, L. D., Jr.; Hui, K. M.; Huang, L. *Mol Ther* **2001**, *3*, 368.

(283) (a) Noonan, E. J.; Place, R. F.; Giardina, C.; Hightower, L. E. *Cell Stress Chaperon* **2007**, *12*, 219(b) Kohler, H. R.; Rahman, B.; Graff, S.; Berkus, M.; Triebskorn, R. *Chemosphere* **1996**, *33*, 1327.

(284) Kim, T.-H.; Shah, S.; Yang, L.; Yin, P. T.; Hossain, M. K.; Conley, B.; Choi, J.-W.; Lee, K.-B. *Acs Nano* **2015**, *9*, 3780.

(285) Reissis, Y.; Garcia-Gareta, E.; Korda, M.; Blunn, G. W.; Hua, J. *Stem cell research & therapy* **2013**, *4*, 139.

(286) (a) Kurbanov, B. M.; Geilen, C. C.; Fecker, L. F.; Orfanos, C. E.; Eberle, J. *The Journal of investigative dermatology* **2005**, *125*, 1010(b) Arts, H. J.; de Jong, S.; Hollema, H.; ten Hoor, K.; van der Zee, A. G.; de Vries, E. G. *Gynecologic oncology* **2004**, *92*, 794.

(287) Deng, Y.; Lin, Y.; Wu, X. *Genes & development* **2002**, *16*, 33.

(288) Ashkenazi, A.; Pai, R. C.; Fong, S.; Leung, S.; Lawrence, D. A.; Marsters, S. A.; Blackie, C.; Chang, L.; McMurtrey, A. E.; Hebert, A.; DeForge, L.; Koumenis, I. L.; Lewis, D.; Harris, L.; Bussiere, J.; Koeppen, H.; Shahrokh, Z.; Schwall, R. H. *The Journal of clinical investigation* **1999**, *104*, 155.

(289) (a) Yamaguchi, M.; Ito, A.; Ono, A.; Kawabe, Y.; Kamihira, M. *ACS synthetic biology* **2014**, *3*, 273(b) Ortner, V.; Kaspar, C.; Halter, C.; Tollner, L.;

Mykhaylyk, O.; Walzer, J.; Gunzburg, W. H.; Dangerfield, J. A.; Hohenadl, C.; Czerny, T. *J Control Release* **2012**, *158*, 424(c) Tang, Q.-s.; Zhang, D.-s.; Cong, X.-m.; Wan, M.-l.; Jin, L.-q. *Biomaterials* **2008**, *29*, 2673(d) Ito, A.; Shinkai, M.; Honda, H.; Kobayashi, T. *Cancer gene therapy* **2001**, *8*, 649.

(290) Kelly, M. M.; Hoel, B. D.; Voelkel-Johnson, C. *Cancer Biol Ther* **2002**, *1*, 520.

(291) Hageman, J.; Kampinga, H. H. *Cell Stress Chaperon* **2009**, *14*, 1.

(292) (a) Savla, R.; Garbuzenko, O. B.; Chen, S.; Rodriguez-Rodriguez, L.; Minko, T. *Pharmaceutical research* **2014**, *31*, 3487(b) Zhang, M.; Garbuzenko, O. B.; Reuhl, K. R.; Rodriguez-Rodriguez, L.; Minko, T. *Nanomedicine (Lond)* **2012**, *7*, 185.